1-1-2012

Performance analysis of diversity techniques in wireless communication systems: Cooperative systems with CCI and MIMO-OFDM systems

Mohammed Akhoirshida
University of Mississippi

PERFORMANCE ANALYSIS OF DIVERSITY TECHNIQUES IN WIRELESS COMMUNICATION SYSTEMS:

COOPERATIVE AND NON-COOPERATIVE SYSTEMS WITH CCI AND MIMO-OFDM SYSTEMS

By

Mohammed Shaker Akhoirshida

A Dissertation
submitted to the faculty
of the University of Mississippi
in partial fulfillment of the requirements
for the degree of Doctor of Philosophy
with a Major in Engineering Science
in the School of Engineering

THE UNIVERSITY OF MISSISSIPPI

December 2012

ABSTRACT

The fast increasing demands in the applications of wireless communication systems have motivated researchers to modify existing techniques, propose new techniques, and evaluate the system performance of these techniques under different channel fading scenarios. This dissertation analyzes the performance of efficient digital communication systems, the performance analysis includes the bit error rate (BER) of different binary and M-ary modulation schemes, and the average channel capacity (ACC) under different adaptive transmission protocols, namely, the simultaneous power and rate adaptation protocol (OPRA), the optimal rate with fixed power protocol (ORA), the channel inversion with fixed rate protocol (CIFR), and the truncated channel inversion with fixed transmit power protocol (CTIFR). In this dissertation, BER and ACC performance of interference-limited dual-hop decode-and-forward (DF) relaying cooperative systems with co-channel interference (CCI) at both the relay and destination nodes is analyzed in small-scale multipath Nakagami-m fading channels with arbitrary (integer as well as non-integer) values of m. This channel condition is assumed for both the desired signal as well as co-channel interfering signals. In addition, the practical case of unequal average fading powers between the two hops is assumed in the analysis. The analysis assumes an arbitrary number of independent and non-identically distributed (i.n.i.d.) interfering signals at both relay (R) and destination (D) nodes.

The ACC performance of non-cooperative wireless systems with co-channel interference (CCI) at destination node is analyzed in small-scale multipath Nakagami-m fading channels with arbitrary (integer as well as non-integer) values of m. This channel condition is assumed for both the desired signal as well as co-channel interfering signals. In addition, the practical case of unequal average fading powers

between the fading and CCI channels is assumed in the analysis. The analysis assumes an arbitrary number of independent and non-identically distributed (i.n.i.d.) interfering signals at the destination (D) node.

Also, the work extended to the case when the receiver employs the maximum ratio combining (MRC) and the equal gain combining (EGC) schemes to exploit the diversity gain in multipath fading channel. The effect of MRC and EGC diversity on the system BER and ACC performance analysis was considered with k elements at the receiver antenna, and the results show that for a given BER or ACC, increasing K decreases the required SIR in order to meet the required quality of service (QoS). So, the system performance can be improved by saving the energy of the transmitted signal. Beside that, the characteristic function approach is used to derive a limited integral form of the average BER of M-ary modulation schemes.

Also, the large computational complexity in the encoding/decoding process in the multiple-input multiple-output and orthogonal frequency division multiplexing (MIMO-OFDM) systems is reduced by the proposed technique. The process of precoding/decoding in combined MIMO-OFDM systems requires the computation of the conventional singular value decomposition (SVD) for each of the data-carrying OFDM tones. Since MIMO-OFDM systems involve large number of data-carriers, the corresponding computational complexity becomes significantly large. In this study, we present a computationally efficient technique for precoding/decoding MIMO-OFDM symbols at the transmitter/receiver, respectively, which depends on applying the conventional SVD process for only a limited number of subcarriers. Making the advantage of the fact that the inverse FFT (IFFT) and FFT processes are inherently implemented in the MIMO-OFDM transmitter and receiver, respectively, we propose to use the F.T-based interpolation method at the receiver to estimate the SVD decompositions for the remaining MIMO-OFDM subcarriers. The computation results show that the new proposed technique results in reduced computational complexity

in encoding/decoding MIMO-OFDM symbols as compared to other schemes known in literature. The derived expressions as well as the generated performance curves are useful for several applications in the wireless communication theory, especially in the design phase of cellular network planning. Also, the work extended to investigate the effect of this computational complexity reduction on the system BER performance.

Finally, dissertation conclusions and proposed future plan are presented at the end of this manuscript. Numerical and simulation results are obtained for the derived expressions. The derived expressions as well as the generated performance curves are useful for several applications in the wireless communication theory, especially in the design phase of cellular network planning, and they are simple and easy to evaluate as compared to the exact one using simulation. The derived expressions in this dissertation are new and have not been previously reported in the literature. The dissertation has analyzed different aspects of the wireless communication systems and obtained expressions for different performance measures. Further investigations can be conducted to extend our research work to include more practical systems and channel conditions.

This work is dedicated to my loving parents, to my loving wife, to my loving siblings, and my loving son Abd Al Rhman, and I do not forget my friends and all those who pray for my success wherever I head.

ACKNOWLEDGEMENTS

First of all, without enlightenment from God, the greatest, the merciful, this work would not have been successful. I would like to express my sincere gratitude to my academic supervisor, the chairperson of my dissertation committee, Prof. Mustafa Matalgah, an Associate Professor of Electrical Engineering, for his endless help and continuous support during this dissertation work. His support helped me to solve all of the problems I encountered and I will not forget his kindness and help even in my personal issues. I would like to thank the Department of Electrical Engineering, especially Professor Glisson for the all support provided during my study. It is my pleasure to appreciate the advice and the constructive comments from my Ph.D. examining committee: Professor Ramanarayanan "Vish" Viswanathan, Electrical Engineering Department chairman; Associate Professor Lei Cao, an Associate Professor of Electrical Engineering; and Associate Professor Xin Dang, an Associate Professor of Mathematics. Last but not least, I am thankful to my great parents, my wife, my loving son Abd AlRhman, and to my siblings for all their help, support, and encouragement.

Oxford, Mississippi, USA. Mohammed Shaker Akhoirshida

December, 2012

Table of Contents

List of Figures

List of Tables

LIST OF ACRONYMS

AF	Amplify and Forward
ASER	Average Symbol Error Rate
AWGN	Additive White Gaussian Noise
BER	Bite Error Rate
BFSK	Binary Frequency Shift Keying
BPSK	Binary Phase Shift Keying
CDF	Cumulative Distribution Function
CF	Characteristic Function
CIFR	Channel Inversion with Fixed Rate
CSI	Channel State Information
DES	Data Encryption Standard
DPSK	Differential Phase shift Keying
EGC	Equal Gain Combining
HARQ	Hybrid Automatic Repeat Request
i.i.d.	Independent and Identically Distributed
MGF	Moment Generating Function
MIMO	Multiple Input Multiple Output

MISO	Multiple Input Single Output
MRC	Maximal Ratio Combining
MSK	Minimum Shift Keying
OPRA	Optimal Power and Rate Adaptation
ORA	Optimal Rate Adaptation
PAM	Pulse Amplitude Modulation
PC	Processing Cycle
PDF	Probability Distribution Function
PSK	Phase Shift Keying
QAM	Quadrature Amplitude Modulation
QoS	Quality of Service
QPSK	Quadrature Phase Shift Keying
RF	Radio Frequency
RV	Random Variable
SC	Selection Combining
SC-PL	Switching Combining with Preferable Link
SEC	Switch and Examine Combining
SEC-PD	Switch and Examine Combining with Post Detection
SIMO	Single Input Multiple Output

SISO Single Input Single Output

SNR Signal-to-Noise Ratio

SSC Switch and Stay Combining

TIFR Truncated Channel Inversion with Fixed Rate

UE User Equipment

ADSL Asymmetric Digital Subscriber Line

ANSI American National Standards Institute

AWGN Additive White Gaussian Noise

Bps Bit per second

BPSK Binary phase shift keying

BWA Broadband Wireless Access

CBR Constant Bit Rate

CDMA Code division multiple access

CMOS Capacity Mapping Ordering Scheme

CP Cyclic prefix

CRC Cyclic Redundancy Check

DAB Digital Audio Broadcasting

DMT Discrete multi-tone modulation

DSSS Direct sequence spread spectrum

DTMF Dual Tone Multi frequency

DVBT Digital Video Broadcast Terrestrial

FCS Frame Check Sequence

FDM Frequency division multiplexing

FEC Forward Error Corrections

Flop Floating point operation

FFT Fast Fourier transform

GI Guard interval

IFFT Inverse Fast Fourier Transform

IFT Inverse Fourier Transform

ISDN Integrated Services Digital Network

ISI Inter symbol interference

kbp kilo bit per second

LAN Local Area Network

MAC Media Access Control

MEAs Multiple-element antennas

MIMO Multiple Input Multiple Output

MISO Multiple inputs single output

MMSE Minimum mean square error receiver

NLOS Non-Line-of-Sight

ODEMOD OFDM- demodulator

OMOD OFDM-modulator

ODO Optimization the detection order

OFDM Orthogonal Frequency division multiplexing

PAPR Peak-to average power ratio

PCM Pulse Code Modulated

P-SQRD parallel -sorted QR decomposition

PTS partial transmit sequence

QAM Quadrature amplitude modulation

QOS Quality of Service

QPSK Quadrature phase shift keying

QRD QR Decomposition

SC Single-carrier

SCR Successive cancellation receiver

SIC Successive interference cancellation

SIMO single input multiple outputs

SINR Signal to Interference-plus-Noise Ratio

INTRODUCTION

In wireless communication systems, multipath fading degrades the average signal-to-interference ratio (SIR) due to destructive combination of the same information signal replicas, and hence drastically affects the overall communication system performance. Many distributions have been considered in the literature to model small scale variations of the signal envelope in multipath fading channels, such as Rayleigh, Nakagami-m, Rican, etc. In this part, the Nakagami-m distribution has been considered to model the small-scale fading channels much better than the previously mentioned ones. Multipath fading is the main cause of signal strength deterioration, which is mainly classified into two types, small-scale and large-scale (shadowing). In large-scale fading, the average signal strength decreases due to path loss, whereas in small-scale fading, the instantaneous signal strength fluctuates randomly around the average mean value. Small-scale multipath fading can follow different distribution models, such as Rayleigh, Rician, Nakagami-m, Weibull, the $\alpha-\mu$ model, etc. Many distributions were considered in the literature; however, selection of the multipath channel model depends on the exact channel environment that might fit one distribution and not the others.

The cooperative diversity combining, which is a promising technique for the next generation of wireless communication systems. In cooperative diversity, there exists one or more relay nodes, as virtual antennas, distributed between the transmitter (source node) and the receiver (destination node). These nodes simply relay the

information data from the transmitter to receiver side, especially when the direct channel link (between the source and the destination nodes) is in severe condition. Moreover, the relay nodes are categorized into two types, the regenerative and the non-regenerative types. In the regenerative, also known as decode and forward (DF), the relay nodes receive the broadcasted signal in the first time slot, demodulate it, and then regenerate the original signal and retransmit it to the destination side. In non-regenerative communication, also known as amplify and forward (AF), the relay nodes simply receive the broadcasted signal in the first time slot, amplify it with a suitable gain, and then retransmit it to the destination side. In this part, the average BER and ACC performance of interference-limited dual-hop decode-and-forward (DF) relaying cooperative systems with co-channel interference (CCI) at both the relay and destination nodes is analyzed in small-scale multipath Nakagami-m fading channels with arbitrary (integer as well as non-integer) values of m. This channel condition is assumed for both the desired signal as well as co-channel interfering signals. Having such study, with the evaluation of several performance metrics available in the literature, enables system engineers and designers to enhance and refine their designs before actual deployment in real life. Many researchers have always been attracted to the notion of expressing their results in closed-form expressions in order to avoid conducting real-time experiments or running different simulations. The quality of the closed-form solution is usually judged by the complexity of its form and the difficulty in evaluating it numerically. In addition to that, different approximations can be used to derive alternative and precise expressions that can be applicable in situations where closed-form solutions are ordinarily unobtainable. The obtained

expressions for the performance of digital communication systems, such as the BER, computational complexity, and channel capacity, over fading channels with CCI can help the designers in building the transceivers in many meritorious and important aspects, such as power optimization, cell planning, and utilizing the wireless environmental resources. Also, the work extended to the case when the receiver employs the maximum ratio combining (MRC) and the equal gain combining (EGC) combining schemes to exploit the diversity gain. The effect of MRC and EGC diversity on the system BER and ACC performance analysis was considered with k elements at the receiver antenna, and the results show that for a given BER or ACC, increasing K decreases the required SIR.

Motivations

Cooperative wireless relaying communication system is a promising technique to combat fading in wireless channels and to ensure high network reliability, especially in severe fading wireless communication channels. In recent years, cooperative wireless relaying communication systems have attracted a lot of research interest due to their improvement in cellular, ad-hoc networks, and military communication systems, and due to their numerous benefits over direct transmission systems, such as good scalability, increased connectivity, robustness to channel impairments, and energy efficiency. Moreover, cooperative wireless relaying communication systems ensure low transmit RF power, and improve the utilization of wireless communication system resources. On the other hand, in light of the demand for wireless communication

services constantly increasing, frequency reuse has proved to be a practical strategy for an efficient use of the radio spectrum. However, as is well known, frequency reuse rise the so called co-channel interference (CCI).

Merit of Work

Having such study, with the evaluation of several performance metrics available in the literature, enables system engineers and designers to enhance and refine their designs before actual deployment in real life. Many researchers have always been attracted to the notion of expressing their results in closed-form expressions in order to avoid conducting real-time experiments or running different simulations. The quality of the closed-form solution is usually judged by the complexity of its form and the difficulty in evaluating it numerically. In addition to that, different approximations can be used to derive alternative and precise expressions that can be applicable in situations where closed-form solutions are ordinarily unobtainable. The obtained expressions for the performance of digital communication systems, such as the BER, computational complexity, and channel capacity, over fading channels with CCI can help the designers in building the transceivers in many meritorious and important aspects, such as power optimization, cell planning, and utilizing the wireless environmental resources.

Chapter 1

DUAL-HOP DF COOPERATIVE SYSTEMS: APPROXIMATION AND SIMULATION OF SIR PDF

1.1 Overview

In recent years, cooperative wireless relaying communication systems have attracted a lot of research interest due to their improvement in cellular, ad-hoc networks, and military communication systems, and due to their numerous benefits over direct transmission systems. The performance analyses are very important for wireless communication system designers as they provide feedback on the quality of the designs and hence, provide a chance for enhancements and refining. The remainder of this chapter is organized as follows. In Section 1.2, we introduce the system model under study. In Sections 1.3 and 1.4 the PDF approximation and simulation steps are explained. In Section 1.5, we present the numerical and simulation results to quantitatively assess and verify the accuracy of the obtained expressions. Finally, some conclusions are drawn in section 1.6.

1.2 System Model

We consider an interference-limited dual-hop DF relaying cooperative wireless communication system operating over independent and non identical distributed (i.n.i.d.) Nakagami-m fading channels with arbitrary integer as well as non-integer fading severity parameter m and with multiple CCI at both R and D nodes, where a source node (S) communicates with D using R as shown in fig. 1.1. The communication is performed in two time slots and no direct link between S and D is assumed to be available due to sever channel impairments conditions. The signal on the direct link between the source and destination nodes is assumed to be insignificant and is ignored in our analysis. This assumption is practical due to sever channel impairments conditions, which justifies cooperative communication. All nodes are single antenna devices. We assumed both R and D operate in interference-limited conditions; i.e., the channel noise is dominated by the total interfering signals. Multiple co-channel N_R and N_D interferers are assumed to be present at R and D, respectively. Each one of the N_R (or N_D) interfering signals (i.e., ith interfering signal, where $i = 1, 2, \cdots, N_R$ (or $i = 1, 2, \cdots, N_D$)) has an average transmit power P_{ri} (or P_{di}), fading severity parameter m_{ri} (or m_{di}), fading power parameter Ω_{ri} (or Ω_{di}), and experiences link fading coefficient h_{ri} (or h_{di}). Let the modulated signal transmitted by S, during the first time slot, denoted by S_S with transmit power P_S. Then the received signal at R in the first time slot is given by

$$y_R = \sqrt{P_S} h_1 S_S + \sum_{i=1}^{N_R} \sqrt{P_{ri}} h_{ri} S_{ri}, \qquad i = 1, 2, \cdots, N_R \tag{1.1}$$

and the received signal at D in the second time slot is given by

$$y_D = \sqrt{P_R} h_2 S_R + \sum_{i=1}^{N_D} \sqrt{P_{di}} h_{di} S_{di}, \qquad i = 1, 2, \cdots, N_D \tag{1.2}$$

where,h_1, and h_2 are the channel gain coefficients of the first and the second hop with fading severity parameter m_1 and m_2, and fading power parameter Ω_1 (or Ω_2), respectively. All of h_{ri}, h_{di}, h_1, and h_2 are i.n.i.d. Nakagami-m random variables. In (1.1) and (1.2), S_R is the transmitted symbol from R to D with transmit power P_D, S_{ri} is the transmitted symbol from ith interferer to R with transmit power P_{ri}, and S_{di} is the transmitted symbol from ith interferer to D with transmit power P_{di}. The transmitted symbols S_S and S_R and the interfering symbols S_{ri} and S_{di} are assumed to be mutually independent and uniformly distributed with zero mean and unit variance. The fading channels average power parameters are given by

$$\Omega_1 = E[|h_1|^2], \tag{1.3}$$

$$\Omega_2 = E[|h_2|^2], \tag{1.4}$$

$$\Omega_{ri} = E[|h_{ri}|^2], \tag{1.5}$$

and

$$\Omega_{di} = E[|h_{di}|^2]. \tag{1.6}$$

The SIR is the ratio between the transmitted signal power and the total interference power. So, at R the SIR is simply given by

$$\gamma_R = \frac{P_S |h_1|^2}{\sum_{i=1}^{N_R} P_{ri} |h_{ri}|^2}, \tag{1.7}$$

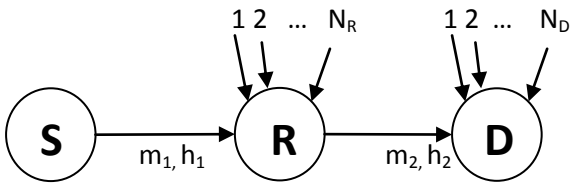

Figure 1.1. A dual-hop DF relaying cooperative wireless communication system over Nakagami-m fading channels with multiple CCI at both the relay and the destination nodes.

and at D is given by

$$\gamma_D = \frac{P_R|h_2|^2}{\sum_{i=1}^{N_D} P_{di}|h_{di}|^2}. \tag{1.8}$$

Since h_{ri}, h_{di}, h_2, and h_1 are i.n.i.d. Nakagami-m random variables, then the square of each of the fading coefficients h_{ri}, h_{di}, h_2, and h_1 follows Gamma distribution. The summation of Nakagami-m random variables is accurately approximated by another Nakagami-m random variable with new different fading parameter and fading power coefficient according to [40]. Also, the summation of Gamma random variables is accurately approximated by another Gamma random variable with different fading parameter and fading power coefficient according to [40] and [24]. So, according to the above the, each of γ_R in (1.7) or γ_D in (1.8) expression is a ratio of two normalized Gamma random variables.

1.3 PDF Approximation Procedure

In this section we explain the PDF approximation that have been used in [24] to derive the outage probability. But they did not simulate the exact PDF and compare it with approximate one to show the accuracy. So, we fill this gap and give more explanations related to this PDF approximation. In our analysis we assumed that

no power control is used (i.e., $P_{ri} = P_r$, and $P_{di} = P_d$) and the transmit powers normalized to one (i.e., $P_S = 1$, $P_R = 1$, $P_{ri} = P_r = 1$, and $P_{di} = P_d = 1$). Now, let R_1 and R_2 follow the Nakagami-m distribution with fading parameters m_{R1}, ω_1, and m_{R2}, ω_2, respectively. Then, the ratio F which is given as

$$F = \frac{R_1^2 \omega_2}{R_2^2 \omega_1}, \tag{1.9}$$

has a PDF $f_F(f)$ follows Fisher-Snedecor PDF as [35, Eq. (92)]

$$f_F(f) = \frac{\Gamma(m_{R1}+m_{R2})}{\Gamma(m_{R1})\Gamma(m_{R2})} \left(\frac{m_{R1}}{m_{R2}}\right)^{m_{R1}} f^{m_{R1}-1} \left(1+\frac{m_{R1}}{m_{R2}} f\right)^{-(m_{R1}+m_{R2})}, \tag{1.10}$$

where $\Gamma(.)$ denotes the Gamma function [36, Eq. 8.310.1]. The SIR in either one (1.7) or (1.8) is a ratio between squared Nakagami-m random variable $|h_1|^2$ (or $|h_2|^2$). Using corollary (1) in Appendix (A) we can accurately approximate the PDF of each of the following two summations $\sum_{i=1}^{N_R} |h_{ri}|^2$ and $\sum_{i=1}^{N_D} |h_{di}|^2$ by another Gamma distribution with new values of the fading parameters and average fading powers, m_r and ω_r, m_d and ω_d, respectively, given as follows [40]

$$m_r = \frac{(\omega_r)^2}{E[{\xi_r}^2] - (\omega_r)^2} \quad , \omega_r = \sum_{i=1}^{N_R} \Omega_{ri} = E[\xi_r], \tag{1.11}$$

and

$$m_d = \frac{(\omega_d)^2}{E[{\xi_d}^2] - (\omega_d)^2} \quad , \omega_d = \sum_{i=1}^{N_D} \Omega_{di} = E[\xi_d], \tag{1.12}$$

where $\xi_r = \sum_{i=1}^{N_R} |h_{ri}|^2$ and $\xi_d = \sum_{i=1}^{N_D} |h_{di}|^2$. The moments of ξ_r and ξ_d can be calculated by means of the multinomial expansion as follows

$$\begin{aligned} E[(\xi_r)^n] &= \sum_{p=0}^{n} \sum_{j=0}^{p} \cdots \sum_{n_{N_R-1}}^{n_{N_R-2}} \binom{n}{p} \binom{p}{j} \cdots \binom{n_{N_R-2}}{n_{N_R-1}} \\ &\quad \times E[|h_{r1}|^{2(n-p)}] E[|h_{r2}|^{2(p-j)}] \cdots E[|h_{rN_R}|^{2(n_{N_R-1})}], \end{aligned} \tag{1.13}$$

and

$$E[(\xi_d)^n] = \sum_{p=0}^{n}\sum_{j=0}^{p}\cdots\sum_{n_{N_D-1}}^{n_{N_D-2}}\binom{n}{p}\binom{p}{j}\cdots\binom{n_{N_D-2}}{n_{N_D-1}} \times E[|h_{d1}|^{2(n-p)}]E[|h_{d2}|^{2(p-j)}]\cdots E[|h_{dN_D}|^{2(n_{N_D-1})}]. \quad (1.14)$$

The nth moment of $|h_{ri}|$ and $|h_{di}|$ can be given as [35, Equ. (17)]

$$E[|h_{ri}|^n] = \frac{\Gamma(m_{ri}+n/2)}{\Gamma(m_{ri})}\binom{\Omega_{ri}}{m_{ri}}^{\frac{n}{2}}, \quad i = 1, 2, 3, \cdots, N_R, \quad (1.15)$$

and

$$E[|h_{di}|^n] = \frac{\Gamma(m_{di}+n/2)}{\Gamma(m_{di})}\binom{\Omega_{di}}{m_{di}}^{\frac{n}{2}}, \quad i = 1, 2, 3, \cdots, N_D. \quad (1.16)$$

The proof of the results in (1.13) and (1.14) is founded in Appendix (A). Now, if we compare (1.9) with (1.7), then the PDF of γ_R, $f_{\gamma_R}(f)$, can be approximated by $f_F(f)$ with $f = \frac{P_r\omega_r\gamma_R}{P_S\Omega_1}$, where $m_{R1} = m_1$ and $m_{R2} = m_r$. Also by comparing (1.9) with (1.8) the PDF of γ_D, $f_{\gamma_D}(f)$, can be approximated by $f_F(f)$ with $f = \frac{P_d\omega_d\gamma_D}{P_R\Omega_2}$, where $m_{R1} = m_2$ and $m_{R2} = m_d$. By substituting these parameters appropriately in (1.10) yields [24]

$$f_{\gamma_R}(\gamma_R) = \frac{\Gamma(m_1+m_r)}{\Gamma(m_1)\Gamma(m_r)}\left(\frac{m_1}{m_r}\right)^{m_1}\left(\frac{P_r\omega_r\gamma_R}{P_S\Omega_1}\right)^{m_1-1}\left(1+\frac{m_1}{m_r}\frac{P_r\omega_r\gamma_R}{P_S\Omega_1}\right)^{-(m_1+m_r)} \quad (1.17)$$

and

$$f_{\gamma_D}(\gamma_D) = \frac{\Gamma(m_2+m_d)}{\Gamma(m_2)\Gamma(m_d)}\left(\frac{m_2}{m_d}\right)^{m_2}\left(\frac{P_d\omega_d\gamma_D}{P_R\Omega_2}\right)^{m_2-1}\left(1+\frac{m_2}{m_d}\frac{P_d\omega_d\gamma_D}{P_R\Omega_2}\right)^{-(m_2+m_d)} \quad (1.18)$$

In the following we present the simulation procedure to verify the accuracy of the PDF approximation.

1.4 PDF Simulation Procedure

The probability density function (PDF) of either one of the random variables γ_R in (1.7) or γ_D in (1.8) is unknown, but we approximated it in the previous section. Moreover, we simulate the exact one using MonteCarlo simulation process according to the following steps. First, for the first run of the Monte Carlo process, we generate 1000 samples for each of the the Nakagami-m random variables (i.e., h_{ri}, h_{di}, h_2, and h_1). Second, we took the square of each of them. Third, after the previous steps we took the ratio between them as in (1.7) (or (1.8)), the result represents the random variables γ_R in (1.7) (or γ_D in (1.8)). As a result of the previous steps, we have γ_R (or γ_D) as a group of observations (i.e., vector of the random variable γ_R (or γ_D) events). Forth, to find the exact PDF, we find the frequency of each observation of the random variable γ_R (or γ_D), dividing these frequencies by the total number of the observations results in a pdf according to this specific run. Finally, we repeated this procedure 10^8 times and average the results to get the exact pdf.

1.5 Numerical and Simulation Results

In the following we introduce sample of the numerical and simulation results of the SIR PDF. Fig. 1.2 shows the probability density function (PDF) of either one the random variable γ_R in (1.7) or γ_D in (1.8) versus the average SIR (in linear scale) in interference-limited DF relaying dual-hop wireless communication system with two interferers at both relay and destination nodes over Nakagami-m fading channels, with arbitrary fading parameters values. (i.e., $N_R = 2$; $N_D = 2$ with $m_1 = 2$,

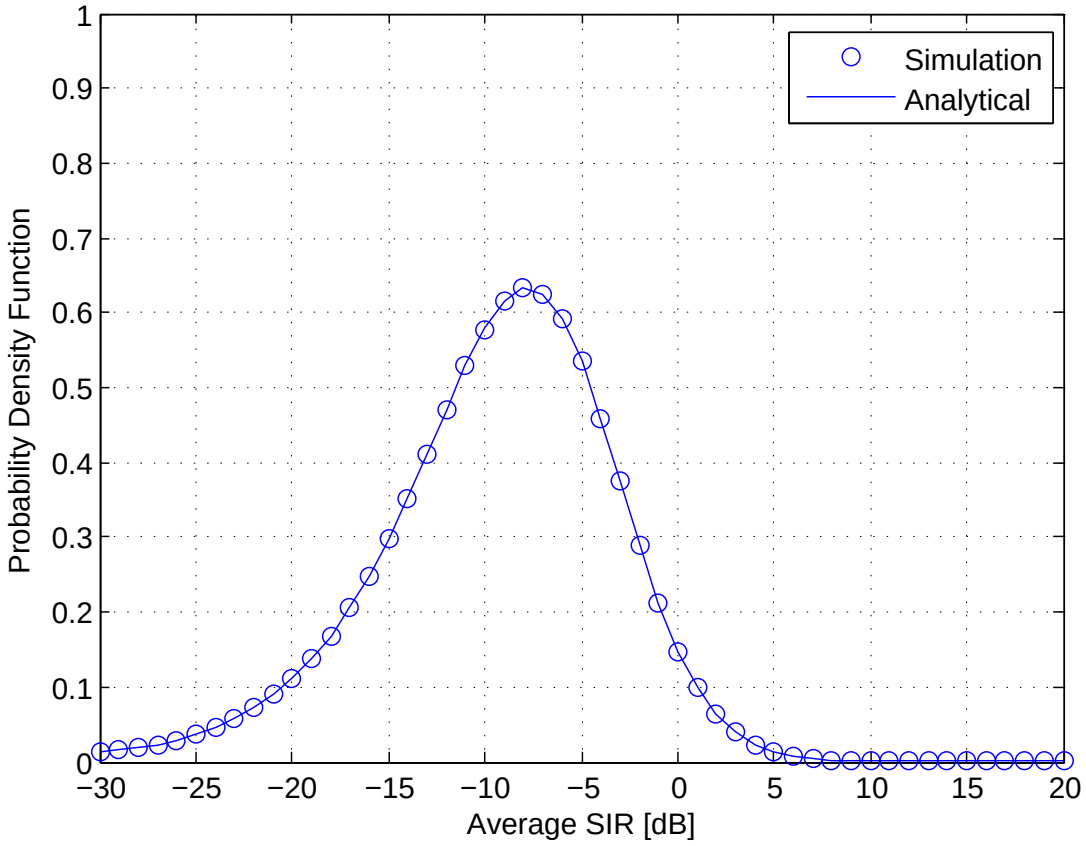

Figure 1.2. The exact and the approximate PDF of γ_D (or γ_R) in linear scale versus the average SIR in dB scale for each hop of the dual-hop DF relaying wireless communication system over Nakagami-m fading channels with multiple CCI.

$\Omega_1 = 1$, $m_{r1} = 1$, $m_{r2} = 1.1$, $m_2 = 2$, $m_{d1} = 1.1$, $m_{d2} = 1$, $\Omega_{r1} = 1$, $\Omega_{r2} = 1$, $\Omega_{d1} = 1$, $\Omega_{d2} = 1$,). The figure shows the accuracy of the proposed approximation. Fig. 1.3 shows the same results in the logarithm scale.

1.6 Conclusions

In this chapter of the dissertation we present an approximation and simulation steps of the probability density function (PDF) of the signal-to-interference ratio (SIR) of

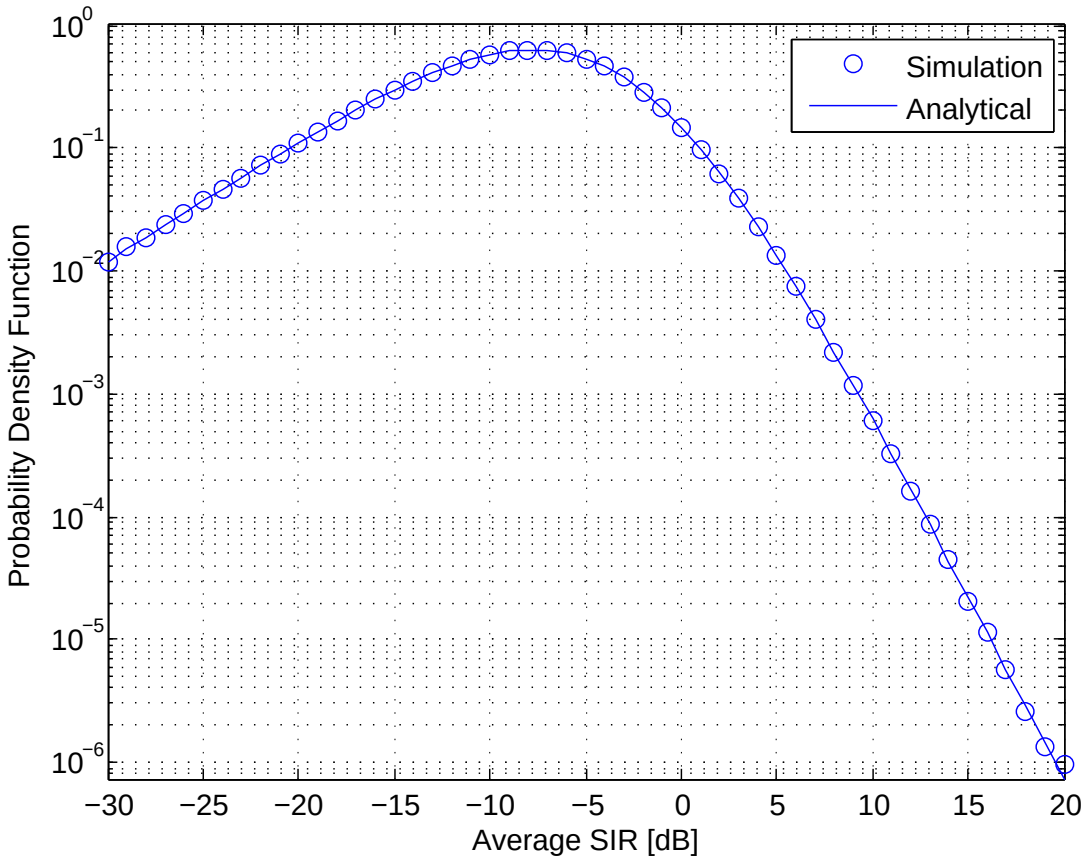

Figure 1.3. The exact and the approximate PDF of γ_D (or γ_R) versus the average SIR in dB scale for each hop of the dual-hop DF relaying wireless communication system over Nakagami-m fading channels with multiple CCI.

the system model under study. The numerical and simulation results are presented at the end of the chapter. The results show the accuracy of the approximate PDF.

Chapter 2

DUAL-HOP DF COOPERATIVE SYSTEMS: BER PERFORMANCE ANALYSIS

2.1 Overview

In wireless communication systems, multipath fading can degrade the average signal-to-interference ratio (SIR) due to destructive combination of the same information-bearing signal replicas, and hence drastically affects the wireless communication systems performance. Many distributions have been considered in the literature to model small scale variations of the signal envelope in multipath fading channels such as Rayleigh (no line of sight channel model), Rician (line of sight channel model), Nakagami-m, etc. The Nakagami-m distribution has been considered in the literature to model the small-scale fading channels much better than the previously mentioned ones. The system performance degradation due to multipath fading, can be minimized by applying a diversity combining at the receiver side in order to utilize all received replicas and combine them together to effectively increase the overall combined SIR. If the communication system is subject to sever fading channel such that

the SIR falls below the required SIR threshold level (which is specify the required quality of service (QoS)), then the communication could be unreliable. So, the need to use cooperative communication systems flows to the surface. In cooperative communication systems intermediate nodes are used to relay the signals between the source and the destination terminals.

Accurate closed-form approximate expressions for the BER performance of different modulation schemes are derived. The analysis assumes an arbitrary number of independent and non-identically distributed (i.n.i.d.) interfering signals at both R and D nodes. The derived closed-form expressions are simple and easy to evaluate. We verify the accuracy of the derived expressions using MonteCarlo Simulation.

The remainder of this chapter is organized as follows. In sections 2.2 and 2.3, the related work and contributions to the chapter are summarized. In Section 2.4, we analyze the performance of the model under study in terms of bit error rate and derive closed-form expressions for the average BER assuming different modulation schemes. In Section 2.5 the analysis extended to include the coherent M-ary modulation schemes. In Section 2.6 the characteristic function approach is used to derive the BER of coherent M-ary modulation schemes in a finite integral form. In Section 2.7, we present the numerical and simulation results to quantitatively assess and verify the accuracy of our obtained expressions. Finally some conclusions are drawn in section 2.8.

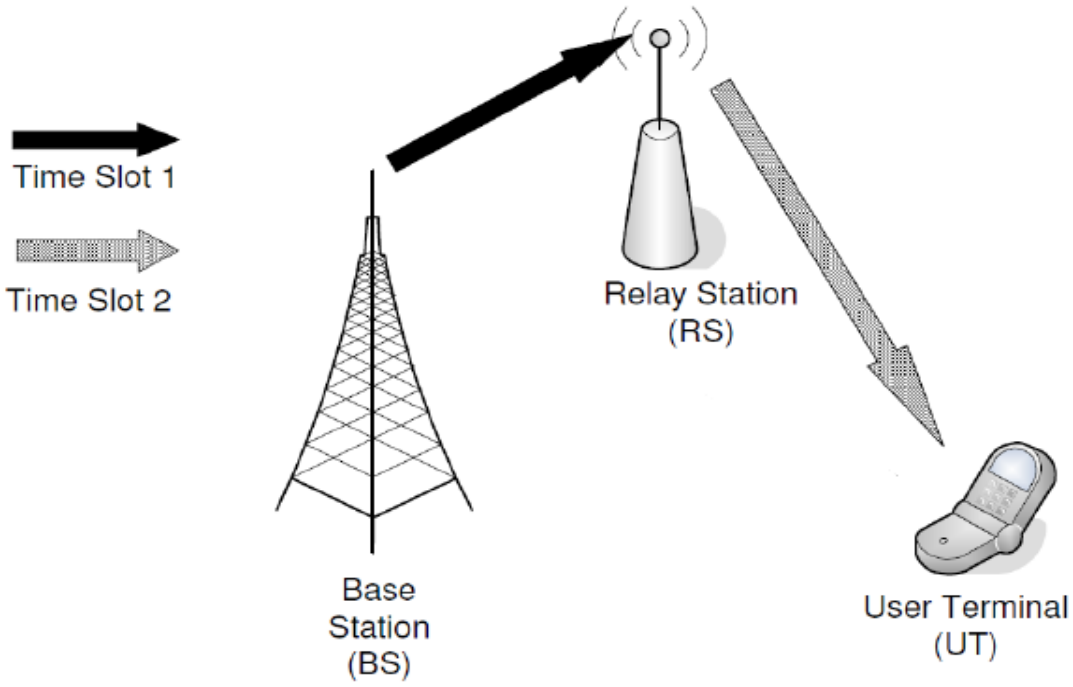

Figure 2.1. A Dual-hop DF relaying cooperative wireless communication system, where the source node (the base Station) communicates with the destination node (user terminal) using the DF relay node (relay station) during two time slots.

2.2 Related Work

In this section, we review the related research work. In [2], a class of cooperative communication protocols with arbitrary N-relay nodes is proposed for wireless networks, in which each relay coherently combines the signals received from previous relays in addition to the signal from the source. Exact symbol-error-rate (SER) expressions for an arbitrary N-node network employing M-ary phase shift-keying (M-PSK) modulation or quadrature-amplitude modulation (QAM) are provided for the proposed class of protocols. Further, approximate expressions for the SER are derived and shown to be tight at high enough signal-to-noise ratio (SNR). The class of cooperative protocols shares the same asymptotic performance at high enough SNR and does not depend on the number of previous relays, the number of previous nodes involved in coherent detection. Hence, the asymptotic performance of a simple cooperative scenario in which each relay combines the signals from the source and the previous relay is exactly the same as that for a much more complicated scenario in which each relay combines the signals from the source and all the previous relays. In [31], the author derived closed-form expressions for the average BER of both coherent and non-coherent binary frequency-shift keying (BFSK) and binary phase shift keying (BPSK) modulation schemes in an interference-limited wireless communication system. The analysis assumes an arbitrary number of independent and but identically distributed Nakagami-m interferers. The study extended to investigate the effect of maximal ratio combining diversity technique at the receiver end. In [125], the authors propose various relaying protocols, and the two most commonly

used are AF and DF. In the AF scheme, the relay node simply forwards a scaled version of the received signal from the source to the intended destination node. In the DF scheme, the relay node decodes the received signal from the source and then transmits the re-encoded version of the received signal to the intended destination node. It has received great interest from both academia and industry due to its simplicity and ease of implementation.

In [9], [10], Hasna and Alouini study the average bit error probability (ABEP) of dual-hop systems with AF relaying over Rayleigh and Nakagami-m fading channels. In [11], the authors analyze the error performance of a DF-based multi-antenna relay network in the presence of Nakagami-m fading. In [12] and [13], the authors study the performance bounds of AF multi-hop transmissions over non-identically distributed Nakagami-m fading channels. In [14], Ikki and Ahmed present a tight lower bound for the performance of an AF multi-relay network over non-identical Nakagami-m fading channels, especially in the medium and high signal-to-noise (SNR) region. In [15], the authors present closed-form expressions for the average bit error probability (ABEP) of BPSK, QPSK and M-QAM of an amplify-and-forward average power scaling dual-hop relay transmission, over non-identical Nakagami-m fading channels, with integer values of m. In [16] and [17] , the authors investigate the performance of a dual-hop amplify-and-forward relay system in Nakagami-m fading channels in the presence of multiple interferers. Based on the new closed-form expression for the cumulative distribution function of a new type of random variable involving a number of independent gamma random variables, they present closed-form expressions for the outage probability, general moments for the end-to-end signal to interference

and noise ratio, and ergodic capacity of the system. In addition, they look into the high signal-to-noise ratio regime and characterize the diversity order and coding gain achieved by the system. In [22], the average BER of DF cooperative systems is analyzed assuming that the channel gain amplitude is real and follows Gaussian distributed. In [23], the average SER of multihop transmission is analyzed assuming that there is no direct link between the source and the destination. In [24], the outage performance of dual-hop DF relaying systems with multiple CCI at both nodes, namely relay and destination, and subject to arbitrary Nakagami-m fading is investigated. More specifically, an indeed highly accurate closed form approximate expression for the end-to-end outage probability is derived that is simple to calculate and yields results instantaneously independently of the number of interferers. In [25], the authors consider a dual-hop relay communication system with channel state information (CSI)-assisted AF relaying protocol. Assuming that the system operates in the presence of Nakagami-m fading, novel closed-form expressions for the exact BER of BPSK signals and the ergodic capacity are derived.

In [26], the authors consider performance of a dual hop AF system with co-channel interference at relay. They consider a channel state information assisted system in the Nakagami-m channel. The outage probability and the average bit error probability of the system are determined. The influence of the interference, as well as the influence of other system's parameters, such as the fading parameter m and outage probability threshold on the system's performance, are considered. In [27], the authors investigate the outage performance of dual-hop DF cooperative systems in an interference-limited Nakagami-m fading environment. More specifically, assum-

ing the presence of Nakagami-m faded multiple CCI at the DF relay and a noisy destination, simple accurate closed-form approximations for the end-to-end outage probability are derived. In [28], the authors investigate the effect of co-channel interference on the performance of dual-hop communications with AF relaying. Based on the derivation of the effective signal-to-interference-plus-noise ratio (SINR) at the destination node of the system, taking into account co-channel interference, they obtain expressions for the error and outage probabilities. In [29], the authors study the performance of a dual-hop non-regenerative relay fading channel in an interference-limited environment. The relay and destination nodes are corrupted by co-channel interference. New closed-form expressions for the probability density function and cumulative distribution function of the output SIR ratio are derived. Analytical expressions for the outage probability of both the channel-state-information-assisted relay and the fixed-gain relay channels are derived. In [30], the authors study the outage probability performance of DF cognitive dual-hop systems for Nakagami-m fading channels, with consideration of an interference limit. An exact outage probability expression is derived, and the impact of various key system parameters, such as interference and fading severity, are investigated.

2.3 Contributions

Many contributions have been achieved in this chapter as follows. First, we derived accurate approximate closed-form expression for the BER of different coherent and non-coherent binary modulation schemes such as, binary phase shift keying (BPSK),

binary frequency shift keying (BFSK), and differential phase shift keying (DPSK) modulation schemes of interference-limited DF dual-hop relaying co-operative wireless communication systems with multiple co-channel interference at both R and D nodes in independent identical and non-identical Nakagami-m fading channels (which is the real situation in practical wireless relaying systems) with arbitrary integer and non-integer fading parameters, the fading shape and the fading power parameters m and ω, respectively. Second, we generalized the BER expressions of binary modulation schemes to the M-ary PSK modulation schemes. Finally, the characteristic function approach is used to derive a finite integral form of the average BER of the M-ary modulation schemes.To the authors best knowledge, there is no research work has been done before that considers the average error probability performance analysis of interference-limited DF dual-hop relaying cooperative wireless communication system operating over independent but not necessarily identically distributed (i.n.i.d.) Nakagami-m fading channels with multiple co-channel interference at both the relay and destination nodes over general non-identical Nakagami-m fading channels with arbitrary (integer and non-integer) values of m. Unlike many studies reported in the literature, we considered the Nakagami-m co-channel interference at both the relay and destination nodes. Also, many studies reported in the literature restrict the BER performance analysis to a certain type of modulation scheme, our closed-form expressions are valid for different modulation schemes (coherent binary and M-ary, and non-coherent binary modulation schemes) known in the communication systems. Beside that, the characteristic function approach is used to derive a finite integral form of the average BER of the M-ary modulation schemes.

2.4 BER Analysis and Derivation

Bit error rate (BER) performance analyses are very important metric for wireless communication system designers as they provide feedback on the quality of the designs and hence, provide a chance for enhancements and refining. This chapter of the dissertation will focus on conducting performance evaluation studies for next generation wireless systems, mainly from an analytical point of view. In general when fading is present, the average BER is obtained by averaging conditional bit error rate (CEP) in Gussian channel over the fading distribution as follows.

$$\overline{P}_e = \int_0^\infty P_e(\gamma)\, f_\gamma(\gamma) d\gamma, \tag{2.1}$$

where $f_\gamma(\gamma)$ is the PDF of SIR and $P_e(\gamma)$ is the conditional BER of a specific modulation scheme in Gaussian channel. Equation (2.1) is general and valid for any modulation scheme and for any wireless communication fading channel. To find $\overline{P}_e$ for our system model we need first to find $f_\gamma(\gamma)$ (which is what we already did in chapter 1, $f_\gamma(\gamma)$ approximated as F-distribution) and then solve the integration in equation (2.1) to derive the BER closed-form expressions for different modulation schemes. By the way $P_e(\gamma)$ depends on the the modulation scheme, and in general is well known in literature for many modulation schemes.

By substituting (1.17) into (2.1) yields,

$$\overline{P}_{e1} = \int_0^\infty P_e(\gamma) \frac{\Gamma(m_1+m_r)}{\Gamma(m_1)\Gamma(m_r)} \left(\frac{m_1}{m_r}\right)^{m_1} \left(\frac{P_r\omega_r\gamma_R}{P_S\Omega_1}\right)^{m_1-1} \left(1+\frac{m_1}{m_r}\frac{P_r\omega_r\gamma_R}{P_S\Omega_1}\right)^{-(m_1+m_r)} d\gamma_R, \tag{2.2}$$

and by substituting (1.18) into (2.1) yields,

First-hop	Second-hop	End-to-end
Yes	Yes	No
Yes	No	Yes
No	Yes	Yes
No	No	No

Table 2.1. Error occurrence throughout the different stages and the overall end-to-end error in a dual-hop DF relaying communication systems

$$\overline{P}_{e2} = \int_0^\infty P_e(\gamma) \frac{\Gamma(m_2+m_d)}{\Gamma(m_2)\Gamma(m_d)} \left(\frac{m_2}{m_d}\right)^{m_2} \left(\frac{P_d\omega_d\gamma_D}{P_R\Omega_2}\right)^{m_2-1} \left(1+\frac{m_2}{m_d}\frac{P_d\omega_d\gamma_D}{P_R\Omega_2}\right)^{-(m_2+m_d)} d\gamma_D, \tag{2.3}$$

where P_{e1} is the average BER of the first hop, and P_{e2} is the average BER of the second hop of the system under study. For DF relaying dual-hop wireless communication system and according to Table (2.1) the end-to-end average BER is then given by [130, Eq. (11.4.12)] as

$$\overline{P}_e = P_{e1} + P_{e2} - 2P_{e1}P_{e2} \tag{2.4}$$

In the following, we will derive the BER closed-form expressions for different binary coherent and non-coherent modulation schemes for the second hop, and then extend the result to the first hop. Then, we will extend the results to include the coherent M-ary modulation schemes. Finally, we will extend the analysis to investigate the BER using characteristic function approach.

2.4.1 Coherent Binary Phase Shift Keying (BPSK) Modulation Scheme

For the BPSK modulation scheme, the conditional BER in Gussian channel is given by $P_e(\gamma) = Q\left(\sqrt{2\gamma}\right)$. Given this $P_e(\gamma)$ and the PDF of γ_D in (1.18) or the PDF of γ_R in (1.17), the integration in (2.1) can not be solved in closed form. However, if we express the Q-function in terms of the confluent hypergeometric function, then we will be able to solve the integral in (2.1) in closed form in the sequel. The conditional BER of BPSK is given in terms of the confluent hypergeometric function by [133, Eq. (7.1.2)] as

$$\begin{aligned} P_e(\gamma) &= Q\left(\sqrt{2\gamma}\right) \\ &= 0.5\left(1 - 2\sqrt{\gamma/\pi}\ \times {}_1F_1\left(0.5; 1.5; -\gamma\right)\right), \end{aligned} \tag{2.5}$$

where ${}_1F_1(.;.;.)$ is the confluent hypergeometric function of the first kind [36, Eq. (9.210.1)]. By substituting (2.5) into (2.1) and using the PDF in (1.18) the average BER of the BPSK that of the second hop can be written as

$$\begin{aligned} \overline{P}_{e2} \;=\; & \int_0^\infty \frac{\Gamma(m_2+m_d)}{\Gamma(m_2)\Gamma(m_d)} \left(\frac{m_2}{m_d}\right)^{m_2} \left(\frac{P_d\omega_d\gamma_D}{P_R\Omega_2}\right)^{m_2-1} \left(\frac{P_d\omega_d}{P_R\Omega_2}\right) \left(1 + \frac{m_2}{m_d}\frac{P_d\omega_d\gamma_D}{P_R\Omega_2}\right)^{-(m_2+m_d)} \\ & \times 0.5\left(1 - 2\sqrt{\gamma_D/\pi}{}_1F_1\left(0.5; 1.5; -\gamma_D\right)\right) d\gamma_D. \end{aligned} \tag{2.6}$$

Now, using the integral form of the confluent hypergeometric function of the first kind which is given in [133, Eq. (13.2.1)] as

$${}_1F_1(a;b;c) = \frac{\Gamma(b)}{\Gamma(b-a)\Gamma(a)} \int_0^1 t^{a-1}(1-t)^{b-a-1}e^{ct}dt,$$

we show that,

$$
\begin{aligned}
{}_1F_1\left(0.5;1.5;-\gamma_D\right) &= \frac{\Gamma(1.5)}{\Gamma(1)\Gamma(0.5)}\int_0^1 t^{-0.5}e^{-\gamma_D t}dt \\
&= 0.5\int_0^1 t^{-0.5}e^{-\gamma_D t}dt. \qquad (2.7)
\end{aligned}
$$

Then, by substituting (2.7) into (2.6) yields

$$
\begin{aligned}
\overline{P}_{e2} &= \int_0^\infty \frac{\Gamma(m_2+m_d)}{\Gamma(m_2)\Gamma(m_d)}\left(\frac{m_2}{m_d}\right)^{m_2}\left(\frac{P_d\omega_d\gamma_D}{P_R\Omega_2}\right)^{m_2-1}\left(\frac{P_d\omega_d}{P_R\Omega_2}\right)\left(1+\frac{m_2}{m_d}\frac{P_d\omega_d\gamma_D}{P_R\Omega_2}\right)^{-(m_2+m_d)} \\
&\quad \times 0.5\left(1-\sqrt{\gamma_D/\pi}\int_0^1 t^{-0.5}e^{-\gamma_D t}dt\right)d\gamma_D \\
&= \frac{1}{2}\int_0^\infty \frac{\Gamma(m_2+m_d)}{\Gamma(m_2)\Gamma(m_d)}\left(\frac{m_2}{m_d}\right)^{m_2}\left(\frac{P_d\omega_d\gamma_D}{P_R\Omega_2}\right)^{m_2-1}\left(\frac{P_d\omega_d}{P_R\Omega_2}\right)\left(1+\frac{m_2}{m_d}\frac{P_d\omega_d\gamma_D}{P_R\Omega_2}\right)^{-(m_2+m_d)}d\gamma_D \\
&\quad -\frac{1}{2}\int_0^\infty \frac{\Gamma(m_2+m_d)}{\Gamma(m_2)\Gamma(m_d)}\left(\frac{m_2}{m_d}\right)^{m_2}\left(\frac{P_d\omega_d\gamma_D}{P_R\Omega_2}\right)^{m_2-1} \\
&\quad \times\left(\frac{P_d\omega_d}{P_R\Omega_2}\right)\left(1+\frac{m_2}{m_d}\frac{P_d\omega_d\gamma_D}{P_R\Omega_2}\right)^{-(m_2+m_d)}\times\left(\sqrt{\gamma_D/\pi}\int_0^1 t^{-0.5}e^{-\gamma_D t}dt\right)d\gamma_D. \qquad (2.8)
\end{aligned}
$$

It is obvious to the reader that the integrand in the first term of (2.8) is a PDF of γ_D ($\gamma_D \geq 0$), and hence the first integration results in 0.5. Interchanging the order of integration in the second term and solving the integral (of γ_D) using [36, Eq. (3.383.5)] yields

$$
\begin{aligned}
\overline{P}_{e2} &= 0.5-\frac{\Gamma(m_2+m_d)\Gamma(m_2+0.5)}{2\Gamma(m_2)\Gamma(m_d)}\sqrt{\frac{1}{\frac{m_2}{m_d}\frac{P_d\omega_d}{P_R\Omega_2}\pi}} \\
&\quad \times\int_0^1 t^{-0.5}U\left(m_2+0.5;1.5-m_d;\frac{P_R\Omega_2 m_d t}{m_2 P_d\omega_d}\right)dt, \qquad (2.9)
\end{aligned}
$$

where $U\left(.;.;.\right)$ is the confluent hypergeometric function of the second kind [36, Eq. (9.211.4)]. This confluent hypergeometric function could be written in terms of the confluent hypergeometric function of the first kind as follows [133, Eq. (13.1.3)]

$$
U\left(a;b;c\right) = \frac{\pi\ \times {}_1F_1\left(a;b;c\right)}{\sin(\pi b)\Gamma(a-b+1)\Gamma(b)}-\frac{{}_1F_1\left(a-b+1;2-b;c\right)c^{1-b}\pi}{\sin(\pi b)\Gamma(a)\Gamma(2-b)}. \qquad (2.10)
$$

Therefore,

$$U\left(m_2+0.5;1.5-m_d;\frac{P_R\Omega_2 m_d t}{m_2 P_d\omega_d}\right)=\frac{\pi}{\sin(\pi 1.5-\pi m_d)\Gamma(m_2+m_d)\Gamma(1.5-m_d)} \times {}_1F_1\left(m_2+0.5;1.5-m_d;\frac{P_R\Omega_2 m_d t}{m_2 P_d\omega_d}\right) -\frac{\frac{P_R\Omega_2 m_d t}{m_2 P_d\omega_d}^{m_d-0.5}\pi}{\sin(\pi 1.5-\pi m_d)\Gamma(m_2+0.5)\Gamma(0.5+m_d)} \times {}_1F_1\left(m_2+m_d;0.5+m_d;\frac{P_R\Omega_2 m_d t}{m_2 P_d\omega_d}\right) \quad (2.11)$$

Substituting (2.11) into (2.9) results in

$$\begin{aligned}\overline{P}_{e2} &= 0.5-\frac{\Gamma(m_2+m_d)\Gamma(m_2+0.5)}{2\Gamma(m_2)\Gamma(m_d)}\sqrt{\frac{1}{\frac{m_2}{m_d}\frac{P_d\omega_d}{P_R\Omega_2}\pi}}\int_0^1 \frac{\pi t^{-0.5}}{\sin(\pi 1.5-m_d)\Gamma(m_2-m_d)\Gamma(1.5-m_d)} \\ &\times {}_1F_1\left(m_2+0.5;1.5-m_d;\frac{P_R\Omega_2 m_d t}{m_2 P_d\omega_d}\right)-\frac{\frac{P_R\Omega_2 m_d t}{m_2 P_d\omega_d}^{-0.5-m_d}\pi}{\sin(\pi 1.5-m_d)\Gamma(m_2+0.5)\Gamma(0.5-m_d)} \\ &{}_1F_1\left(m_2-m_d;0.5-m_d;\frac{P_R\Omega_2 m_d t}{m_2 P_d\omega_d}\right)dt. \end{aligned} \quad (2.12)$$

To evaluate the integral in (2.12) we use [36, Eq. (7.512.12)] to obtain

$$\begin{aligned}\overline{P}_{e2}=0.5&-\frac{\Gamma(m_2+m_d)\Gamma(m_2+0.5)\sqrt{\pi}}{\Gamma(m_2)\Gamma(m_d)\cos(\pi m_d)}\left(\frac{\left(\frac{P_R\Omega_2 m_d}{m_2 P_d\omega_d}\right)^{m_d}}{2m_d\Gamma(m_d+0.5)\Gamma(m_2+0.5)}\right) \\ &\times {}_2F_2\left(m_d,m_d+m_2;m_d+1,m_d+0.5;\frac{P_R\Omega_2 m_d}{m_2 P_d\omega_d}\right) \\ -\frac{\Gamma(m_2+m_d)\Gamma(m_2+0.5)\sqrt{\pi}}{\Gamma(m_2)\Gamma(m_d)\cos(\pi m_d)}&\left(\frac{{}_2F_2\left(0.5,m_2+0.5;1.5,1.5-m_d;\frac{P_R\Omega_2 m_d}{m_2 P_d\omega_d}\right)\sqrt{\frac{P_R\Omega_2 m_d}{m_2 P_d\omega_d}}}{\Gamma(m_2+m_d)\Gamma(1.5-m_d)}\right), \end{aligned} \quad (2.13)$$

where ${}_2F_2\left(a_1,a_2;b-1,b_2;x\right)$ is the generalized hypergeometric function [134, Eq. (1.1.5)]. In (2.13) $\Gamma(x)$ is the incomplete Gamma function which is given in [36, Eq. 8.310.1]. The BER expression in (2.13) represnts the end-to-end BER for case one, in which the relay node drops the errored data. Using the same steps that have been

used to derive (2.13), P_{e1} can be given as

$$\begin{aligned} P_{e1} &= \int_0^\infty P_e\left(\gamma_R\right) f_{\gamma_R}(\gamma_R) d\gamma_R \\ &= \int_0^\infty P_e\left(\gamma_R\right) \frac{\Gamma(m_1+m_r)}{\Gamma(m_1)\Gamma(m_r)} \left(\frac{m_1}{m_r}\right)^{m_1} \left(\frac{P_r\omega_r\gamma_R}{P_S\Omega_1}\right)^{m_1-1} \\ &\quad \times \left(\frac{P_d\omega_d}{P_R\Omega_2}\right) \left(1+\frac{m_1}{m_r}\frac{P_r\omega_r\gamma_R}{P_S\Omega_1}\right)^{-(m_1+m_r)} d\gamma_R. \end{aligned} \tag{2.14}$$

$$\begin{aligned} \overline{P}_{e1} = 0.5 - \frac{\Gamma(m_1+m_r)\Gamma(m_1+0.5)\sqrt{\pi}}{\Gamma(m_1)\Gamma(m_r)\cos(\pi m_r)} \left(\frac{\left(\frac{P_S\Omega_1 m_r}{m_1 P_r\omega_r}\right)^{m_r}}{2m_r\Gamma(m_r+0.5)\Gamma(m_1+0.5)}\right) \\ \times {}_2F_2\left(m_r, m_r+m_1; m_r+1, m_r+0.5; \frac{P_S\Omega_1 m_r}{m_1 P_r\omega_r}\right) \\ - \frac{\Gamma(m_1+m_r)\Gamma(m_1+0.5)\sqrt{\pi}}{\Gamma(m_1)\Gamma(m_r)\cos(\pi m_r)} \left(\frac{{}_2F_2\left(0.5, m_1+0.5; 1.5, 1.5-m_r; \frac{P_S\Omega_1 m_r}{m_1 P_r\omega_r}\right)\sqrt{\frac{P_S\Omega_1 m_r}{m_1 P_r\omega_r}}}{\Gamma(m_1+m_r)\Gamma(1.5-m_r)}\right), \end{aligned} \tag{2.15}$$

The end-to-end average BER (for case two, in which the relay node does not drop the errored data) of the DF dual-hop cooperative system can be obtained by substituting (2.13) and (2.14) into (2.4) to get the result as follows.

$$
\begin{aligned}
\overline{P}_e &= P_{e1} + P_{e2} - 2P_{e1}P_{e2} \\
&= 0.5 - \frac{\Gamma(m_2+m_d)\Gamma(m_2+0.5)\sqrt{\pi}}{\Gamma(m_2)\Gamma(m_d)\cos(\pi m_d)} \\
&\quad \times \left(\frac{{}_2F_2\left(m_d, m_d+m_2; m_d+1, m_d+0.5; \frac{P_R\Omega_2 m_d}{m_2 P_d \omega_d}\right)\left(\frac{P_R\Omega_2 m_d}{m_2 P_d \omega_d}\right)^{m_d}}{2m_d\Gamma(m_d+0.5)\Gamma(m_2+0.5)} \right) \\
&\quad - \frac{\Gamma(m_2+m_d)\Gamma(m_2+0.5)\sqrt{\pi}}{\Gamma(m_2)\Gamma(m_d)\cos(\pi m_d)} \\
&\quad \times \left(\frac{{}_2F_2\left(0.5, m_2+0.5; 1.5, 1.5-m_d; \frac{P_R\Omega_2 m_d}{m_2 P_d \omega_d}\right)\sqrt{\frac{P_R\Omega_2 m_d}{m_2 P_d \omega_d}}}{\Gamma(m_2+m_d)\Gamma(1.5-m_d)} \right) \\
&\quad + 0.5 - \frac{\Gamma(m_1+m_r)\Gamma(m_1+0.5)\sqrt{\pi}}{\Gamma(m_1)\Gamma(m_r)\cos(\pi m_r)} \\
&\quad \times \left(\frac{{}_2F_2\left(m_r, m_r+m_1; m_r+1, m_r+0.5; \frac{P_S\Omega_2 m_r}{m_1 P_S \omega_r}\right)\left(\frac{P_S\Omega_1 m_r}{m_1 P_r \omega_r}\right)^{m_r}}{2m_r\Gamma(m_r+0.5)\Gamma(m_1+0.5)} \right) \\
&\quad - \frac{\Gamma(m_1+m_r)\Gamma(m_1+0.5)\sqrt{\pi}}{\Gamma(m_1)\Gamma(m_r)\cos(\pi m_r)} \\
&\quad \times \left(\frac{{}_2F_2\left(0.5, m_1+0.5; 1.5, 1.5-m_r; \frac{P_S\Omega_1 m_r}{m_1 P_r \omega_r}\right)\sqrt{\frac{P_S\Omega_1 m_r}{m_1 P_r \omega_r}}}{\Gamma(m_1+m_r)\Gamma(1.5-m_r)} \right) \\
&\quad - 1 - \frac{2\Gamma(m_2+m_d)\Gamma(m_2+0.5)\sqrt{\pi}}{\Gamma(m_2)\Gamma(m_d)\cos(\pi m_d)} \\
&\quad \times \left(\frac{{}_2F_2\left(m_d, m_d+m_2; m_d+1, m_d+0.5; \frac{P_R\Omega_2 m_d}{m_2 P_d \omega_d}\right)\left(\frac{P_R\Omega_2 m_d}{m_2 P_d \omega_d}\right)^{m_d}}{2m_d\Gamma(m_d+0.5)\Gamma(m_2+0.5)} \right) \\
&\quad - \frac{\Gamma(m_2+m_d)\Gamma(m_2+0.5)\sqrt{\pi}}{\Gamma(m_2)\Gamma(m_d)\cos(\pi m_d)} \\
&\quad \times \left(\frac{{}_2F_2\left(0.5, m_2+0.5; 1.5, 1.5-m_d; \frac{P_R\Omega_2 m_d}{m_2 P_d \omega_d}\right)\sqrt{\frac{P_R\Omega_2 m_d}{m_2 P_d \omega_d}}}{\Gamma(m_2+m_d)\Gamma(1.5-m_d)} \right) \\
&\quad \times 0.5 - \frac{\Gamma(m_1+m_r)\Gamma(m_1+0.5)\sqrt{\pi}}{\Gamma(m_1)\Gamma(m_r)\cos(\pi m_r)} \\
&\quad \times \left(\frac{{}_2F_2\left(m_r, m_r+m_1; m_r+1, m_r+0.5; \frac{P_S\Omega_2 m_r}{m_1 P_S \omega_r}\right)\left(\frac{P_S\Omega_1 m_r}{m_1 P_r \omega_r}\right)^{m_r}}{2m_r\Gamma(m_r+0.5)\Gamma(m_1+0.5)} \right) \\
&\quad - \frac{\Gamma(m_1+m_r)\Gamma(m_1+0.5)\sqrt{\pi}}{\Gamma(m_1)\Gamma(m_r)\cos(\pi m_r)} \\
&\quad \times \left(\frac{{}_2F_2\left(0.5, m_1+0.5; 1.5, 1.5-m_r; \frac{P_S\Omega_1 m_r}{m_1 P_r \omega_r}\right)\sqrt{\frac{P_S\Omega_1 m_r}{m_1 P_r \omega_r}}}{\Gamma(m_1+m_r)\Gamma(1.5-m_r)} \right).
\end{aligned} \tag{2.16}
$$

For simplicity, we can rewrite (2.13) and (2.14) as follows

$$
\overline{P}_e = 0.5 - G\left(m_i, m_x, \omega_i, \Omega_x, P_i, P_y\right), \tag{2.17}
$$

where $G\left(m_i, m_x, \omega_i, \Omega_x, P_i, P_y\right)$ represent the second and third terms in (2.13) (or 2.14), and $i = d(or \quad r), x = 2(or \quad 1)$ and $y = R(or \quad D)$. Later, in the numerical results section we will explore some insights of the result in (2.16).

2.4.2 Non-Coherent Binary Frequency Shift Keying (NCBFSK) Modulation Scheme

For a non-coherent binary frequency shift keying (NCBFSK) modulation scheme, the conditional BER for a given SIR γ_e is given as

$$P_e^{NCBFSK} = 0.5\exp(-\frac{\gamma_e}{2}) \tag{2.18}$$

by substituting (2.18) and (1.17) into (2.1) yields

$$\begin{aligned}\overline{P}_{e1}^{NCBFSK} &= 0.5\int_0^{\infty}\frac{\Gamma(m_1+m_r)}{\Gamma(m_1)\Gamma(m_r)}\left(\frac{m_1}{m_r}\right)^{m_1}\left(\frac{P_r\omega_r\gamma_R}{P_S\Omega}\right)^{m_1-1} \\ &\quad\times\left(1+\frac{m_1}{m_r}\frac{P_r\omega_r\gamma_R}{P_D\Omega}\right)^{-(m_1+m_r)}\exp(-\frac{\gamma_R}{2})d\gamma_R,\end{aligned} \tag{2.19}$$

and by substituting (2.18) and (1.18) into (2.1) yields

$$\begin{aligned}\overline{P}_{e2}^{NCBFSK} &= 0.5\int_0^{\infty}\frac{\Gamma(m_2+m_d)}{\Gamma(m_2)\Gamma(m_d)}\left(\frac{m_2}{m_d}\right)^{m_2}\left(1+\frac{m_2}{m_d}\frac{P_d\omega_d\gamma_D}{P_R\Omega}\right)^{-(m_2+m_d)} \\ &\quad\times\left(\frac{P_d\omega_d\gamma_D}{P_R\Omega}\right)^{m_2-1}\exp(-\frac{\gamma_D}{2})d\gamma_D,\end{aligned} \tag{2.20}$$

the average BER of the system under study and subject to the NCBFSK modulation scheme can be obtained by solving the integrals in (2.19) and (2.20) using [36] to get the result as follows

$$\overline{P}_{e1}^{NCBFSK} = \frac{\Gamma(m_1+m_r)}{2\Gamma(m_r)}U\left(m_1; 1-m_r; \frac{P_S\Omega m_r}{2m_1P_r\omega_r}\right). \tag{2.21}$$

and

$$\overline{P}_{e2}^{NCBFSK} = \frac{\Gamma(m_2+m_d)}{2\Gamma(m_d)}U\left(m_2; 1-m_d; \frac{P_R\Omega m_d}{2m_2P_d\omega_d}\right). \tag{2.22}$$

The end-to-end average BER of the NCBFSK DF dual hop system can be obtained by substituting (2.21) and (2.22) into (2.4).

2.4.3 Differential Binary Phase Shift Keying (DBPSK) Modulation Scheme

For a differential binary phase shift keying (DBPSK) modulation scheme, the conditional BER for a given SIR γ_e is given as

$$P_e^{DBPSK} = 0.5\exp(-\gamma_e), \tag{2.23}$$

by substituting (2.23) and (1.17) into (2.1) yields

$$\begin{aligned}\overline{P}_{e1}^{DBPSK} = \quad & 0.5\int_0^{\infty}\frac{\Gamma(m_1+m_r)}{\Gamma(m_1)\Gamma(m_r)}\left(\frac{m_1}{m_r}\right)^{m_1}\left(\frac{P_r\omega_r\gamma_R}{P_S\Omega}\right)^{m_1-1} \\ & \times\left(1+\frac{m_1}{m_r}\frac{P_r\omega_r\gamma_R}{P_D\Omega}\right)^{-(m_1+m_r)}\exp(-\gamma_R)d\gamma_R,\end{aligned} \tag{2.24}$$

and by substituting (2.23) and (1.18) into (2.1) yields

$$\begin{aligned}\overline{P}_{e2}^{DBPSK} = \quad & 0.5\int_0^{\infty}\frac{\Gamma(m_2+m_d)}{\Gamma(m_2)\Gamma(m_d)}\left(\frac{m_2}{m_d}\right)^{m_2}\left(\frac{P_d\omega_d\gamma_D}{P_R\Omega}\right)^{m_2-1} \\ & \times\left(1+\frac{m_2}{m_d}\frac{P_d\omega_d\gamma_D}{P_R\Omega}\right)^{-(m_2+m_d)}\exp(-\gamma_D)d\gamma_D,\end{aligned} \tag{2.25}$$

the average BER of the system under study and subject to the DBPSK modulation scheme can be obtained by solving the integrals in (2.24) and (2.25) using [36] to get the result as follows

$$\overline{P}_{e1}^{DBPSK} = \frac{\Gamma(m_1+m_r)}{2\Gamma(m_r)}U\left(m_1;1-m_r;\frac{P_S\Omega m_r}{m_1P_r\omega_r}\right), \tag{2.26}$$

and

$$\overline{P}_{e2}^{DBPSK} = \frac{\Gamma(m_2+m_d)}{2\Gamma(m_d)}U\left(m_2;1-m_d;\frac{P_R\Omega m_d}{m_2P_d\omega_d}\right), \tag{2.27}$$

where $U(.;.;.)$ is the confluent hypergeometric function of the second kind [134]. The end-to-end average BER of the DPSK DF dual hop system can be obtained fby substituting (2.26) and (2.27) into (2.4).

2.5 M-ary Modulation Schemes

For M-ary coherent modulation schemes, like quadrature phase shift keying (QPSK), four quadrature amplitude modulation (4QAM), M-ary-pulse amplitude modulation (MPAM), M-ary phase shift keying (MPSK), rectangular M-ary quadrature amplitude modulation (MQAM), and non rectangular MQAM the conditional bit error probabilities Gaussian channel are approximated as in [135, Table 6.1] in the following general form,

$$P_e(\gamma) \approx AQ(\sqrt{B\gamma}). \tag{2.28}$$

For a specific coherent M-ary modulation scheme, A and B are constants with a proper value as in [135, Table 6.1]. For examples, $A = \frac{2}{\log_2 M}$ and $B = 2\log_2 M \sin(\frac{\pi}{M})$ for MPSK modulation scheme, and $A = 1$ and $B = 2$ for quadrature phase shift keying (QPSK) or four quadrature amplitude modulation schemes (4QAM). Using the same steps that have been used to derive (2.13) the general form of the BER of the first hop in DF dual hop system P_{e1}^{M-ary} can be given as

$$\begin{aligned} P_{e1}^{M-ary} &= \int_0^\infty P_e\left(\gamma_R\right) f_{\gamma_R}(\gamma_R) d\gamma_R \\ &= \int_0^\infty AQ(\sqrt{B\gamma_R}) \frac{\Gamma(m_1+m_r)}{\Gamma(m_1)\Gamma(m_r)} \left(\frac{m_1}{m_r}\right)^{m_1} \left(\frac{P_r\omega_r\gamma_R}{P_S\Omega_1}\right)^{m_1-1} \\ &\quad \times \left(\frac{P_r\omega_r}{P_S\Omega_1}\right) \left(1+\frac{m_1}{m_r}\frac{P_r\omega_r\gamma_R}{P_S\Omega_1}\right)^{-(m_1+m_r)} d\gamma_R. \end{aligned} \tag{2.29}$$

$$P_{e1}^{M-ary} = 0.5A - \frac{A\Gamma(m_1+m_r)\Gamma(m_1+0.5)\sqrt{\pi}}{\Gamma(m_1)\Gamma(m_r)\cos(\pi m_r)} \left(\frac{\left(\frac{BP_S\Omega_1 m_r}{2m_1 P_r \omega_r}\right)^{m_r}}{2m_r\Gamma(m_r+0.5)\Gamma(m_1+0.5)} \right) \times {}_2F_2\left(m_r, m_r+m_1; m_r+1, m_r+0.5; \frac{BP_S\Omega_1 m_r}{2m_1 P_r\omega_r}\right) - \frac{\Gamma(m_1+m_r)\Gamma(m_1+0.5)\sqrt{\pi}}{\Gamma(m_1)\Gamma(m_r)\cos(\pi m_r)} \left(\frac{{}_2F_2\left(0.5, m_1+0.5; 1.5, 1.5-m_r; \frac{BP_S\Omega_1 m_r}{2m_1 P_r\omega_r}\right)\sqrt{\frac{BP_S\Omega_1 m_r}{2m_1 P_r\omega_r}}}{\Gamma(m_1+m_r)\Gamma(1.5-m_r)} \right) \quad (2.30)$$

and the general form of the BER of the second hop in DF dual hop system P_{e2}^{M-ary} can be given as

$$\begin{aligned} P_{e2}^{M-ary} &= \int_0^\infty P_e(\gamma_D) f_{\gamma_D}(\gamma_D) d\gamma_D \\ &= \int_0^\infty AQ(\sqrt{B\gamma_D}) \frac{\Gamma(m_2+m_d)}{\Gamma(m_2)\Gamma(m_d)} \left(\frac{m_2}{m_d}\right)^{m_2} \left(\frac{P_d\omega_d\gamma_D}{P_R\Omega_2}\right)^{m_2-1} \\ &\quad \times \left(\frac{P_r\omega_d}{P_S\Omega_2}\right) \left(1 + \frac{m_2}{m_d}\frac{P_r\omega_r\gamma_R}{P_S\Omega_1}\right)^{-(m_1+m_r)} d\gamma_R. \end{aligned} \quad (2.31)$$

$$P_{e2}^{M-ary} = 0.5A - \frac{A\Gamma(m_2+m_d)\Gamma(m_2+0.5)\sqrt{\pi}}{\Gamma(m_2)\Gamma(m_d)\cos(\pi m_d)} \left(\frac{\left(\frac{BP_R\Omega_2 m_d}{2m_2 P_d \omega_d}\right)^{m_d}}{2m_d\Gamma(m_d+0.5)\Gamma(m_2+0.5)} \right) \times {}_2F_2\left(m_d, m_d+m_2; m_d+1, m_d+0.5; \frac{BP_R\Omega_2 m_d}{2m_2 P_d\omega_d}\right) - \frac{\Gamma(m_2+m_d)\Gamma(m_2+0.5)\sqrt{\pi}}{\Gamma(m_2)\Gamma(m_d)\cos(\pi m_d)} \left(\frac{{}_2F_2\left(0.5, m_2+0.5; 1.5, 1.5-m_d; \frac{BP_R\Omega_2 m_d}{2m_2 P_d\omega_d}\right)\sqrt{\frac{BP_R\Omega_2 m_d}{2m_2 P_d\omega_d}}}{\Gamma(m_2+m_d)\Gamma(1.5-m_d)} \right) \quad (2.32)$$

The end-to-end average BER of M-ary coherent modulation DF dual hop system can be obtained by substituting (2.30) and (2.32) into (2.4).

As example, the average BER of QPSK (also known as 4QAM) modulation scheme is given by substituting the proper value of A and B (as in [135, Table 6.1]) in (2.31) and (2.32) to yield

$$P_{e1}^{QPSK} = 1 - \frac{2\Gamma(m_1+m_r)\Gamma(m_1+0.5)\sqrt{\pi}}{\Gamma(m_1)\Gamma(m_r)\cos(\pi m_r)} \left(\frac{\left(\frac{2P_S\Omega_1 m_r}{2m_1 P_r \omega_r}\right)^{m_r}}{2m_r\Gamma(m_r+0.5)\Gamma(m_1+0.5)} \right)$$
$$\times {}_2F_2\left(m_r, m_r+m_1; m_r+1, m_r+0.5; \frac{2P_S\Omega_1 m_r}{2m_1 P_r\omega_r}\right)$$
$$-\frac{2\Gamma(m_1+m_r)\Gamma(m_1+0.5)\sqrt{\pi}}{\Gamma(m_1)\Gamma(m_r)\cos(\pi m_r)} \left(\frac{{}_2F_2\left(0.5, m_1+0.5; 1.5, 1.5-m_r; \frac{2P_S\Omega_1 m_r}{2m_1 P_r\omega_r}\right)\sqrt{\frac{2P_S\Omega_1 m_r}{2m_1 P_r\omega_r}}}{\Gamma(m_1+m_r)\Gamma(1.5-m_r)} \right), \quad (2.33)$$

and

$$P_{e2}^{QPSK} = 1 - \frac{2\Gamma(m_2+m_d)\Gamma(m_2+0.5)\sqrt{\pi}}{\Gamma(m_2)\Gamma(m_d)\cos(\pi m_d)} \left(\frac{\left(\frac{2P_R\Omega_2 m_d}{2m_2 P_d \omega_d}\right)^{m_d}}{2m_d\Gamma(m_d+0.5)\Gamma(m_2+0.5)} \right)$$
$$\times {}_2F_2\left(m_d, m_d+m_2; m_d+1, m_d+0.5; \frac{2P_R\Omega_2 m_d}{2m_2 P_d\omega_d}\right)$$
$$-\frac{2\Gamma(m_2+m_d)\Gamma(m_2+0.5)\sqrt{\pi}}{\Gamma(m_2)\Gamma(m_d)\cos(\pi m_d)} \left(\frac{{}_2F_2\left(0.5, m_2+0.5; 1.5, 1.5-m_d; \frac{2P_R\Omega_2 m_d}{2m_2 P_d\omega_d}\right)\sqrt{\frac{2P_R\Omega_2 m_d}{2m_2 P_d\omega_d}}}{\Gamma(m_2+m_d)\Gamma(1.5-m_d)} \right). \quad (2.34)$$

The end-to-end average BER of QPSK DF dual hop system can be obtained by substituting (2.33) and (2.33) into (2.4).

2.6 BER of M-ary Modulation Using Characteristic Function (CF) Approach

Different approaches can be used to evaluate the system performance, such as the PDF approach, the CF approach, or the MGF approach. However, evaluation of the BER performance of the system under study can only be obtained using the PDF approach or the CF approach since the MGF of the F-distribution is not exist. In this section we extend our study to include the CF approach. The CF of the

F-distribution is given as [32]

$$\begin{aligned} C_F(\omega) &= \int_0^{\infty} f_\gamma(\gamma) e^{-j\omega\gamma} d\gamma \\ &= \frac{\Gamma(m_2+m_d)}{\Gamma(m_d)} U\left(m_2; 1-m_d; -j\frac{m_d}{m_2}\omega\right), \end{aligned} \tag{2.35}$$

where $U(.;.;.)$ is the confluent hypergeometric function of the second kind [36, Eq. (9.211.4)].

In [33], the author derived an exact average probability of error for arbitrary M-ary signal constellations in AWGN using geometric relations. The conditional error probability (CEP) is expressed in finite integral form as

$$P_{eM} = \frac{1}{\pi}\int_0^{\pi-\psi} e^{\frac{-\gamma sin^2(\psi)}{sin^2(\phi)}} d\phi, \tag{2.36}$$

where $\psi = \pi/M$ radian. Substituting (2.36) in the general expression of the average bit error rate and after simple manipulation results in

$$\begin{aligned} \overline{P}_e &= \int_0^{\infty} P_{eM} f_\gamma(\gamma) d\gamma \\ &= \int_0^{\infty} \frac{1}{\pi}\int_0^{\pi-\frac{\pi(M-1)}{M}} e^{\frac{-\gamma sin^2(\frac{\pi(M-1)}{M})}{sin^2(\phi)}} d\phi f_\gamma(\gamma) d\gamma \\ &= \frac{1}{\pi}\int_0^{\pi-\frac{\pi(M-1)}{M}} \int_0^{\infty} e^{\frac{-j(-j\gamma sin^2(\frac{\pi(M-1)}{M}))}{sin^2(\phi)}} f_\gamma(\gamma) d\gamma d\phi, \end{aligned} \tag{2.37}$$

in (2.37), the inner integral is equivalent to the definition of the characteristic function $C_F(\omega)$, with $\omega = \frac{(-jsin^2(\frac{\pi(M-1)}{M}))}{sin^2(\phi)}$. So, (2.37) can be rewritten as

$$\overline{P}_e = \frac{1}{\pi}\int_0^{\pi-\frac{\pi(M-1)}{M}} C_F\left(\frac{-jsin^2(\frac{\pi(M-1)}{M})}{sin^2(\phi)}\gamma\right) d\phi, \tag{2.38}$$

substituting (2.35) into (2.38) results in

$$\begin{aligned}\overline{P}_e &= \frac{1}{\pi}\int_0^{\pi-\frac{\pi(M-1)}{M}} C_F\left(\frac{-jsin^2(\frac{\pi(M-1)}{M})}{sin^2(\phi)}\gamma\right)d\phi \\ &= \frac{\Gamma(m_2+m_d)}{\pi\Gamma(m_d)}\int_0^{\pi-\frac{\pi(M-1)}{M}} U\left(m_2;1-m_d;-j\frac{m_d}{m_2}\frac{(-jsin^2(\frac{\pi(M-1)}{M}))}{sin^2(\phi)}\right)d\phi \quad (2.39)\end{aligned}$$

It is noteworthy that the result in (2.39) is new and has not been reported in the literature before. By the way, even though the exact form of average probability of error for arbitrary M-ary signal constellations in AWGN is used but the result in (2.39) is still an approximate result since $f_\gamma(\gamma)$ is approximated as F-distribution. The numerical and the simulation results show that the expression in (2.39) is accurate and the obtained curves are useful in the engineering design process.

2.7 Numerical and Simulation Results

In this section, we provide numerical and simulation results for the expressions that have been derived in this chapter for arbitrary values of the Nakagami-m fading parameters. Without loss of generality we assume that $P_S = P_R = P_{ri} = P_{di} = 1$. The simulation results are obtained using MonteCarlo simulation method, with number of runs equal to $1,000,000$ times. Fig. 2.2 shows the BER versus SIR for BPSK modulation scheme of a dual-hop DF relaying communication over Nakagami-m fading channels with arbitrary fading parameters values. (i.e., $N_R = 3$; $N_D = 3$ with $m_1 = 1.5, 2, 3$, and 4, $\Omega_1 = 3.5$, $m_{r1} = 1$, $m_{r2} = 1$, $m_{r3} = 1$, m_2 =1.5, 2, 3 and 4, $m_{d1} = 1$, $m_{d2} = 1$, $m_{d3} = 1$, $\Omega_{r1} = 1.8$, $\Omega_{r2} = 1.8$, $\Omega_{r3} = 2$, $\Omega_{d1} = 1.1$, $\Omega_{d2} = 1.8$, $\Omega_{d3} = 1.2$). The figure shows that the derived approximated closed-form expression is highly close to the exact one obtained using MonteCarlo simulation, and confirms

the accuracy. Also, the BER increases as the value of m_1 and m_2 decreases and decreases as the value of m_1 and m_2 increases. In other words, the BER improved by the improvement of the channel conditions of the first and the second hop.

Fig. 2.3 shows the BER versus SIR for BFSK and DPSK in interference-limited DF dual hop wireless communication system with three interferers at both relay and destination nodes over Nakagami-m fading channels, with arbitrary fading parameters values. (i.e., $N_R = 3$; $N_D = 3$ with $m_1 = 1, 1.5, 2.5$, and 3.1, $\Omega_1 = 3.5$, $m_{r1} = 1$, $m_{r2} = 1$, $m_{r3} = 1.1$, $m_2 = 1, 1.5, 2.5$, and 3.1, $m_{d1} = 1$, $m_{d2} = 1.1$, $m_{d3} = 1$, $\Omega_{r1} = 1.8$, $\Omega_{r2} = 1.8$, $\Omega_{r3} = 2$, $\Omega_{d1} = 1.1$, $\Omega_{d2} = 1.8$, $\Omega_{d3} = 1.4$). The figure shows that the BER increases as the value of m_1 and m_2 decreases and decreases as the value of m_1 and m_2 increases. In other words, the BER improved by the channel conditions of the first and the second hop improvement. Alos, the figure shows that the DBPSK modulation scheme outperforms the BFSK modulation schemes.

Fig. 2.4 shows the BER versus SIR for BPSK and DPSK in interference-limited DF dual hop wireless communication system with three interferers at both relay and destination nodes over Nakagami-m fading channels, with arbitrary fading parameters values. (i.e., $N_R = 3$; $N_D = 3$ with $m_1 = 1, 1.5, 2.5$, and 3.1, $\Omega_1 = 3.5$, $m_{r1} = 1$, $m_{r2} = 1$, $m_{r3} = 1.1$, $m_2 = 1, 1.5, 2.5$, and 3.1, $m_{d1} = 1$, $m_{d2} = 1.1$, $m_{d3} = 1$, $\Omega_{r1} = 1.8$, $\Omega_{r2} = 1.8$, $\Omega_{r3} = 2$, $\Omega_{d1} = 1.1$, $\Omega_{d2} = 1.8$, $\Omega_{d3} = 1.4$). The figure shows that the BER increases as the value of m_1 and m_2 decreases and decreases as the value of m_1 and m_2 increases. In other words, the BER improved by the improvement of the channel conditions of the first and the second hop. Alos, the figure shows that the BPSK modulation scheme outperforms the DPSK modulation scheme.

Fig. 2.5 shows the BER versus SIR for BPSK and BFSK in interference-limited DF dual hop wireless communication system with three interferers at both relay and destination nodes over Nakagami-m fading channels, with arbitrary fading parameters values. (i.e., $N_R = 3$; $N_D = 3$ with $m_1 = 0.5, 1, 1.2, 1.5, 2$, and 3.1, $\Omega_1 = 3.5$, $m_{r1} = 1$, $m_{r2} = 1$, $m_{r3} = 1.1$, $m_2 = 1, 1.5, 2.5$, and 3.1, $m_{d1} = 1$, $m_{d2} = 1.1$, $m_{d3} = 1$, $\Omega_{r1} = 1.8$, $\Omega_{r2} = 1.8$, $\Omega_{r3} = 2$, $\Omega_{d1} = 1.1$, $\Omega_{d2} = 1.8$, $\Omega_{d3} = 1.4$). The figure shows that the BER increases as the value of m_1 and m_2 decreases and decreases as the value of m_1 and m_2 increases. In other words, the BER improved by the improvement of the channel conditions of the first and the second hop. Alos, the figure shows that the BPSK modulation scheme outperforms the BFSK modulation scheme.

Fig. 2.6 shows the BER versus SIR for QPSK interference-limited DF dual hop wireless communication system with three interferers at both relay and destination nodes over Nakagami-m fading channels, with arbitrary fading parameters values. (i.e., $N_R = 3$; $N_D = 3$ with $m_1 = 1, 1.5, 2.5$, and 3.1, $\Omega_1 = 3.5$, $m_{r1} = 1$, $m_{r2} = 1$, $m_{r3} = 1.1$, $m_2 = 1, 1.5, 2.5$, and 3.1, $m_{d1} = 1$, $m_{d2} = 1.1$, $m_{d3} = 1$, $\Omega_{r1} = 1.8$, $\Omega_{r2} = 1.8$, $\Omega_{r3} = 2$, $\Omega_{d1} = 1.1$, $\Omega_{d2} = 1.8$, $\Omega_{d3} = 1.4$). The figure shows that the BER increases as the value of m_1 and m_2 decreases and decreases as the value of m_1 and m_2 increases. In other words, the BER improved by the improvement of the channel conditions of the first and the second hop improvement. Alos, the figure shows the accuracy of the derived expressions.

Fig. 2.7 shows the derived BER using CF method versus SIR for QPSK DF dual hop in interference-limited wireless communication system with two interferers at both relay and destination nodes over Nakagami-m fading channels, with arbitrary

fading parameters values. (i.e., $N_R = 2$; $N_D = 2$ with $m_1 = 0.5, 1$,and 2, $\Omega_1 = 3.5$, $m_{r1} = 0.5$, $m_{r2} = 0.5$, , $m_2 = 0.5, 1$,and 2, $m_{d1} = 0.5$, $m_{d2} = 0.55$, $\Omega_{r1} = 1.8$, $\Omega_{r2} = 1.8$, $\Omega_{r3} = 2$, $\Omega_{d1} = 1.1$, $\Omega_{d2} = 1.8$, $\Omega_{d3} = 1.4$). The figure shows that the BER increases as the value of m_1 and m_2 decreases and decreases as the value of m_1 and m_2 increases. In other words, the BER improved by the channel conditions of the first and the second hop improvement. Also, the figure shows that the accuracy of derived expressions using both the CF and the PDF methods.

These results are very useful to evaluate the error performance analysis of the system under study. Moreover, these results are very useful to evaluate the error performance analysis. Such analysis is very important for wireless communication systems engineering design process.

2.8 Conclusions

In this chapter, we considered an interference-limited DF relaying cooperative system with multiple CCI at both relay and destination nodes. Assuming that the system operates in presence of (i.n.i.d.) Nakagami-m fading channels with arbitrary (integer and non-integer) values of fading parameter m, highly accurate approximate closed-form expressions for the BER of different modulation schemes are derived. The proposed analysis is accompanied by numerical and simulation results to show the accuracy of the derived expressions. The proposed approximate expressions of the BER are indeed simple and highly accurate regardless the number of interfering signals. Beside that, allow for arbitrary integer and non-integer values of the

Nakagami-m fading parameters and unequal fading powers between the first and the second hop.

For comprehensive study, we extend the performance derivations to include different coherent and non-coherent modulation schemes such as, Coherent BPSK, non-coherent BFSK and DPSK, and M-ary coherent modulation schemes. Using the BER general form of coherent M-ary modulation schemes in Gaussian channels, the analysis extended to derive ABER general form for wide range of coherent M-ary modulation schemes. The numerical results show that the DPSK modulation scheme outperforms the BFSK modulation scheme, where as the BPSK modulation scheme outperforms both of them. Also, we extend our study to include the CF approach to derive a finite integral form for the BER of the M-ary modulation schemes, and we provide the simulation results to show the accuracy of this expression.

Having such a study enables system engineers and designers to optimize their designs before actual deployment in real situations and save time and cost that may occur according to mistakes in system hardware implementation.

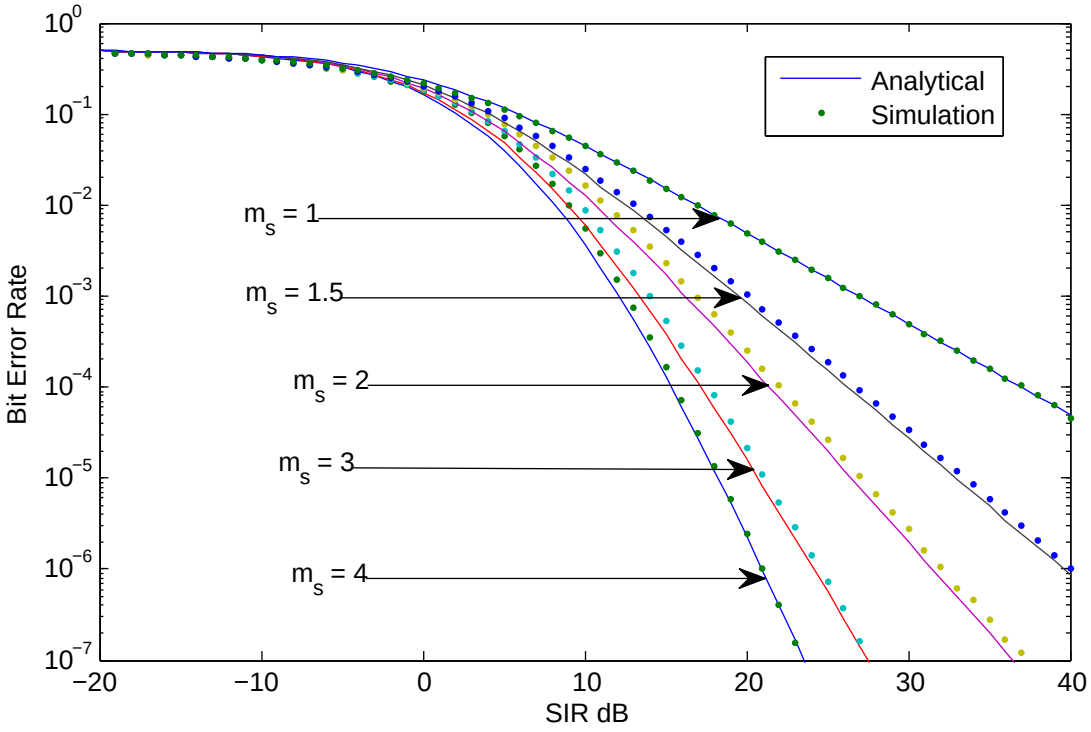

Figure 2.2. The average BER versus SIR for interference-limited BPSK DF dual-hop communication system with three interferers at both the relay and the destination nodes over Nakagami-m fading channels with arbitrary fading parameters values.

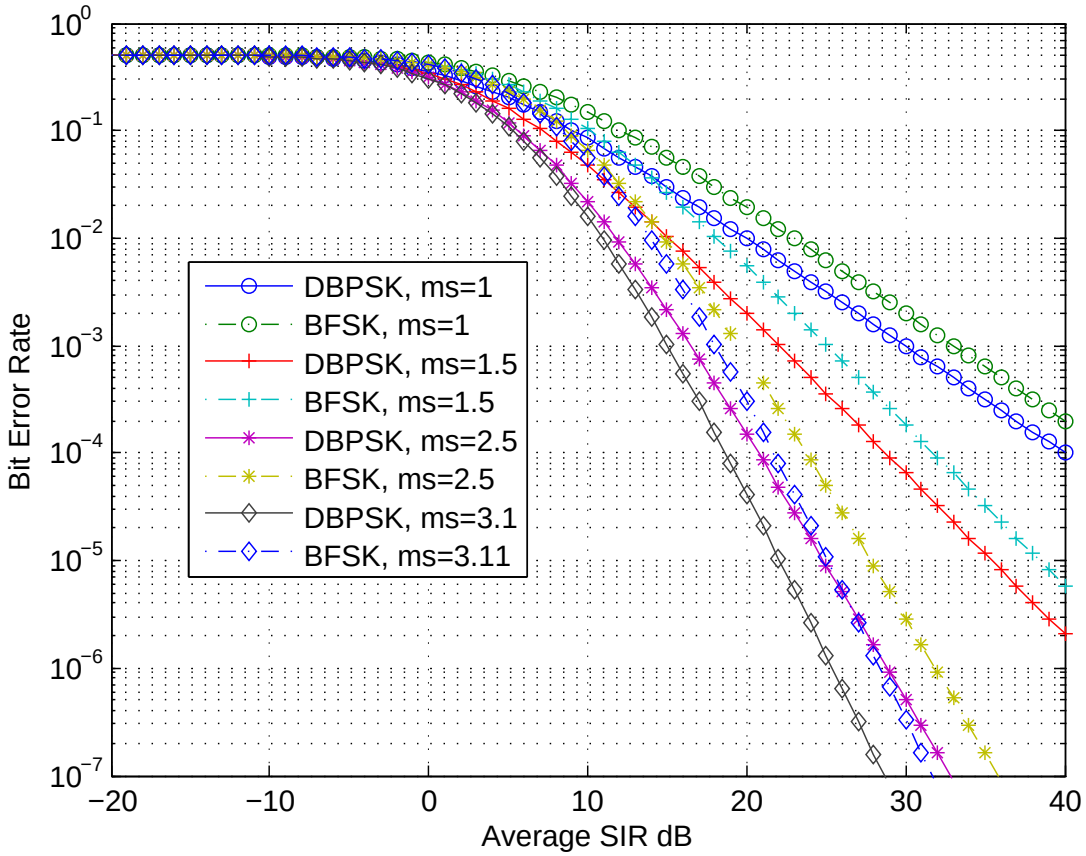

Figure 2.3. BER versus SIR for BFSK and DPSK in interference-limited DF dual hop wireless communication system with three interferers at both relay and destination nodes over Nakagami-m fading channels.

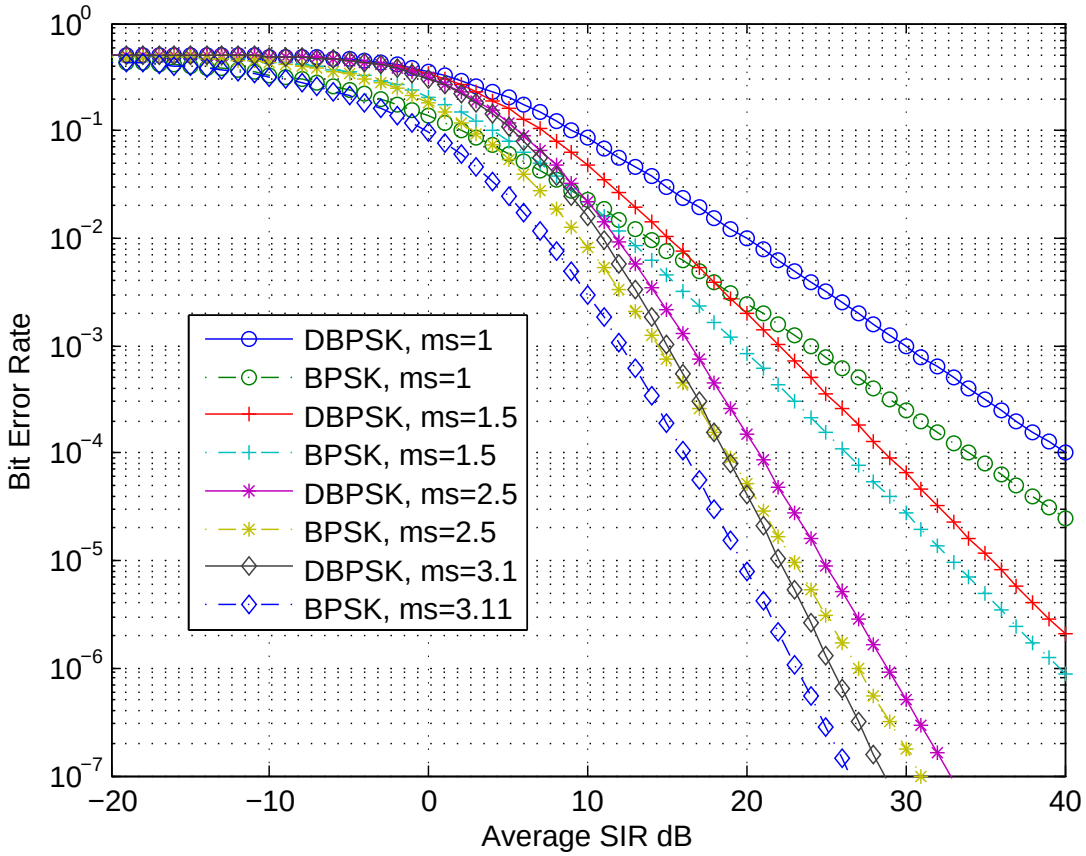

Figure 2.4. BER versus SIR for BPSK and DPSK in interference-limited DF dual hop wireless communication system for three interferers at both relay and destination nodes over Nakagami-m fading channels.

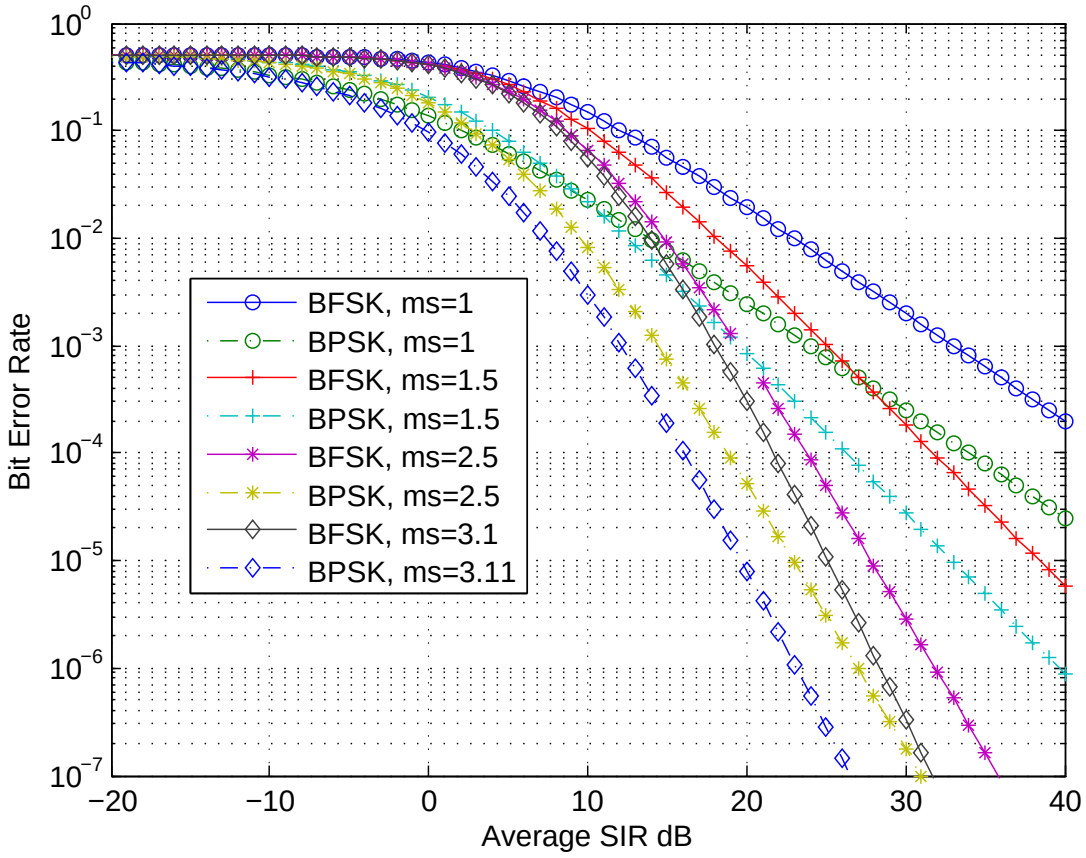

Figure 2.5. BER versus SIR for BFSK and BPSK in interference-limited DF dual hop wireless communication system for three interferers at both relay and destination nodes over Nakagami-m fading channels.

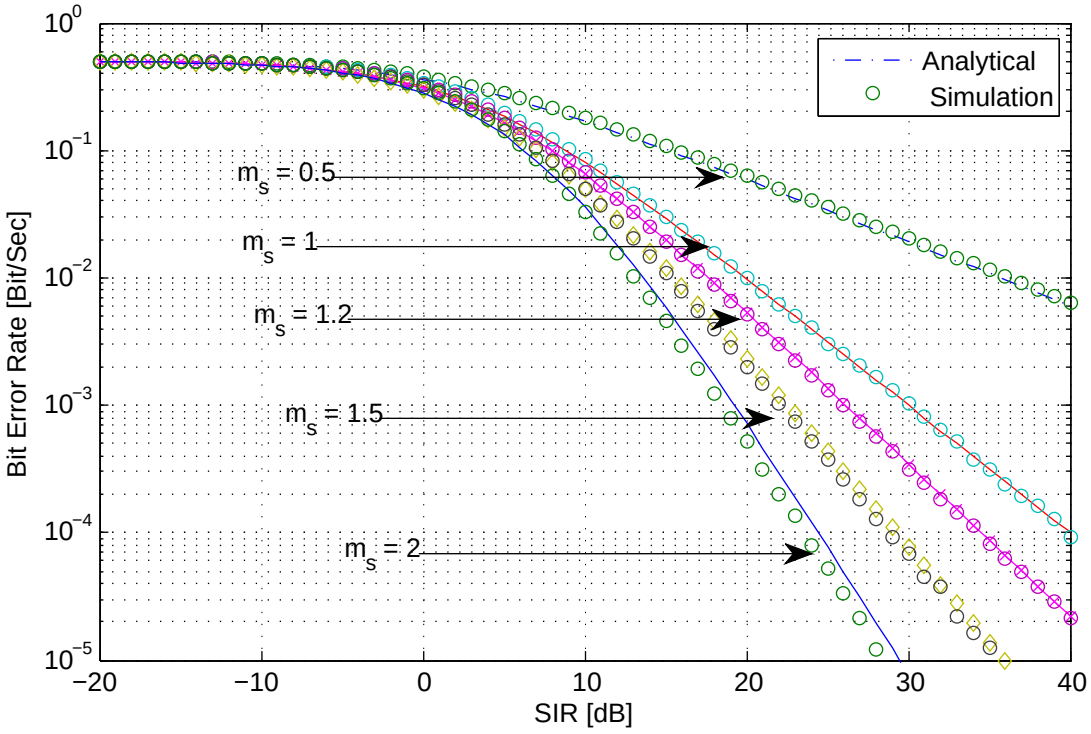

Figure 2.6. The average BER versus SIR for interference-limited QPSK DF dual-hop communication system with three interferers at both the relay and the destination nodes over Nakagami-m fading channels with arbitrary fading parameters values.

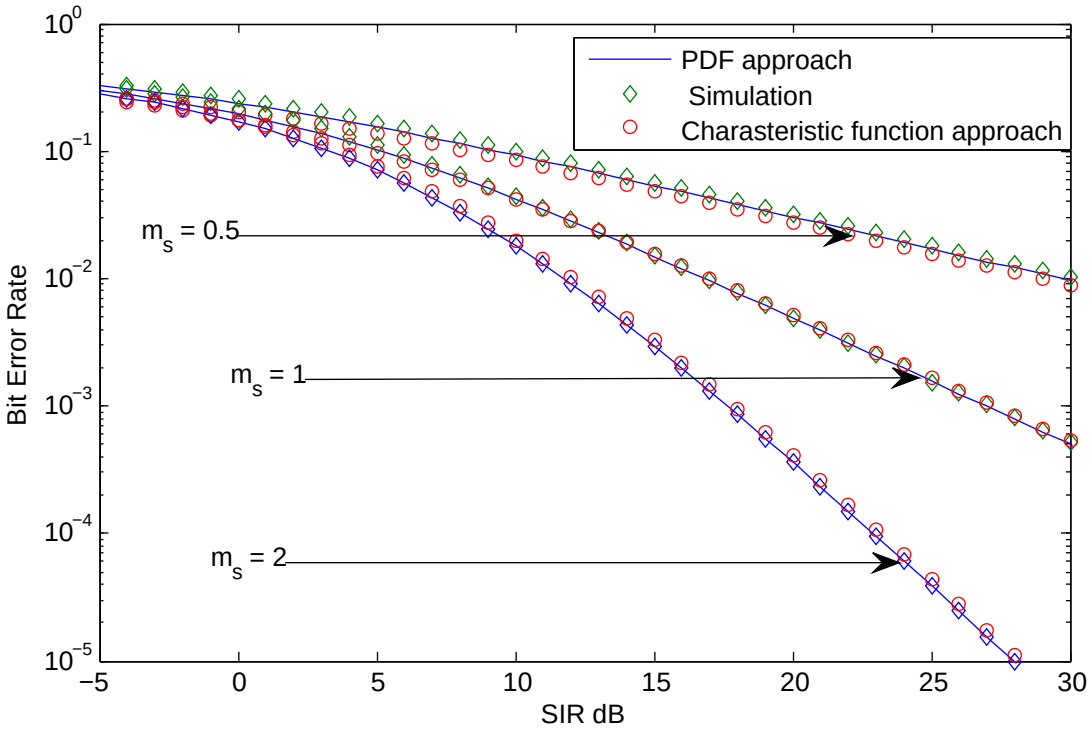

Figure 2.7. The derived BER using CF method versus SIR for QPSK DF dual hop in interference-limited wireless communication system with two interferers at both relay and destination nodes over Nakagami-m fading channels, with arbitrary fading parameters values.

Chapter 3

DUAL-HOP DF COOPERATIVE SYSTEMS: CAPACITY PERFORMANCE ANALYSIS

3.1 Chapter Overview

The channel capacity, which can be defined as the upper bound on the amount of information that can be reliably transmitted over a noisy wireless channel with a certain probability of error [54], is an important performance metric for any wireless communication system. This channel capacity is always bounded by an upper limit defined by Shannon theorem (sometimes called the Shannon-Hartley theorem) [55]-[58]. Shannon theorem states that for an additive white Gaussian noise (AWGN) channel, there exist coding schemes such that it is possible to communicate error free data over the channel provided that the data rate $\mathcal{R}_b$ [bits/sec] is less than or equal to the channel capacity $\mathcal{C}$ [bits/sec] [56] and [57], where $\mathcal{C}$ is defined as:

$$\mathcal{C} = W \log_2 \left(1 + \frac{P}{N_o W}\right), \tag{3.1}$$

where W is the transmission bandwidth, P is the signal power, and N_o is the one-sided power spectral density level of the additive noise. It is noteworthy that if

$\mathcal{R}_b > \mathcal{C}$, then it is impossible to achieve an error free transmission no matter what the coding scheme is. Therefore, Shannon capacity is considered as the optimistic theoretical bound against which to compare all practical transmission systems. In this chapter we study the normalized Shannon capacity, C, measured in [bits/sec/Hz], under different adaptive transmission protocols assuming a small-scale fading channel following the Nakagami-m distribution with cochannel interference (CCI).

In Section 3.2, the related work is summarized. The chapter contributions are provided in Section 3.3. The capacity analysis is presented in section 3.5, which mainly derives optimal expressions for the channel capacity under different adaptive transmission protocols, namely, the simultaneous optimal power and rate adaptation, optimal rate adaptation with constant transmit power, and the channel inversion with fixed rate protocol. We provide numerical and simulation results in section 3.6. Finally, the chapter conclusions are provided in section 3.7.

3.2 Related Work

Large amount of research papers reported in the literature has considered performance analysis of cooperative communication systems.

In [124] the authors studied the ergodic capacity in Rayleigh fading of multi-hop wireless transmission systems employing either amplify-and- forward relaying or decode-and-forward relaying , the results shown that multi-hop transmission systems employing a decode-and-forward relaying scheme achieve higher ergodic capacities than multi-hop transmission systems with amplify-and-forward relaying schemes. In

[126] the authors derived an expression for the exact ergodic capacity, simplified closed-form expressions for the high SNR regime, and tight closed-form upper and lower bounds of the ergodic capacity of amplify-and-forward (AF) MIMO dual-hop relay channels, assuming that the channel state information is available at the destination terminal only. In contrast to prior results, our expressions apply for arbitrary numbers of interferers and arbitrary values of the Nakagami-m fading parameters.

[31], the effect of cochannel interference on the performance of digital mobile radio systems in a Nakagami fading channel is studied. The performance of maximal ratio combining (MRC) diversity is analyzed in the presence of multiple equal-power cochannel interferers and additive white Gaussian noise. The results are expressed in terms of the confluent hypergeometric function of the second kind, a function that can be easily evaluated numerically. The analysis assumes an arbitrary number of independent and identically distributed Nakagami interferers. In [117], the authors investigate the performance of a dual-hop AF relay system in Nakagami-m fading channels in the presence of multiple cochannel interference (CCI). They present integral-form expressions for the outage probability, general moments for the end-to-end signal to interference and noise ratio, and ergodic capacity of the system. In addition, they look into the high SNR regime and characterize the diversity order and coding gain achieved by the system. In [118], a highly accurate integral-form approximate expression for the end-to-end outage probability of dual-hop DF relaying systems with multiple CCI and subject to arbitrary (integer and non-integer) Nakagami-m fading channel is derived. In [119], the authors obtained the average channel capacity with channel side information at the transmitter and the receiver

and at the receiver alone. In their paper, the optimal power and rate adaptation (OPRA) and channel inversion with fixed rate (CIFR) were implemented when the channel state information (CSI) is known at both the transmitter and the receiver sides. The optimal rate adaptation with fixed power is implemented when the CSI is known only at the receiver side. The Rayleigh fading distribution was used to model small-scale variations of the channel envelope. It should be noted that in the OPRA the better the channel conditions, the more power is transmitted under the constraint of total transmitted power, while the ORA scheme is simply the well-known AWGN channel capacity averaged over the distribution of the fading model. The authors in [119] shown that the CIFR results in a large channel capacity penalty in severe fading. Consequently, a slightly modified version of the CIFR, the truncated channel inversion with fixed rate (TIFR), was also proposed in the same paper. The same system model as in [119] was adapted by the authors in [120] under the same channel fading model but with diversity schemes, namely, the selection combining and the maximal ratio combining schemes. The channel capacity under the three power adaptation policies was also considered in [121] assuming Nakagami-m multipath fading with diversity combining at the receiver side.

In [123] the authors investigate the efficacy of a novel moment generating function (MGF) based analytical framework for calculating the ergodic channel capacities of cooperative dual-hop amplify-and-forward relay networks under three distinct source-adaptive transmission policies in Rice and Nakagami-m fading environments. The proposed analytical approach reduces the computational complexity of evaluating the ergodic capacities of AF multi-relay networks with the optimal joint power-and-rate

adaptation (when the channel side information is available at both the transmitter and the receiver) and the optimal rate-adaptation with a constant transmit power (when channel side information is available at the receiver only) protocols.

In [124] the authors studied the ergodic capacity in Rayleigh fading of multi-hop wireless transmission systems employing either amplify-and- forward relaying or decode-and-forward relaying , the results shown that multi-hop transmission systems employing a decode-and-forward relaying scheme achieve higher ergodic capacities than multi-hop transmission systems with amplify-and-forward relaying schemes. In [126] the authors derived an expression for the exact ergodic capacity, simplified integral-form expressions for the high SNR regime, and tight integral-form upper and lower bounds of the ergodic capacity of amplify-and-forward (AF) MIMO dual-hop relay channels, assuming that the channel state information is available at the destination terminal only. In contrast to prior results, our integral expressions apply for dual hop relaying system over Nakagami-m fading and CCI channels with arbitrary number of interferers, but limited to value of the Nakagami-m fading parameter $m = 2$.

3.3 Contributions

In this chapter, we derived integral-form approximate expressions for the average channel capacity performance analysis of interference-limited dual-hop wireless communication systems with cochannel interference over small scale multipath nakagami-m fading channels under different adaptive transmission protocols is investigated.

The CCI at both relay and destination nodes is considered in interference limited Nakagami-m fading channels with arbitrary number of interferers, but limited to value of the Nakagami-m fading parameter $m = 2$. This channel condition is assumed for both the desired signal as well as co-channel interfering signals. In addition, the practical case of unequal average fading powers between the two hops is assumed in the analysis. Considering this channel distribution under different adaptive transmission protocols; namely, the simultaneous power and rate adaptation protocol (OPRA), the optimal rate with fixed power protocol (ORA), the channel inversion with fixed rate protocol (CIFR), and the truncated channel inversion with fixed transmit power protocol (CTIFR). We show numerical and simulation results to verify the accuracy of our derived expressions. To the best of the authors' knowledge, the derived integral-expressions in this chapter are new and have not been previously reported in the literature.

3.4 System and signal Models

We consider the same system and signal model of the previous chapter.

3.5 Average Channel Capacity Performance Analysis

Average channel capacity (ACC) performance analysis is very important metric for wireless communication system designers as they provide feedback on the quality of the designs and hence, provide a chance for enhancements and refining. This

section will focus on conducting performance evaluation studies for next generation wireless systems, mainly from an analytical point of view. In Df dual-hop wireless communication systems, the received signal at each relay node is fully decoded, re-encoded and then retransmitted to the destination node. Thus, the overall system achievable ACC should be the minimum of the achievable ACC's over each individual hop. On the other hand, according to [124] the overall system capacity cannot be larger than the capacity of each individual link. Therefore, the overall capacity in a DF dual-hop transmission system is given by [124] as

$$C_{DF} = min\left(C_1, C_2\right), \tag{3.2}$$

where C_1 and C_2 are the average channel capacity of the first and the second hop, respectively. In general, in cooperative systems with L DF relays when fading is present, the channel capacity can be found by averaging the AWGN channel capacity given by the Shannon theorem over the PDF distribution of the small-scale fading model, which is here the Nakagami-m distribution, as follows [124]:

$$\begin{aligned} C &= \frac{1}{1+L} E\left[\log_2\left(1+\gamma\right)\right] \\ &= \frac{1}{1+L} \int_0^\infty \log_2\left(1+\gamma\right) f_{\gamma_m}(\gamma) d\gamma. \end{aligned} \tag{3.3}$$

In dual-hop system $L = 1$ [124],

$$\begin{aligned} C &= \frac{1}{2} E\left[\log_2\left(1+\gamma\right)\right] \\ &= \frac{1}{2} \int_0^\infty \log_2\left(1+\gamma\right) f_{\gamma_m}(\gamma) d\gamma. \end{aligned} \tag{3.4}$$

where C is the normalized channel capacity [bits/sec/Hz], and γ is the instantaneous signal-to-interference ratio, and $f_{\gamma_m}(\gamma)$ is the PDF of γ_m given as

$$\gamma_m = min\left(\gamma_1, \gamma_2\right), \tag{3.5}$$

$$f_{\gamma_m}(\gamma) = f_{\gamma_1}(\gamma) + f_{\gamma_2}(\gamma) - f_{\gamma_1}(\gamma)F_{\gamma_2}(\gamma) - f_{\gamma_2}(\gamma)F_{\gamma_1}(\gamma) \tag{3.6}$$

where

$$f_{\gamma_1}(\gamma) = \frac{\Gamma(m_1+m_r)}{\Gamma(m_1)\Gamma(m_r)}\left(\frac{m_1}{m_r}\right)^{m_1}\left(\frac{P_r\omega_r\gamma}{P_S\Omega_1}\right)^{m_1-1}\left(1+\frac{m_1}{m_r}\frac{P_r\omega_r\gamma}{P_S\Omega_1}\right)^{-(m_1+m_r)}, \tag{3.7}$$

$$f_{\gamma_2}(\gamma) = \frac{\Gamma(m_2+m_d)}{\Gamma(m_2)\Gamma(m_d)}\left(\frac{m_2}{m_d}\right)^{m_2}\left(\frac{P_d\omega_d\gamma}{P_R\Omega_2}\right)^{m_2-1}\left(1+\frac{m_2}{m_d}\frac{P_d\omega_d\gamma}{P_R\Omega_2}\right)^{-(m_2+m_d)}. \tag{3.8}$$

$$F_{\gamma_1}(\gamma) = \frac{\Gamma(m_1+m_r)}{m_1\Gamma(m_1)\Gamma(m_r)}\left(\frac{m_1}{m_r}\right)^{m_1}\left(\frac{P_r\omega_r\gamma}{P_S\Omega_1}\right)^{m_1}{}_2F_1\left(m_1, m_1+m_r; 1+m_1; -\frac{m_1}{m_r}\frac{P_r\omega_r\gamma}{P_R\Omega_1}\right), \tag{3.9}$$

$$F_{\gamma_2}(\gamma) = \frac{\Gamma(m_2+m_d)}{m_2\Gamma(m_2)\Gamma(m_d)}\left(\frac{m_2}{m_d}\right)^{m_2}\left(\frac{P_d\omega_d\gamma}{P_R\Omega_2}\right)^{m_2}{}_2F_1\left(m_2, m_2+m_d; 1+m_2; -\frac{m_2}{m_d}\frac{P_d\omega_d\gamma}{P_R\Omega_2}\right), \tag{3.10}$$

where $f_{\gamma_1}(\gamma)$ and $f_{\gamma_2}(\gamma)$ are the PDF's of the first and the second hop, respectively. Also, $F_{\gamma_1}(\gamma)$ and $F_{\gamma_2}(\gamma)$ are the CDF's of the first and the second hop, respectively. In general, there are four different power and rate adaptation scenarios, namely, the optimal rate adaptation with constant transmit power (ORA), the optimal simultaneous power and rate adaptation (OPRA), the truncated channel inversion with fixed rate (CTIFR), and the channel inversion with fixed rate (CIFR). In the following, we will derive the ACC integral-expressions for different adaptive transmission protocols.

3.5.1 Optimal Rate Adaptation with Constant Transmit Power (ORA)

The optimal rate adaptation to the channel fading with constant transmit power is simply the ergodic channel capacity C_{ora}, which can be evaluated as

$$\begin{aligned} C_{\text{ora}} &= \frac{1}{L+1} E\left[\log_2\left(1+\gamma\right)\right] \\ &= \frac{1}{L+1}\int_0^{\infty} \log_2\left(1+\gamma\right) f_{\gamma_m}(\gamma) d\gamma. \end{aligned} \tag{3.11}$$

By substituting (3.6) into (3.11) yields

$$\begin{aligned} C_{ora} &= \frac{1}{L+1}\int_0^{\infty} \log_2\left(1+\gamma\right) f_{\gamma m}(\gamma) d\gamma \\ &= \frac{1}{L+1}\int_0^{\infty} \log_2\left(1+\gamma\right) f_{\gamma_1}(\gamma) d\gamma + \frac{1}{L+1}\int_0^{\infty} \log_2\left(1+\gamma\right) f_{\gamma_2}(\gamma) d\gamma \\ &- \frac{1}{L+1}\int_0^{\infty} \log_2\left(1+\gamma\right) f_{\gamma_1}(\gamma) F_{\gamma_2}(\gamma) d\gamma - \frac{1}{L+1}\int_0^{\infty} \log_2\left(1+\gamma\right) f_{\gamma_2}(\gamma) F_{\gamma_1}(\gamma) d\gamma, \end{aligned} \tag{3.12}$$

Representing the logarithm in (3.12) in terms of the natural logarithm function results in

$$\begin{aligned} C_{ora} &= \frac{1}{(L+1)\ln 2}\int_0^{\infty} \ln\left(1+\gamma\right) f_{\gamma m}(\gamma) d\gamma \\ &= \frac{1}{(L+1)\ln 2}\int_0^{\infty} \ln\left(1+\gamma\right) f_{\gamma_1}(\gamma) d\gamma + \frac{1}{(L+1)\ln 2}\int_0^{\infty} \ln\left(1+\gamma\right) f_{\gamma_2}(\gamma) d\gamma \\ &- \frac{1}{(L+1)\ln 2}\int_0^{\infty} \ln\left(1+\gamma\right) f_{\gamma_1}(\gamma) F_{\gamma_2}(\gamma) d\gamma - \frac{1}{(L+1)\ln 2}\int_0^{\infty} \ln\left(1+\gamma\right) f_{\gamma_2}(\gamma) F_{\gamma_1}(\gamma) d\gamma, \end{aligned} \tag{3.13}$$

The integrals of the first two terms in in (3.13) can not be solved unless we represent the natural logarithm functions in terms of the Meijer's G-function as follows:

$$\ln\left(1+\gamma\right) = G_{2,2}^{1,2}\left(\gamma \left| \begin{matrix} 1,1 \\ 1,0 \end{matrix} \right.\right), \tag{3.14}$$

where $G_{p,q}^{m,n}\left(\cdot\right)$ is the Meijer's G-function defined in [127, pp. 348]. The integrals in the first two terms of (3.12) can be solved with help of [132, Eq. (7.811.5)] as

$$\int_0^{\infty} \log_2\left(1+\gamma\right) f_{\gamma_1}(\gamma) d\gamma = \frac{1}{\Gamma(m_1)\Gamma(m_r)\ln 2}\; G_{3,3}^{2,3}\left(\frac{p_S \omega_1 m_r}{p_r \omega_r m_1}\middle| \begin{matrix} 1-m_1, 1, 1 \\ m_r, 1, 0 \end{matrix}\right),$$

$$\int_0^{\infty} \log_2(1+\gamma)\, f_{\gamma_2}(\gamma) d\gamma = \frac{1}{\Gamma(m_2)\Gamma(m_d)\ln 2}\; G_{3,3}^{2,3}\left(\frac{p_R \omega_2 m_d}{p_d \omega_d m_2} \middle| \begin{matrix} 1-m_2, 1, 1 \\ m_d, 1, 0 \end{matrix} \right),$$

but there is no solution for the integrals in the last two terms of (3.12). The expression in (3.13) is new, novel, and has not been reported in the literature before. However, the fading parameter $m = 2$ is the only restriction on the result in (3.13).

3.5.2 Optimal Simultaneous Transmit Power and Rate Adaptation (OPRA)

Given an average power constraint, the average channel capacity of a fading channel assuming optimal power and rate adaptation was given as [119]:

$$C_{\text{opra}} = \frac{1}{(L+1)\ln 2} \int_{\gamma_{th}}^{\infty} \ln\left(\frac{\gamma}{\gamma_{th}}\right) f_{\gamma_m}(\gamma) d\gamma, \tag{3.15}$$

By substituting (3.6) into (3.15) yields

$$\begin{aligned} C_{\text{opra}} &= \frac{1}{(L+1)\ln 2} \int_{\gamma_{th}}^{\infty} \ln\left(\frac{\gamma}{\gamma_{th}}\right) f_{\gamma_m}(\gamma) d\gamma \\ &= \frac{1}{(L+1)\ln 2} \int_{\gamma_{th}}^{\infty} \ln\left(\frac{\gamma}{\gamma_{th}}\right) f_{\gamma_1}(\gamma) d\gamma + \frac{1}{(L+1)\ln 2} \int_{\gamma_{th}}^{\infty} \ln\left(\frac{\gamma}{\gamma_{th}}\right) f_{\gamma_2}(\gamma) d\gamma \\ &- \frac{1}{(L+1)\ln 2} \int_{\gamma_{th}}^{\infty} \ln\left(\frac{\gamma}{\gamma_{th}}\right) f_{\gamma_1}(\gamma) F_{\gamma_2}(\gamma) d\gamma - \frac{1}{(L+1)\ln 2} \int_{\gamma_{th}}^{\infty} \ln\left(\frac{\gamma}{\gamma_{th}}\right) f_{\gamma_2}(\gamma) F_{\gamma_1}(\gamma) d\gamma, \end{aligned} \tag{3.16}$$

where γ_{th} is the threshold SIR below which the transmission is suspended. The integrals in the first two terms of (3.16) can not be solved unless we represent the natural logarithm function in terms of the limit's expression as follows [132, Eq. 1.512.4]:

$$\ln x = \lim_{\epsilon \to 0} \left(\frac{x^{\epsilon} - 1}{\epsilon} \right), \tag{3.17}$$

$$\ln\left(\frac{\gamma}{\gamma_{th}}\right) = \lim_{\epsilon \to 0}\left(\frac{\left(\frac{\gamma}{\gamma_{th}}\right)^{\epsilon} - 1}{\epsilon}\right), \tag{3.18}$$

The integrals in the first two terms of (3.16) can be solved with the help of [132, Eq. 1.512.4] as

$$\begin{aligned}
\frac{1}{(L+1)\ln 2}\int_{\gamma_{th}}^{\infty} \ln\left(\frac{\gamma}{\gamma_{th}}\right) f_{\gamma_1}(\gamma)d\gamma \quad = \quad & \lim_{\epsilon \to 0} \frac{\frac{\Gamma(m_1+m_r)}{\Gamma(m_1)\Gamma(m_r)}\left(\frac{m_1}{m_r}\right)^{m_1}}{\epsilon \ln 2} \\
& \times \frac{\gamma_{th}^{-m_1}}{\left(\frac{m_1 P_r \omega_r}{m_r P_S \Omega_1}\right)^{m_1+m_r}(m_1-\epsilon)} {}_2F_1\left(m_1+m_r, m_r-\epsilon; m_r-\epsilon+1; \frac{-1}{\left(\frac{m_1 P_r \omega_r}{m_r P_S \Omega_1}\right)\gamma_{th}}\right) \\
& - \frac{\gamma_{th}^{-m_1}}{\left(\frac{m_1 P_r \omega_r}{m_r P_R \Omega_1}\right)^{m_1+m_r}(m_1)} {}_2F_1\left(m_1+m_r, m_r; m_r+1; \frac{-1}{\left(\frac{m_1 P_r \omega_r}{m_r P_S \Omega_1}\right)\gamma_{th}}\right)
\end{aligned} \tag{3.19}$$

$$\begin{aligned}
\frac{1}{(L+1)\ln 2}\int_{\gamma_{th}}^{\infty} \ln\left(\frac{\gamma}{\gamma_{th}}\right) f_{\gamma_2}(\gamma)d\gamma \quad = \quad & \lim_{\epsilon \to 0} \frac{\frac{\Gamma(m_2+m_d)}{\Gamma(m_2)\Gamma(m_d)}\left(\frac{m_2}{m_d}\right)^{m_2}}{\epsilon \ln 2} \\
& \times \frac{\gamma_{th}^{-m_2}}{\left(\frac{m_2 P_d \omega_d}{m_d P_R \Omega_2}\right)^{m_2+m_d}(m_2-\epsilon)} {}_2F_1\left(m_2+m_d, m_d-\epsilon; m_d-\epsilon+1; \frac{-1}{\left(\frac{m_2 P_d \omega_d}{m_d P_R \Omega_2}\right)\gamma_{th}}\right) \\
& - \frac{\gamma_{th}^{-m_2}}{\left(\frac{m_2 P_d \omega_d}{m_d P_R \Omega_2}\right)^{m_2+m_d}(m_2)} {}_2F_1\left(m_2+m_d, m_d; m_d+1; \frac{-1}{\left(\frac{m_2 P_d \omega_d}{m_d P_R \Omega_2}\right)\gamma_{th}}\right)
\end{aligned} \tag{3.20}$$

The integral-expression in (3.16) is new, novel, and has not been reported in the literature before. However, $m = 2$ is the only restriction on the result in (3.16). Also, the numerical results show that it converges into infinitesimally small neighborhoods around $\epsilon = 0$. In our numerical results, we use $\epsilon = 10^{-7}$ to plot the results of the optimal simultaneous transmit power and rate adaptation (OPRA).

3.5.3 Channel Inversion with Fixed Rate (CIFR)

In this transmission policy, the transmitter adapts its transmitted power in order to achieve a constant SIR level at the receiver side, where the transmitter side is assumed to have full knowledge of the channel envelope variations. It is noteworthy that a fixed modulation as well as a fixed code rate are employed under this policy since the SIR is held constant, and the channel (after the channel inversion policy)

will appear as a time-invariant channel at the receiver side. Under this policy, the channel capacity in [bit/sec/Hs] is given by [119]

$$\begin{aligned} C_{\text{cifr}} &= \frac{1}{(L+1)}\log_2\left[1+\frac{1}{\int_0^\infty \gamma^{-1}\, f_{\gamma_m}(\gamma)d\gamma}\right] \\ &= \frac{1}{(L+1)}\log_2\left[1+\frac{1}{E[\gamma^{-1}]}\right]. \end{aligned} \tag{3.21}$$

By substituting (3.6) into (3.21) yields

$$C_{\text{cifr}} = \frac{1}{(L+1)}\log_2\left[1+\frac{1}{\int_0^\infty \gamma^{-1} f_{\gamma_1}(\gamma)d\gamma + \int_0^\infty \gamma^{-1} f_{\gamma_2}(\gamma)d\gamma - \int_0^\infty \gamma^{-1} f_{\gamma_1}(\gamma)F_{\gamma_2}(\gamma)d\gamma - \int_0^\infty \gamma^{-1} f_{\gamma_2}(\gamma)F_{\gamma_1}(\gamma)d\gamma}\right] \tag{3.22}$$

The integrals in the first two terms of (3.22) can be solved with the help of [132, Eq. (3.194.3)] and after some simplifications results in

$$\int_0^\infty \gamma^{-1} f_{\gamma_1}(\gamma)d\gamma = \frac{\Gamma(m_1+m_r)}{\Gamma(m_1)\Gamma(m_r)}\left(\frac{m_1}{m_r}\right)\left(\frac{\omega_r}{\Omega_1}\right) B\left(m_r-1, 1+m_1\right) d\gamma. \tag{3.23}$$

$$\int_0^\infty \gamma^{-1} f_{\gamma_2}(\gamma)d\gamma = \frac{\Gamma(m_2+m_d)}{\Gamma(m_2)\Gamma(m_d)}\left(\frac{m_2}{m_d}\right)\left(\frac{\omega_d}{\Omega_2}\right) B\left(m_d-1, 1+m_2\right) d\gamma. \tag{3.24}$$

The integral-expression in (3.22) is new, novel, and has not been reported in the literature before. However, $m = 2$ is the only restriction on the result in (3.22).

3.5.4 Truncated Channel Inversion with Fixed Rate (TIFR)

A truncated channel inversion with fixed transmit power C_{tifr} is given as [119]:

$$C_{\text{tifr}} = \frac{1}{(L+1)}\log_2\left(1+\frac{1}{\int_{\gamma_{th}}^\infty \gamma^{-1}\, f_{\gamma_m}(\gamma)d\gamma}\right)\left(1-P_{\text{out}}\right), \tag{3.25}$$

$$C_{\text{tifr}} = \frac{1}{(L+1)}\log_2\left(1+\frac{1}{\int_{\gamma_{th}}^\infty \gamma^{-1} f_{\gamma_1}(\gamma)d\gamma + \int_0^\infty \gamma^{-1} f_{\gamma_2}(\gamma)d\gamma - \int_0^\infty \gamma^{-1} f_{\gamma_1}(\gamma)F_{\gamma_2}(\gamma)d\gamma - \int_0^\infty \gamma^{-1} f_{\gamma_2}(\gamma)F_{\gamma_1}(\gamma)d\gamma}\right) \times \left(1-P_{\text{out}}\right), \tag{3.26}$$

where γ_{th} here is the cutoff SIR value. P_{out} is the outage probability defined as the probability that the instantaneous SIR drops below the threshold γ_{th}, P_{out} is given as [118]

$$\begin{aligned} P_{\text{out}}(\gamma_{th}) &= \frac{\Gamma(m_2+m_d)}{m_2\Gamma(m_2)\Gamma(m_d)}\left(\frac{m_2}{m_d}\right)^{m_2}\left(\frac{P_d\omega_d\gamma_{th}}{P_R\Omega_2}\right)^{m_2} \\ &\quad \times {}_2F_1\left(m_2, m_2+m_d; 1+m_2; -\frac{m_2}{m_d}\frac{P_d\omega_d\gamma_{th}}{P_R\Omega_2}\right). \end{aligned} \tag{3.27}$$

Solving the integrals in the first two terms of (3.26) using [132, Eq. (3.194.2)] and after simple manipulation and simplifications results in

$$\begin{aligned} \int_{\gamma_{th}}^{\infty}\gamma^{-1}f_{\gamma_2}(\gamma)d\gamma &= \frac{\Gamma(m_1+m_r)}{\Gamma(m_1)\Gamma(m_r)}\left(\frac{m_1\omega_r}{m_r\omega_1}\right)^{-m_1}\left(\frac{\gamma_{th}}{m_r+1}\right)^{-m_1-1} \\ &\quad \times {}_2F_1\left(m_1+m_1; 1+m_r; 2+m_r; \frac{-m_r\omega_1}{\gamma_{th}m_1\omega_r}\right). \end{aligned} \tag{3.28}$$

$$\begin{aligned} \int_{\gamma_{th}}^{\infty}\gamma^{-1}f_{\gamma_1}(\gamma)d\gamma &= \frac{\Gamma(m_2+m_d)}{\Gamma(m_2)\Gamma(m_d)}\left(\frac{m_2\omega_d}{m_d\omega_2}\right)^{-m_2}\left(\frac{\gamma_{th}}{m_d+1}\right)^{-m_2-1} \\ &\quad \times {}_2F_1\left(m_2+m_d; 1+m_d; 2+m_d; \frac{-m_d\omega_2}{\gamma_{th}m_2\omega_d}\right). \end{aligned} \tag{3.29}$$

The result in (3.26) is new and has not been reported in the literature before. However, $m = 2$ is the only restriction on the result in (3.26).

3.6 Numerical and Simulation Results

In this section, we provide numerical and simulation results for the integral-expressions derived in this chapter for the different transmission protocols in dual-hop DF relaying cooperative system ($L = 1$). Without loss of generality we assume that

$P_S = P_R = P_{ri} = P_{di} = 1$. The simulation results are obtained using MonteCarlo simulation method, with number of runs equal to $1,000,000$ times. The simulation has been done by simulating the PDF and the SIR that has been used in this chapter to derive the expressions of ACC under different adaptive transmission protocols, and then substitute them properly in the ACC general formula of each transmission protocol. However, The results are accurate for $m = 2$ especially in high range of SIR.

In Fig. 3.1, the normalized average channel capacity per unit bandwidth according to the ORA transmission policy is presented in dual-hop DF relaying cooperative system ($L = 1$) assuming the Nakagami-m fading channel model for $m = 2$.

The normalized capacity per unit bandwidth according to the simultaneous optimal and rate adaptation policy (OPRA) is shown in Fig. 3.2 at the threshold SIR equal to 2 dB. The figure shows that as the SIR increases, the capacity increases as expected.

In Fig. 3.3, the normalized average channel capacity per unit bandwidth [Bit/sec/Hz] versus the average SIR in dual-hop DF relaying cooperative system ($L = 1$) over the Nakagami-m fading channel model with the channel inversion with fixed rate protocol (CIFR) for $m = 2$. The figure shows that as the SIR increases, the capacity increases as expected.

In Fig. 3.4, the normalized average channel capacity per unit bandwidth [Bit/sec/Hz] versus the average SIRin dual-hop DF relaying cooperative system ($L = 1$) over the Nakagami-m fading channel model with the truncated channel inversion with fixed rate protocol (TIFR) for a $m = 2$. The figure shows that as the SIR increases, the

capacity increases as expected.

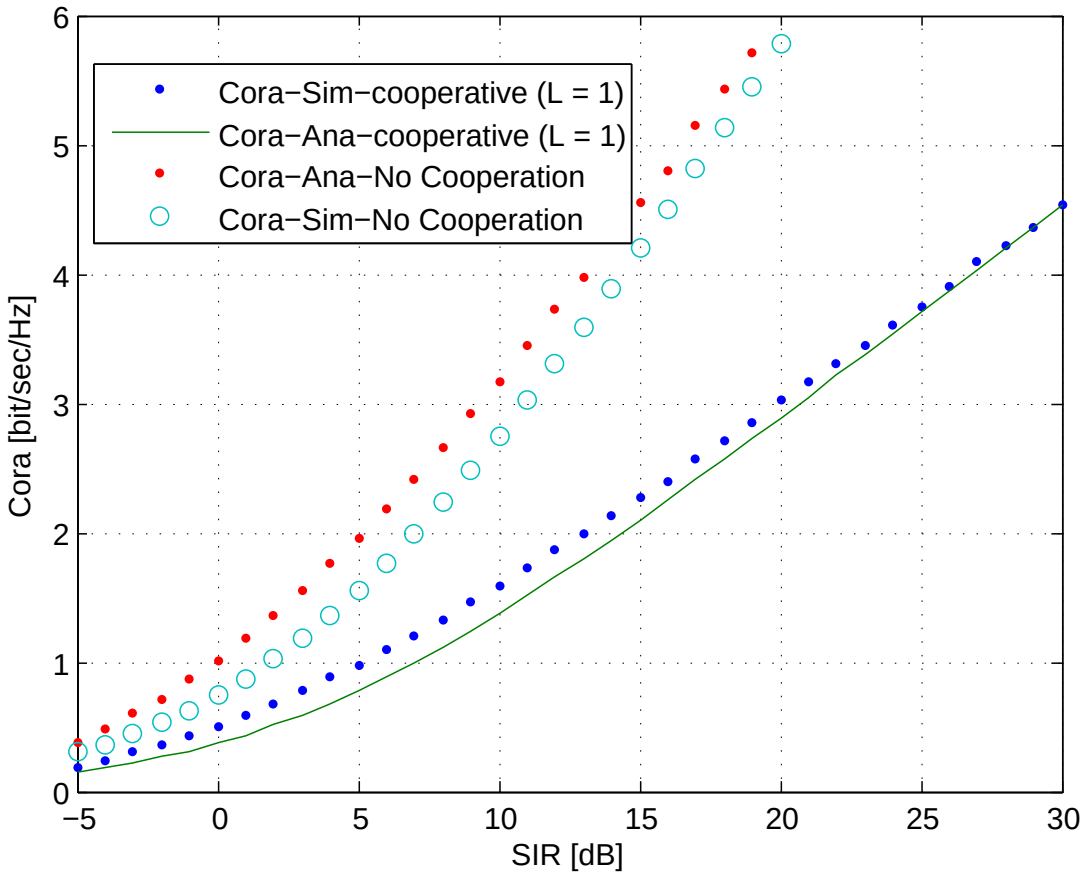

Figure 3.1. The normalized average channel capacity per unit bandwidth [Bit/sec/Hz] versus the average SIR for non-cooperative and dual-hop DF relaying cooperative system ($L = 1$) over the Nakagami-m fading channel model with optimal rate adaptation and fixed power protocol (ORA) for $m = 2$.

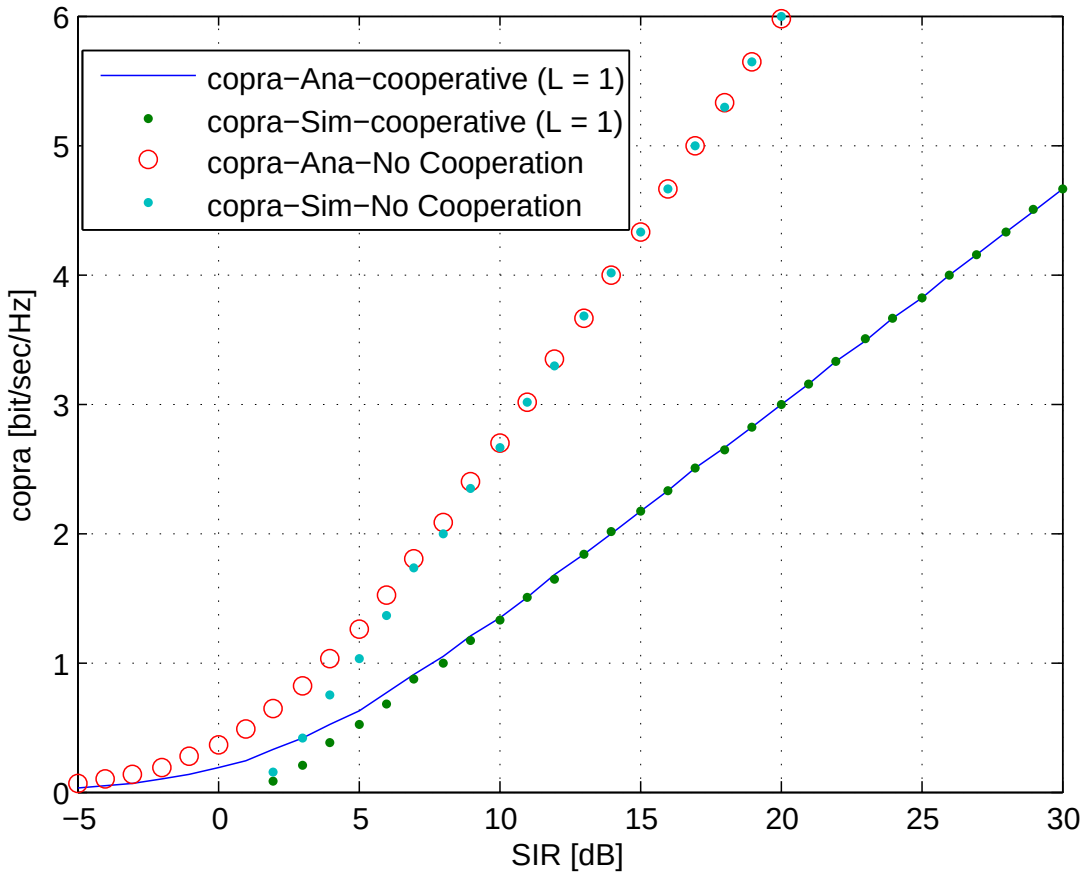

Figure 3.2. The normalized average channel capacity per unit bandwidth [Bit/sec/Hz] versus the average SIR for non-cooperative and dual-hop DF relaying cooperative system ($L = 1$) over the Nakagami-m fading channel model with simultaneous optimal power and rate adaptation protocol (OPRA) for $m = 2$.

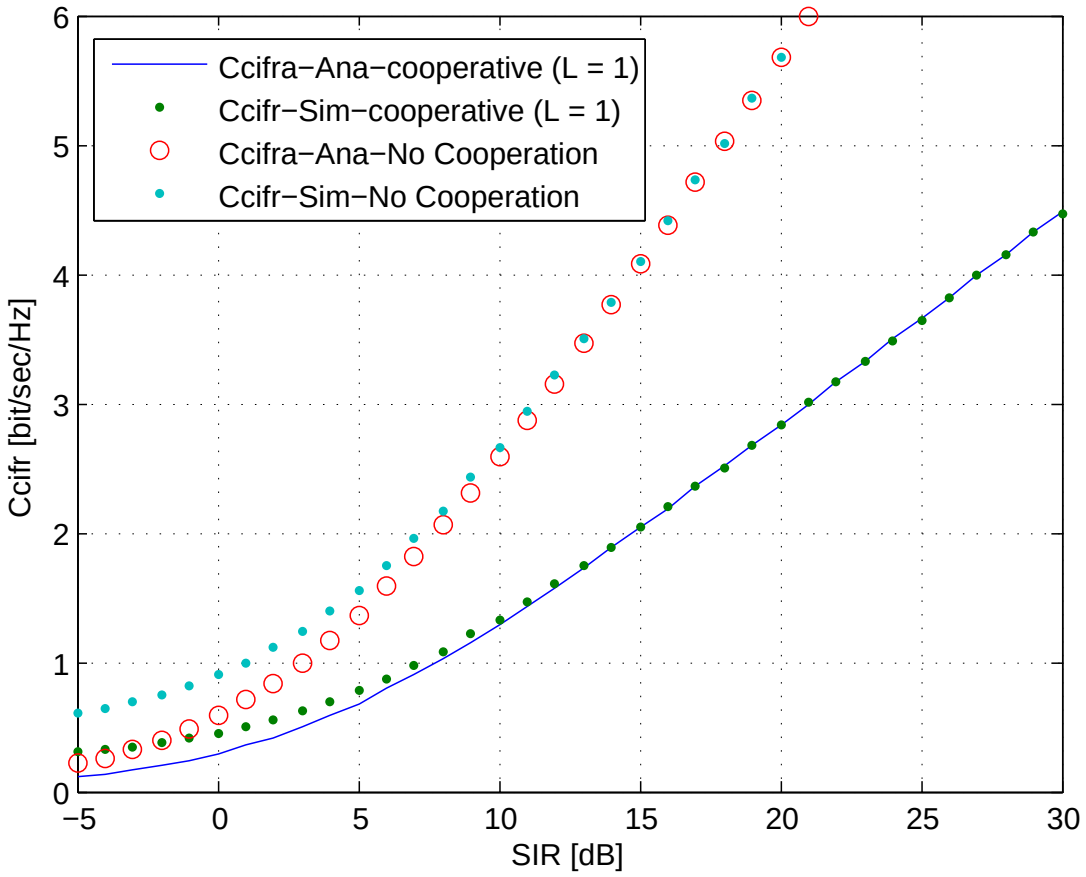

Figure 3.3. The normalized average channel capacity per unit bandwidth [Bit/sec/Hz] versus the average SIR for non-cooperative and dual-hop DF relaying cooperative system ($L = 1$) over the Nakagami-m fading channel model with the channel inversion with fixed rate protocol (CIFR) for $m = 2$.

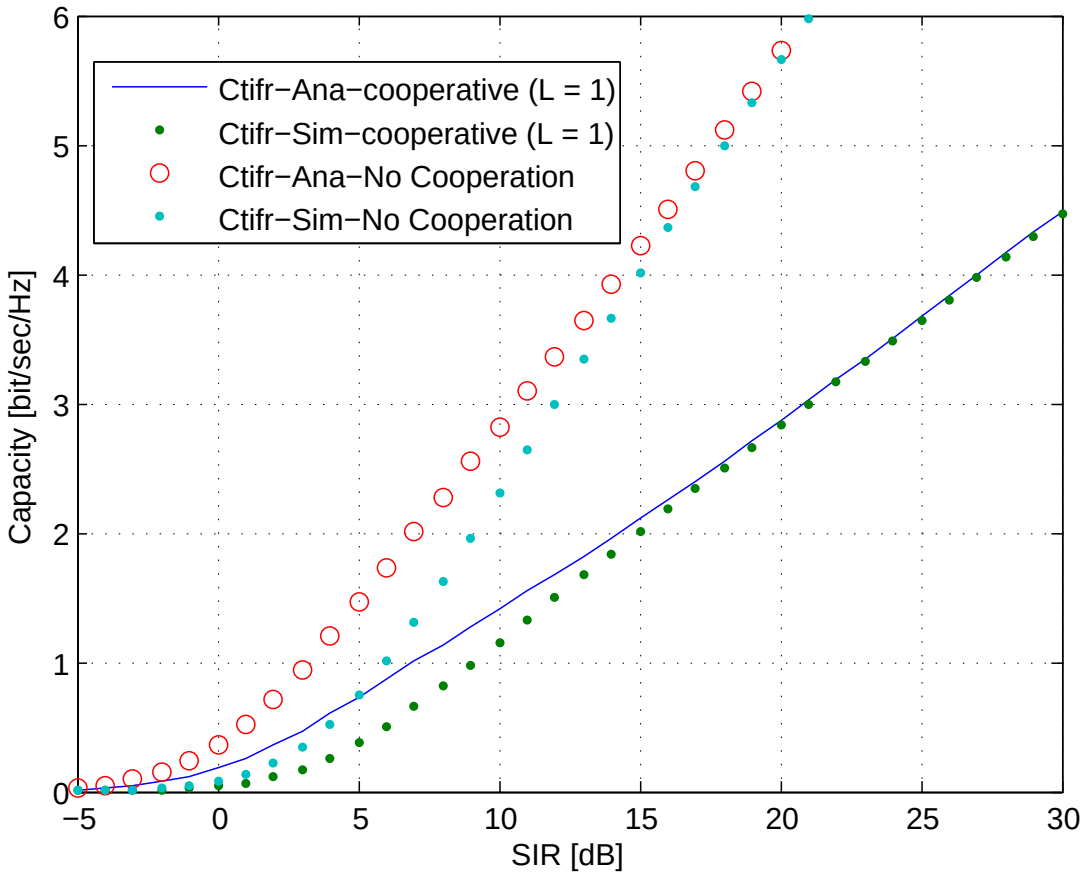

Figure 3.4. The normalized average channel capacity per unit bandwidth [Bit/sec/Hz] versus the average SIR for non-cooperative and dual-hop DF relaying cooperative system ($L = 1$) over the Nakagami-m fading channel model with truncated channel inversion with fixed rate protocol (TIFR) for $m = 2$.

3.7 Conclusions

In this chapter, we considered a dual-hop DF relaying wireless communication system over the Nakagami-m small-scale fading channels with multiple CCI at both the relay and the destination nodes. Assuming that the system operates in presence of (i.n.i.d.) Nakagami-m fading channels with $m = 2$, accurate approximated integral-expressions for the average channel capacity (ACC) for different adaptive transmission protocols especially in high range of SIR are derived. The normalized channel capacity different transmission protocols; the optimal rate adaptation with fixed transmitted power (ORA), the simultaneous power and rate adaptation transmission (OPRA), the truncated channel inversion with fixed rate transmission protocol (TIFR), and the channel inversion with fixed rate transmission protocol (CIFR). Having such a study with the enables system engineers and designers to optimize their designs before actual deployment in real situations and save the cost that may occur according to mistakes in system hardware implementation. The proposed analysis is accompanied by numerical and simulation results to verify the accuracy of the derived expressions for $m = 2$ especially in high range of SIR.

Chapter 4

NON-COOPERATIVE SYSTEMS: CAPACITY PERFORMANCE ANALYSIS

4.1 Chapter Overview

The channel capacity is always bounded by an upper limit defined by Shannon theorem (sometimes called the Shannon-Hartley theorem) [55]-[58]. Shannon theorem states that for an additive white Gaussian noise (AWGN) channel, there exist coding schemes such that it is possible to communicate error free data over the channel provided that the data rate $\mathcal{R}_b$ [bits/sec] is less than or equal to the channel capacity $\mathcal{C}$ [bits/sec] [56] and [57]. It is noteworthy that if $\mathcal{R}_b > \mathcal{C}$, then it is impossible to achieve an error free transmission no matter what the coding scheme is. Therefore, Shannon capacity is considered as the optimistic theoretical bound against which to compare all practical transmission systems. In this chapter we study the normalized Shannon capacity, C, measured in [bits/sec/Hz], of non-cooperative communication system under different adaptive transmission protocols assuming a small-scale fading channel following the Nakagami-m distribution with Nakagami-m cochannel inter-

ference (CCI) at destination node.

In Section 4.2, the related work is summarized. The chapter contributions are provided in Section 4.3. The capacity analysis is presented in section 4.5, which mainly derives optimal closed-form expressions for the channel capacity under different adaptive transmission protocols, namely, the simultaneous optimal power and rate adaptation, optimal rate adaptation with constant transmit power, and the channel inversion with fixed rate protocol. We provide numerical and simulation results in section 4.6. Finally, the chapter conclusions are provided in section 4.7.

4.2 Related Work

Large amount of research papers reported in the literature has considered performance analysis of cooperative communication systems. The channel capacity under the three power adaptation policies was considered in [121] assuming Nakagami-m fading with diversity combining at the receiver side. In [120] under the same channel fading model but with diversity schemes, namely, the selection combining and the maximal ratio combining schemes. [31], the effect of cochannel interference on the performance of digital mobile radio systems in a Nakagami fading channel is studied. The performance of maximal ratio combining (MRC) diversity is analyzed in the presence of multiple equal-power cochannel interferers and additive white Gaussian noise. The results are expressed in terms of the confluent hypergeometric function of the second kind, a function that can be easily evaluated numerically. The analysis assumes an arbitrary number of independent and identically distributed Nakagami

interferers. In [119], the authors obtained the average channel capacity with channel side information at the transmitter and the receiver and at the receiver alone. In their paper, the optimal power and rate adaptation (OPRA) and channel inversion with fixed rate (CIFR) were implemented when the channel state information (CSI) is known at both the transmitter and the receiver sides. The optimal rate adaptation with fixed power is implemented when the CSI is known only at the receiver side. The Rayleigh fading distribution was used to model small-scale variations of the channel envelope. It should be noted that in the OPRA the better the channel conditions, the more power is transmitted under the constraint of total transmitted power, while the ORA scheme is simply the well-known AWGN channel capacity averaged over the distribution of the fading model. The authors in [119] shown that the CIFR results in a large channel capacity penalty in severe fading. Consequently, a slightly modified version of the CIFR, the truncated channel inversion with fixed rate (TIFR), was also proposed in the same paper. The same system model as in [119] was adapted by the authors in [120] under the same channel fading model but with diversity schemes, namely, the selection combining and the maximal ratio combining schemes. The channel capacity under the three power adaptation policies was also considered in [121] assuming Nakagami-m fading with diversity combining at the receiver side.

4.3 Contributions

In this chapter, we derived closed-form approximate expressions for the average channel capacity performance analysis of interference-limited wireless communication systems with cochannel interference over small scale Nakagami-m fading channels under different adaptive transmission protocols is investigated. The CCI at the destination node is considered in interference limited Nakagami-m fading channels with arbitrary (integer as well as non-integer) values of m. This channel condition is assumed for both the desired signal as well as co-channel interfering signals. Considering this channel distribution under different adaptive transmission protocols; namely, the simultaneous power and rate adaptation protocol (OPRA), the optimal rate with fixed power protocol (ORA), the channel inversion with fixed rate protocol (CIFR), and the truncated channel inversion with fixed transmit power protocol (CTIFR). We show numerical and simulation results to verify the accuracy of our derived expressions. To the best of the authors' knowledge, the derived expressions in this chapter are new and have not been previously reported in the literature. Unlike many studies reported in the literature which is restrict the identical cochannel interference to the destination node, we consider the independent and non- identical Nakagami-m cochannel interference at the destination node. The channels are assumed to experience fading modeled as independent but not necessarily identically distributed (i.n.i.d.) Nakagami-m with arbitrary (integer as well as non-integer) values of fading parameter, m.

4.4 System and signal Models

We consider an interference-limited single-hop wireless communication system operating over independent and non identical distributed (i.n.i.d.) Nakagami-m fading channels with arbitrary integer as well as non-integer fading severity parameter m and with multiple CCI at D node, where a source node (S) communicates with D as shown in fig.4.1. All nodes are single antenna devices. We assumed D operates in interference-limited conditions; i.e., the channel noise is dominated by the total interfering signals. Multiple co-channel N_D interferers are assumed to be present at D. Each one of N_D interfering signals (i.e., ith interfering signal, where $i = 1, 2, \cdots, N_D$)) has an average transmit power P_{di}, fading severity parameter m_{di}, fading power parameter Ω_{di}, and experiences link fading coefficient h_{di}. Let the modulated signal transmitted by S denoted by S_S with transmit power P_S. Then the received signal at D is given by

$$y_D = \sqrt{P_S} h_2 S_S + \sum_{i=1}^{N_D} \sqrt{P_{di}} h_{di} S_{di}, \qquad i = 1, 2, \cdots, N_D \tag{4.1}$$

where h_2 is the channel gain coefficients with fading severity parameter m and fading power parameter Ω_2. All of h_{di},and h_2 are i.n.i.d. Nakagami-m random variables. In (4.1), S_S is the transmitted symbol from S to D with transmit power P_S, S_{di} is the transmitted symbol from ith interferer to D with transmit power P_{di}. The fading channels average power parameters are given by

$$\Omega_2 = E[|h_2|^2], \tag{4.2}$$

$$\Omega_{di} = E[|h_{di}|^2]. \tag{4.3}$$

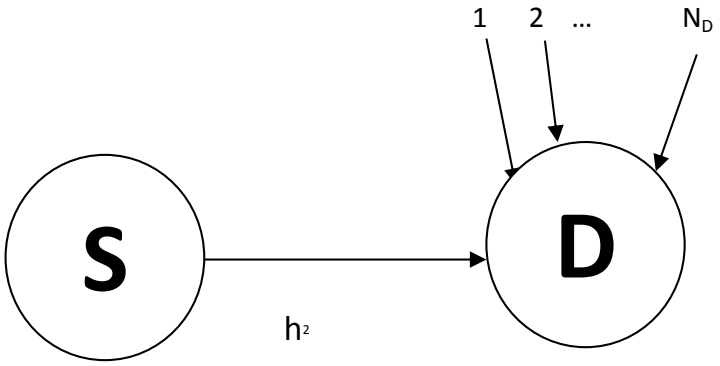

Figure 4.1. An interference-limited single-hop wireless communication system over Nakagami-m fading channel with multiple co-channel interference at the destination node.

The SIR is the ratio between the transmitted signal power and the total interference power. So, at D is given by

$$\gamma_D = \frac{P_R|h_2|^2}{\sum_{i=1}^{N_D} P_{di}|h_{di}|^2}. \tag{4.4}$$

4.5 Average Channel Capacity Performance Analysis

In general, when fading is present, the channel capacity can be found by averaging the AWGN channel capacity given by the Shannon theorem over the PDF distribution of the small-scale fading model, which is here the Nakagami-m distribution, as follows:

$$\begin{aligned} C &= E\left[\log_2\left(1+\gamma\right)\right] \\ &= \int_0^\infty \log_2\left(1+\gamma\right) f_\gamma(\gamma) d\gamma. \end{aligned} \tag{4.5}$$

where C is the normalized channel capacity [bits/sec/Hz], and γ is the instantaneous signal-to-interference ratio. In general, there are four different power and rate adaptation scenarios, namely, the optimal rate adaptation with constant transmit power (ORA), the optimal simultaneous power and rate adaptation (OPRA), the truncated channel inversion with fixed rate (CTIFR), and the channel inversion with fixed rate (CIFR).

In the following, we will derive the ACC closed-form expressions for different adaptive transmission protocols.

4.5.1 Optimal Rate Adaptation with Constant Transmit Power (ORA)

The optimal rate adaptation to the channel fading with constant transmit power is simply the ergodic channel capacity C_{ora}, which can be evaluated as

$$\begin{aligned} C_{\text{ora}} &= E\left[\log_2\left(1+\gamma\right)\right] \\ &= \int_0^{\infty} \log_2\left(1+\gamma\right) f_\gamma(\gamma) d\gamma. \end{aligned} \tag{4.6}$$

By representing the logarithm in (4.6) in terms of the natural logarithm function results in

$$C_{\text{ora}} = \frac{1}{\ln 2} \int_0^{\infty} \ln\left(1+\gamma\right) f_\gamma(\gamma) d\gamma. \tag{4.7}$$

The integral in (4.7) can not be solved unless we represent the natural logarithm

functions in terms of the Meijer's G-function as follows:

$$\ln\left(1+\gamma\right) \;=\; G_{2,2}^{1,2}\left(\gamma\left|\begin{array}{c}1,1\\1,0\end{array}\right.\right), \tag{4.8}$$

where $G_{p,q}^{m,n}\left(\cdot\right)$ is the Meijer's G-function defined in [127, pp. 348]. Using (4.8) in (4.6) results in

$$C_{\text{ora}} \;=\; \frac{1}{\ln 2}\int_0^{\infty} f_{\gamma}(\gamma) G_{2,2}^{1,2}\left(\gamma\left|\begin{array}{c}1,1\\1,0\end{array}\right.\right) d\gamma, \tag{4.9}$$

$$C_{\text{ora}} \;=\; \frac{1}{\ln 2}\int_0^{\infty} \frac{\Gamma(m_2+m_d)}{\Gamma(m_2)\Gamma(m_d)}\left(\frac{m_2}{m_d}\right)^{m_2}\left(\frac{P_d\omega_d\gamma}{P_R\Omega_2}\right)^{m_2-1}\left(1+\frac{m_2}{m_d}\frac{P_d\omega_d\gamma}{P_R\Omega_2}\right)^{-(m_2+m_d)} G_{2,2}^{1,2}\left(\gamma\left|\begin{array}{c}1,1\\1,0\end{array}\right.\right) d\gamma, \tag{4.10}$$

The integral in (4.10) can be solved with the help of [132, Eq. (7.811.5)] as

$$C_{\text{ora}} = \frac{1}{\Gamma(m_1)\Gamma(m_d)\ln 2}\; G_{3,3}^{2,3}\left(\frac{p_R\omega_2 m_d}{p_d\omega_d m_2}\left|\begin{array}{c}1-m_2,1,1\\m_d,1,0\end{array}\right.\right), \tag{4.11}$$

The expression in (4.11) is new, novel, and has not been reported in the literature before, and valid for integer and non-integer values of the fading severity parameters. However, $m_d > 1$ is the only restriction on the result in (4.11).

4.5.2 Optimal Simultaneous Transmit Power and Rate Adaptation (OPRA)

Given an average power constraint, the average channel capacity of a fading channel assuming optimal power and rate adaptation was given as [119]:

$$C_{\text{opra}} = \frac{1}{\ln 2}\int_{\gamma_{th}}^{\infty} \ln\left(\frac{\gamma}{\gamma_{th}}\right) f_{\gamma}(\gamma) d\gamma, \tag{4.12}$$

$$\begin{aligned} C_{\text{opra}} &= \frac{1}{\ln 2}\int_{\gamma_{th}}^{\infty} \ln\left(\frac{\gamma}{\gamma_{th}}\right) \frac{\Gamma(m_2+m_d)}{\Gamma(m_2)\Gamma(m_d)} \left(\frac{m_2}{m_d}\right)^{m_2} \left(\frac{P_d\omega_d\gamma_D}{P_R\Omega_2}\right)^{m_2-1} \\ &\quad \times \left(1+\frac{m_2}{m_d}\frac{P_d\omega_d\gamma_D}{P_R\Omega_2}\right)^{-(m_2+m_d)} d\gamma, \end{aligned} \tag{4.13}$$

where γ_{th} is the threshold SIR below which the transmission is suspended. The integral in (4.13) can not be solved unless we represent the natural logarithm function in terms of the limit's expression as follows [132, Eq. 1.512.4]:

$$\ln x = \lim_{\epsilon\to 0}\left(\frac{x^{\epsilon}-1}{\epsilon}\right), \tag{4.14}$$

$$\ln\left(\frac{\gamma}{\gamma_{th}}\right) = \lim_{\epsilon\to 0}\left(\frac{\left(\frac{\gamma}{\gamma_{th}}\right)^{\epsilon}-1}{\epsilon}\right), \tag{4.15}$$

substituting (4.15) into (4.13) results in

$$\begin{aligned} C_{\text{opra}} &= \frac{1}{\ln 2}\int_{\gamma_{th}}^{\infty} \lim_{\epsilon\to 0}\left(\frac{\left(\frac{\gamma}{\gamma_{th}}\right)^{\epsilon}-1}{\epsilon}\right) \frac{\Gamma(m_2+m_d)}{\Gamma(m_2)\Gamma(m_d)} \left(\frac{m_2}{m_d}\right)^{m_2} \left(\frac{P_d\omega_d\gamma_D}{P_R\Omega_2}\right)^{m_2-1} \\ &\quad \times \left(1+\frac{m_2}{m_d}\frac{P_d\omega_d\gamma_D}{P_R\Omega_2}\right)^{-(m_2+m_d)} d\gamma \end{aligned}$$

$$
\begin{aligned}
C_{\text{opra}} &= \lim_{\epsilon\to 0}\frac{1}{\epsilon\,\ln 2}\int_{\gamma_{th}}^{\infty}\left(\frac{\gamma}{\gamma_{th}}\right)^{\epsilon}\frac{\Gamma(m_2+m_d)}{\Gamma(m_2)\Gamma(m_d)}\left(\frac{m_2}{m_d}\right)^{m_2}\left(\frac{P_d\omega_d\gamma_D}{P_R\Omega_2}\right)^{m_2-1}\left(1+\frac{m_2}{m_d}\frac{P_d\omega_d\gamma_D}{P_R\Omega_2}\right)^{-(m_2+m_d)}d\gamma_D \\
&\quad -\int_{\gamma_{th}}^{\infty}\frac{\Gamma(m_2+m_d)}{\Gamma(m_2)\Gamma(m_d)}\left(\frac{m_2}{m_d}\right)^{m_2}\left(\frac{P_d\omega_d\gamma_D}{P_R\Omega_2}\right)^{m_2-1}\left(1+\frac{m_2}{m_d}\frac{P_d\omega_d\gamma_D}{P_R\Omega_2}\right)^{-(m_2+m_d)}d\gamma_D, \qquad (4.16)
\end{aligned}
$$

The integrals in (4.16) can be solved with the help of [132, Eq. 1.512.4] as

$$
\begin{aligned}
C_{\text{opra}} &= \lim_{\epsilon\to 0}\frac{\frac{\Gamma(m_2+m_d)}{\Gamma(m_2)\Gamma(m_d)}\left(\frac{m_2}{m_d}\right)^{m_2}}{\epsilon\,\ln 2} \\
&\quad\times\frac{\gamma_{th}^{-m_2}}{\left(\frac{m_2P_d\omega_d}{m_dP_R\Omega_2}\right)^{m_2+m_d}(m_2-\epsilon)}{}_2F_1\left(m_2+m_d,m_d-\epsilon;m_d-\epsilon+1;\frac{-1}{\left(\frac{m_2P_d\omega_d}{m_dP_R\Omega_2}\right)\gamma_{th}}\right) \\
&\quad-\frac{\gamma_{th}^{-m_2}}{\left(\frac{m_2P_d\omega_d}{m_dP_R\Omega_2}\right)^{m_2+m_d}(m_2)}{}_2F_1\left(m_2+m_d,m_d;m_d+1;\frac{-1}{\left(\frac{m_2P_d\omega_d}{m_dP_R\Omega_2}\right)\gamma_{th}}\right) \qquad (4.17)
\end{aligned}
$$

The expression in (4.17) is new, novel, and has not been reported in the literature before. The result in (4.17) converges for integer and non-integer values of the fading parameters m. Also, the numerical results show that it converges into infinitesimally small neighborhoods around $\epsilon = 0$. In our numerical results, we use $\epsilon = 10^{-7}$ to plot the results of the optimal simultaneous transmit power and rate adaptation (OPRA).

4.5.3 Channel Inversion with Fixed Rate (CIFR)

In this transmission policy, the transmitter adapts its transmitted power in order to achieve a constant SIR level at the receiver side, where the transmitter side is assumed to have full knowledge of the channel envelope variations. It is noteworthy that a fixed modulation as well as a fixed code rate are employed under this policy since the SIR is held constant, and the channel (after the channel inversion policy) will appear as a time-invariant channel at the receiver side. Under this policy, the

channel capacity in [bit/sec/Hs] is given by [119]

$$\begin{aligned} C_{\text{cifr}} &= \log_2\left[1+\frac{1}{\int_0^\infty \gamma^{-1}\, f_\gamma(\gamma)d\gamma}\right] \\ &= \log_2\left[1+\frac{1}{E[\gamma^{-1}]}\right]. \end{aligned} \tag{4.18}$$

$$C_{\text{cifr}} = \log_2\left[1+\frac{1}{\int_0^\infty \gamma^{-1}\, \frac{\Gamma(m_2+m_d)}{\Gamma(m_2)\Gamma(m_d)}\left(\frac{m_2}{m_d}\right)^{m_2}\left(\frac{P_d\omega_d\gamma_D}{P_R\Omega_2}\right)^{m_2-1}\left(1+\frac{m_2}{m_d}\frac{P_d\omega_d\gamma_D}{P_R\Omega_2}\right)^{-(m_2+m_d)} d\gamma}\right],$$

using [132, Eq. (3.194.3)] and after some simplifications results in

$$C_{\text{cifr}} = \log_2\left[1+\frac{1}{\frac{\Gamma(m_2+m_d)}{\Gamma(m_2)\Gamma(m_d)}\left(\frac{m_2}{m_d}\right)\left(\frac{\omega_d}{\Omega_2}\right) B\left(m_d-1, 1+m_2\right) d\gamma}\right]. \tag{4.19}$$

The expression in (4.19) is new, novel, and has not been reported in the literature before, and valid for integer and non-integer values of the fading severity parameters. However, $m_d > 1$ is the only restriction on the result in (4.19).

4.5.4 Truncated Channel Inversion with Fixed Rate (TIFR)

A truncated channel inversion with fixed transmit power C_{tifr} is given as [119]:

$$C_{\text{tifr}} = \log_2\left(1+\frac{1}{\int_{\gamma_{th}}^\infty \gamma^{-1}\, f_\gamma(\gamma)d\gamma}\right)\left(1-P_{\text{out}}\right), \tag{4.20}$$

$$\begin{aligned} C_{\text{tifr}} &= \log_2\left(1+\frac{1}{\int_{\gamma_{th}}^\infty \gamma^{-1}\, \frac{\Gamma(m_2+m_d)}{\Gamma(m_2)\Gamma(m_d)}\left(\frac{m_2}{m_d}\right)^{m_2}\left(\frac{P_d\omega_d\gamma_D}{P_R\Omega_2}\right)^{m_2-1}\left(1+\frac{m_2}{m_d}\frac{P_d\omega_d\gamma_D}{P_R\Omega_2}\right)^{-(m_2+m_d)} d\gamma}\right) \\ &\quad \times\left(1-P_{\text{out}}\right), \end{aligned} \tag{4.21}$$

where γ_{th} here is the cutoff SIR value. P_{out} is the outage probability defined as the probability that the instantaneous SIR drops below the threshold γ_{th}, P_{out} is given as [118]

$$\begin{aligned} P_{\text{out}}(\gamma_{th}) &= \frac{\Gamma(m_2+m_d)}{m_2\Gamma(m_2)\Gamma(m_d)}\left(\frac{m_2}{m_d}\right)^{m_2}\left(\frac{P_d\omega_d\gamma_{th}}{P_R\Omega_2}\right)^{m_2} \\ &\quad \times {}_2F_1\left(m_2, m_2+m_d; 1+m_2; -\frac{m_2}{m_d}\frac{P_d\omega_d\gamma_{th}}{P_R\Omega_2}\right). \end{aligned} \tag{4.22}$$

Solving the integral in (4.21) using [132, Eq. (3.194.2)] and after simple manipulation and simplifications results in

$$\begin{aligned} C_{\text{tifr}} &= \log_2\left(1+\frac{1}{\frac{\Gamma(m_2+m_d)}{\Gamma(m_2)\Gamma(m_d)}\left(\frac{m_2\omega_d}{m_d\omega_2}\right)^{-m_2}\left(\frac{\gamma_{th}}{m_d+1}\right)^{-m_2-1}{}_2F_1\left(m_2+m_d; 1+m_d; 2+m_d; \frac{-m_d\omega_2}{\gamma_{th}m_2\omega_d}\right)}\right) \\ &\quad \times (1-P_{\text{out}}). \end{aligned} \tag{4.23}$$

The result in (4.23) is new and has not been reported in the literature before. These expressions are very useful to evaluate the average capacity performance analysis of the system under study. Moreover, they are simple, accurate and very useful to evaluate the ACC performance analysis of the system under study.

4.6 Numerical and Simulation Results

In this section, we provide numerical and simulation results for the expressions derived in this chapter for arbitrary values of the Nakagami-m fading parameters for the different transmission protocols. Without loss of generality we assume that $P_S = P_R = P_{ri} = P_{di} = 1$. The simulation results are obtained using MonteCarlo

simulation method, with number of runs equal to $1,000,000$ times. The simulation has been done by simulating the PDF and the SIR that has been used in this chapter to derive the closed-form expressions of ACC under different adaptive transmission protocols, and then substitute them properly in the ACC general formula of each transmission protocol.

Fig. 4.2 shows a comparison for the normalized channel capacity under all of the adaptive transmission protocols. The ORA is the best protocol among all of the prescribed policies in terms of the achievable channel capacity with a small improvement over the OPRA transmission policy. The simulation also presented in the figure to verify the accuracy of the obtained results.

In Fig. 4.3, the normalized average channel capacity per unit bandwidth according to the ORA transmission policy is presented assuming the Nakagami-m fading channel model for different combinations of the fading parameters. As the fading parameters increase, the amount of fading decreases, and, hence, the capacity increases as expected.

The normalized capacity per unit bandwidth according to the simultaneous optimal and rate adaptation policy (OPRA) is shown in Fig. 4.4 at the threshold SIR equal to 2 dB. The figure shows that as the fading parameters increase, the amount of fading decreases, and, hence, the capacity increases as expected.

In Fig. 4.5, the normalized average channel capacity per unit bandwidth [Bit/sec/Hz] versus the average SIR, for a wireless communication system over the Nakagami-m fading channel model with the channel inversion with fixed rate protocol (CIFR) for a different fading parameters. As the fading parameters increase, the amount of

fading decreases, and, hence, the capacity increases as expected.

In Fig. 4.6, the normalized average channel capacity per unit bandwidth [Bit/sec/Hz] versus the average SIR, for a wireless communication system over the Nakagami-m fading channel model with the truncated channel inversion with fixed rate protocol (TIFR) for a different fading parameters. The figure shows that as the fading parameters increase, the amount of fading decreases, and, hence, the capacity increases as expected.

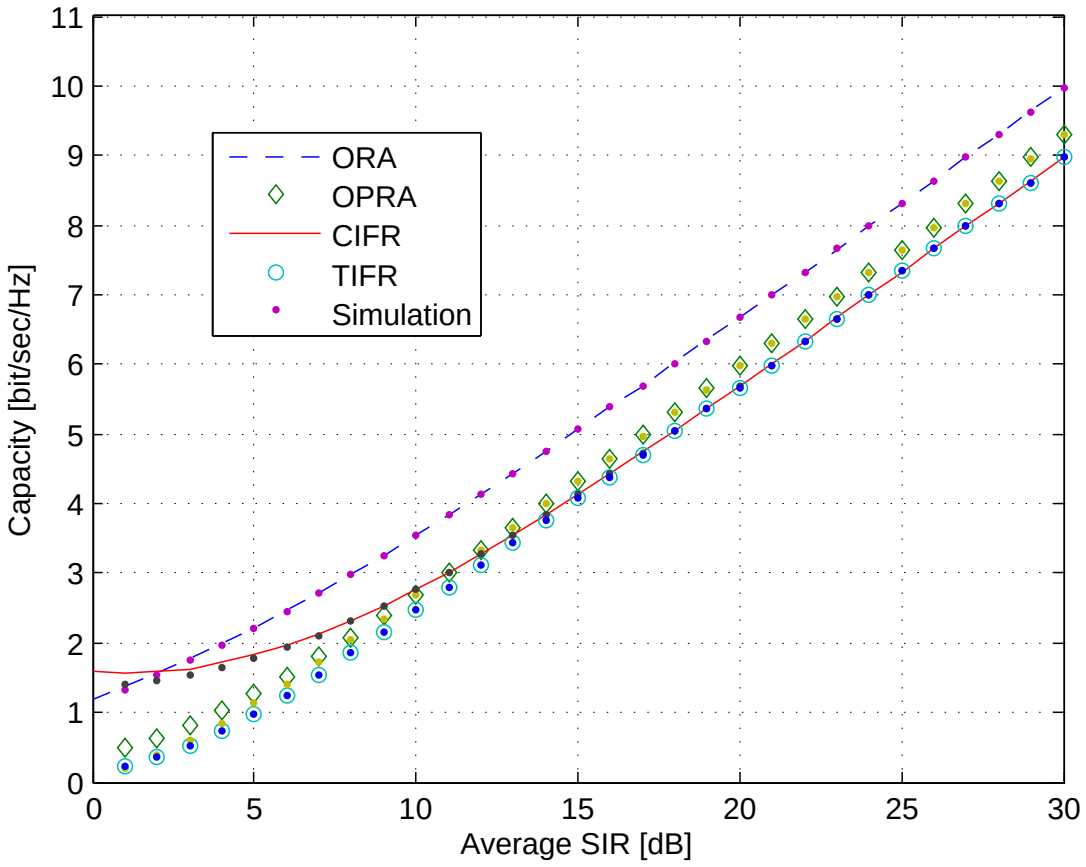

Figure 4.2. The normalized average channel capacity per unit bandwidth [Bit/sec/Hz] for the all transmission protocols versus the average SIR in dB for wireless communication system over the Nakagami-m fading channels with multiple CCI.

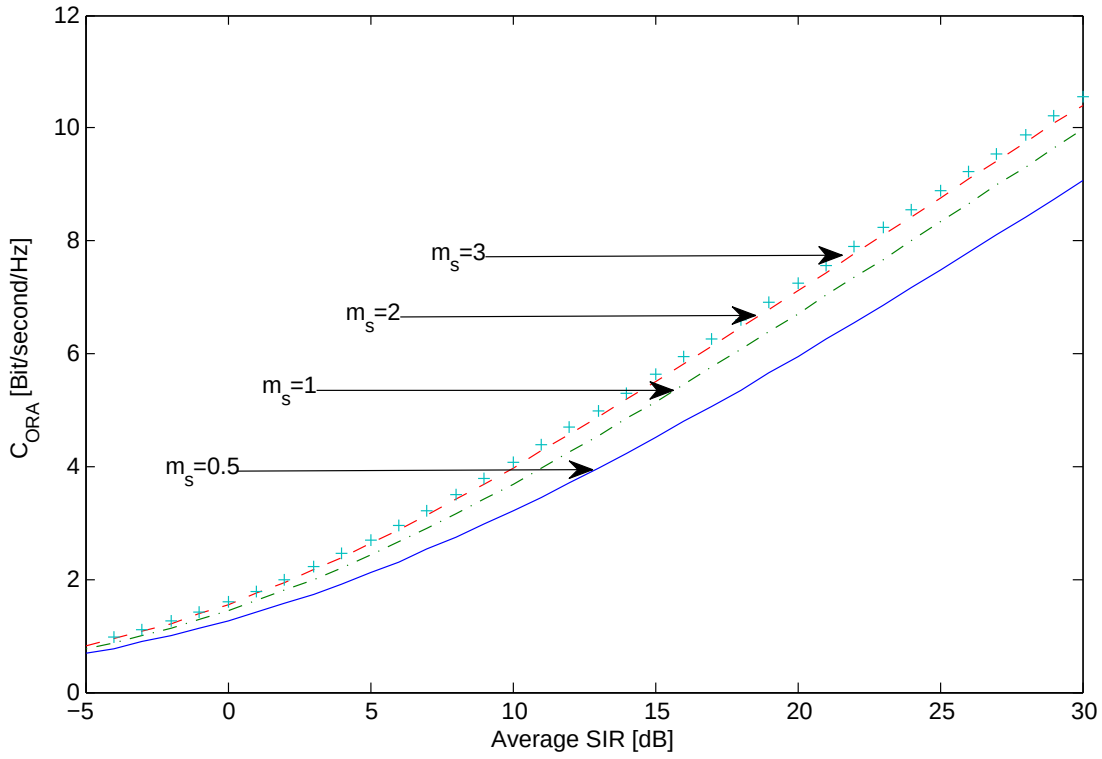

Figure 4.3. The normalized average channel capacity per unit bandwidth [Bit/sec/Hz] versus the average SIR, for a wireless communication system over the Nakagami-m fading channel model with optimal rate adaptation and fixed power protocol (ORA) for a different fading parameters.

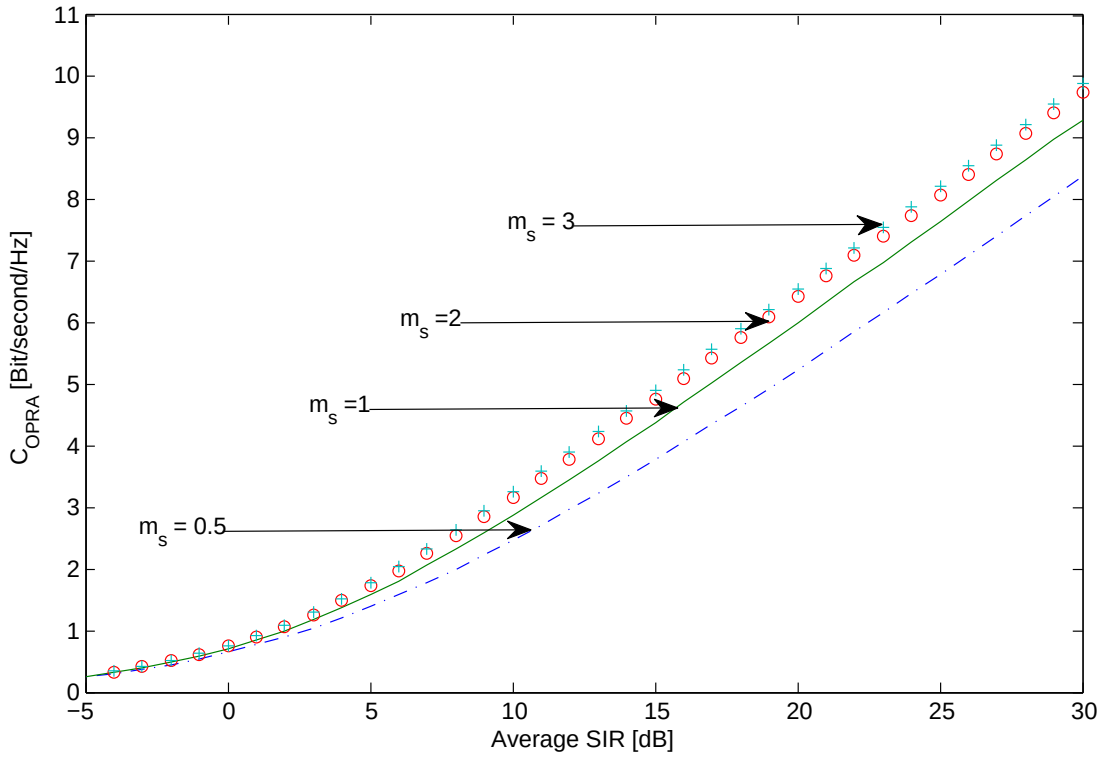

Figure 4.4. The normalized average channel capacity per unit bandwidth [Bit/sec/Hz] versus the average SIR, for a wireless communication system over the Nakagami-m fading channel model with simultaneous optimal power and rate adaptation protocol (OPRA) for a different fading parameters.

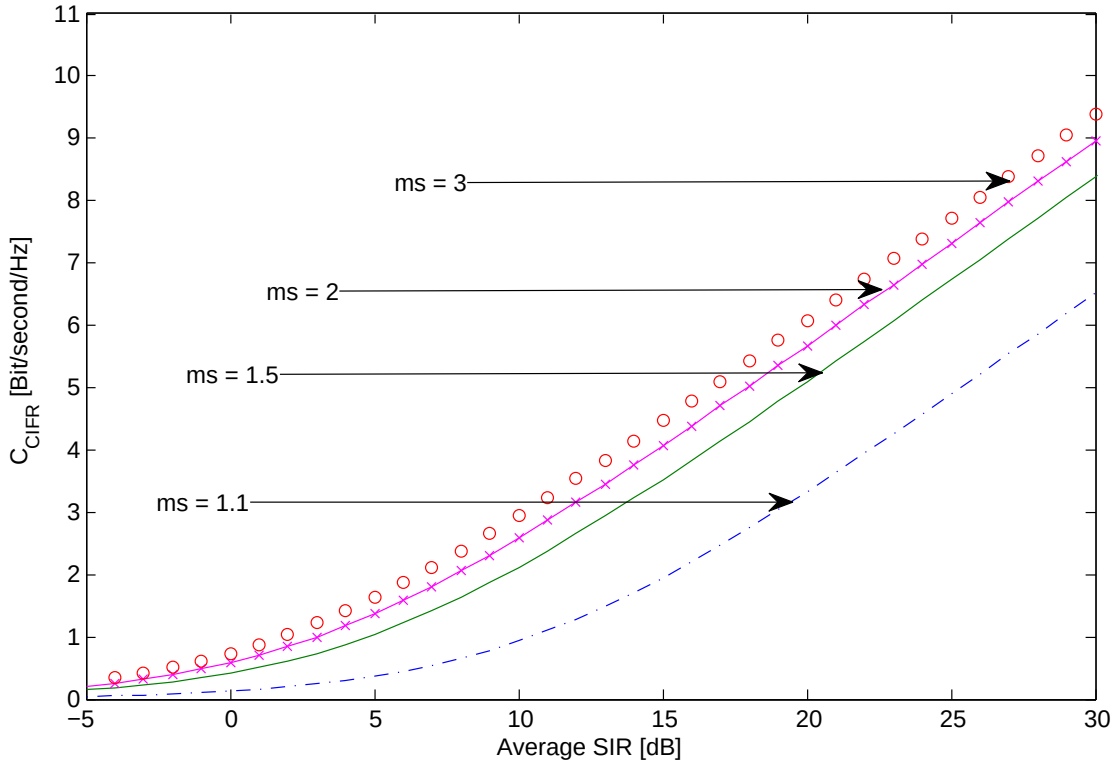

Figure 4.5. The normalized average channel capacity per unit bandwidth [Bit/sec/Hz] versus the average SIR, for a wireless communication system over the Nakagami-m fading channel model with the channel inversion with fixed rate protocol (CIFR) for a different fading parameters.

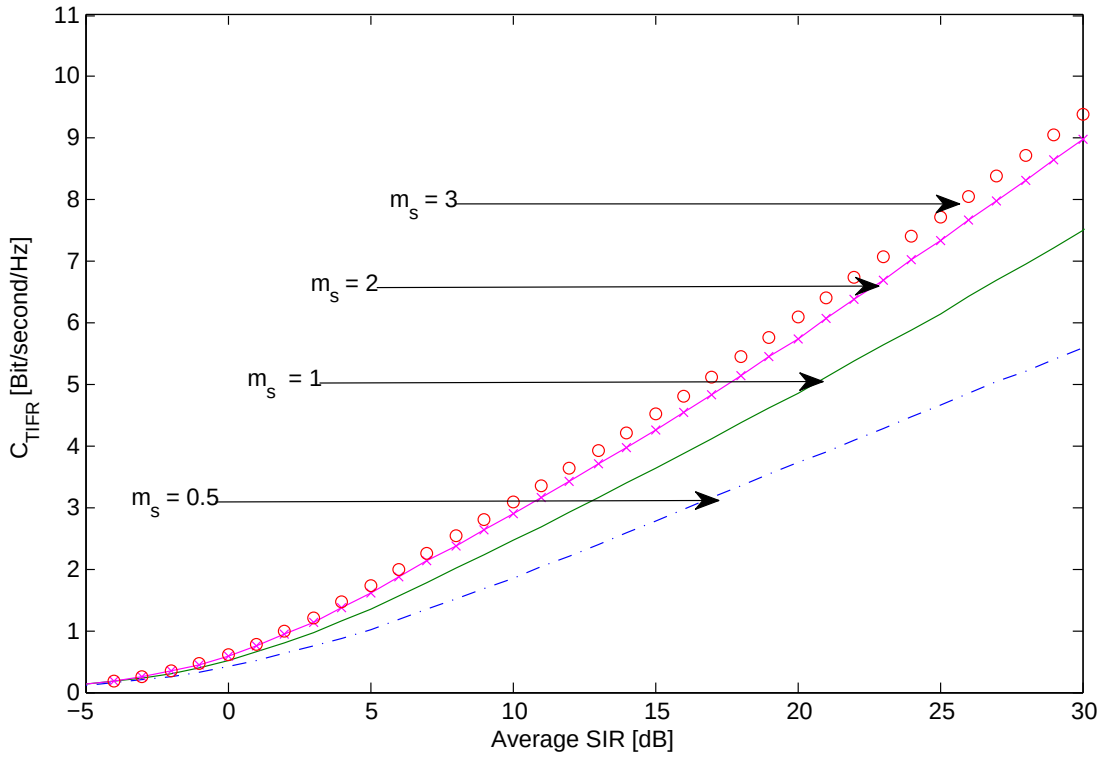

Figure 4.6. The normalized average channel capacity per unit bandwidth [Bit/sec/Hz] versus the average SIR, for a wireless communication system over the Nakagami-m fading channel model with truncated channel inversion with fixed rate protocol (TIFR) for a different fading parameters.

The above results are very useful to evaluate the ACC performance analysis of the system under study. In general, as the channel conditions improve, the amount of fading decreases, and the normalized channel capacity increases regardless of the transmission policy adopted. such analysis is very important for wireless communication systems engineering design process.

4.7 Conclusions

In this chapter, we considered a wireless communication system over the Nakagami-m small-scale fading channels with multiple CCI at both the destination nodes. Assuming that the system operates in presence of (i.n.i.d.) Nakagami-m fading channels with arbitrary (integer and non-integer) values of fading parameter m, highly accurate approximated closed-form expressions for the average channel capacity (ACC) for different adaptive transmission protocols are derived. The normalized channel capacity different transmission protocols; the optimal rate adaptation with fixed transmitted power (ORA), the simultaneous power and rate adaptation transmission (OPRA), the truncated channel inversion with fixed rate transmission protocol (TIFR), and the channel inversion with fixed rate transmission protocol (CIFR). Having such a study with the enables system engineers and designers to optimize their designs before actual deployment in real situations and save the cost that may occur according to mistakes in system hardware implementation.

Chapter 5

DUAL-HOP DF COOPERATIVE SYSTEMS WITH DIVERSITY: BER PERFORMANCE ANALYSIS

5.1 Overview

In this chapter, the work extended to the case when the receiver employs the maximum ratio combining (MRC) and the equal gain combining (EGC) combining schemes to exploit the diversity gain in multipath fading channels. The effect of MRC and the EGC diversity on the system BER performance analysis was considered with k elements at the receiver antenna, and the results show that for a given BER, increasing K decreases the required SIR. So, the system performance can be improved by saving the energy of the transmitted signal. We analyze the average BER performance of an multipath interference-limited dual-hop DF relaying cooperative system with multiple co-channel interferers at both relay and destination nodes and subject to independent and both identical (i.i.d.) and non identical distributed (i.n.i.d.) Nakagami-m fading channels with arbitrary values of the fading severity

parameter m (integers and non-integers).

The remainder of this chapter is organized as follows. In sections 5.2 and 5.3, the related work and contributions to the chapter are summarized. In Section 5.5 the BER derivation extended to the case when the receiver employs the maximum ratio combining scheme to exploit the diversity gain. In Section 5.6 the BER derivation extended to the case when the receiver employs the equal gain combining scheme to exploit the diversity gain. In Section 5.7, we present the numerical and simulation results to quantitatively assess and verify the accuracy of our obtained expressions. Finally some conclusions are drawn in section 5.8.

5.2 Related Work

A large amount of published research papers reported in the literature have considered performance analysis of cooperative relaying wireless communication systems, both the AF and DF types, under different system models. Many of them focused on the capacity, diversity gain, BER, and outage performance analysis, over fading channel environments. In [1], the authors present an exact average symbol error rate analysis for the distributed spatial diversity wireless system with k amplifying relays in a Rayleigh-fading environment. The average symbol error rate formula clearly illustrates the advantage that the distributed diversity system has in overcoming the severe penalty in signal-to-noise ratio caused by Rayleigh fading. In [5], the lower-bound SER performance of cooperative digital communication schemes is investigated, where multiple dual-hop relays are invoked for achieving the cooperative

diversity with the aid of the maximal ratio combining (MRC). A range of closed-form expressions are obtained for the probability density functions (PDFs) of the relay-channels output signal-to-noise ratio (SNR). Accurate approximate closed-form expressions are derived for computing the SER. Using the closed-form expressions obtained in this contribution, the SER performance of the relay-assisted digital communications schemes, which may employ various classes of coherent modulations, can be readily evaluated in the context of a variety of fading scenarios that the cooperative signals might experience. In [31], the author derived closed-form expressions for the average BER of both coherent and non-coherent binary frequency-shift keying (BFSK) and binary phase shift keying (BPSK) modulation schemes in an interference-limited wireless communication system. The analysis assumes an arbitrary number of independent and identically distributed Nakagami-m interferers. The study extended to investigate the effect of maximal ratio combining diversity technique at the receiver end. In [6], the authors focus on the diversity order of the DF cooperative networks with relay selection. Many detection schemes have been proposed for the DF; but it has been shown that the cooperative maximum ratio combining (C-MRC) can achieve almost the same performance as the optimum maximum likelihood detector and has a much lower complexity. Therefore, they first combine the C-MRC with the relay selection and show that it achieves the full diversity order by deriving an upper bound of its BER. In order to reduce the signaling overhead, they then combine the link-adaptive regeneration (LAR) with the relay selection by deriving an upper bound of the BER. In [4], the author evaluates outage performance of a cooperative transmission protocol over fading channels that requires a number of

relaying nodes to employ a distributed space-time coding scheme. Diversity provided by this technique has been widely analyzed for the Rayleigh fading case. However, ad-hoc and sensor networks often experience propagation environments where the line-of-sight component is either non-zero or, in some cases, dominates compared to the random non-line-of-sight components. By considering the Nakagami-m as a generic framework for describing the statistic of fading impairments, the author evaluates a set of fading inequalities that define settings where the benefits of collaborative transmission from multiple relays when fading parameters vary. In [7], the authors examine the SER performance of DF cooperative communications. They focus on the scenario in which multiple dual-hop relays are employed and the channel environment is described by Nakagami-m fading. Cooperative diversity is observed from the derived error-rate expressions, and some insight into how channel conditions in the relay nodes affect the SER performance is obtained. In addition, with the knowledge of the partial channel state information (CSI) at the transmitting sides, they derive an optimal power allocation scheme to further enhance the SER performance. In [18], the decouple-and-forward (DCF) relaying for dual-hop Alamouti transmissions is proposed as enhanced AF relaying to achieve spatial diversity gain especially provided by a two-antenna relay. DCF relaying that consists of decoupling, re-encoding and amplifying needs a little more complicated relay than AF relaying but a less complicated one than DF relaying. Assuming uncorrelated Rayleigh fading channels, the authors derive a probability density function (PDF) of end-to-end signal-to-noise ratio (SNR) for the DCF system and provide its BER performance.

5.3 Contributions

In this chapter, the work extended to the case when the receiver employs the most common diversity techniques; maximum ratio (MRC) and equal gain combining (EGC) schemes to exploit the diversity gain in DF cooperative communication system with multipath fading channel. The effect of both MRC and EGC diversity on the system BER performance analysis was considered with k finger at the destination receiver antenna. We derive closed-form BER expressions for i.n.i.d Nakagami-m branches (or finger) with an MRC combiner. Each branch, has an arbitrary fading parameters. We consider the uncorrelated independent branches in evaluating the BER at the MRC combiner output. In addition to that, we also derive another BER at the EGC combiner output. Also, we provide numerical and simulation results to show the accuracy of the derived expressions. Finally, we extend the BER analysis to cover different binary and M-ary modulation schemes.

5.4 System and signal Models

We consider an interference-limited dual-hop DF relaying cooperative wireless communication system operating over independent and non identical distributed (i.n.i.d.) Nakagami-m multipath fading channels with arbitrary integer as well as non-integer fading severity parameter m and with multiple CCI at both R and D nodes, where a source node (S) communicates with D using R as shown in fig. 5.1. The communication is performed in two time slots and no direct link between S and D is assumed to be available due to sever channel impairments conditions. The signal on the direct

link between the source and destination nodes is assumed to be insignificant and is ignored in our analysis. This assumption is practical due to sever channel impairments conditions, which justifies cooperative communication. We assumed both R and D operate in interference-limited conditions; i.e., the channel noise is dominated by the total interfering signals. Multiple co-channel N_R and N_D interferers are assumed to be present at R and D, respectively. Each one of the N_R (or N_D) interfering signals (i.e., ith interfering signal, where $i = 1, 2, \cdots, N_R$ (or $i = 1, 2, \cdots, N_D$)) has an average transmit power P_{ri} (or P_{di}), fading severity parameter m_{ri} (or m_{di}), fading power parameter Ω_{ri} (or Ω_{di}), and experiences link fading coefficient h_{ri} (or h_{di}). Let the modulated signal transmitted by S, during the first time slot, denoted by S_S with transmit power P_S. Then the received signal at R in the first time slot is given by

$$y_R = \sum_{j=1}^{N_{m1}} \sqrt{P_S} h_{1j} S_S + \sum_{i=1}^{N_R} \sqrt{P_{ri}} h_{ri} S_{ri}, \qquad i = 1, 2, \cdots, N_R \tag{5.1}$$

and the received signal at D in the second time slot is given by

$$y_D = \sum_{j=1}^{N_{m2}} \sqrt{P_R} h_{2j} S_R + \sum_{i=1}^{N_D} \sqrt{P_{di}} h_{di} S_{di}, \qquad i = 1, 2, \cdots, N_D \tag{5.2}$$

where N_{m1} and N_{m2} are the total number of the multipath channels of the first and the second hop, respectively. h_1, and h_2 are the channel gain coefficients of the first and the second hop with fading severity parameter m_1 and m_2, and fading power parameter Ω_1 (or Ω_2), respectively. All of h_{ri}, h_{di}, h_{1j}, and h_{2j} are i.n.i.d. Nakagami-m random variables. In (5.1) and (5.2), S_R is the transmitted symbol from R to D with transmit power P_D, S_{ri} is the transmitted symbol from ith interferer to R with transmit power P_{ri}, and S_{di} is the transmitted symbol from ith interferer to D with

transmit power P_{di}. The transmitted symbols S_S and S_R and the interfering symbols S_{ri} and S_{di} are assumed to be mutually independent and uniformly distributed with zero mean and unit variance. The fading channels average power parameters are given by

$$\Omega_{1j} = E[|h_{1j}|^2], \tag{5.3}$$

$$\Omega_{2j} = E[|h_{2j}|^2], \tag{5.4}$$

$$\Omega_{ri} = E[|h_{ri}|^2], \tag{5.5}$$

and

$$\Omega_{di} = E[|h_{di}|^2]. \tag{5.6}$$

The SIR is the ratio between the transmitted signal power and the total interference power. So, at R the SIR is simply given by

$$\gamma_R = \frac{\sum_{j=1}^{N_{m1}} P_S |h_{1j}|^2}{\sum_{i=1}^{N_R} P_{ri} |h_{ri}|^2}, \tag{5.7}$$

and at D is given by

$$\gamma_D = \frac{\sum_{j=1}^{N_{m2}} P_R |h_{2j}|^2}{\sum_{i=1}^{N_D} P_{di} |h_{di}|^2}. \tag{5.8}$$

Since h_{ri}, h_{di}, h_{2j}, and h_{1j} are i.n.i.d. Nakagami-m random variables, then the square of each of the fading coefficients h_{ri}, h_{di}, h_{2j}, and h_{1j} follows Gamma distribution. Also, the summation of Gamma random variables is accurately approximated by another Gamma random variable with different fading parameter and fading power coefficient according to [40] and [24]. So, according to the above the, each of γ_R in (5.7) or γ_D in (5.8) expression is a ratio of two normalized Gamma random variables, which is given as F-distribution [24].

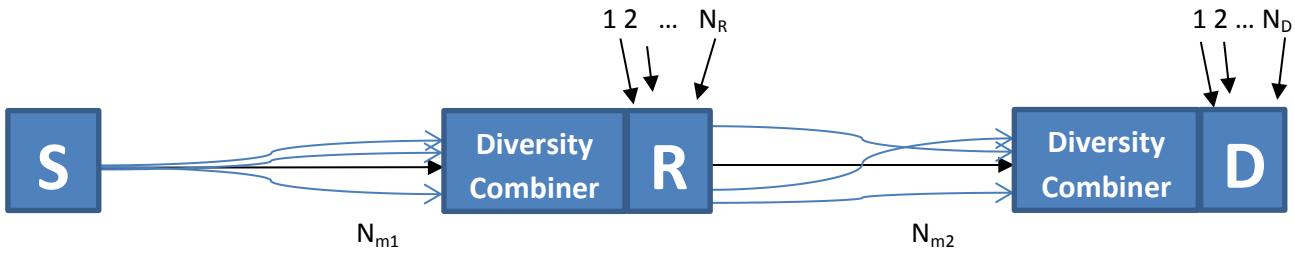

Figure 5.1. A dual-hop DF relaying cooperative wireless communication system over Nakagami-m multipath fading channels with multiple CCI at both the relay and the destination nodes.

5.5 Maximal Ratio Combining (MRC) Diversity Analysis

In receiver diversity the independent fading paths associated with multiple receive antennas are combined to obtain a better resultant signal. The maximal ratio combining (MRC) diversity is one of the most effective techniques that is commonly used to combat the bad effect of the multiple CCI and multipath fading channels in wireless communication systems. In maximal ratio combining (MRC) the output is a weighted sum of all branches, so the $\alpha_i s$ in figure 5.2 are all non zero.

The equivalent SIR γ_e at the output of the MRC combiner is given by [135]

$$\gamma_e = \sum_{l=1}^{K} \gamma_{D_l}. \tag{5.9}$$

Using the same previous procedure in section (2.4), which used to approximate the pdf of the SIR , the pdf of γ_e is approximated as

$$\begin{aligned} f_{\gamma_e}(\gamma_e) &= \frac{\Gamma(m_e+m_d)}{\Gamma(m_e)\Gamma(m_d)} \left(\frac{m_e}{m_d}\right)^{m_e} \left(\frac{P_d\omega_d\gamma_e}{P_S\Omega_e}\right)^{m_e-1} \\ &\quad \times \left(1+\frac{m_e}{m_d}\frac{P_d\omega_d\gamma_e}{P_S\Omega_e}\right)^{-(m_e+m_d)}, \end{aligned} \tag{5.10}$$

where m_e and Ω_e are the fading shape and power parameters of the received signal at the output of the MRC combiner, respectively, and they can be given as follows.

$$\Omega_e = \sum_{l=1}^{K} \Omega_{D_l} = E[\xi_D], \tag{5.11}$$

$$m_e = \frac{(\Omega_e)^2}{E[{\xi_{D_l}}^2] - (\Omega_e)^2}, \tag{5.12}$$

where $\xi_D = \sum_{l=1}^{K} |h_{Dl}|^2$. The moments of ξ_D can be calculated by means of the multinomial expansion given as

$$\begin{aligned} E[(\xi_D)^n] \;=\; & \sum_{p=0}^{n}\sum_{j=0}^{p}\cdots\sum_{l=n_{K-1}}^{n_{K-2}} \binom{n}{p}\binom{p}{j}\cdots\binom{n_{K-2}}{n_{K-1}} \\ & \times E[|h_{D1}|^{2(n-p)}]E[|h_{D2}|^{2(p-j)}] \\ & \times \cdots E[|h_{DK}|^{2(n_{K-1})}], \end{aligned} \tag{5.13}$$

the $E[|h_{Dl}|^n]$ is given by

$$E[|h_{Dl}|^n] = \frac{\Gamma(m_{dl} + n/2)}{\Gamma(m_{dl})}\binom{\Omega_{dl}}{m_{dl}}^{\frac{n}{2}}, \qquad l = 1, 2, 3, \cdots, K. \tag{5.14}$$

Using the same previous steps that have been used in section (2.4) to derive the average BER for different modulation schemes, we get the following results:

$$\begin{aligned} \overline{P}_{e1}^{BPSKMRC} = 0.5 - & \frac{\Gamma(m_e + m_r)\Gamma(m_e + 0.5)\sqrt{\pi}}{\Gamma(m_1)\Gamma(m_r)\cos(\pi m_r)} \left(\frac{\left(\frac{P_S\Omega_e m_r}{m_1 P_r \omega_r}\right)^{m_r}}{2m_r\Gamma(m_r + 0.5)\Gamma(m_1 + 0.5)} \right) \\ & \times {}_2F_2\left(m_r, m_r + m_1; m_r + 1, m_r + 0.5; \frac{P_S\Omega_e m_r}{m_1 P_r \omega_r}\right) \\ & - \frac{\Gamma(m_1 + m_r)\Gamma(m_1 + 0.5)\sqrt{\pi}}{\Gamma(m_1)\Gamma(m_r)\cos(\pi m_r)} \left(\frac{{}_2F_2\left(0.5, m_1 + 0.5; 1.5, 1.5 - m_r; \frac{P_S\Omega_e m_r}{m_1 P_r \omega_r}\right)\sqrt{\frac{P_S\Omega_e m_r}{m_1 P_r \omega_r}}}{\Gamma(m_1 + m_r)\Gamma(1.5 - m_r)} \right) \end{aligned} \tag{5.15}$$

$$\overline{P}_{e2}^{BPSKMRC} = 0.5 - \frac{\Gamma(m_e+m_d)\Gamma(m_e+0.5)\sqrt{\pi}}{\Gamma(m_e)\Gamma(m_d)\cos(\pi m_d)}\left(\frac{\left(\frac{P_S\Omega_e m_d}{m_e P_d\omega_d}\right)^{m_d}}{2m_d\Gamma(m_d+0.5)\Gamma(m_e+0.5)}\right)$$
$$\times {}_2F_2\left(m_d, m_d+m_e; m_d+1, m_d+0.5; \frac{P_S\Omega_e m_d}{m_e P_d\omega_d}\right)$$
$$-\frac{\Gamma(m_e+m_d)\Gamma(m_e+0.5)\sqrt{\pi}}{\Gamma(m_e)\Gamma(m_d)\cos(\pi m_d)}\left(\frac{{}_2F_2\left(0.5, m_e+0.5; 1.5, 1.5-m_d; \frac{P_S\Omega_e m_d}{m_e P_d\omega_d}\right)\sqrt{\frac{P_S\Omega_e m_d}{m_e P_d\omega_d}}}{\Gamma(m_e+m_d)\Gamma(1.5-m_d)}\right) \quad (5.16)$$

$$\overline{P}_{e1}^{DBPSKMRC} = \frac{\Gamma(m_1+m_r)}{2\Gamma(m_r)}U\left(m_1; 1-m_r; \frac{P_S\Omega m_r}{m_1 P_r\omega_r}\right), \quad (5.17)$$

$$\overline{P}_{e2}^{DBPSKMRC} = \frac{\Gamma(m_e+m_d)}{2\Gamma(m_d)}U\left(m_e; 1-m_d; \frac{P_R\Omega_e m_d}{m_e P_d\omega_d}\right), \quad (5.18)$$

$$\overline{P}_{e1}^{NCBFSKMRC} = \frac{\Gamma(m_1+m_r)}{2\Gamma(m_r)}U\left(m_1; 1-m_r; \frac{P_S\Omega m_r}{2m_1 P_r\omega_r}\right). \quad (5.19)$$

and

$$\overline{P}_{e2}^{NCBFSKMRC} = \frac{\Gamma(m_e+m_d)}{2\Gamma(m_d)}U\left(m_e; 1-m_d; \frac{P_R\Omega_e m_d}{2m_e P_d\omega_d}\right). \quad (5.20)$$

For DF dual hop system, the end-to-end bit error occurs according to two events as in Table (2.1) The end-to-end average BER is given by [130, Eq. (11.4.12)] as

$$\overline{P}_e^{MRC} = P_{e1}^{MRC} + P_{e2}^{MRC} - 2P_{e1}^{MRC}P_{e2}^{MRC} \quad (5.21)$$

where P_{e1} is the average BER related to the first hop, and P_{e2} is the average BER related to the second hop of the system under study. By a proper substituting in (5.21), the end-to-end BER of DF dual hop system with MRC diversity combining technique in multipath fading channel can be evaluated.

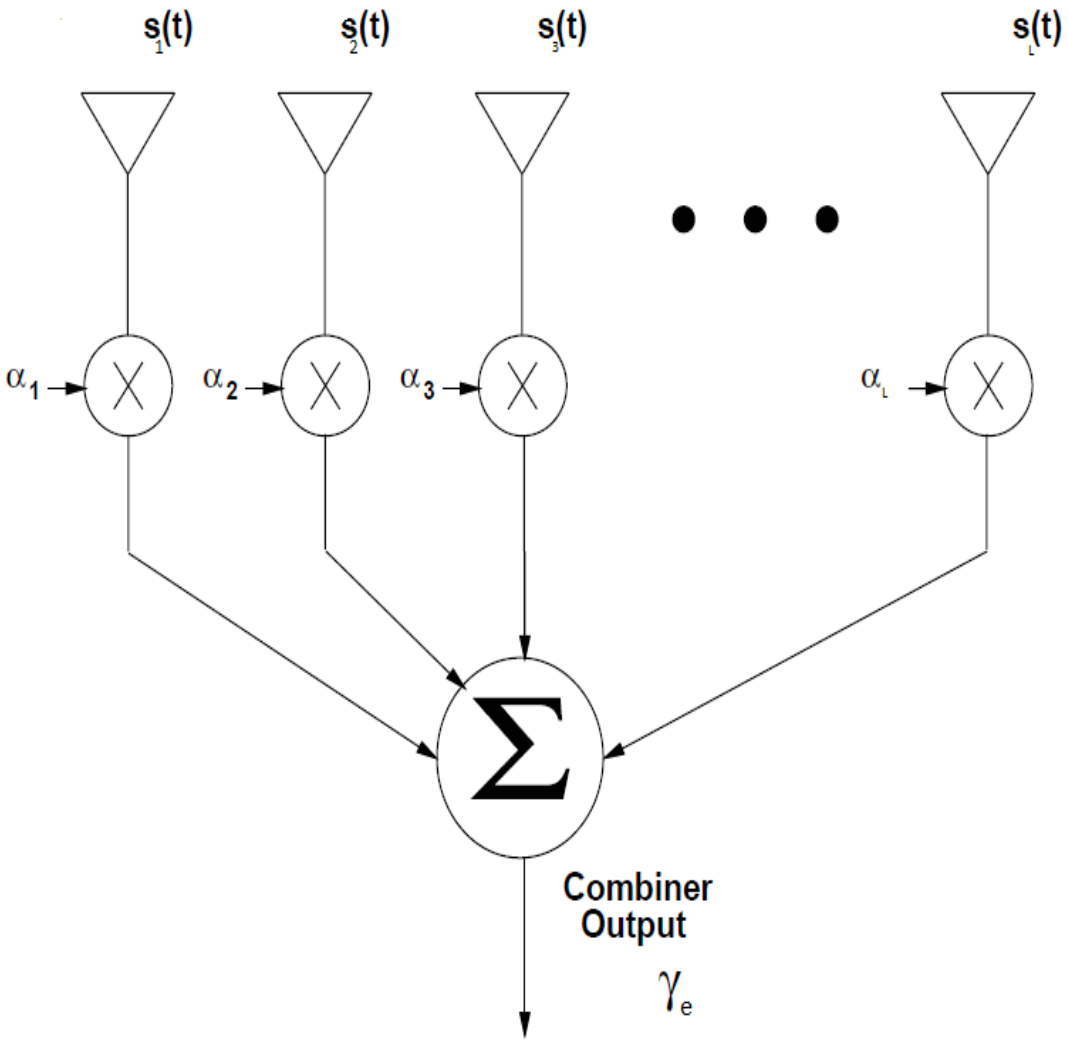

Figure 5.2. Receiver diversity combiner diagram.

5.6 Equal-Gain Combining (EGC) Diversity Analysis

The MRC requires knowledge of the time-varying SIR on each branch, which can be very difficult to measure. A simpler technique is equal-gain combining, which co-phases the signals on each branch and then combines them with equal weighting, so the $\alpha_i s$ in figure 5.2 are all equal. We extend the previous average BER performance analysis to include the effect of K-order EGC diversity in a multipath interference-limited dual-hop system with independent and non-identical Nakagami-m CCI fading channels.

The equivalent SIR γ_e at the output of the EGC combiner is given by [135]

$$\gamma_e = \frac{(\sum_{l=1}^{K} |h_{D_l}|)^2}{\sum_{i=1}^{N_D} |h_{di}|^2}, \qquad l = 1, 2, \cdots, K, \tag{5.22}$$

in (5.22) the $\sum_{l=1}^{K} |h_{D_l}|$ is approximated in [34] as a new Nakagami-m random variable with new fading shape and power parameters m_e and Ω_e, respectively. Using the same previous procedure in section (2.4) the pdf of γ_e is given by

$$\begin{aligned} f_{\gamma_e}(\gamma_e) &= \frac{\Gamma(m_e + m_d)}{\Gamma(m_e)\Gamma(m_d)} \left(\frac{m_e}{m_d}\right)^{m_e} \left(\frac{K P_d \omega_d \gamma_e}{P_S \Omega_e}\right)^{m_e - 1} \\ &\quad \times \left(1 + \frac{m_e}{m_d} \frac{K P_d \omega_d \gamma_e}{P_S \Omega_e}\right)^{-(m_e + m_d)}, \end{aligned} \tag{5.23}$$

where m_e and Ω_e are the fading shape and power parameters of the received signal at the output of the EGC combiner, respectively, and they can be given as follows

$$\Omega_e = \sum_{l=1}^{K} \Omega_{D_l} = E[\xi_D], \tag{5.24}$$

$$m_e = \frac{(\Omega_e)^2}{E[{\xi_{D_l}}^2] - (\Omega_e)^2}, \tag{5.25}$$

where $\xi_D = \sum_{l=1}^{K} |h_{Dl}|^2$. The moments of ξ_D can be calculated by means of the multinomial expansion given by [34]

$$\begin{aligned} E[(\xi_D)^n] &= \sum_{p=0}^{n} \sum_{j=0}^{p} \cdots \sum_{l=n_{K-1}}^{n_{K-2}} \binom{n}{p} \binom{p}{j} \cdots \binom{n_{K-2}}{n_{K-1}} \\ &\quad \times E[|h_{D1}|^{(n-p)}] E[|h_{D2}|^{(p-j)}] \cdots E[|h_{DK}|^{(n_{K-1})}], \end{aligned} \tag{5.26}$$

the $E[|h_{Dl}|^n]$ is given by

$$E[|h_{Dl}|^n] = \frac{\Gamma(m_{dl} + n/2)}{\Gamma(m_{dl})} \binom{\Omega_{dl}}{m_{dl}}^{\frac{n}{2}}, \qquad l = 1, 2, 3, \cdots, K. \tag{5.27}$$

Using the same previous steps that have been used in section (2.4) to derive the average BER for different non-coherent modulation schemes, we get the following results:

$$\overline{P}_{e1}^{DBPSKEGC} = \frac{\Gamma(m_1+m_r)}{2\Gamma(m_r)} U\left(m_1; 1-m_r; \frac{P_S \Omega m_r}{m_1 K P_r \omega_r}\right), \tag{5.28}$$

$$\overline{P}_{e2}^{DBPSKEGC} = \frac{\Gamma(m_e+m_d)}{2\Gamma(m_d)} U\left(m_e; 1-m_d; \frac{P_R \Omega_e m_d}{m_e K P_d \omega_d}\right), \tag{5.29}$$

$$\overline{P}_{e1}^{NCBFSKEGC} = \frac{\Gamma(m_1 + m_r)}{2\Gamma(m_r)} U\left(m_1; 1-m_r; \frac{P_S \Omega m_r}{2m_1 K P_r \omega_r}\right). \tag{5.30}$$

and

$$\overline{P}_{e2}^{NCBFSKEGC} = \frac{\Gamma(m_e + m_d)}{2\Gamma(m_d)} U\left(m_e; 1-m_d; \frac{P_R \Omega_e m_d}{2m_e K P_d \omega_d}\right). \tag{5.31}$$

The end-to-end average BER is then given by [130, Eq. (11.4.12)] as

$$\overline{P}_e^{EGC} = P_{e1}^{EGC} + P_{e2}^{EGC} - 2P_{e1}^{EGC} P_{e2}^{EGC} \tag{5.32}$$

where P_{e1} is the average BER related to the first hop, and P_{e2} is the average BER related to the second hop of the system under study. By a proper substituting in (5.32), the end-to-end BER of a DF dual hop system with EGC diversity combining technique can be evaluated.

5.7 Numerical and Simulation Results

In this section, we provide numerical and simulation results for the expressions that have been derived in this chapter for arbitrary values of the Nakagami-m fading parameters. Without loss of generality we assume that $P_S = P_R = P_{ri} = P_{di} = 1$. The simulation results are obtained using MonteCarlo simulation method, with number of runs equal to $1,000,000$ times. Fig. 5.3 shows the BER versus SIR for BPSK of interference-limited DF dual hop wireless communication system with three interferers at both the relay and the destination node over Nakagami-m fading channels with arbitrary values of m (i.e., $N_R = 3$, $N_D = 3$ with $me = 1, 2$, and 4, $m_{di} = 1$, $m_{ri} = 1$, $\Omega_1 = 1.5$, $\Omega_2 = 1.3$, $\Omega_{di} = 1.1$, $\Omega_{ri} = 1.2$) and with different MRC diversity order K (i.e., $K = 1$, 2, 4). The figure shows that the BER decreases with the increasing of the MRC diversity order K. Also, it shows that for a given BER, increasing K decreases the required SIR. So, the system performance can be improved by saving the energy of the transmitted signal. Fig. 5.4 shows the BER versus SIR for BFSK and DBPSK of interference-limited DF dual hop wireless communication system with three interferers at both the relay and the destination node over Nakagami-m fading channels with arbitrary values of m (i.e., $N_R = 3$,

$N_D = 3$ with $me = 1, 2$, and 4, $m_{di} = 1$, $m_{ri} = 1$, $\Omega_1 = 1.5$, $\Omega_2 = 1.3$, $\Omega_{di} = 1.1$, $\Omega_{ri} = 1.2$) and with different EGC diversity order K (i.e., $K = 1$, 2, 4). The figure shows that the BER decreases with the increasing of the EGC diversity order K. Also, it shows that for a given BER, increasing K decreases the required SIR. So, the system performance can be improved by saving the energy of the transmitted signal. These results are very useful to evaluate the error performance analysis for wireless communication systems engineering design process.

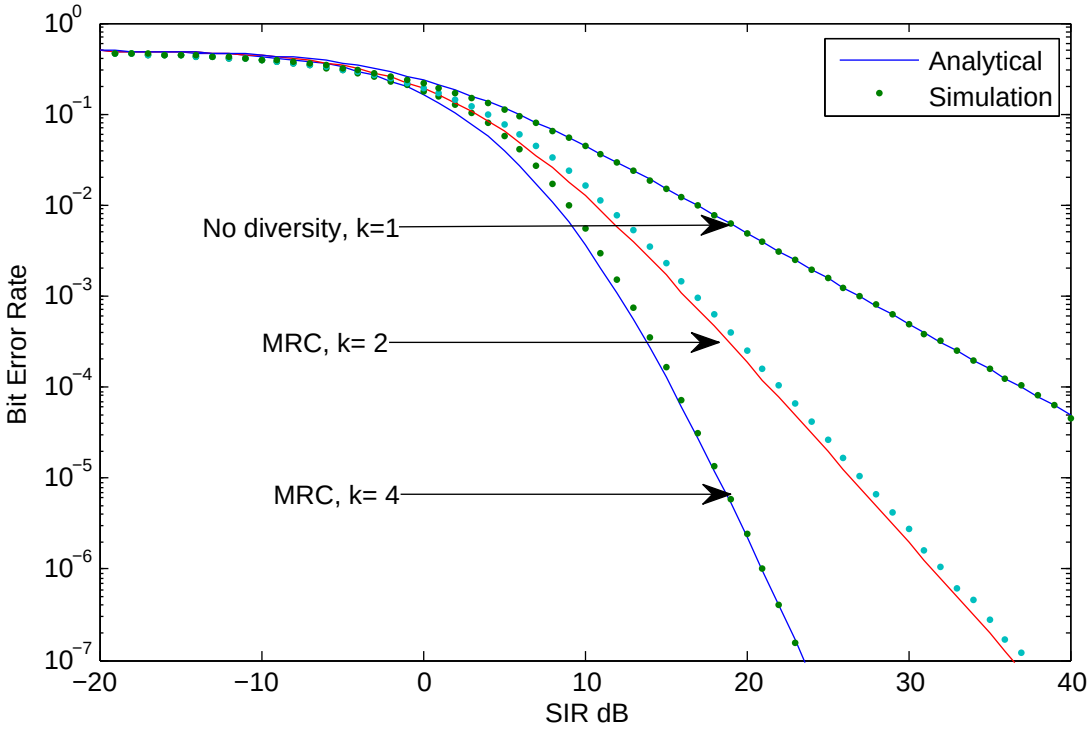

Figure 5.3. BER versus SIR for interference-limited BPSK DF dual hop wireless communication system with three interferers at both the relay and the destination node over Nakagami-m fading channels with different MRC diversity order K (i.e., K = 1, 2, 4).

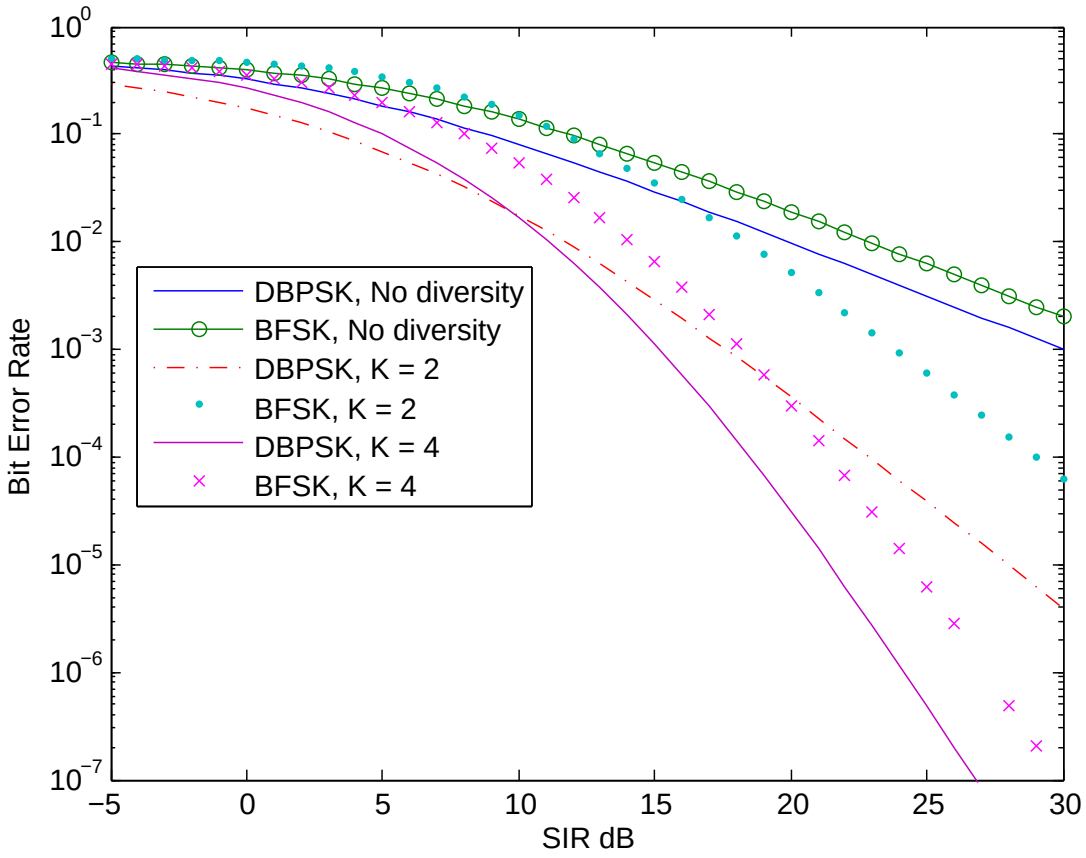

Figure 5.4. BER versus SIR for interference-limited BFSK and DBPSK DF dual hop wireless communication system with three interferers at both the relay and the destination node over Nakagami-m fading channels with different EGC diversity order K (i.e., K = 1, 2, 4).

5.8 Conclusions

The maximum ratio combining (MRC) and the equal gain combining (EGC) diversity effect on the interference-limited DF relaying system BER performance was investigated in multipath fading channel, and the results shows that for a given BER, increasing K decreases the required SIR. So, the system performance can be improved by saving the energy of the transmitted signal. Having such a study enables system engineers and designers to optimize their designs before actual deployment in real situations and save the time and cost that may occur according to mistakes in system hardware implementation.

Chapter 6

DUAL-HOP DF COOPERATIVE SYSTEMS WITH DIVERSITY: CAPACITY PERFORMANCE ANALYSIS

6.1 Chapter Overview

In this chapter, the work extended to the case when the receiver employs the maximum ratio combining (MRC) and the equal gain combining (EGC) combining schemes to exploit the diversity gain. The effect of MRC and the EGC diversity on the ACC performance analysis was considered with k elements at the receiver antenna, and the results show that for a given ACC, increasing K decreases the required SIR. So, the system performance can be improved by saving the energy of the transmitted signal.

In Section 6.2, the related work is summarized. The chapter contributions are provided in Section 6.3. In sections 6.5 and 6.6 the analysis based MRC and EGC are presented. We provide numerical and simulation results in section 6.7. Finally, the chapter conclusions are provided in section 6.8.

6.2 Related Work

In this section we introduce some of the research work reported in the literature that has been considered the ACC performance analysis of cooperative communication systems. In [31], the effect of cochannel interference on the performance of digital mobile radio systems in a Nakagami fading channel is studied. The performance of maximal ratio combining (MRC) diversity is analyzed in the presence of multiple equal-power cochannel interferers and additive white Gaussian noise. The results are expressed in terms of the confluent hypergeometric function of the second kind, a function that can be easily evaluated numerically. The analysis assumes an arbitrary number of independent and identically distributed Nakagami interferers. The same system model as in [119] was adapted by the authors in [120] under the same channel fading model but with diversity schemes, namely, the selection combining and the maximal ratio combining schemes. The channel capacity under the three power adaptation policies was also considered in [121] assuming Nakagami-m multipath fading with diversity combining at the receiver side. We assumed a single branch dual hop cooperation network, which includes a single source node, a single destination node, and a single relay node in between. There is no direct path between the source and destination nodes, the signal on the direct link between the source and destination nodes is assumed to be insignificant and is ignored in our analysis. This assumption is practical due to sever channel impairments conditions, which justifies cooperative communication. Nakagami-m fading channels with arbitrary values of the fading severity parameter m are assumed at each hop stage, namely the source-relay and

relay-destination stages. Multiple CCI are assumed at both nodes, namely relay and destination nodes, and subject to arbitrary Nakagami-m wireless fading channels. Unlike many studies reported in the literature which is restrict the cochannel interference to the relay node, we consider the Nakagami-m cochannel interference at both relay and destination nodes, also we assume arbitrary values of the fading parameters.

6.3 Contributions

In this chapter, the work extended to the case when the receiver employs the maximum ratio combining (MRC) and the equal-gain combining (EGC) schemes to exploit the diversity gain. The effect of MRC and the EGC diversity on the system BER performance analysis was considered with k elements at the receiver antenna. We derive closed-form expressions for the average channel capacity over the Nakagami-m fading model under different adaptive transmission protocols, namely, namely, the simultaneous power and rate adaptation protocol (OPRA), the optimal rate with fixed power protocol (ORA), the channel inversion with fixed rate protocol (CIFR), and the truncated channel inversion with fixed transmit power protocol (CTIFR). To the best of the authors' knowledge, the derived expressions in this chapter are new and have not been previously reported in the literature. In this chapter, we consider the average channel capacity performance analysis of interference-limited dual-hop DF relaying communication system with multiple CCI. Unlike many studies reported in the literature which is restrict the cochannel interference to the relay

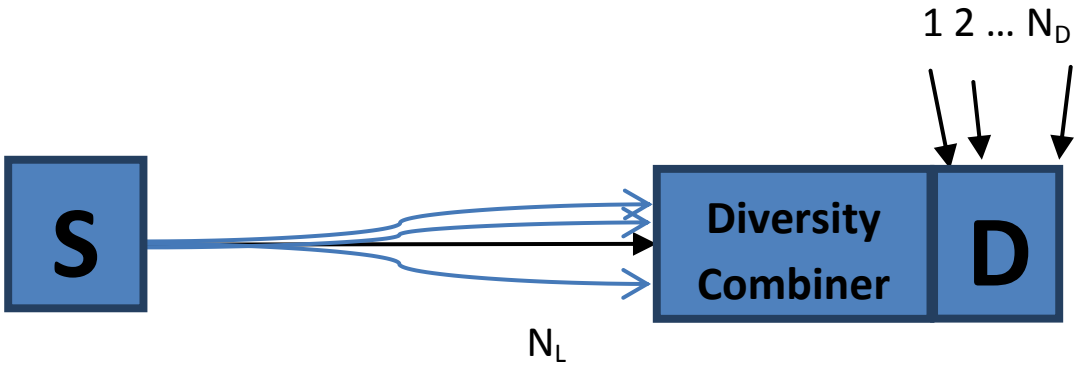

Figure 6.1. An interference-limited single-hop wireless communication system over multi-path Nakagami-m fading channels with multiple co-channel interference at the destination node.

node, we consider the Nakagami-m cochannel interference at both relay and destination nodes. The channels are assumed to experience fading modeled as independent but not necessarily identically distributed (i.n.i.d.) Nakagami-m with arbitrary (integer as well as non-integer) values of fading parameter, m. The signal on the direct link between the source and destination nodes is assumed to be insignificant and is ignored in our analysis. This assumption is practical due to sever channel impairments conditions, which justifies cooperative communication. We show numerical and simulation results to verify the accuracy of our derived expressions. In this chapter, many contributions have been achieved as follows.

6.4 System and signal Models

In this chapter we considered the same system and signal models in the previous chapter.

6.5 ACC with Maximal Ratio Combining (MRC) Diversity Analysis

We extend the previous ACC performance analysis to include the effect of the MRC diversity. Using the same previous procedure in the previous chapter the pdf of γ_e is given by

$$\begin{aligned} f_{\gamma_e}(\gamma_e) &= \frac{\Gamma(m_e+m_d)}{\Gamma(m_e)\Gamma(m_d)}\left(\frac{m_e}{m_d}\right)^{m_e}\left(\frac{P_d\omega_d\gamma_e}{P_S\Omega_e}\right)^{m_e-1} \\ &\quad\times\left(1+\frac{m_e}{m_d}\frac{P_d\omega_d\gamma_e}{P_S\Omega_e}\right)^{-(m_e+m_d)}, \end{aligned} \tag{6.1}$$

where the fading parameters in (6.1) are presented in the previous chapter. Using the same previous steps that have been used in the previous chapter to derive the ACC for different adaptive transmission protocols, The following results are obtained.

6.5.1 Optimal Rate Adaptation with Constant Transmit Power with MRC (ORA-MRC)

$$\begin{aligned} C_{\text{ora}}^{MRC} &= \frac{1}{\ln 2}\int_0^\infty \frac{\Gamma(m_e+m_d)}{\Gamma(m_e)\Gamma(m_d)}\left(\frac{m_e}{m_d}\right)^{m_e}\left(\frac{P_d\omega_d\gamma_D}{P_R\Omega_e}\right)^{m_e-1}\left(1+\frac{m_e}{m_d}\frac{P_d\omega_d\gamma_D}{P_R\Omega_e}\right)^{-(m_e+m_d)} \\ &\quad\times G_{2,2}^{1,2}\left(\gamma\middle|\begin{matrix}1,1\\1,0\end{matrix}\right)d\gamma, \end{aligned} \tag{6.2}$$

The integral in (6.11) can be solved with the help of [132, Eq. (7.811.5)] as

$$C_{\text{ora}}^{MRC} = \frac{1}{\Gamma(m_1)\Gamma(m_r)\ln 2}\; G_{3,3}^{2,3}\left(\frac{p_R\omega_e m_d}{p_d\omega_d m_e}\middle|\begin{matrix}1-m_e, 1, 1\\ m_d, 1, 0\end{matrix}\right), \tag{6.3}$$

The expression in (6.12) is new, novel, and has not been reported in the literature before, and valid for integer and non-integer values of the fading severity parameters. However, $m_d > 1$ is the only restriction on the result in (6.12).

6.5.2 Optimal Simultaneous Transmit Power and Rate Adaptation with MRC (OPRA-MRC)

$$C_{\text{opra}}^{MRC} = \frac{1}{\ln 2}\int_{\gamma_{th}}^{\infty} \ln\left(\frac{\gamma}{\gamma_{th}}\right) f_\gamma(\gamma) d\gamma, \tag{6.4}$$

$$\begin{aligned} C_{\text{opra}}^{MRC} &= \frac{1}{\ln 2}\int_{\gamma_{th}}^{\infty} \ln\left(\frac{\gamma}{\gamma_{th}}\right) \frac{\Gamma(m_e+m_d)}{\Gamma(m_e)\Gamma(m_d)} \left(\frac{m_e}{m_d}\right)^{m_e} \left(\frac{P_d\omega_d\gamma_D}{P_R\Omega_e}\right)^{m_e-1} \\ &\quad \times \left(1+\frac{m_e}{m_d}\frac{P_d\omega_d\gamma_D}{P_R\Omega_e}\right)^{-(m_e+m_d)} d\gamma, \end{aligned} \tag{6.5}$$

The integrals in (6.5) can be solved with the help of [132, Eq. 1.512.4] as

$$\begin{aligned} C_{\text{opra}}^{MRC} &= \lim_{\epsilon\to 0} \frac{\frac{\Gamma(m_e+m_d)}{\Gamma(m_e)\Gamma(m_d)}\left(\frac{m_e}{m_d}\right)^{m_e}}{\epsilon\,\ln 2} \\ &\quad \times \frac{\gamma_{th}^{-m_e}}{\left(\frac{m_eP_d\omega_d}{m_dP_R\Omega_e}\right)^{m_e+m_d}(m_e-\epsilon)} {}_2F_1\left(m_e+m_d, m_d-\epsilon; m_d-\epsilon+1; \frac{-1}{\left(\frac{m_eP_d\omega_d}{m_dP_R\Omega_e}\right)\gamma_{th}}\right) \\ &\quad - \frac{\gamma_{th}^{-m_e}}{\left(\frac{m_eP_d\omega_d}{m_dP_R\Omega_e}\right)^{m_e+m_d}(m_e)} {}_2F_1\left(m_e+m_d, m_d; m_d+1; \frac{-1}{\left(\frac{m_eP_d\omega_d}{m_dP_R\Omega_e}\right)\gamma_{th}}\right) \end{aligned}$$

where γ_{th} is an optimal cutoff SIR below which the transmission is suspended.

6.5.3 Channel Inversion with Fixed Rate with MRC (CIFR-MRC)

$$C_{\text{cifr}}^{MRC} = \log_2\left[1+\frac{1}{\int_0^\infty \gamma^{-1}\,\frac{\Gamma(m_e+m_d)}{\Gamma(m_e)\Gamma(m_d)}\left(\frac{m_e}{m_d}\right)^{m_e}\left(\frac{P_d\omega_d\gamma_D}{P_R\Omega_e}\right)^{m_e-1}\left(1+\frac{m_e}{m_d}\frac{P_d\omega_d\gamma_D}{P_R\Omega_e}\right)^{-(m_e+m_d)}d\gamma}\right],$$

using [132, Eq. (3.194.3)] and after some simplifications results in

$$C_{\text{cifr}}^{MRC} = \log_2\left[1+\frac{1}{\frac{\Gamma(m_e+m_d)}{\Gamma(m_e)\Gamma(m_d)}\left(\frac{m_e}{m_d}\right)\left(\frac{\omega_d}{\Omega_e}\right)B\left(m_1-1,1+m_e\right)d\gamma}\right]. \quad (6.6)$$

The expression in (6.6) is new, novel, and has not been reported in the literature before, and valid for integer and non-integer values of the fading severity parameters. However, $m_d > 1$ is the only restriction on the result in (6.6).

6.5.4 Truncated Channel Inversion with Fixed Rate with MRC (TIFR-MRC)

$$C_{\text{tifr}}^{MRC} = \log_2\left(1+\frac{1}{\int_{\gamma_{th}}^\infty \gamma^{-1}\,\frac{\Gamma(m_e+m_d)}{\Gamma(m_e)\Gamma(m_d)}\left(\frac{m_e}{m_d}\right)^{m_e}\left(\frac{P_d\omega_d\gamma_D}{P_R\Omega_e}\right)^{m_e-1}\left(1+\frac{m_e}{m_d}\frac{P_d\omega_d\gamma_D}{P_R\Omega_e}\right)^{-(m_e+m_d)}d\gamma}\right) \times\left(1-P_{\text{out}}\right), \quad (6.7)$$

where γ_{th} here is the cutoff SIR value. P_{out} is the outage probability defined as the probability that the instantaneous SIR drops below the threshold γ_{th}, P_{out} is given as [118]

$$P_{\text{out}}(\gamma_{th}) = \frac{\Gamma(m_e+m_d)}{m_e\Gamma(m_e)\Gamma(m_d)}\left(\frac{m_e}{m_d}\right)^{m_e}\left(\frac{P_d\omega_d\gamma_{th}}{P_R\Omega_e}\right)^{m_e} \times {}_2F_1\left(m_e,m_e+m_d;1+m_e;-\frac{m_e}{m_d}\frac{P_d\omega_d\gamma_{th}}{P_R\Omega_e}\right). \quad (6.8)$$

Solving the integral that appeared in (6.17) using [132, Eq. (3.194.2)] and after simple manipulation and simplifications results in

$$C_{\text{tifr}}^{MRC} = \log_2\left(1+\frac{1}{\frac{\Gamma(m_e+m_d)}{\Gamma(m_e)\Gamma(m_d)}\left(\frac{m_e\omega_d}{m_d\omega_e}\right)^{-m_e}\left(\frac{\gamma_{th}}{m_d+1}\right)^{-m_e-1}{}_2F_1\left(m_e+m_d;1+m_d;2+m_d;\frac{-m_d\omega_e}{\gamma_{th}m_e\omega_d}\right)}\right) \times(1-P_{\text{out}}), \tag{6.9}$$

The result in (6.9) is new and has not been reported in the literature before.

6.6 ACC with Equal-Gain Combining (EGC) Diversity Analysis

We extend the previous ACC performance analysis to include the effect of the EGC diversity. In an K-order EGC diversity interference-limited communicaction system with CCI at the destination node over independent and non-identical Nakagami-m multipath fading channels. Using the same previous procedure in the previous chapter, the pdf of γ_e is given by

$$f_{\gamma_e}(\gamma_e) = \frac{\Gamma(m_e+m_d)}{\Gamma(m_e)\Gamma(m_d)}\left(\frac{m_e}{m_d}\right)^{m_e}\left(\frac{KP_d\omega_d\gamma_e}{P_S\Omega_e}\right)^{m_e-1} \times\left(1+\frac{m_e}{m_d}\frac{KP_d\omega_d\gamma_e}{P_S\Omega_e}\right)^{-(m_e+m_d)}, \tag{6.10}$$

where the fading parameters in (6.10) are presented in previous chapter.

Using the same previous steps that have been used in the previous chapter to derive the ACC for different adaptive transmission protocols, we obtained the following results.

6.6.1 Optimal Rate Adaptation with Constant Transmit Power with EGC (ORA-EGC)

$$C_{\text{ora}}^{EGC} = \frac{1}{\ln 2}\int_0^{\infty}\frac{\Gamma(m_e+m_d)}{\Gamma(m_e)\Gamma(m_d)}\left(\frac{m_e}{m_d}\right)^{m_e}\left(\frac{P_d\omega_d\gamma_D}{P_R\Omega_e}\right)^{m_e-1}\left(1+\frac{m_e}{m_d}\frac{P_d\omega_d\gamma_D}{P_R\Omega_e}\right)^{-(m_e+m_d)} \times G_{2,2}^{1,2}\left(\gamma\middle|\begin{matrix}1,1\\1,0\end{matrix}\right)d\gamma, \tag{6.11}$$

The integral in (6.11) can be solved with the help of [132, Eq. (7.811.5)] as

$$C_{\text{ora}}^{EGC} = \frac{1}{\Gamma(m_1)\Gamma(m_r)\ln 2}\ G_{3,3}^{2,3}\left(\frac{p_R\omega_e m_d}{p_d\omega_d m_e}\middle|\begin{matrix}1-m_e,1,1\\m_d,1,0\end{matrix}\right), \tag{6.12}$$

The expression in (6.12) is new, novel, and has not been reported in the literature before, and valid for integer and non-integer values of the fading severity parameters. However, $m_d > 1$ is the only constraint on the result in (6.12).

6.6.2 Optimal Simultaneous Transmit Power and Rate Adaptation with EGC (OPRA-EGC)

$$C_{\text{opra}}^{EGC} = \frac{1}{\ln 2}\int_{\gamma_{th}}^{\infty}\ln\left(\frac{\gamma}{\gamma_{th}}\right)f_{\gamma}(\gamma)d\gamma, \tag{6.13}$$

$$C_{\text{opra}}^{EGC} = \frac{1}{\ln 2}\int_{\gamma_{th}}^{\infty}\ln\left(\frac{\gamma}{\gamma_{th}}\right)\frac{\Gamma(m_e+m_d)}{\Gamma(m_e)\Gamma(m_d)}\left(\frac{m_e}{m_d}\right)^{m_e}\left(\frac{P_d\omega_d\gamma_D}{P_R\Omega_e}\right)^{m_e-1} \times\left(1+\frac{m_e}{m_d}\frac{P_d\omega_d\gamma_D}{P_R\Omega_e}\right)^{-(m_e+m_d)}d\gamma, \tag{6.14}$$

The integrals in (6.14) can be solved with the help of [132, Eq. 1.512.4] as

$$\begin{aligned} C_{\text{opra}}^{EGC} &= \lim_{\epsilon\to 0} \frac{\frac{\Gamma(m_e+m_d)}{\Gamma(m_e)\Gamma(m_d)}\left(\frac{m_e}{m_d}\right)^{m_e}}{\epsilon\,\ln 2} \\ &\quad \times \frac{\gamma_{th}^{-m_e}}{\left(\frac{m_e P_d\omega_d}{m_d P_R\Omega_e}\right)^{m_e+m_d}(m_e-\epsilon)} {}_2F_1\left(m_e+m_d, m_d-\epsilon; m_d-\epsilon+1; \frac{-1}{\left(\frac{m_e P_d\omega_d}{m_d P_R\Omega_e}\right)\gamma_{th}}\right) \\ &\quad - \frac{\gamma_{th}^{-m_e}}{\left(\frac{m_e P_d\omega_d}{m_d P_R\Omega_e}\right)^{m_e+m_d}(m_e)} {}_2F_1\left(m_e+m_d, m_d; m_d+1; \frac{-1}{\left(\frac{m_e P_d\omega_d}{m_d P_R\Omega_e}\right)\gamma_{th}}\right) \end{aligned} \quad (6.15)$$

where γ_{th} is an optimal cutoff SIR below which the transmission is suspended.

6.6.3 Channel Inversion with Fixed Rate with EGC (CIFR-EGC)

$$C_{\text{cifr}}^{EGC} = \log_2\left[1+\frac{1}{\int_0^\infty \gamma^{-1}\,\frac{\Gamma(m_e+m_d)}{\Gamma(m_e)\Gamma(m_d)}\left(\frac{m_e}{m_d}\right)^{m_e}\left(\frac{P_d\omega_d\gamma_D}{P_R\Omega_e}\right)^{m_e-1}\left(1+\frac{m_e}{m_d}\frac{P_d\omega_d\gamma_D}{P_R\Omega_e}\right)^{-(m_e+m_d)}d\gamma}\right],$$

using [132, Eq. (3.194.3)] and after some simplifications results in

$$C_{\text{cifr}}^{EGC} = \log_2\left[1+\frac{1}{\frac{\Gamma(m_e+m_d)}{\Gamma(m_e)\Gamma(m_d)}\left(\frac{m_e}{m_d}\right)\left(\frac{\omega_d}{\Omega_e}\right)B\left(m_1-1,1+m_e\right)d\gamma}\right]. \quad (6.16)$$

The expression in (6.16) is new, novel, and has not been reported in the literature before, and valid for integer and non-integer values of the fading severity parameters. However, $m_d > 1$ is the only restriction on the result in (6.16).

6.6.4 Truncated Channel Inversion with Fixed Rate with EGC (TIFR-EGC)

$$C_{\text{tifr}}^{EGC} = \log_2\left(1+\frac{1}{\int_{\gamma_{th}}^{\infty}\gamma^{-1}\,\frac{\Gamma(m_e+m_d)}{\Gamma(m_e)\Gamma(m_d)}\left(\frac{m_e}{m_d}\right)^{m_e}\left(\frac{P_d\omega_d\gamma_D}{P_R\Omega_e}\right)^{m_e-1}\left(1+\frac{m_e}{m_d}\frac{P_d\omega_d\gamma_D}{P_R\Omega_e}\right)^{-(m_e+m_d)}d\gamma}\right) \times(1-P_{\text{out}}), \tag{6.17}$$

where γ_{th} here is the thresholda SIR value. P_{out} is the outage probability defined as the probability that the instantaneous SIR drops below the threshold γ_{th}, P_{out} is given as [118]

$$P_{\text{out}}(\gamma_{th}) = \frac{\Gamma(m_e+m_d)}{m_e\Gamma(m_e)\Gamma(m_d)}\left(\frac{m_e}{m_d}\right)^{m_e}\left(\frac{P_d\omega_d\gamma_{th}}{P_R\Omega_e}\right)^{m_e} \times {}_2F_1\left(m_e, m_e+m_d; 1+m_e; -\frac{m_e}{m_d}\frac{P_d\omega_d\gamma_{th}}{P_R\Omega_e}\right). \tag{6.18}$$

Solving the integral that appeared in (6.17) using [132, Eq. (3.194.2)] and after simple manipulation and simplifications results in

$$C_{\text{tifr}}^{EGC} = \log_2\left(1+\frac{1}{\frac{\Gamma(m_e+m_d)}{\Gamma(m_e)\Gamma(m_d)}\left(\frac{m_e\omega_d}{m_d\omega_e}\right)^{-m_e}\left(\frac{\gamma_{th}}{m_d+1}\right)^{-m_e-1}{}_2F_1\left(m_e+m_d; 1+m_d; 2+m_d; \frac{-m_d\omega_e}{\gamma_{th}m_e\omega_d}\right)}\right) \times(1-P_{\text{out}}), \tag{6.19}$$

6.7 Numerical and Simulation Results

In this section, we provide numerical and simulation results for the expressions derived in this chapter for arbitrary values of the Nakagami-m fading parameters for the different transmission protocols. Without loss of generality we assume that

$P_S = P_R = P_{ri} = P_{di} = 1$. The simulation results are obtained using MonteCarlo simulation method, with number of runs equal to $1,000,000$ times.

In Fig. 6.2, the normalized average channel capacity per unit bandwidth under ORA transmission policy is presented for different MRC diversity order K (i.e., $K = 1, 2, 4$). The figure shows that the ACC increases with the increase of the MRC diversity order K. Also, it shows that for a given desired ACC, increasing K decreases the required SIR. So, the system performance can be improved by saving the required energy of the transmitted signal as expected.

In Fig. 6.3 the normalized capacity per unit bandwidth under simultaneous optimal and rate adaptation policy (OPRA) and with different MRC diversity order K (i.e., $K = 1, 2, 4$) is shown at the threshold SIR equal to 2 dB. The figure shows that the ACC increases with the increase of the MRC diversity order K as expected. Also, it shows that for a given desired ACC, increasing K decreases the required SIR. So, the system performance can be improved by saving the required energy of the transmitted signal.

In Fig. 6.4, the normalized average channel capacity per unit bandwidth [Bit/sec/Hz] versus the average SIR, for a wireless communication system over the Nakagami-m multipath fading channel model under the channel inversion with fixed rate protocol (CIFR) and with different MRC diversity order K (i.e., $K = 1, 2, 4$). The figure shows that the ACC increases with the increase of the MRC diversity order K. Also, it shows that for a given desired ACC, increasing K decreases the required SIR. So, the system performance can be improved by saving the required energy of the transmitted signal.

In Fig. 6.5, the normalized average channel capacity per unit bandwidth [Bit/sec/Hz] versus the average SIR, for a wireless communication system over the Nakagami-m multipath fading channel model under the truncated channel inversion with fixed rate protocol (TIFR) and with different MRC diversity order K (i.e., $K = 1, 2, 4$). The figure shows that the ACC increases with the increase of the MRC diversity order K. Also, it shows that for a given desired ACC, increasing K decreases the required SIR. So, the system performance can be improved by saving the required energy of the transmitted signal.

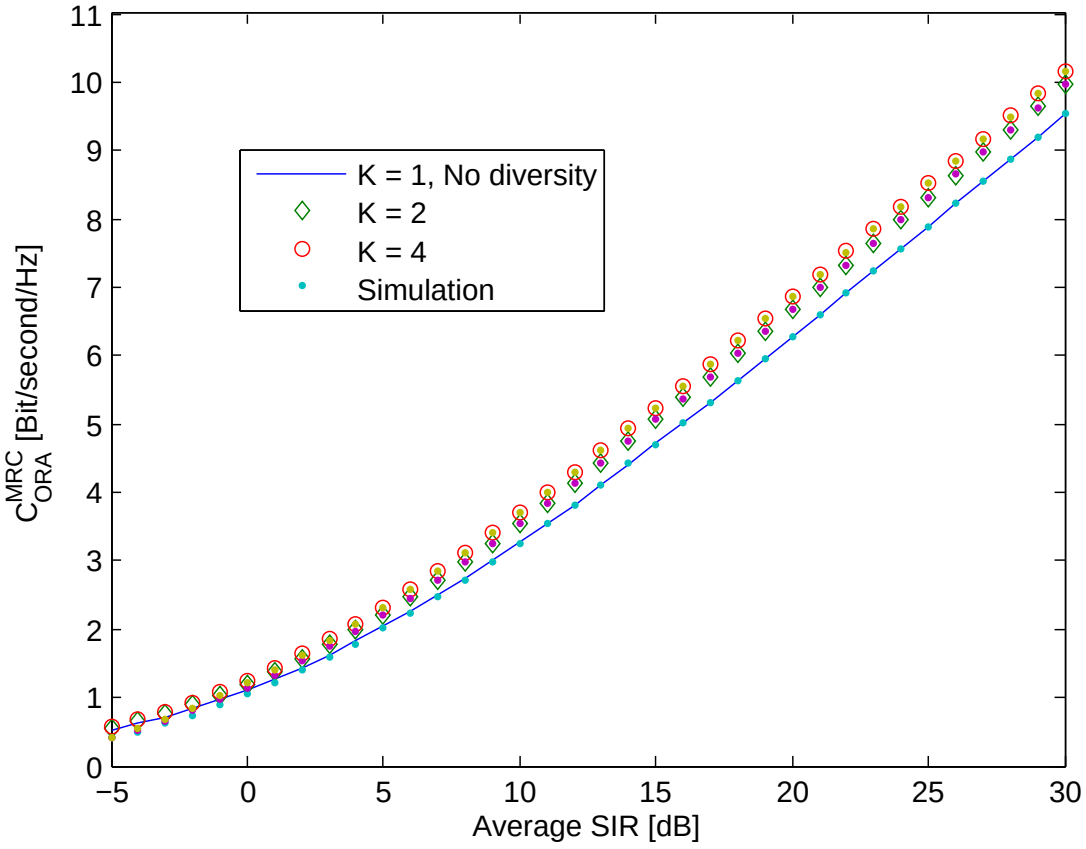

Figure 6.2. The normalized average channel capacity per unit bandwidth [Bit/sec/Hz] versus the average SIR, for a wireless communication system over the Nakagami-m multipath fading channel model with MRC under the optimal rate adaptation and fixed power protocol (ORA) for a different fading parameters.

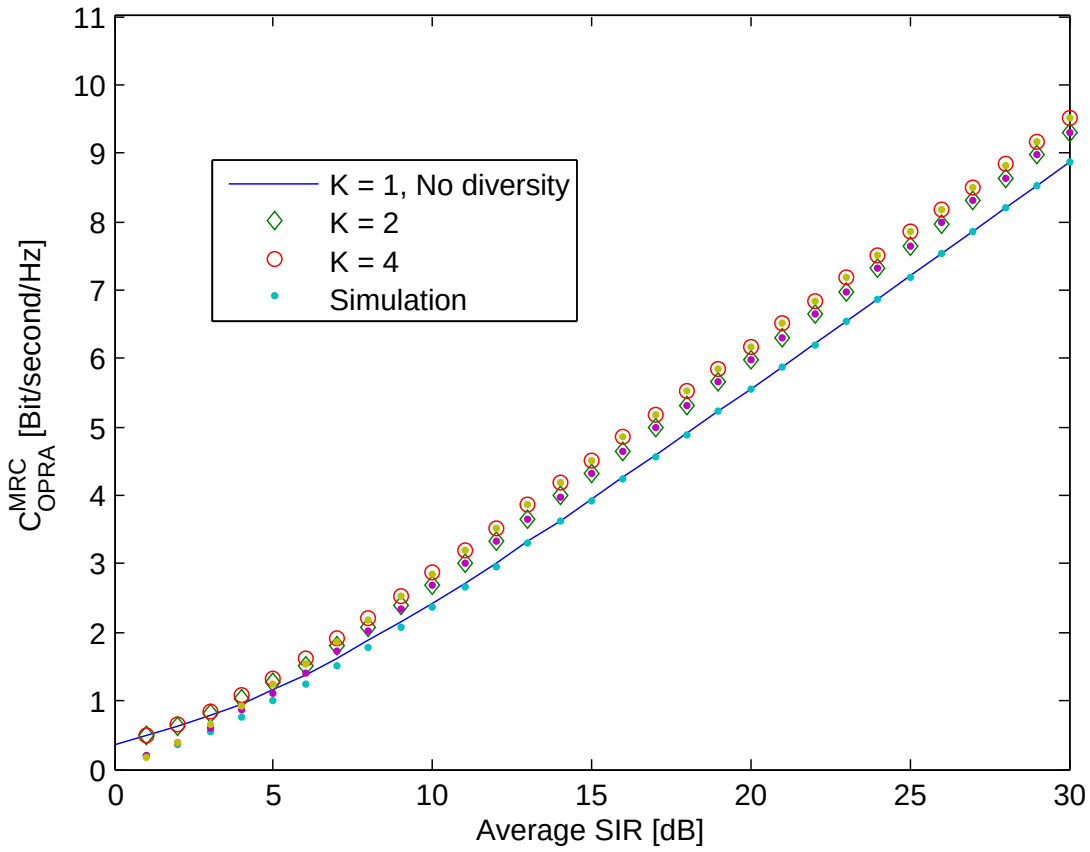

Figure 6.3. The normalized average channel capacity per unit bandwidth [Bit/sec/Hz] versus the average SIR, for a wireless communication system over the Nakagami-m multipath fading channel model with MRC under the simultaneous optimal power and rate adaptation protocol (OPRA) for a different fading parameters.

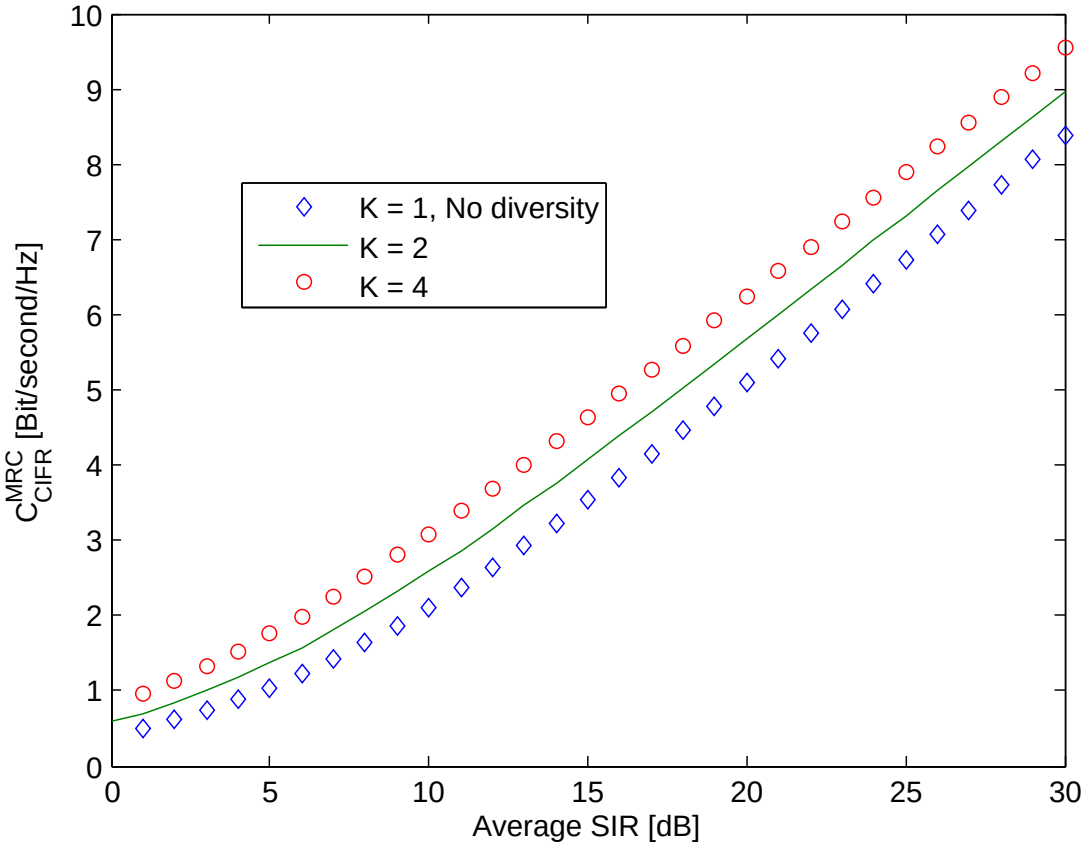

Figure 6.4. The normalized average channel capacity per unit bandwidth [Bit/sec/Hz] versus the average SIR, for a wireless communication system over the Nakagami-m multipath fading channel model with MRC under the the channel inversion with fixed rate protocol (CIFR) for a different fading parameters.

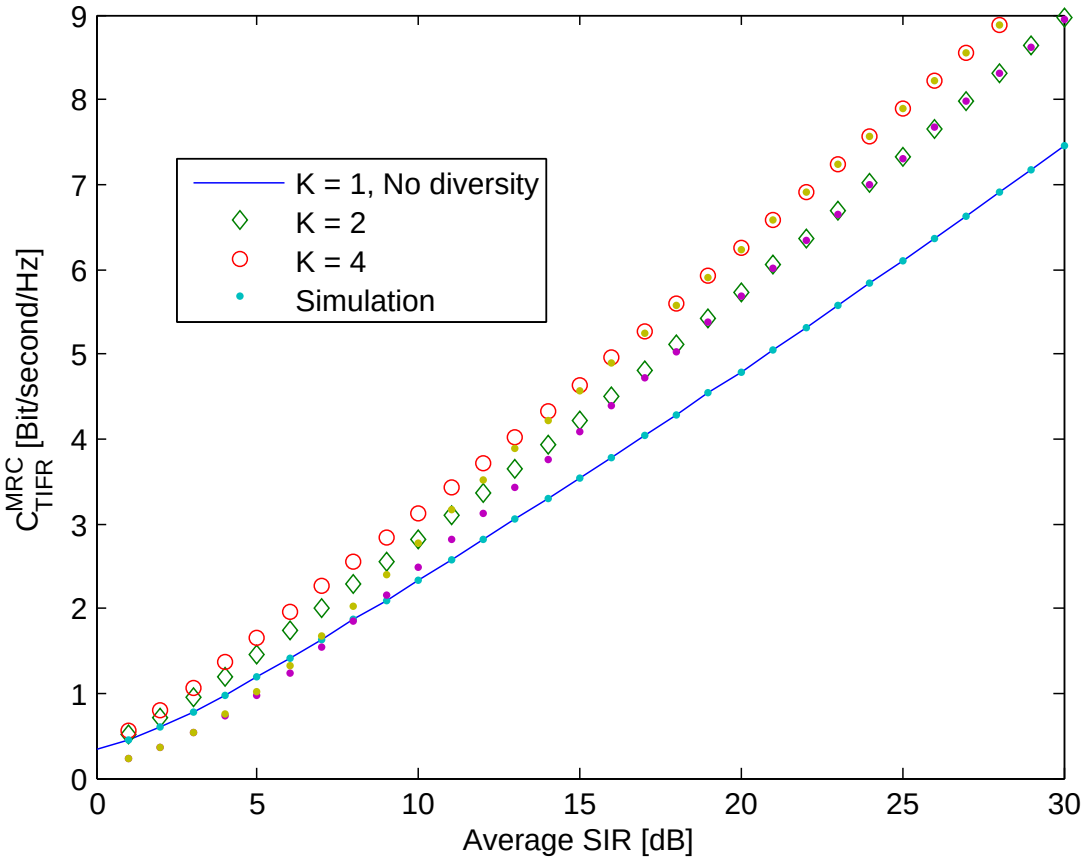

Figure 6.5. The normalized average channel capacity per unit bandwidth [Bit/sec/Hz] versus the average SIR, for a wireless communication system over the Nakagami-m multipath fading channel model with MRC under the truncated channel inversion with fixed rate protocol (TIFR) for a different fading parameters.

In Fig. 6.6, the normalized average channel capacity per unit bandwidth according to the ORA transmission policy is presented in interference-limited wireless communication system with two interferers at destination node over Nakagami-m multipath fading channels, with arbitrary fading parameters values. (i.e., $N_R = 2$; $N_D = 2$ with $m_1 = 1$, $\Omega_1 = 1$, $m_{r1} = 1$, $m_{r2} = 1$, $m_2 = 1$, $m_{d1} = 1$, $m_{d2} = 1$, $\Omega_{r1} = 1$, $\Omega_{r2} = 1$, $\Omega_{d1} = 1$, $\Omega_{d2} = 1$,). with different EGC diversity order K (i.e., $K = 1$, 2, 4). The figure shows that the ACC increases with the increase of the EGC diversity order K. Also, it shows that for a given desired ACC, increasing K decreases the required SIR. So, the system performance can be improved by saving the required energy of the transmitted signal as expected.

In Fig. 6.7 the normalized capacity per unit bandwidth according to the simultaneous optimal and rate adaptation policy (OPRA) in interference-limited wireless communication system with two interferers at destination node over Nakagami-m multipath fading channels, with arbitrary fading parameters values. (i.e., $N_R = 2$; $N_D = 2$ with $m_1 = 1$, $\Omega_1 = 1$, $m_{r1} = 1$, $m_{r2} = 1$, $m_2 = 1$, $m_{d1} = 1$, $m_{d2} = 1$, $\Omega_{r1} = 1$, $\Omega_{r2} = 1$, $\Omega_{d1} = 1$, $\Omega_{d2} = 1$,). with different EGC diversity order K (i.e., $K = 1$, 2, 4), and with different EGC diversity order K (i.e., $K = 1$, 2, 4) is shown at the threshold SIR equal to 2 dB. The figure shows that the ACC increases with the increase of the EGC diversity order K as expected. Also, it shows that for a given desired ACC, increasing K decreases the required SIR. So, the system performance can be improved by saving the required energy of the transmitted signal.

In Fig. 6.8, the normalized average channel capacity per unit bandwidth [Bit/sec/Hz] versus the average SIR, in interference-limited wireless communication system with

two interferers at destination node over Nakagami-m multipath fading channels, with arbitrary fading parameters values. (i.e., $N_R = 2$; $N_D = 2$ with $m_1 = 1$, $\Omega_1 = 1.1$, $m_{r1} = 1$, $m_{r2} = 1$, $m_2 = 1.1$, $m_{d1} = 1$, $m_{d2} = 1$, $\Omega_{r1} = 1$, $\Omega_{r2} = 1$, $\Omega_{d1} = 1$, $\Omega_{d2} = 1$,). with different EGC diversity order K (i.e., $K = 1, 2, 4$), with the channel inversion with fixed rate protocol (CIFR) and with different EGC diversity order K (i.e., $K = 1, 2, 4$). The figure shows that the ACC increases with the increase of the EGC diversity order K. Also, it shows that for a given desired ACC, increasing K decreases the required SIR. So, the system performance can be improved by saving the required energy of the transmitted signal.

In Fig. 6.9, the normalized average channel capacity per unit bandwidth [Bit/sec/Hz] versus the average SIR in interference-limited wireless communication system with two interferers at destination node over Nakagami-m multipath fading channels, with arbitrary fading parameters values. (i.e., $N_R = 2$; $N_D = 2$ with $m_1 = 1$, $\Omega_1 = 1$, $m_{r1} = 1$, $m_{r2} = 1$, $m_2 = 1$, $m_{d1} = 1$, $m_{d2} = 1$, $\Omega_{r1} = 1$, $\Omega_{r2} = 1$, $\Omega_{d1} = 1$, $\Omega_{d2} = 1$,). with different EGC diversity order K (i.e., $K = 1, 2, 4$), with the truncated channel inversion with fixed rate protocol (TIFR) and with different EGC diversity order K (i.e., $K = 1, 2, 4$). The figure shows that the ACC increases with the increase of the EGC diversity order K. Also, it shows that for a given desired ACC, increasing K decreases the required SIR. So, the system performance can be improved by saving the required energy of the transmitted signal.

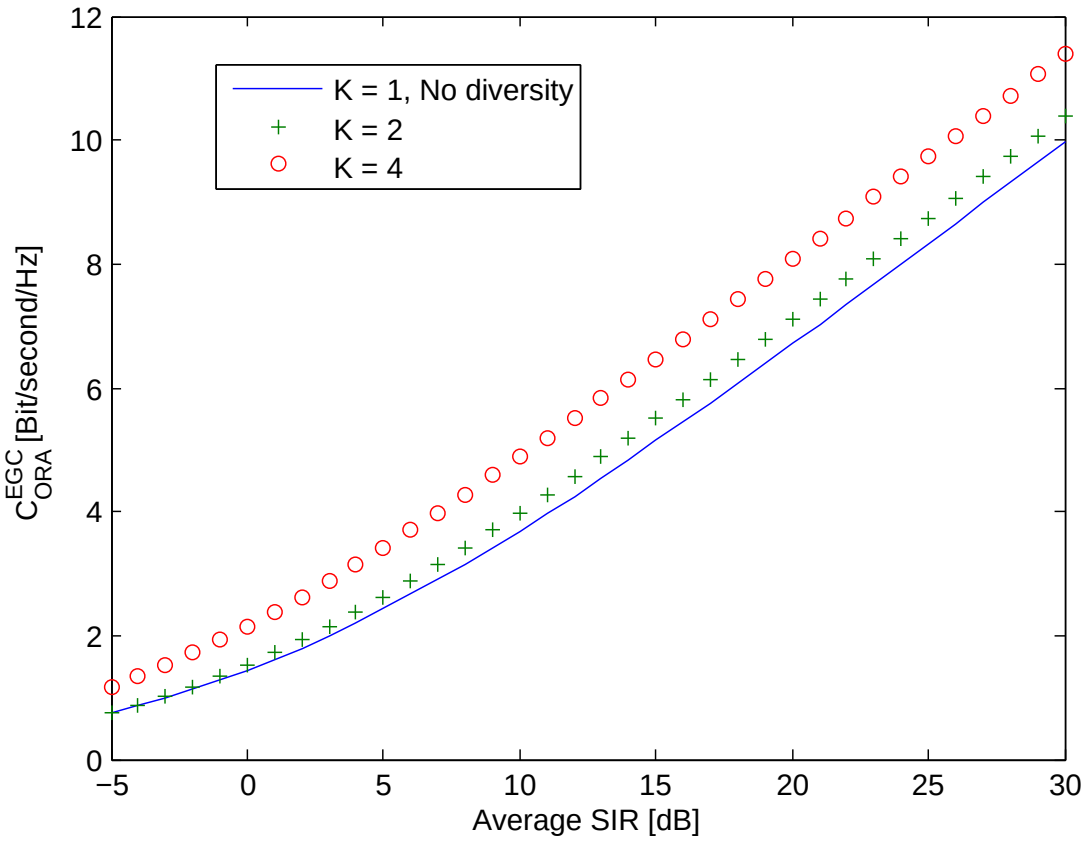

Figure 6.6. The normalized average channel capacity per unit bandwidth [Bit/sec/Hz] versus the average SIR, for a wireless communication system over the Nakagami-m multipath fading channel model with EGC under the optimal rate adaptation and fixed power protocol (ORA) for a different fading parameters.

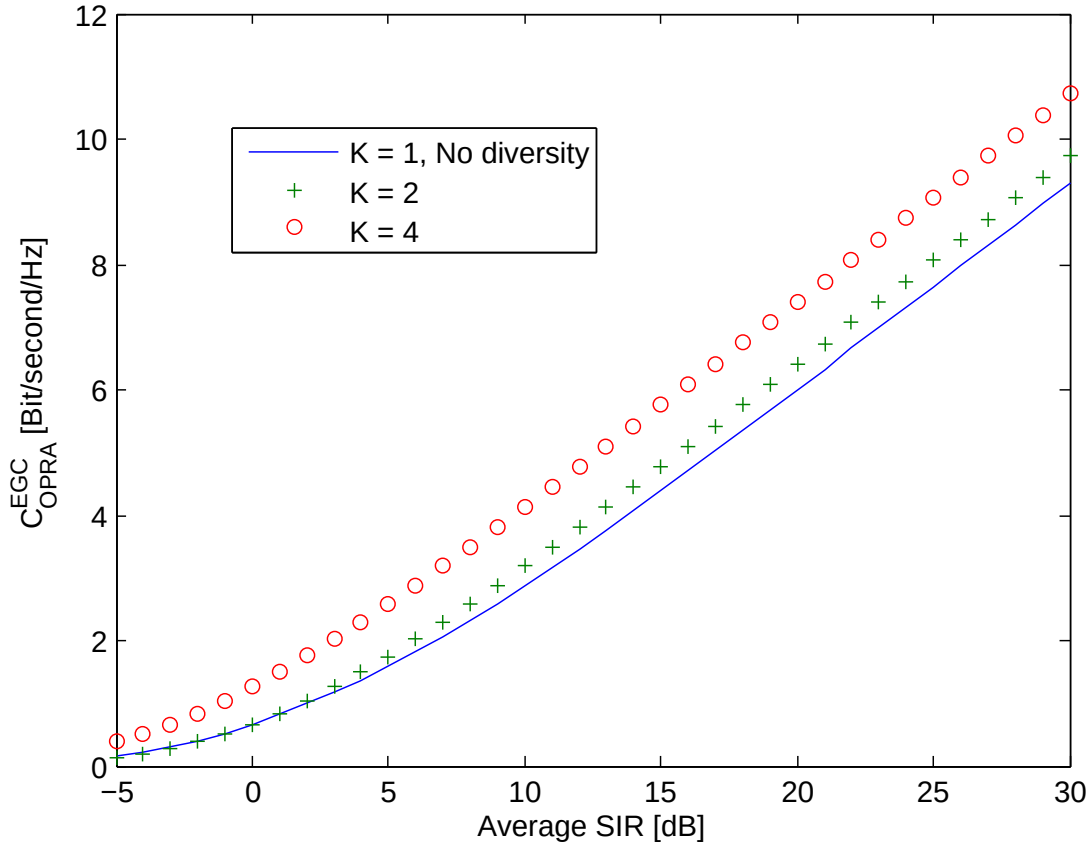

Figure 6.7. The normalized average channel capacity per unit bandwidth [Bit/sec/Hz] versus the average SIR, for a wireless communication system over the Nakagami-m multipath fading channel model with EGC under the simultaneous optimal power and rate adaptation protocol (OPRA) for a different fading parameters.

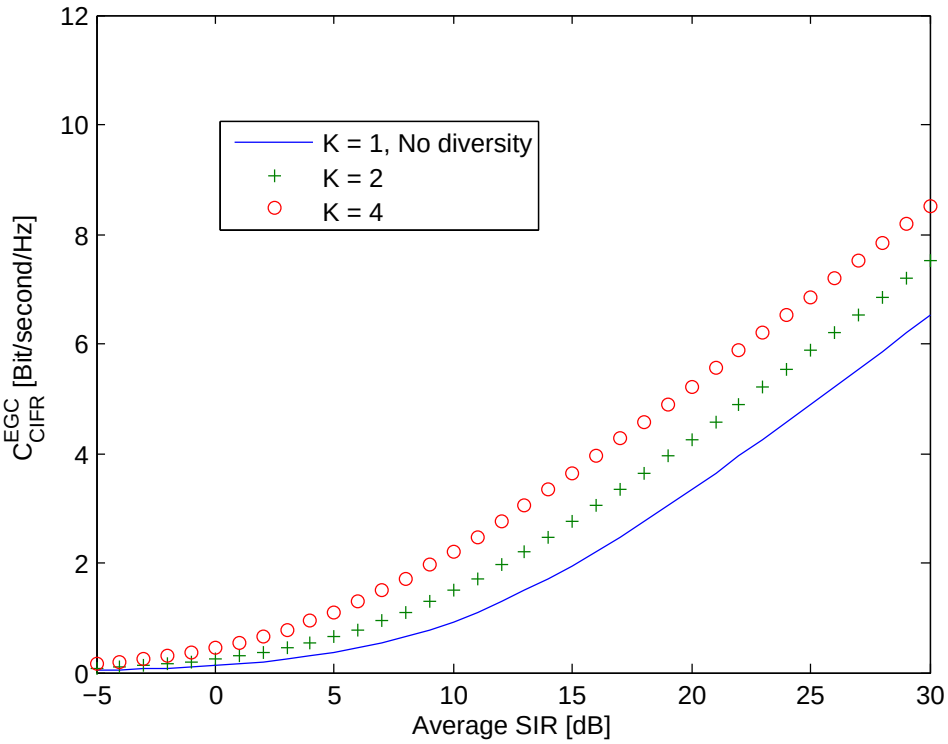

Figure 6.8. The normalized average channel capacity per unit bandwidth [Bit/sec/Hz] versus the average SIR, for a wireless communication system over the Nakagami-m multipath fading channel model with EGC under the the channel inversion with fixed rate protocol (CIFR) for a different fading parameters.

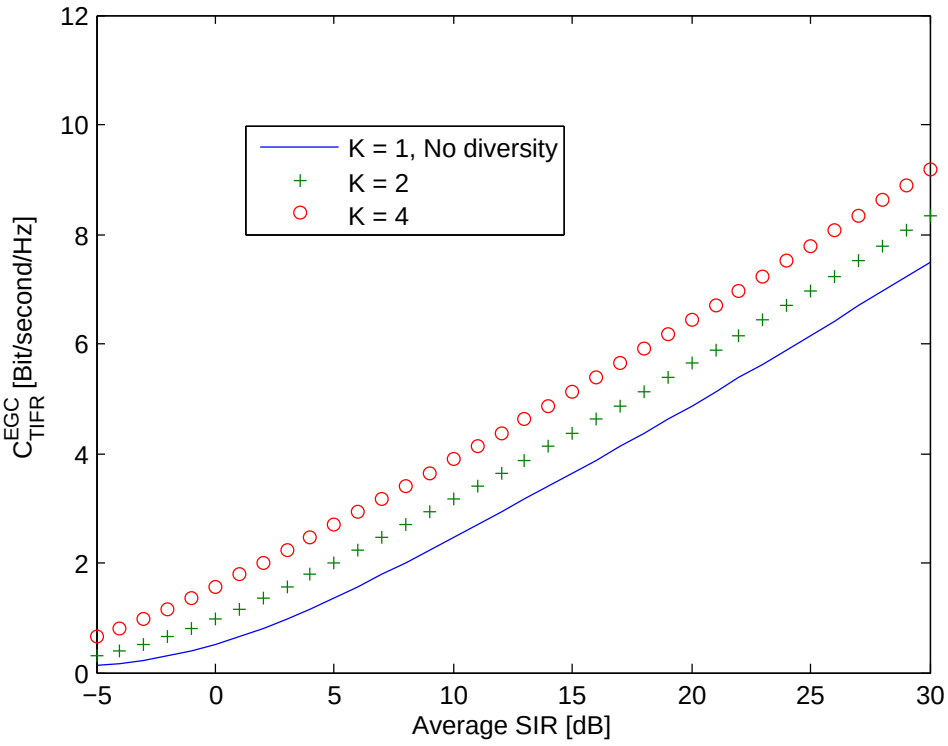

Figure 6.9. The normalized average channel capacity per unit bandwidth [Bit/sec/Hz] versus the average SIR, for a wireless communication system over the Nakagami-m multipath fading channel model with EGC under the truncated channel inversion with fixed rate protocol (TIFR) for a different fading parameters.

The above results are very useful to evaluate the ACC performance analysis of the system under study. In general, as the channel conditions improve, the amount of fading decreases, and the normalized channel capacity increases regardless of the transmission policy adopted. such analysis is very important for wireless communication systems engineering design process.

6.8 Conclusions

The MRC and the EGC diversity effect on the ACC system performance analysis was considered, and the results show that for a given ACC, increasing K decreases the required SIR. So, the system performance can be improved by saving the energy of the transmitted signal. Also, we verify the high accuracy level of the derived expressions by simulating the PDF and the SIR that has been used in this chapter to derive the closed-form expressions of ACC under different adaptive transmission protocols. A highly accurate closed-form approximate expressions for different adaptive transmission protocols are derived in this chapter, which proved to be an excellent tools in engineering design process.

Chapter 7

DUAL-HOP MULTIPLE DF RELAYS COOPERATIVE SYSTEMS WITH DIVERSITY: BER PERFORMANCE ANALYSIS

7.1 Overview

In this chapter,we analyze the average BER performance of an multiple DF relays interference-limited dual-hop DF relaying cooperative system with multiple co-channel interferers at both relay and destination nodes and subject to independent and both identical (i.i.d.) and non identical distributed (i.n.i.d.) Nakagami-m fading channels with arbitrary values of the fading severity parameter m (integers and non-integers).

The remainder of this chapter is organized as follows. In sections 7.2 and 7.3, the related work and contributions to the chapter are summarized. In Section 7.5 the BER derivation extended to the case when the receiver employs the maximum

ratio combining scheme to exploit the diversity gain. In Section 7.6, we present the numerical and simulation results at the end of the chapter. Finally some conclusions are drawn in section 7.7.

7.2 Related Work

In [5], the lower-bound SER performance of cooperative digital communication schemes is investigated, where multiple dual-hop relays are invoked for achieving the cooperative diversity with the aid of the maximal ratio combining (MRC). A range of closed-form expressions are obtained for the probability density functions (PDFs) of the relay-channels output signal-to-noise ratio (SNR). Accurate approximate closed-form expressions are derived for computing the SER. Using the closed-form expressions obtained in this contribution, the SER performance of the relay-assisted digital communications schemes, which may employ various classes of coherent modulations, can be readily evaluated in the context of a variety of fading scenarios that the cooperative signals might experience. In [31], the author derived closed-form expressions for the average BER of both coherent and non-coherent binary frequency-shift keying (BFSK) and binary phase shift keying (BPSK) modulation schemes in an interference-limited wireless communication system. The analysis assumes an arbitrary number of independent and identically distributed Nakagami-m interferers. The study extended to investigate the effect of maximal ratio combining diversity technique at the receiver end. In [6], the authors focus on the diversity order of the DF cooperative networks with relay selection. Many detection schemes have been

proposed for the DF; but it has been shown that the cooperative maximum ratio combining (C-MRC) can achieve almost the same performance as the optimum maximum likelihood detector and has a much lower complexity. Therefore, they first combine the C-MRC with the relay selection and show that it achieves the full diversity order by deriving an upper bound of its BER. In order to reduce the signaling overhead, they then combine the link-adaptive regeneration (LAR) with the relay selection by deriving an upper bound of the BER. In [4], the author evaluates outage performance of a cooperative transmission protocol over fading channels that requires a number of relaying nodes to employ a distributed space-time coding scheme. Diversity provided by this technique has been widely analyzed for the Rayleigh fading case. However, ad-hoc and sensor networks often experience propagation environments where the line-of-sight component is either non-zero or, in some cases, dominates compared to the random non-line-of-sight components. By considering the Nakagami-m as a generic framework for describing the statistic of fading impairments, the author evaluates a set of fading inequalities that define settings where the benefits of collaborative transmission from multiple relays when fading parameters vary. In [7], the authors examine the SER performance of DF cooperative communications. They focus on the scenario in which multiple dual-hop relays are employed and the channel environment is described by Nakagami-m fading. Cooperative diversity is observed from the derived error-rate expressions, and some insight into how channel conditions in the relay nodes affect the SER performance is obtained. In addition, with the knowledge of the partial channel state information (CSI) at the transmitting sides, they derive an optimal power allocation scheme to further enhance the SER per-

formance. In [18], the decouple-and-forward (DCF) relaying for dual-hop Alamouti transmissions is proposed as enhanced AF relaying to achieve spatial diversity gain especially provided by a two-antenna relay. DCF relaying that consists of decoupling, re-encoding and amplifying needs a little more complicated relay than AF relaying but a less complicated one than DF relaying. Assuming uncorrelated Rayleigh fading channels, the authors derive a probability density function (PDF) of end-to-end signal-to-noise ratio (SNR) for the DCF system and provide its BER performance.

7.3 Contributions

In this chapter, the work extended to the case when the receiver employs the most common diversity techniques; maximum ratio (MRC) combining scheme to exploit the diversity gain in multiple DF cooperative communication system with nakagami-m fading channel. The effect of both MRC diversity on the system BER performance analysis was considered with k finger at the destination receiver antenna. We derive integral-form BER expressions for i.n.i.d Nakagami-m branches (or finger) with an MRC combiner. Each branch, has an arbitrary fading parameters. We consider the uncorrelated independent branches in evaluating the BER at the MRC combiner output. Also, we provide numerical and simulation results at the end of the chapter.

7.4 System and signal Models

We consider an interference-limited dual-hop multiple DF relaying cooperative wireless communication system operating over independent and non identical distributed

(i.n.i.d.) Nakagami-m fading channels with arbitrary integer as well as non-integer fading severity parameter m and with multiple CCI at both R and D nodes, where a source node (S) communicates with D using R_l as shown in fig. 7.1. The communication is performed in two time slots and no direct link between S and D is assumed to be available due to sever channel impairments conditions. The signal on the direct link between the source and destination nodes is assumed to be insignificant and is ignored in our analysis. This assumption is practical due to sever channel impairments conditions, which justifies cooperative communication. We assumed both R_l and D operate in interference-limited conditions; i.e., the channel noise is dominated by the total interfering signals. Multiple co-channel N_R and N_D interferers are assumed to be present at R and D, respectively. Each one of the N_R (or N_D) interfering signals (i.e., ith interfering signal, where $i = 1, 2, \cdots, N_R$ (or $i = 1, 2, \cdots, N_D$)) has an average transmit power P_{ri} (or P_{di}), fading severity parameter m_{ri} (or m_{di}), fading power parameter Ω_{ri} (or Ω_{di}), and experiences link fading coefficient h_{ri} (or h_{di}). Let the modulated signal transmitted by S, during the first time slot, denoted by S_S with transmit power P_S.

The transmitted symbols S_S and S_R and the interfering symbols S_{ri} and S_{di} are assumed to be mutually independent and uniformly distributed with zero mean and unit variance. The fading channels average power parameters are given by

$$\Omega_{1l} = E[|h_{1l}|^2], \tag{7.1}$$

$$\Omega_{2l} = E[|h_{2l}|^2], \tag{7.2}$$

$$\Omega_{ri} = E[|h_{ri}|^2], \tag{7.3}$$

and

$$\Omega_{di} = E[|h_{di}|^2]. \tag{7.4}$$

According to [24], the pdf and the cdf of hops number one and two of branch l is given by:

$$f_{\gamma_{1,l}}(\gamma) = \frac{\Gamma(m_1+m_r)}{\Gamma(m_1)\Gamma(m_r)}\left(\frac{m_1}{m_r}\right)^{m_1}\left(\frac{P_r\omega_r\gamma}{P_S\Omega_1}\right)^{m_1-1}\left(1+\frac{m_1}{m_r}\frac{P_r\omega_r\gamma}{P_S\Omega_1}\right)^{-(m_1+m_r)} \tag{7.5}$$

$$f_{\gamma_{2,l}}(\gamma) = \frac{\Gamma(m_2+m_d)}{\Gamma(m_2)\Gamma(m_d)}\left(\frac{m_2}{m_d}\right)^{m_2}\left(\frac{P_d\omega_d\gamma}{P_R\Omega_2}\right)^{m_2-1}\left(1+\frac{m_2}{m_d}\frac{P_d\omega_d\gamma}{P_R\Omega_2}\right)^{-(m_2+m_d)} \tag{7.6}$$

$$\begin{aligned} F_{\gamma_{1,l}}(\gamma) &= \frac{\Gamma(m_1+m_r)}{m_1\Gamma(m_1)\Gamma(m_r)}\left(\frac{m_1}{m_r}\right)^{m_1}\left(\frac{P_r\omega_r\gamma}{P_S\Omega_1}\right)^{m_1} \\ &\quad \times {}_2F_1\left(m_1, m_1+m_r; 1+m_1; -\frac{m_1}{m_r}\frac{P_r\omega_r\gamma}{P_R\Omega_1}\right), \end{aligned} \tag{7.7}$$

and

$$\begin{aligned} F_{\gamma_{2,l}}(\gamma) &= \frac{\Gamma(m_2+m_d)}{m_2\Gamma(m_2)\Gamma(m_d)}\left(\frac{m_2}{m_d}\right)^{m_2}\left(\frac{P_d\omega_d\gamma}{P_R\Omega_2}\right)^{m_2} \\ &\quad \times {}_2F_1\left(m_2, m_2+m_d; 1+m_2; -\frac{m_2}{m_d}\frac{P_d\omega_d\gamma}{P_R\Omega_2}\right). \end{aligned} \tag{7.8}$$

The end-to-end instantaneous signal-to-interference ratio pdf of branch l $f_{\gamma_l}(\gamma)$ is given as [24]

$$f_{\gamma_l}(\gamma) = f_{\gamma_{1,l}}(\gamma) + f_{\gamma_{2,l}}(\gamma) - f_{\gamma_{1,l}}(\gamma)F_{\gamma_{2,l}}(\gamma) - f_{\gamma_{2,l}}(\gamma)F_{\gamma_{1,l}}(\gamma) \tag{7.9}$$

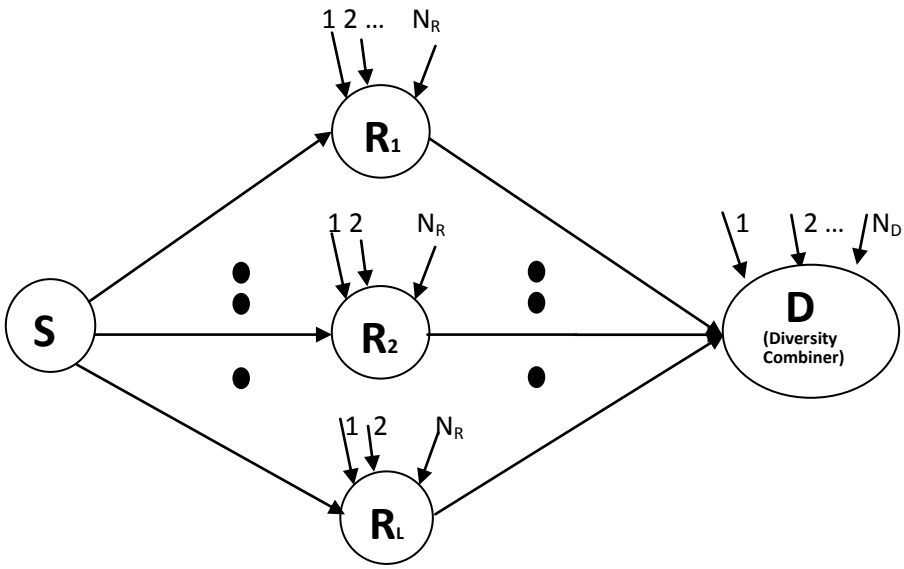

Figure 7.1. A dual-hop multiple DF relays cooperative wireless communication system over Nakagami-m fading channels with multiple CCI at both the relay and the destination nodes.

7.5 Maximal Ratio Combining (MRC) Diversity Analysis

In maximal ratio combining (MRC) the output is a weighted sum of all branches, so the $\alpha_i s$ in figure 7.2 are all non zero.

The equivalent SIR γ_e at the output of the MRC combiner is given by [135]

$$\gamma_{MRC} = \sum_{l=1}^{L} \gamma_l. \tag{7.10}$$

where γ_l is the end-to-end instantaneous signal-to-interference ratio of branch l. So, the PDF of γ_{MRC}, $f_{\gamma_{MRC}}(\gamma)$, is given by

$$f_{\gamma_{MRC}}(\gamma) = Convolution(f_{\gamma_1}(\gamma), f_{\gamma_2}(\gamma), f_{\gamma_3}(\gamma), ..., f_{\gamma_L}(\gamma)) \tag{7.11}$$

$f_{\gamma_{MRC}}(\gamma)$ can be obtained by substituting equations (7.5)-(7.9) into (7.11) properly.

7.5.1 Binary Phase Shift Keying (BPSK) Modulation Scheme

The conditional BER of BPSK in Gaussian channel is given in terms of the confluent hypergeometric function as

$$\begin{aligned} P_e(\gamma) &= Q\left(\sqrt{2\gamma}\right) \\ &= 0.5\left(1 - 2\sqrt{\gamma/\pi}\ \times {}_1F_1\left(0.5; 1.5; -\gamma\right)\right), \end{aligned} \tag{7.12}$$

where ${}_1F_1(.;.;.)$ is the confluent hypergeometric function of the first kind [36, Eq. (9.210.1)]

$$\begin{aligned} P^{BPSKMRC} &= E\left[0.5\left(1 - 2\sqrt{\gamma/\pi}\ \times {}_1F_1\left(0.5; 1.5; -\gamma\right)\right)\right] \\ &= \int_0^\infty 0.5\left(1 - 2\sqrt{\gamma/\pi}\ \times {}_1F_1\left(0.5; 1.5; -\gamma\right)\right) f_{\gamma_{MRC}}(\gamma)d\gamma \\ &= \int_0^\infty 0.5\left(1 - 2\sqrt{\gamma/\pi}\ \times {}_1F_1\left(0.5; 1.5; -\gamma\right)\right) \\ &\quad \times Convol(f_{\gamma_1}(\gamma), f_{\gamma_2}(\gamma), f_{\gamma_3}(\gamma), ..., f_{\gamma_L}(\gamma))d\gamma \end{aligned} \tag{7.13}$$

There is no solution for the above integrals in (7.13), they are complicated since they include double integrals, Hypergeometric functions, logarithmical and other algebraic expressions, as example for just two branches of multi-relay system, we got the following integral expression,

$$\begin{aligned} P^{BPSKMRC} &= E\left[0.5\left(1 - 2\sqrt{\gamma/\pi}\ \times {}_1F_1\left(0.5; 1.5; -\gamma\right)\right)\right] \\ &= \int_0^\infty 0.5\left(1 - 2\sqrt{\gamma/\pi}\ \times {}_1F_1\left(0.5; 1.5; -\gamma\right)\right) f_{\gamma_{MRC}}(\gamma)d\gamma \\ &= \int_0^\infty 0.5\left(1 - 2\sqrt{\gamma/\pi}\ \times {}_1F_1\left(0.5; 1.5; -\gamma\right)\right) Convolution(f_{\gamma_1}(\gamma), f_{\gamma_2}(\gamma))d\gamma \\ &= \int_0^\infty 0.5\left(1 - 2\sqrt{\gamma/\pi}\ \times {}_1F_1\left(0.5; 1.5; -\gamma\right)\right) \int_0^\infty f_{\gamma_1}(\gamma - x) f_{\gamma_2}(x)dxd\gamma \\ &= \int_0^\infty 0.5\left(1 - 2\sqrt{\gamma/\pi}\ \times {}_1F_1\left(0.5; 1.5; -\gamma\right)\right) \int_0^\infty (f_{\gamma_{1,l}}(\gamma - x) + f_{\gamma_{2,l}}(\gamma - x) - f_{\gamma_{1,l}}(\gamma - x)F_{\gamma_{2,l}}(\gamma - x) - f_{\gamma_{2,l}}(\gamma - x)F_{\gamma_{1,l}}(\gamma - x)) \\ &\quad \times (f_{\gamma_{1,l}}(x) + f_{\gamma_{2,l}}(x) - f_{\gamma_{1,l}}(x)F_{\gamma_{2,l}}(x) - f_{\gamma_{2,l}}(x)F_{\gamma_{1,l}}(x))dxd\gamma \end{aligned} \tag{7.14}$$

by substituting equations (7.5)-(7.9) into (7.14) properly, the above expression expanded to 16-terms.

Also, the conditional BER (i.e., Gaussian channel BER) can be expressed in Q-function form to obtain the following integral form,

$$\begin{aligned}
P^{BPSKMRC} &= E\left[Q\left(\sqrt{2\gamma}\right)\right] \\
&= \int_0^\infty Q\left(\sqrt{2\gamma}\right) f_{\gamma_{MRC}}(\gamma)d\gamma \\
&= \int_0^\infty Q\left(\sqrt{2\gamma}\right) Convol(f_{\gamma_1}(\gamma), f_{\gamma_2}(\gamma)d\gamma \\
&= \int_0^\infty Q\left(\sqrt{2\gamma}\right) \int_0^\infty f_{\gamma_1}(\gamma - x) f_{\gamma_2}(x)dxd\gamma \\
&= \int_0^\infty Q\left(\sqrt{2\gamma}\right) \int_0^\infty (f_{\gamma_{1,l}}(\gamma - x) + f_{\gamma_{2,l}}(\gamma - x) - f_{\gamma_{1,l}}(\gamma - x)F_{\gamma_{2,l}}(\gamma - x) - f_{\gamma_{2,l}}(\gamma - x)F_{\gamma_{1,l}}(\gamma - x)) \\
&\quad \times (f_{\gamma_{1,l}}(x) + f_{\gamma_{2,l}}(x) - f_{\gamma_{1,l}}(x)F_{\gamma_{2,l}}(x) - f_{\gamma_{2,l}}(x)F_{\gamma_{1,l}}(x))dxd\gamma \qquad (7.15)
\end{aligned}$$

The above expression expanded to 16-terms.

7.5.2 Differential Binary Phase Shift Keying (DBPSK) Modulation Scheme

For a differential binary phase shift keying (DBPSK) modulation scheme, the conditional BER for a given SIR γ_e is given as

$$P_e^{DBPSK} = 0.5\exp(-\gamma_e), \qquad (7.16)$$

by substituting (7.16) into (7.12) yields

$$\begin{aligned}
P_e^{DBPSKMRC} &= E\left[0.5\exp(-\gamma_e)\right] \\
&= \int_0^\infty 0.5\exp(-\gamma_e) f_{\gamma_{MRC}}(\gamma)d\gamma \\
&= \int_0^\infty 0.5\exp(-\gamma_e) Conv(f_{\gamma_1}(\gamma), f_{\gamma_2}(\gamma), f_{\gamma_3}(\gamma), ..., f_{\gamma_L}(\gamma))d\gamma \qquad (7.17)
\end{aligned}$$

There is no solution for the above integrals in (7.21), they are very complicated since they include the double integrals, Hypergeometric functions, logarithmical and

other algebraic expressions, as example for just two branches of multi-relay system:

$$
\begin{aligned}
P^{DBPSKMRC} &= E\left[0.5\exp(-\gamma_e)\right] \\
&= \int_0^\infty 0.5\exp(-\gamma_e) f_{\gamma_{MRC}}(\gamma) d\gamma \\
&= \int_0^\infty 0.5\exp(-\gamma_e) Conv(f_{\gamma_1}(\gamma), f_{\gamma_2}(\gamma) d\gamma \\
&= \int_0^\infty 0.5\exp(-\gamma_e) \int_0^\infty f_{\gamma_1}(\gamma - x) f_{\gamma_2}(x) dx d\gamma \\
&= \int_0^\infty 0.5\exp(-\gamma_e) \int_0^\infty (f_{\gamma_{1,l}}(\gamma - x) + f_{\gamma_{2,l}}(\gamma - x) - f_{\gamma_{1,l}}(\gamma - x) F_{\gamma_{2,l}}(\gamma - x) - f_{\gamma_{2,l}}(\gamma - x) F_{\gamma_{1,l}}(\gamma - x)) \\
&\quad \times (f_{\gamma_{1,l}}(x) + f_{\gamma_{2,l}}(x) - f_{\gamma_{1,l}}(x) F_{\gamma_{2,l}}(x) - f_{\gamma_{2,l}}(x) F_{\gamma_{1,l}}(x)) dx d\gamma
\end{aligned} \tag{7.18}
$$

by substituting equations (7.5)-(7.9) into (7.18) properly, the above expression expanded to 16-terms. At the end, the above expression expanded to 16-terms, I break each term down and there is no solution for these integrals and the most complicated term is the term that have:
$f_{\gamma_{1,l}}(x) F_{\gamma_{2,l}}(x) \times f_{\gamma_{2,l}}(\gamma - x) F_{\gamma_{1,l}}(\gamma - x)$

$$
\begin{aligned}
f_{\gamma_{1,l}}(x) F_{\gamma_{2,l}}(x) \times f_{\gamma_{2,l}}(\gamma - x) F_{\gamma_{1,l}}(\gamma - x) &= \frac{\Gamma(m_1 + m_r)}{\Gamma(m_1)\Gamma(m_r)} \left(\frac{m_1}{m_r}\right)^{m_1} \left(\frac{P_r \omega_r \gamma}{P_S \Omega_1}\right)^{m_1 - 1} \left(1 + \frac{m_1}{m_r} \frac{P_r \omega_r \gamma}{P_S \Omega_1}\right)^{-(m_1 + m_r)} \\
&\quad \times \frac{\Gamma(m_2 + m_d)}{m_2 \Gamma(m_2)\Gamma(m_d)} \left(\frac{m_2}{m_d}\right)^{m_2} \left(\frac{P_d \omega_d \gamma}{P_R \Omega_2}\right)^{m_2} \\
&\quad \times {}_2F_1\left(m_2, m_2 + m_d; 1 + m_2; -\frac{m_2}{m_d} \frac{P_d \omega_d \gamma}{P_R \Omega_2}\right) \\
&\quad \times \frac{\Gamma(m_2 + m_d)}{\Gamma(m_2)\Gamma(m_d)} \left(\frac{m_2}{m_d}\right)^{m_2} \left(\frac{P_d \omega_d \gamma}{P_R \Omega_2}\right)^{m_2 - 1} \left(1 + \frac{m_2}{m_d} \frac{P_d \omega_d \gamma}{P_R \Omega_2}\right)^{-(m_2 + m_d)} \\
&\quad \times \frac{\Gamma(m_2 + m_d)}{\Gamma(m_2)\Gamma(m_d)} \left(\frac{m_2}{m_d}\right)^{m_2} \left(\frac{P_d \omega_d \gamma}{P_R \Omega_2}\right)^{m_2 - 1} \left(1 + \frac{m_2}{m_d} \frac{P_d \omega_d \gamma}{P_R \Omega_2}\right)^{-(m_2 + m_d)} \\
&\quad \times \frac{\Gamma(m_1 + m_r)}{m_1 \Gamma(m_1)\Gamma(m_r)} \left(\frac{m_1}{m_r}\right)^{m_1} \left(\frac{P_r \omega_r \gamma}{P_S \Omega_1}\right)^{m_1} \\
&\quad \times {}_2F_1\left(m_1, m_1 + m_r; 1 + m_1; -\frac{m_1}{m_r} \frac{P_r \omega_r \gamma}{P_R \Omega_1}\right)
\end{aligned} \tag{7.19}
$$

The numerical and simulation results show that the above BER expression is not accurate, since it contains several multiplication process of the approximated PDF and CDF.

7.5.3 Non-Coherent Binary Frequency Shift Keying (NCBFSK) Modulation Scheme

For a non-coherent binary frequency shift keying (NCBFSK) modulation scheme, the conditional BER for a given SIR γ_e is given as

$$P_e^{NCBFSK} = 0.5\exp(-\frac{\gamma_e}{2}) \tag{7.20}$$

by substituting (7.20) into (7.12) yields

$$\begin{aligned} P_e^{NCBFSKMRC} &= E\left[0.5\exp(-\frac{\gamma_e}{2})\right] \\ &= \int_0^\infty 0.5\exp(-\frac{\gamma_e}{2}) f_{\gamma_{MRC}}(\gamma)d\gamma \\ &= \int_0^\infty 0.5\exp(-\frac{\gamma_e}{2}) Convol(f_{\gamma_1}(\gamma), f_{\gamma_2}(\gamma), f_{\gamma_3}(\gamma), ..., f_{\gamma_L}(\gamma))d\gamma \end{aligned} \tag{7.21}$$

There is no solution for the above integrals in (7.21), they are very complicated since they include the double integrals, Hypergeometric functions, logarithmical and other algebraic expressions, as example for just two branches of multi-relay system:

$$\begin{aligned} P^{NCBFSKMRC} &= E\left[0.5\exp(-\frac{\gamma_e}{2})\right] \\ &= \int_0^\infty 0.5\exp(-\frac{\gamma_e}{2}) f_{\gamma_{MRC}}(\gamma)d\gamma \\ &= \int_0^\infty 0.5\exp(-\frac{\gamma_e}{2}) Convol(f_{\gamma_1}(\gamma), f_{\gamma_2}(\gamma)d\gamma \\ &= \int_0^\infty 0.5\exp(-\frac{\gamma_e}{2}) \int_0^\infty f_{\gamma_1}(\gamma - x) f_{\gamma_2}(x)dxd\gamma \\ &= \int_0^\infty 0.5\exp(-\frac{\gamma_e}{2}) \int_0^\infty (f_{\gamma_{1,l}}(\gamma - x) + f_{\gamma_{2,l}}(\gamma - x) - f_{\gamma_{1,l}}(\gamma - x)F_{\gamma_{2,l}}(\gamma - x) - f_{\gamma_{2,l}}(\gamma - x)F_{\gamma_{1,l}}(\gamma - x)) \\ &\quad \times (f_{\gamma_{1,l}}(x) + f_{\gamma_{2,l}}(x) - f_{\gamma_{1,l}}(x)F_{\gamma_{2,l}}(x) - f_{\gamma_{2,l}}(x)F_{\gamma_{1,l}}(x))dxd\gamma \end{aligned} \tag{7.22}$$

by substituting equations (7.5)-(7.9) into (7.22) properly, the above expression expanded to 16-terms. At the end, the above expression expanded to 16-terms, I break each term down and there is no solution for these integrals and the most complicated term is the term that have:

$f_{\gamma_{1,l}}(x)F_{\gamma_{2,l}}(x) \times f_{\gamma_{2,l}}(\gamma - x)F_{\gamma_{1,l}}(\gamma - x)$

$$
\begin{aligned}
f_{\gamma_{1,l}}(x)F_{\gamma_{2,l}}(x) \times f_{\gamma_{2,l}}(\gamma - x)F_{\gamma_{1,l}}(\gamma - x) &= \frac{\Gamma(m_1 + m_r)}{\Gamma(m_1)\Gamma(m_r)} \left(\frac{m_1}{m_r}\right)^{m_1} \left(\frac{P_r\omega_r\gamma}{P_S\Omega_1}\right)^{m_1-1} \left(1 + \frac{m_1}{m_r}\frac{P_r\omega_r\gamma}{P_S\Omega_1}\right)^{-(m_1+m_r)} \\
&\times \frac{\Gamma(m_2 + m_d)}{m_2\Gamma(m_2)\Gamma(m_d)} \left(\frac{m_2}{m_d}\right)^{m_2} \left(\frac{P_d\omega_d\gamma}{P_R\Omega_2}\right)^{m_2} \\
&\times {}_2F_1\left(m_2, m_2 + m_d; 1 + m_2; -\frac{m_2}{m_d}\frac{P_d\omega_d\gamma}{P_R\Omega_2}\right) \\
&\times \frac{\Gamma(m_2 + m_d)}{\Gamma(m_2)\Gamma(m_d)} \left(\frac{m_2}{m_d}\right)^{m_2} \left(\frac{P_d\omega_d\gamma}{P_R\Omega_2}\right)^{m_2-1} \left(1 + \frac{m_2}{m_d}\frac{P_d\omega_d\gamma}{P_R\Omega_2}\right)^{-(m_2+m_d)} \\
&\times \frac{\Gamma(m_2 + m_d)}{\Gamma(m_2)\Gamma(m_d)} \left(\frac{m_2}{m_d}\right)^{m_2} \left(\frac{P_d\omega_d\gamma}{P_R\Omega_2}\right)^{m_2-1} \left(1 + \frac{m_2}{m_d}\frac{P_d\omega_d\gamma}{P_R\Omega_2}\right)^{-(m_2+m_d)} \\
&\times \frac{\Gamma(m_1 + m_r)}{m_1\Gamma(m_1)\Gamma(m_r)} \left(\frac{m_1}{m_r}\right)^{m_1} \left(\frac{P_r\omega_r\gamma}{P_S\Omega_1}\right)^{m_1} \\
&\times {}_2F_1\left(m_1, m_1 + m_r; 1 + m_1; -\frac{m_1}{m_r}\frac{P_r\omega_r\gamma}{P_R\Omega_1}\right) \qquad (7.23)
\end{aligned}
$$

The numerical and simulation results show that the above BER expression is not accurate, since it contains several multiplication process of the approximated PDF and CDF.

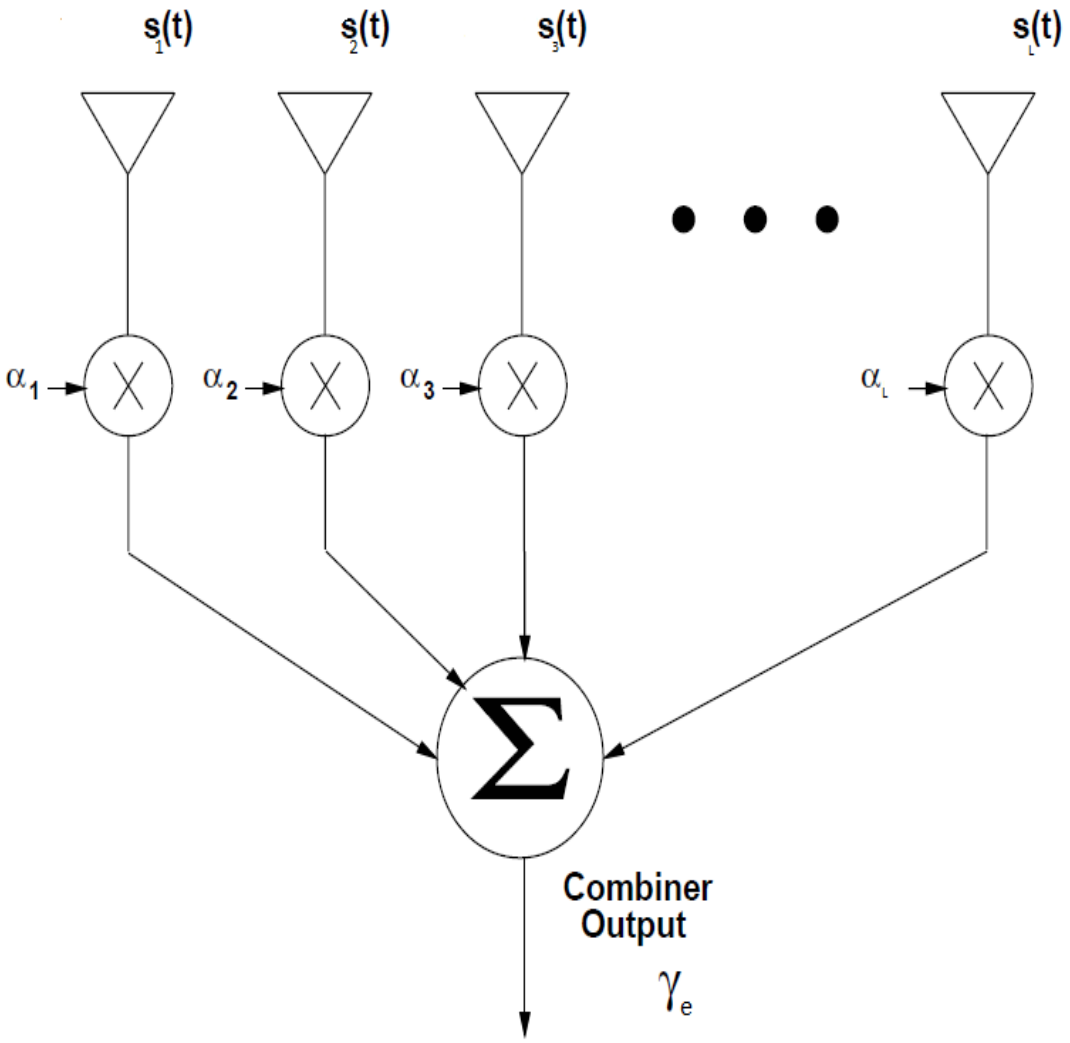

Figure 7.2. Receiver diversity combiner diagram.

7.6 Numerical and Simulation Results

In this section, we provide numerical and simulation results for the integral expressions that have been derived in this chapter for arbitrary values of the Nakagami-m fading parameters. Without loss of generality we assume that $P_S = P_R = P_{ri} = P_{di} = 1$. The simulation results are obtained using MonteCarlo simulation method, with number of runs equal to $1,000,000$ times.

Fig. 7.3 shows the BER versus SIR for BPSK of interference-limited multiple DF dual hop wireless communication system with three interferers at both the relay and the destination node over Nakagami-m fading channels with arbitrary values of m (i.e., $N_R = 3$, $N_D = 3$ with $me = 1.5$, $m_{di} = 1$, $m_{ri} = 1$, $\Omega_1 = 1.5$, $\Omega_2 = 1.3$, $\Omega_{di} = 1.1$, $\Omega_{ri} = 1.2$) and with MRC diversity order K (i.e., $K = 2$). The figure shows that the BER decreases with the increases of the SIR.

Fig. 7.4 shows the BER versus SIR for BFSK of interference-limited multiple DF dual hop wireless communication system with three interferers at both the relay and the destination node over Nakagami-m fading channels with arbitrary values of m (i.e., $N_R = 3$, $N_D = 3$ with $me = 1.5$, $m_{di} = 1$, $m_{ri} = 1$, $\Omega_1 = 1.5$, $\Omega_2 = 1.3$, $\Omega_{di} = 1.1$, $\Omega_{ri} = 1.2$) and with MRC diversity order K (i.e., $K = 2$). The figure shows that the BER decreases with the increases of the SIR.

Fig. 7.5 shows the BER versus SIR for DBSK of interference-limited multiple DF dual hop wireless communication system with three interferers at both the relay and the destination node over Nakagami-m fading channels with arbitrary values of m (i.e., $N_R = 3$, $N_D = 3$ with $me = 1.5$, $m_{di} = 1$, $m_{ri} = 1$, $\Omega_1 = 1.5$, $\Omega_2 = 1.3$,

$\Omega_{di} = 1.1$, $\Omega_{ri} = 1.2$) and with MRC diversity order K (i.e., $K = 2$). The figure shows that the BER decreases with the increases of the SIR.

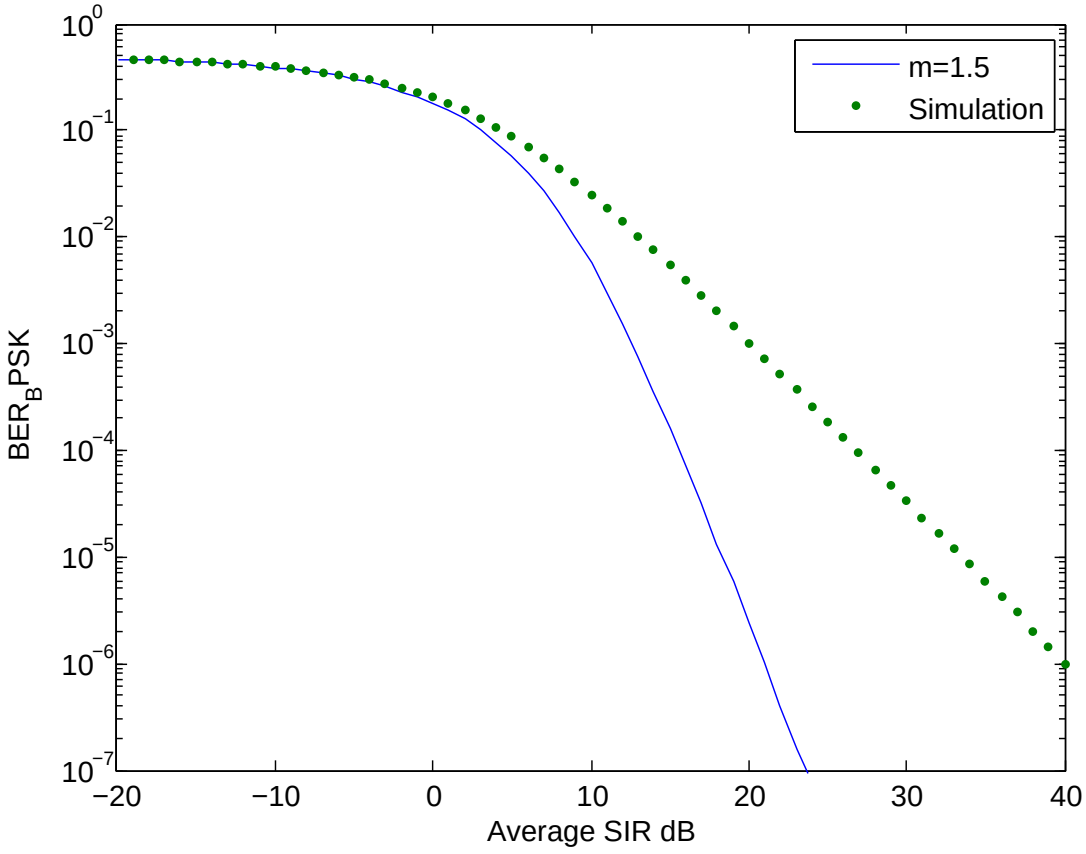

Figure 7.3. BER versus SIR for interference-limited BPSK multiple DF dual hop wireless communication system with three interferers at both the relay and the destination node over Nakagami-m fading channels with MRC diversity.

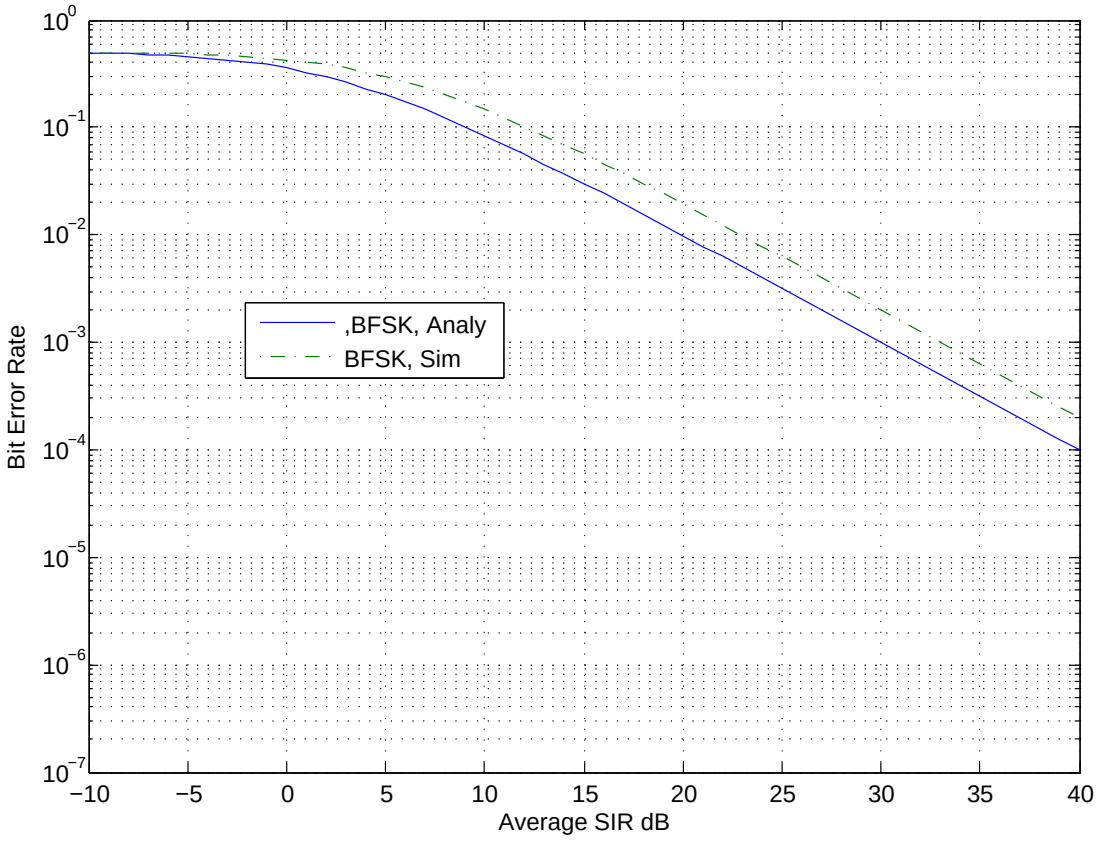

Figure 7.4. BER versus SIR for interference-limited BFSK multiple DF dual hop wireless communication system with three interferers at both the relay and the destination node over Nakagami-m fading channels with MRC diversity order.

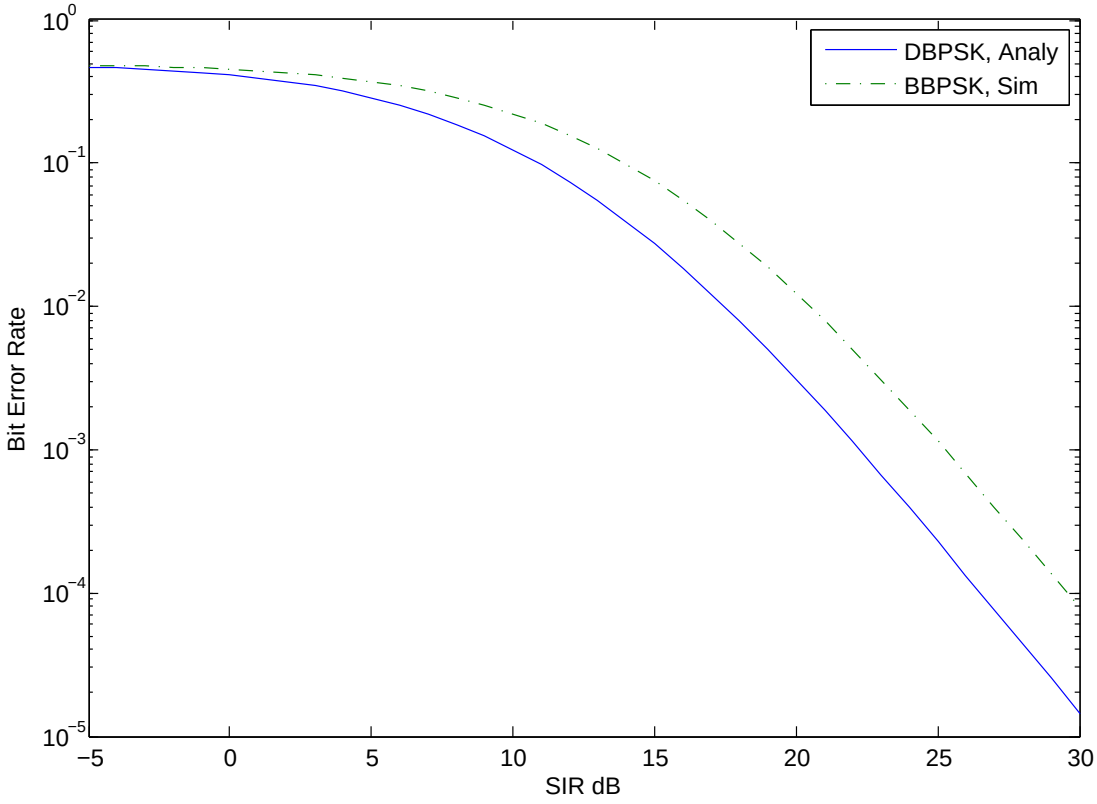

Figure 7.5. BER versus SIR for interference-limited DBPSK multiple DF dual hop wireless communication system with three interferers at both the relay and the destination node over Nakagami-m fading channels with MRC diversity.

7.7 Conclusions

The maximum ratio combining (MRC) effect on the interference-limited multiple DF relays cooperative system BER performance was investigated in Nakagami-m fading channels, and the results shows that for a given BER, increases K decreases the required SIR to achieve certain level of QoS. So, the system performance can be improved by saving the energy of the transmitted signal. Having such a study enables system engineers and designers to optimize their designs.

Chapter 8

DUAL-HOP MULTIPLE DF RELAYS COOPERATIVE SYSTEMS WITH DIVERSITY: CAPACITY PERFORMANCE ANALYSIS

8.1 Chapter Overview

Shannon theorem states that for an additive white Gaussian noise (AWGN) channel, there exist coding schemes such that it is possible to communicate error free data over the channel provided that the data rate $\mathcal{R}_b$ [bits/sec] is less than or equal to the channel capacity $\mathcal{C}$ [bits/sec] [56] and [57], where $\mathcal{C}$ is defined as:

$$\mathcal{C} = W \log_2 \left(1 + \frac{P}{N_o W}\right), \tag{8.1}$$

where W is the transmission bandwidth, P is the signal power, and N_o is the one-sided power spectral density level of the additive noise. It is noteworthy that if $\mathcal{R}_b > \mathcal{C}$, then it is impossible to achieve an error free transmission no matter what the coding scheme is. Therefore, Shannon capacity is considered as the optimistic the-

oretical bound against which to compare all practical transmission systems. In this chapter we study the normalized Shannon capacity, C, measured in [bits/sec/Hz], under different adaptive transmission protocols assuming fading channel following the Nakagami-m distribution with cochannel interference (CCI).

In Section 8.2, the related work is summarized. The chapter contributions are provided in Section 8.3. The capacity analysis is presented in section 8.4. We provide numerical and simulation results in section 8.5. Finally, the chapter conclusions are provided in section 8.6.

8.2 Related Work

In [119], the authors obtained the average channel capacity with channel side information at the transmitter and the receiver and at the receiver alone. In their paper, the optimal power and rate adaptation (OPRA) and channel inversion with fixed rate (CIFR) were implemented when the channel state information (CSI) is known at both the transmitter and the receiver sides. The optimal rate adaptation with fixed power is implemented when the CSI is known only at the receiver side. The Rayleigh fading distribution was used to model small-scale variations of the channel envelope. It should be noted that in the OPRA the better the channel conditions, the more power is transmitted under the constraint of total transmitted power, while the ORA scheme is simply the well-known AWGN channel capacity averaged over the distribution of the fading model. The authors in [119] shown that the CIFR results in a large channel capacity penalty in severe fading. Consequently,

a slightly modified version of the CIFR, the truncated channel inversion with fixed rate (TIFR), was also proposed in the same paper. The same system model as in [119] was adapted by the authors in [120] under the same channel fading model but with diversity schemes, namely, the selection combining and the maximal ratio combining schemes. The channel capacity under the three power adaptation policies was also considered in [121] assuming Nakagami-m multipath fading with diversity combining at the receiver side.

8.3 Contributions

In this chapter, we derived integral-form approximate expressions for the average channel capacity performance analysis of interference-limited dual-hop wireless communication systems with cochannel interference over Nakagami-m fading channels under different adaptive transmission protocols is investigated. Considering this channel distribution under different adaptive transmission protocols; namely, the simultaneous power and rate adaptation protocol (OPRA), the optimal rate with fixed power protocol (ORA), the channel inversion with fixed rate protocol (CIFR), and the truncated channel inversion with fixed transmit power protocol (CTIFR).

8.4 System and signal Models

In this chapter, we considered the same system and signal models of the previous chapter. In Df dual-hop wireless communication systems, the received signal at each relay node is fully decoded, re-encoded and then retransmitted to the destination

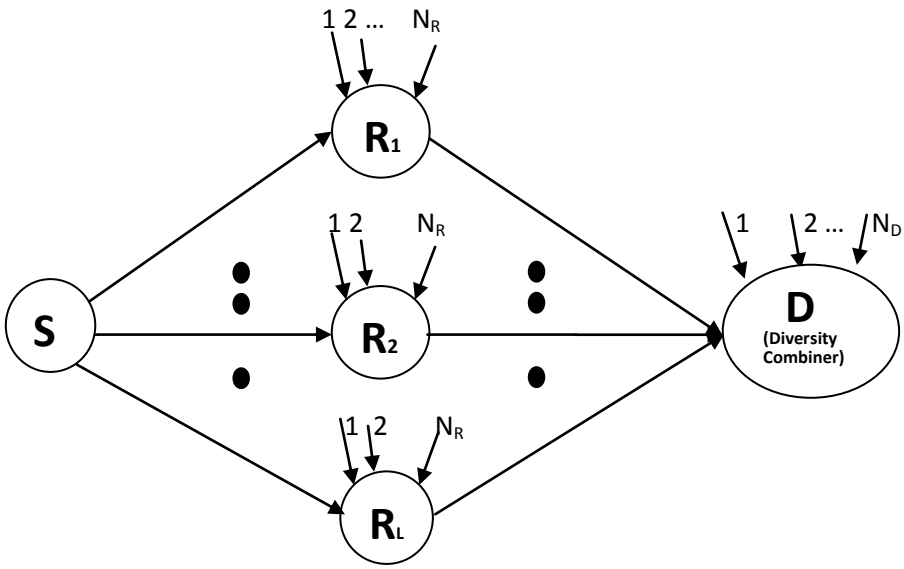

Figure 8.1. A dual-hop multiple DF relaying cooperative wireless communication system over Nakagami-m fading channels with multiple CCI at both the relays and the destination nodes.

node. Thus, the overall system achievable ACC should be the minimum of the achievable ACC's over each individual hop. On the other hand, according to [124] the overall system capacity cannot be larger than the capacity of each individual link. Therefore, the overall capacity of branch 1 of a dual-hop system with multiple DF relays is given by

$$C_{DF1} = min\left(C_{11}, C_{12}\right), \tag{8.2}$$

where C_{11} and C_{12} are the average channel capacity of the first and the second hop of the first branch in a dual-hop system with multiple DF relays, respectively. In general, when fading is present, the channel capacity can be found by averaging the AWGN channel capacity given by the Shannon theorem over the PDF distribution of the small-scale fading model, which is here the Nakagami-m distribution. Assuming

dual-hop with L relays, In this case the transmission takes place over $(1+L)$ time slots as follows

$$\begin{aligned} C_{DF1} &= \frac{1}{1+L} E\left[\log_2\left(1+\gamma\right)\right] \\ &= \frac{1}{1+L}\int_0^\infty \log_2\left(1+\gamma\right) f_{\gamma_{m1}}(\gamma) d\gamma. \end{aligned} \tag{8.3}$$

where C is the normalized channel capacity [bits/sec/Hz], and γ is the instantaneous signal-to-interference ratio with PDF $f_{\gamma_{m1}}(\gamma)$ given as

$$\gamma_{m1} = \frac{1}{1+L} min\left(\gamma_{11}, \gamma_{12}\right), \tag{8.4}$$

$$f_{\gamma_{m1}}(\gamma) = f_{\gamma_{11}}(\gamma) + f_{\gamma_{12}}(\gamma) - f_{\gamma_{11}}(\gamma) F_{\gamma_{12}}(\gamma) - f_{\gamma_{12}}(\gamma) F_{\gamma_{11}}(\gamma) \tag{8.5}$$

where

$$f_{\gamma_{11}}(\gamma) = \frac{\Gamma(m_1+m_r)}{\Gamma(m_1)\Gamma(m_r)} \left(\frac{m_1}{m_r}\right)^{m_1} \left(\frac{P_r\omega_r\gamma}{P_S\Omega_1}\right)^{m_1-1} \left(1+\frac{m_1}{m_r}\frac{P_r\omega_r\gamma}{P_S\Omega_1}\right)^{-(m_1+m_r)}, \tag{8.6}$$

and

$$f_{\gamma_{12}}(\gamma) = \frac{\Gamma(m_2+m_d)}{\Gamma(m_2)\Gamma(m_d)} \left(\frac{m_2}{m_d}\right)^{m_2} \left(\frac{P_d\omega_d\gamma}{P_R\Omega_2}\right)^{m_2-1} \left(1+\frac{m_2}{m_d}\frac{P_d\omega_d\gamma}{P_R\Omega_2}\right)^{-(m_2+m_d)} \tag{8.7}$$

$$F_{\gamma_{11}}(\gamma) = \frac{\Gamma(m_1+m_r)}{m_1\Gamma(m_1)\Gamma(m_r)} \left(\frac{m_1}{m_r}\right)^{m_1} \left(\frac{P_r\omega_r\gamma}{P_S\Omega_1}\right)^{m_1} {}_2F_1\left(m_1, m_1+m_r; 1+m_1; -\frac{m_1}{m_r}\frac{P_r\omega_r\gamma}{P_R\Omega_1}\right), \tag{8.8}$$

$$F_{\gamma_{12}}(\gamma) = \frac{\Gamma(m_2+m_d)}{m_2\Gamma(m_2)\Gamma(m_d)} \left(\frac{m_2}{m_d}\right)^{m_2} \left(\frac{P_d\omega_d\gamma}{P_R\Omega_2}\right)^{m_2} {}_2F_1\left(m_2, m_2+m_d; 1+m_2; -\frac{m_2}{m_d}\frac{P_d\omega_d\gamma}{P_R\Omega_2}\right), \tag{8.9}$$

where $f_{\gamma_{11}}(\gamma)$ and $f_{\gamma_{12}}(\gamma)$ are the PDF's of the first and the second hop of the first branch, respectively. Also, $F_{\gamma_{11}}(\gamma)$ and $F_{\gamma_{12}}(\gamma)$ are the CDF's of the first and the

second hop of the first branch, respectively. The overall equivalent SIR γ_{MRC} at the output of the MRC combiner is given as

$$\gamma_{MRC} = \sum_{l=1}^{L} \gamma_{ml}. \tag{8.10}$$

So, the PDF of γ_{MRC}, $f_{\gamma_{MRC}}(\gamma)$, is given by

$$f_{\gamma_{MRC}}(\gamma) = Convolution(f_{\gamma_{m1}}(\gamma), f_{\gamma_{m2}}(\gamma), f_{\gamma_{m3}}(\gamma), ..., f_{\gamma_{mL}}(\gamma)) \tag{8.11}$$

In the following, we will derive the ACC integral-expressions for different adaptive transmission protocols.

8.4.1 Optimal Transmit Rate Adaptation (ORA)

$$\begin{aligned} C_{ora}^{MRC} &= \frac{1}{1+L} E\left[\log_2(1+\gamma)\right] \\ &= \frac{1}{1+L} \int_0^{\infty} \log_2(1+\gamma) f_{\gamma_{MRC}}(\gamma) d\gamma \\ &= \frac{1}{1+L} \int_0^{\infty} \log_2(1+\gamma) Convolution(f_{\gamma_{m1}}(\gamma), f_{\gamma_{m2}}(\gamma), f_{\gamma_{m3}}(\gamma), ..., f_{\gamma_{mL}}(\gamma)) d\gamma \end{aligned} \tag{8.12}$$

There is no solution for the above integrals in (8.15), they are very complicated since they include the double integrals, Hypergeometric functions, logarithmical and other algebraic expressions, as example for just two branches of multiple relays (i.e., $L = 2$) cooperative system:

$$\begin{aligned} C_{ora}^{MRC} &= \frac{1}{(L+1)} E\left[\log_2(1+\gamma)\right] \\ &= \frac{1}{(L+1)} \int_0^{\infty} \log_2(1+\gamma) f_{\gamma_{MRC}}(\gamma) d\gamma \\ &= \frac{1}{(L+1)} \int_0^{\infty} \log_2(1+\gamma) Convolution(f_{\gamma_{m1}}(\gamma), f_{\gamma_{m2}}(\gamma)) d\gamma \\ &= \frac{1}{(L+1)} \int_0^{\infty} \log_2(1+\gamma) \int_0^{\infty} f_{\gamma_{m1}}(\gamma - x) f_{\gamma_{m2}}(x) dx d\gamma \\ &= \frac{1}{(L+1)} \int_0^{\infty} \log_2(1+\gamma) \int_0^{\infty} (f_{\gamma_{1,l}}(\gamma - x) + f_{\gamma_{2,l}}(\gamma - x) - f_{\gamma_{1,l}}(\gamma - x) F_{\gamma_{2,l}}(\gamma - x) - f_{\gamma_{2,l}}(\gamma - x) F_{\gamma_{1,l}}(\gamma - x)) \\ &\quad \times (f_{\gamma_{1,l}}(x) + f_{\gamma_{2,l}}(x) - f_{\gamma_{1,l}}(x) F_{\gamma_{2,l}}(x) - f_{\gamma_{2,l}}(x) F_{\gamma_{1,l}}(x)) dx d\gamma \end{aligned} \tag{8.13}$$

By substituting equations (8.6),(8.7),(8.8), and (8.9) properly in (8.13), the expression expanded to sixteen terms and there is no solution for these integrals and the

most complicated term is the one that have,

$$
\begin{aligned}
f_{\gamma_{1,l}}(x)F_{\gamma_{2,l}}(x) \times f_{\gamma_{2,l}}(\gamma-x)F_{\gamma_{1,l}}(\gamma-x) &= \frac{\Gamma(m_1+m_r)}{\Gamma(m_1)\Gamma(m_r)}\left(\frac{m_1}{m_r}\right)^{m_1}\left(\frac{P_r\omega_r\gamma}{P_S\Omega_1}\right)^{m_1-1}\left(1+\frac{m_1}{m_r}\frac{P_r\omega_r\gamma}{P_S\Omega_1}\right)^{-(m_1+m_r)} \\
&\times \frac{\Gamma(m_2+m_d)}{m_2\Gamma(m_2)\Gamma(m_d)}\left(\frac{m_2}{m_d}\right)^{m_2}\left(\frac{P_d\omega_d\gamma}{P_R\Omega_2}\right)^{m_2} \\
&\times {}_2F_1\left(m_2, m_2+m_d; 1+m_2; -\frac{m_2}{m_d}\frac{P_d\omega_d\gamma}{P_R\Omega_2}\right) \\
&\times \frac{\Gamma(m_2+m_d)}{\Gamma(m_2)\Gamma(m_d)}\left(\frac{m_2}{m_d}\right)^{m_2}\left(\frac{P_d\omega_d\gamma}{P_R\Omega_2}\right)^{m_2-1}\left(1+\frac{m_2}{m_d}\frac{P_d\omega_d\gamma}{P_R\Omega_2}\right)^{-(m_2+m_d)} \\
&\times \frac{\Gamma(m_2+m_d)}{\Gamma(m_2)\Gamma(m_d)}\left(\frac{m_2}{m_d}\right)^{m_2}\left(\frac{P_d\omega_d\gamma}{P_R\Omega_2}\right)^{m_2-1}\left(1+\frac{m_2}{m_d}\frac{P_d\omega_d\gamma}{P_R\Omega_2}\right)^{-(m_2+m_d)} \\
&\times \frac{\Gamma(m_1+m_r)}{m_1\Gamma(m_1)\Gamma(m_r)}\left(\frac{m_1}{m_r}\right)^{m_1}\left(\frac{P_r\omega_r\gamma}{P_S\Omega_1}\right)^{m_1} \\
&\times {}_2F_1\left(m_1, m_1+m_r; 1+m_1; -\frac{m_1}{m_r}\frac{P_r\omega_r\gamma}{P_R\Omega_1}\right) \qquad (8.14)
\end{aligned}
$$

The numerical and simulation results show the accuracy shortage of this double integral form in (8.13).

8.4.2 Optimal Simultaneous Transmit Power and Rate Adaptation (OPRA)

$$
\begin{aligned}
C_{opra}^{MRC} &= \frac{1}{(1+L)\ln 2}\int_{\gamma_{th}}^{\infty}\ln\left(\frac{\gamma}{\gamma_{th}}\right)f_{\gamma_{MRC}}(\gamma)d\gamma \\
&= \frac{1}{(1+L)\ln 2}\int_{\gamma_{th}}^{\infty}\ln\left(\frac{\gamma}{\gamma_{th}}\right)Conv(f_{\gamma_1}(\gamma), f_{\gamma_2}(\gamma), f_{\gamma_3}(\gamma), ..., f_{\gamma_L}(\gamma))d\gamma, \qquad (8.15)
\end{aligned}
$$

as example for just two branches of multiple relays (i.e., $L = 2$) cooperative system:

$$
\begin{aligned}
C_{opra}^{MRC} &= \frac{1}{(L+1)\ln 2}\int_{\gamma_{th}}^{\infty}\ln\left(\frac{\gamma}{\gamma_{th}}\right)f_{\gamma_{MRC}}(\gamma)d\gamma \\
&= \frac{1}{(L+1)\ln 2}\int_{\gamma_{th}}^{\infty}\ln\left(\frac{\gamma}{\gamma_{th}}\right)Conv(f_{\gamma_1}(\gamma), f_{\gamma_2}(\gamma)d\gamma \\
&= \frac{1}{(L+1)\ln 2}\int_{\gamma_{th}}^{\infty}\ln\left(\frac{\gamma}{\gamma_{th}}\right)\int_0^{\infty}f_{\gamma_1}(\gamma-x)f_{\gamma_2}(x)dxd\gamma \\
&= \frac{1}{(L+1)\ln 2}\int_{\gamma_{th}}^{\infty}\ln\left(\frac{\gamma}{\gamma_{th}}\right)\int_0^{\infty}(f_{\gamma_{1,l}}(\gamma-x)+f_{\gamma_{2,l}}(\gamma-x)-f_{\gamma_{1,l}}(\gamma-x)F_{\gamma_{2,l}}(\gamma-x)-f_{\gamma_{2,l}}(\gamma-x)F_{\gamma_{1,l}}(\gamma-x)) \\
&\quad \times (f_{\gamma_{1,l}}(x)+f_{\gamma_{2,l}}(x)-f_{\gamma_{1,l}}(x)F_{\gamma_{2,l}}(x)-f_{\gamma_{2,l}}(x)F_{\gamma_{1,l}}(x))dxd\gamma \qquad (8.16)
\end{aligned}
$$

By substituting equations (8.6),(8.7),(8.8), and (8.9) properly in (8.16), the expression expanded to sixteen terms and there is no solution for these integrals and the

most complicated term is the one that have,

$$
\begin{aligned}
f_{\gamma_{1,l}}(x)F_{\gamma_{2,l}}(x) \times f_{\gamma_{2,l}}(\gamma-x)F_{\gamma_{1,l}}(\gamma-x) \quad = \quad & \frac{\Gamma(m_1+m_r)}{\Gamma(m_1)\Gamma(m_r)}\left(\frac{m_1}{m_r}\right)^{m_1}\left(\frac{P_r\omega_r\gamma}{P_S\Omega_1}\right)^{m_1-1}\left(1+\frac{m_1}{m_r}\frac{P_r\omega_r\gamma}{P_S\Omega_1}\right)^{-(m_1+m_r)} \\
& \times \frac{\Gamma(m_2+m_d)}{m_2\Gamma(m_2)\Gamma(m_d)}\left(\frac{m_2}{m_d}\right)^{m_2}\left(\frac{P_d\omega_d\gamma}{P_R\Omega_2}\right)^{m_2} \\
& \times {}_2F_1\left(m_2, m_2+m_d; 1+m_2; -\frac{m_2}{m_d}\frac{P_d\omega_d\gamma}{P_R\Omega_2}\right) \\
& \times \frac{\Gamma(m_2+m_d)}{\Gamma(m_2)\Gamma(m_d)}\left(\frac{m_2}{m_d}\right)^{m_2}\left(\frac{P_d\omega_d\gamma}{P_R\Omega_2}\right)^{m_2-1}\left(1+\frac{m_2}{m_d}\frac{P_d\omega_d\gamma}{P_R\Omega_2}\right)^{-(m_2+m_d)} \\
& \times \frac{\Gamma(m_2+m_d)}{\Gamma(m_2)\Gamma(m_d)}\left(\frac{m_2}{m_d}\right)^{m_2}\left(\frac{P_d\omega_d\gamma}{P_R\Omega_2}\right)^{m_2-1}\left(1+\frac{m_2}{m_d}\frac{P_d\omega_d\gamma}{P_R\Omega_2}\right)^{-(m_2+m_d)} \\
& \times \frac{\Gamma(m_1+m_r)}{m_1\Gamma(m_1)\Gamma(m_r)}\left(\frac{m_1}{m_r}\right)^{m_1}\left(\frac{P_r\omega_r\gamma}{P_S\Omega_1}\right)^{m_1} \\
& \times {}_2F_1\left(m_1, m_1+m_r; 1+m_1; -\frac{m_1}{m_r}\frac{P_r\omega_r\gamma}{P_R\Omega_1}\right) \qquad (8.17)
\end{aligned}
$$

The numerical and simulation results show the accuracy shortage of this double integral form in (8.16).

8.4.3 Channel Inversion with Fixed Rate (CIFR)

$$
\begin{aligned}
C_{\text{cifr}}^{MRC} &= \frac{1}{1+L}\log_2\left[1+\frac{1}{\int_0^\infty \gamma^{-1}\, f_{\gamma_{MRC}}(\gamma)d\gamma}\right] \\
&= \frac{1}{1+L}\log_2\left[1+\frac{1}{E[\gamma^{-1}]}\right]. \qquad (8.18)
\end{aligned}
$$

as example for just two branches of multiple relays (i.e., $L=2$) cooperative system:

$$
C_{\text{cifr}}^{MRC} = \frac{1}{(L+1)}\log_2\left[1+\frac{1}{\int_0^\infty \gamma^{-1} Conv(f_{\gamma_1}(\gamma), f_{\gamma_2}(\gamma)d\gamma d\gamma}\right] \qquad (8.19)
$$

There is no solution for the above integrals in (8.19.The numerical and simulation results show the accuracy shortage of this double integral form in (8.13).

8.4.4 Truncated Channel Inversion with Fixed Rate (TIFR)

$$
C_{\text{tifr}}^{MRC} = \frac{1}{1+L}\log_2\left[1+\frac{1}{\int_{\gamma_{th}}^\infty \gamma^{-1}\, f_{\gamma_{MRC}}(\gamma)d\gamma}\right](1-P_{\text{out}}) \qquad (8.20)
$$

as example for just two branches of multiple relays (i.e., $L = 2$) cooperative system:

$$C_{\text{tifr}}^{MRC} = \frac{1}{(L+1)}\log_2\left[1+\frac{1}{\int_{\gamma_{th}}^{\infty}\gamma^{-1}Conv(f_{\gamma_1}(\gamma),f_{\gamma_2}(\gamma)d\gamma d\gamma}\right](1-P_{\text{out}}) \quad (8.21)$$

P_{out} is the outage probability defined as the probability that the instantaneous SIR drops below the threshold γ_{th}, given as

$$P_{\text{out}}(\gamma_{th}) = \frac{\Gamma(m_2+m_d)}{m_2\Gamma(m_2)\Gamma(m_d)}\left(\frac{m_2}{m_d}\right)^{m_2}\left(\frac{P_d\omega_d\gamma_{th}}{P_R\Omega_2}\right)^{m_2}{}_2F_1\left(m_2,m_2+m_d;1+m_2;-\frac{m_2}{m_d}\frac{P_d\omega_d\gamma_{th}}{P_R\Omega_2}\right). \quad (8.22)$$

There is no solution for the above integrals in (8.21).The numerical and simulation results show the accuracy shortage of integral form above.5 in (8.13).

8.5 Numerical and Simulation Results

In this section, we provide numerical and simulation results for the integral-expressions derived in this chapter for the different transmission protocols in dual-hop DF relaying cooperative system with two DF relays($L = 2$). Without loss of generality we assume that $P_S = P_R = P_{ri} = P_{di} = 1$. The simulation results are obtained using MonteCarlo simulation method, with number of runs equal to $1,000,000$ times. The difference between the analytical and simulation results shows the lack in accuracy of the derived expressions due to approximation and complexity of these expressions.

In Fig. 8.2, the normalized average channel capacity per unit bandwidth according to the ORA transmission policy in dual-hop DF relaying cooperative system with two DF relays($L = 2$) is presented assuming the Nakagami-m fading channel model for $m = 1$.

The normalized capacity per unit bandwidth according to the simultaneous optimal and rate adaptation policy (OPRA) in dual-hop DF relaying cooperative system

with two DF relays($L = 2$) is shown in Fig. 8.3 at the threshold SIR equal to 2 dB. The figure shows that as the SIR increases, the capacity increases as expected.

In Fig. 8.4, the normalized average channel capacity per unit bandwidth [Bit/sec/Hz] versus the average SIR, in dual-hop DF relaying cooperative system with two DF relays($L = 2$) over the Nakagami-m fading channel model with the channel inversion with fixed rate protocol (CIFR) for $m = 1$. The figure shows that as the SIR increases, the capacity increases as expected.

In Fig. 8.5, the normalized average channel capacity per unit bandwidth [Bit/sec/Hz] versus the average SIR, in dual-hop DF relaying cooperative system with two DF relays($L = 2$) over the Nakagami-m fading channel model with the truncated channel inversion with fixed rate protocol (TIFR) for a $m = 1$. The figure shows that as the SIR increases, the capacity increases as expected.

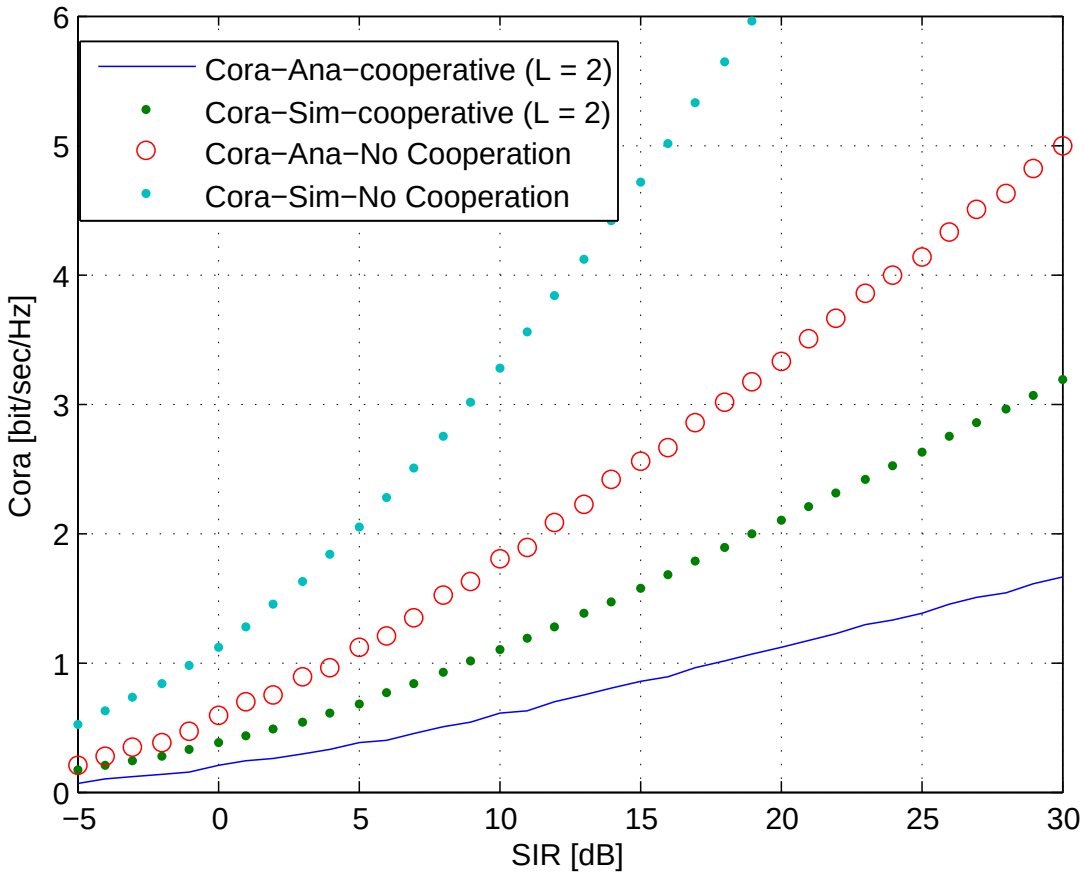

Figure 8.2. The normalized average channel capacity per unit bandwidth [Bit/sec/Hz] versus the average SIR for non-cooperative and cooperative system with two DF relays($L = 2$) over the Nakagami-m fading channel model with optimal rate adaptation and fixed power protocol (ORA).

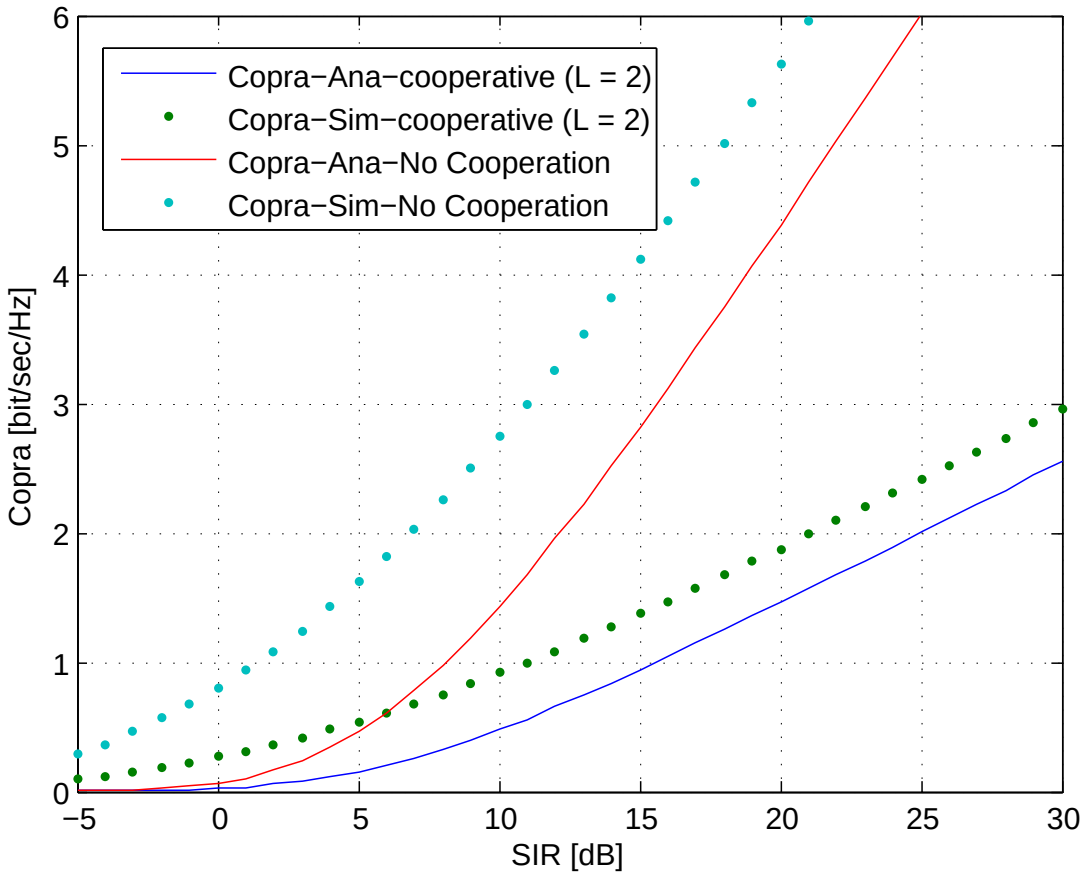

Figure 8.3. The normalized average channel capacity per unit bandwidth [Bit/sec/Hz] versus the average SIR for non-cooperative and cooperative system with two DF relays($L = 2$) over the Nakagami-m fading channel model with simultaneous optimal power and rate adaptation protocol (OPRA).

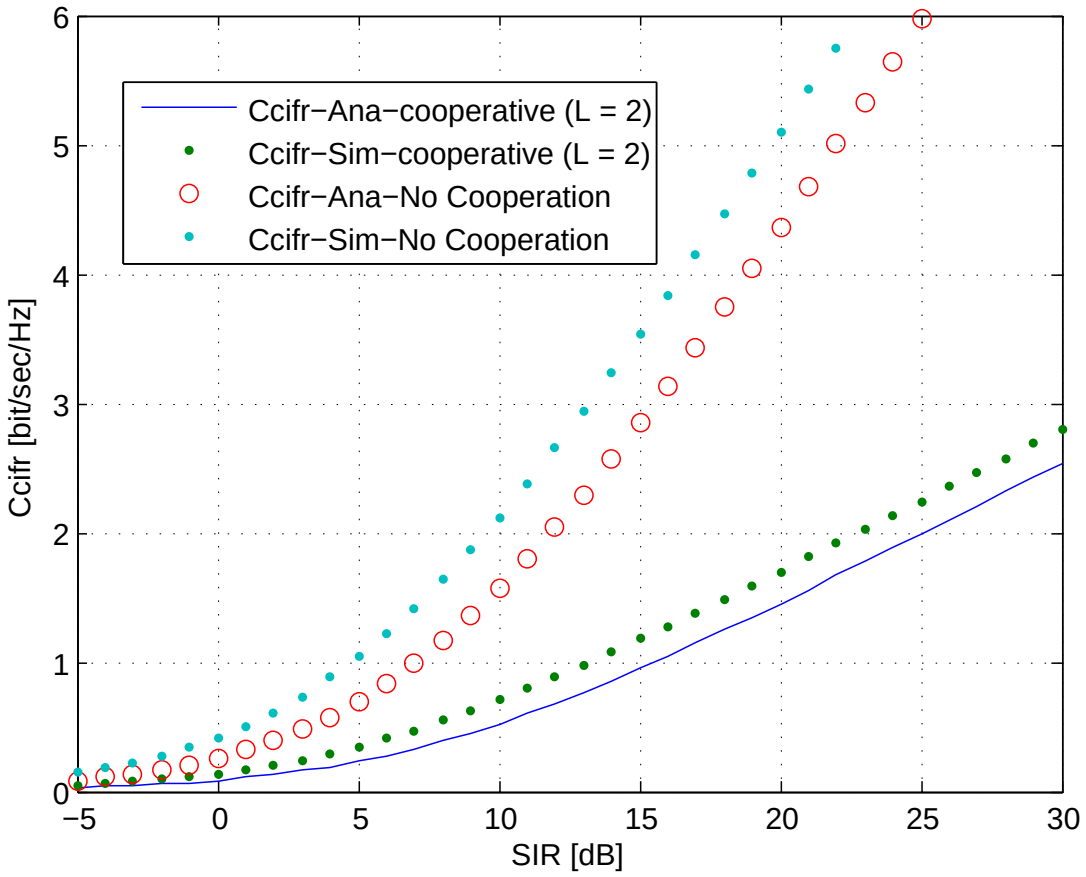

Figure 8.4. The normalized average channel capacity per unit bandwidth [Bit/sec/Hz] versus the average SIR for non-cooperative and cooperative system with two DF relays($L = 2$) over the Nakagami-m fading channel model with the channel inversion with fixed rate protocol (CIFR).

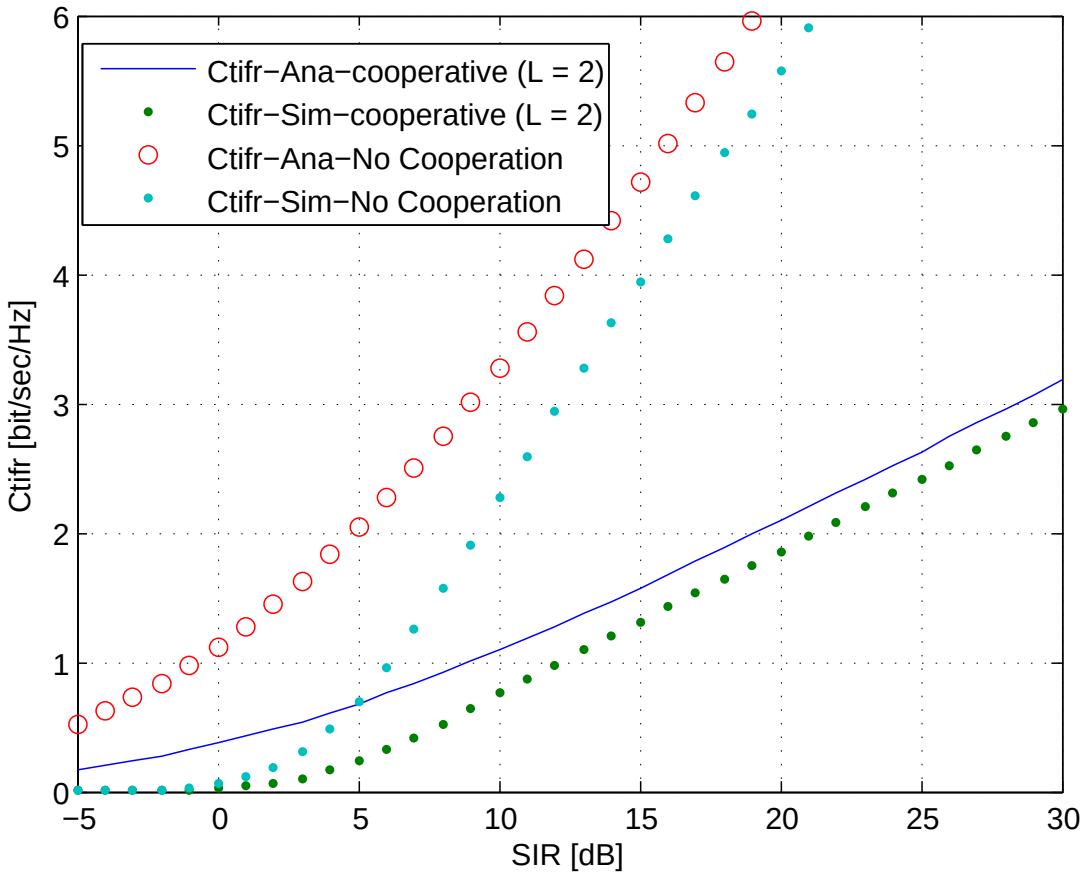

Figure 8.5. The normalized average channel capacity per unit bandwidth [Bit/sec/Hz] versus the average SIR for non-cooperative and cooperative system with two DF relays($L = 2$) over the Nakagami-m fading channel model with truncated channel inversion with fixed rate protocol (TIFR).

8.6 Conclusions

In this chapter, we considered a dual-hop multiple DF relaying wireless communication system over the Nakagami-m small-scale fading channels with multiple CCI at both the relay and the destination nodes. Approximate integral-expressions for the average channel capacity (ACC) for different adaptive transmission protocols are derived. The normalized channel capacity different transmission protocols; the optimal rate adaptation with fixed transmitted power (ORA), the simultaneous power and rate adaptation transmission (OPRA), the truncated channel inversion with fixed rate transmission protocol (TIFR), and the channel inversion with fixed rate transmission protocol (CIFR).The difference between the analytical and simulation results shows the lack in accuracy of the derived expressions due to approximation and complexity of these expressions.

Chapter 9

FT-BASED INTERPOLATION TECHNIQUE FOR SVD COMPLEXITY REDUCTION: ALGORITHM

9.1 Overview

In this chapter, we consider MIMO-OFDM wireless communication systems, and we propose an algorithm-based singular value decomposition (SVD) as an encoding/decoding technique to reduce the computational complexity of the system under study using the Fourier transform interpolation method. In section 9.2, we present our motivations behind the study of such a system model. In section 9.3 we present the merit of the work. In section 9.4, we review work related to interpolation-based techniques for low complexity MIMO-OFDM systems. The chapter contributions are provided in section 9.5. The combination of the MIMO and OFDM systems are provided in section 9.6. In section 9.7, the system model is provided. In section 9.8, we present the singular value decomposition of the channel matrix. In section 9.9, we present the singular value decomposition of the channel matrix through FT-based

interpolation. Finally, Summary and conclusions are provided in section 9.10.

9.2 Motivations

Multiple-Input, Multiple-Output (MIMO) systems use space diversity to enhance performance by implementing multiple antennas at both transmitter and receiver sides. The signals from each transmit antenna take separate paths during propagation to be combined at the receiver in a way to improve the received signal quality. Using Orthogonal Frequency Division Multiplexing (OFDM) in wideband wireless systems decouples the frequency selective fading channel into a set of parallel flat fading subchannels. Hence, using equalizers is no longer needed, which results in reduced receiver complexity.

It is known that in the space between a transmitter and a receiver in a wireless communication system, the signal can take many different directions due to reflection, refraction, scattering, and other propagation phenomena. Therefore, characteristics and numbers of available paths depend on the terrain between transmitters and receivers. Traditionally, these multiple propagation paths were only thought of as a reason to introduce attenuation, degradation, and interference, which result in reduced signal-to-noise ratio and, hence, reduce signal quality. In fact, by using MIMO, these additional multipath signal propagations can be effectively combined to further improve signal quality. As a result of using multiple antennas (space diversity) on transmitters and receivers, MIMO technology is able to effectively increase the capacity of a given wireless communication system. More information can be trans-

mitted through a wireless communication channel with a predefined error probability requirement for a given application. On the other hand, the precoding and decoding computational complexity in MIMO increases as the number of transmit and receive antennas increase, as the detection typically requires computing the eigenvalues and eigenvectors of the channel gain matrix when using the singular value decomposition (SVD) encoding/decoding technique or the Gram-Schmidt orthogonalization process when using the QR decomposition. This complexity increases more in MIMO wireless systems based on OFDM as this computation is needed for each of the OFDM symbols. Therefore, the resulting computational complexity becomes significant for large MIMO size.

9.3 Merit of the Work

The obtained reduction in computational complexity and the evaluation of the BER performance of BPSK modulation scheme in wireless communication system can help engineers to build communication systems in different aspects, such as transmit power optimization, cellular system Planning (i.e, cluster size, frequency reuse factor, cell radius, and type of antennas), and wireless communication system resources utilization.

9.4 Related Work

Large amount of studies related to this subject reported in the literature. In [76], the author has shown that in sufficiently rich scattering environments, MIMO systems

hold the potential for enormous spectral efficiency, and, thus, capacity improvements relative to SISO systems. To combat frequency selective fading, multicarrier systems, such as OFDM systems, are gaining acceptance as multiplexing schemes over single carrier systems for broadband wireless systems due to their large delay tolerance property. It is well known that the capacity of a wireless system in a multipath fading environment can be significantly increased by the use of multiple antennas at the transmitter and receiver [78]. These systems are commonly referred to as MIMO systems and can be classified as space-time signaling, e.g. space-time coding [79], and spatial multiplexing, e.g. a Vertical Bell Labs Space-Time Architecture (V-BLAST) system [80]. These techniques exploit the fact that in rich multipath scattering environments, the signals received at each element of the receiver array are uncorrelated. They have been successfully applied for frequency-selective channels through their combination with OFDM, for example [81, 82].

In [85], the parallel-sorted QR decomposition (P-SQRD) algorithm for a limited number of sub-carriers is applied. The interpolation algorithm to find the QRD for the rest of the sub-carriers, the optimization of detection order, and the reduction of system computational complexity are achieved with good performance. They also proposed that the order of detection has a deep impact on performance of the SIC and should therefore be optimized. With respect to the QRD, this optimization can be achieved by permuting the column of channel matrix by the P(n), denoting an optimized permuting matrix of carrier n, which leads to different decomposition algorithms that are useful for computational complexity reduction issues by applying interpolation methods. Most previous researchers proposed different interpolation

algorithms, such as interpolation-based transmit beamforming for MIMO-OFDM, interpolation-based QR decomposition in MMO-OFDM systems [83]and [84], and interpolation for low complexity SIC for MIMO-OFDM using P-SQRD [85].

In [86]-[87], the authors propose interpolation-based detection algorithms introduced for MIMO-OFDM systems. The idea of these algorithms is based on QR decomposition and efficient matrix inversion. In [106], the author calculates QR decomposition only for a limited number of subcarriers and to determine the matrices $Q(n)$ and $R(n)$ for the remaining carriers by interpolation algorithm before executing SIC detection. Thereby, the computational cost for QR decomposition is reduced, yielding reduction in overall complexity for a sufficiently large number of the sub-carriers. In [91] and [94], several methods and approaches to solve interpolation problems for signal processing issues are investigated, like Canonical basis, Lagrange, Newton and trigonometric, and FT interpolation methods, and they are very useful for complexity reduction issues. In [92], the authors proposed a fast and efficient method for the interpolation of non-stationary seismic data. The method uses the fast Fourier transform to identify the space wave number evolution of non-stationary spatial signals at each temporal frequency. The non-redundant nature of this interpolation method renders a big computational advantage to this interpolation method. In [93], the DFT-based interpolation is applied to design fractional delay FIR filter by using suitable index mapping. The filter coefficients are easily computed because a closed-form design is obtained.

In [94], the authors propose a new transmit beamforming scheme with partial feedback and beamforming interpolation, in which the receiver sends back informa-

tion about only a fraction of beamforming vectors and information for the phase rotation to the transmitter through the feedback channel; and the transmitter computes the beamforming vectors for all subcarriers through proposed spherical linear interpolation. In [106], the authors present computationally efficient implementation for successive interference cancelation (SIC) for a per-antenna-coded MIMO-OFDM system. this implementation utilizes a parallelized version of the sorted QRD (PSQRD) algorithm in order to achieve the same detection order for all subcarriers. In [107], the authors propose an optimal QR decomposition, which they call the equal-diagonal QR decomposition, or the QRS decomposition. They apply the decomposition to pre-coded successive cancellation detection, where they assume that both the transmitter and the receiver have perfect channel state information (CSI) knowledge. In [108], the authors present a novel, computationally efficient algorithm for detecting V-BLAST architectures with respect to the MMSE criterion. It utilizes a sorted QR decomposition of the channel matrix and leads to a simple successive detection structure. In [109], the authors claim that computational complexity can be simplified in the following ways: first, to simplify channel capacity calculation, they prove that eigenvalues of the full channel matrix multiplication equals eigenvalues of the triangular channel matrix multiplication. Second, to simply evaluate the optimal transmission rate constrained constellation, they propose a simplified multiplication of the resulted simple triangular matrix and a transmitted signal vector.

The other commonly used precoding/decoding method in MIMO-OFDM systems is based on the SVD process, which requires computing singular values and corresponding singular vectors of the channel matrix by exploiting the SVD technique.

When the MIMO-OFDM system has a large number of sub-channels, the SVD computation becomes very complex due to computing the SVD for each sub-channel separately. A wide range of research work has been reported in the literature for reducing the computational complexity in precoding/decoding based on SVD decomposition for MIMO-OFDM sub-channels. In [111], the authors propose low computational complexity based on an SVD algorithm with fast convergence speed. The proposed SVD algorithm has the following features: (1) low total computational complexity, (2) fast convergence speed, (3) the ability of reconfiguration to different numbers of transmitter and receiver antennas, and (4) insensitive to the dynamic range problem, which is suitable for hardware implementation. In [112], the authors propose a new approach to eliminate co-space interference and inter-symbol interference (ISI) in time and frequency domains, respectively. By using a polynomial matrix SVD based on a second order sequential best rotation (SBR2) algorithm, the MIMO- OFDM system is decomposed to the parallel decoupled single input, single output (SISO) OFDM systems. In this way, the CSI is eliminated by time-domain broadband beamforming (TBBF) in both transmitter and receiver sides, and the ISI is mitigated in each SISO-OFDM system by frequency-domain equalization. In this dissertation, we present a computationally efficient technique for precoding/decoding MIMO-OFDM symbols at the transmitter/receiver, respectively, which depends on applying the conventional SVD process for only a limited number of subcarriers. Taking advantage of the fact that the inverse FFT (IFFT) and FFT processes are inherently implemented in the MIMO-OFDM transmitter and receiver, respectively, we propose to use the FFT-based interpolation method at the receiver to estimate

the SVD decompositions for the remaining MIMO-OFDM subcarriers. Our objective in this proposed technique is in line with the previous work reported in the literature. However, the results in our study advance the literature in the sense that more reduction in precoding/decoding complexity of MIMO-OFDM symbols is achieved as compared to previously reported work. Throughout the chapter, we quantitatively demonstrate this computational complexity reduction using computer simulations.

9.5 Contributions

We propose a simple and computationally efficient method-based SVD decomposition of channel matrix to detect the received signal. The complexity is reduced significantly compared to the other methods-based QR decomposition for all Nc carriers, which burns heavy computational complexity. Moreover, we extend our work to add more computational complexity reduction by using the proper FT-based interpolation algorithm. We evaluate and compare the other interpolation algorithms and their realizations with the results of this work. Our tool for conducting this study was to use the available MATLAB software to perform the required calculations for the above mentioned algorithms.

9.6 Multiple Input Multiple Output Orthogonal Frequency-Division Multiplexing (MIMO-OFDM) System

The combination between the two techniques will exploit both systems advantages. OFDM is a method for digital modulation in which a signal is split into several narrowband channels at different frequencies. OFDM is a special case of multicarrier transmission, where a single data stream is transmitted over a number of lower rate sub-carriers. It is worth mentioning here that OFDM can be seen as either a modulation technique or a multiplexing technique. One of the main reasons to use OFDM is to increase the robustness against frequency selective fading or narrowband interference. In a single carrier system, a single fade or interferer can cause the entire link to fail, but in a multicarrier system, only a small percentage of the sub carriers will be affected. Error correction coding can then be used to correct for the few erroneous sub-carriers. The main idea of MIMO-OFDM is the spatial multiplexing, which represents the most popular approach to exploit the capacity advantages of multiple antenna systems. Information theoretical results show that MIMO systems can provide enormous capacity gains. MIMO wireless technology seems to meet a lot of demands by offering increased spectral efficiency through spatial multiplexing gain and improved link reliability due to antenna diversity gain. Even though there are still a large number of open research problems in the area of MIMO-OFDM wireless systems, both from theoretical and hardware implementation perspectives, the technology has been considered ready for use in practical systems. On the other

hand, there are many of difficulties facing MIMO-OFDM systems which prevent them from being widely used and extensively deployed. With the fact that spectrum is a scarce resource, and the propagation conditions are hostile due to fading caused by destructive addition of multipath components and interference from other users, this requirement calls for means to radically increase spectral efficiency and to improve link reliability. The heavy computational complexity of interference cancellation at the receiver side per carrier transmitting of a MIMO-OFDM system is the main challenge in our study. One of the key problems is keeping the good performance level with minimum computational complexity for interference cancellation process at the receiver side and minimizing the receiver cost. Various studies exist on this key problem to use various interpolation methods to reduce the MIMO-OFDM receiver complexity. The problem that we study in this work is to investigate an interpolation method and to get less computational complexity than other common methods. The MIMO-OFDM system consists of many receive and transmit antennas connected together via wireless communication media. One of the main types of the MIMO-OFDM receivers is the interference cancellation receiver which use the concept of channel matrix decomposition method to extract the receive signal at certain antenna without any interference from other antennas.

9.7 System and Channel Model

A multiple transmit and receive antennas system with n_t transmit antennas at transmitter and n_r receive antennas at receiver is assumed, assuming $n_r \geq n_t$ to get the

best diversity gains in additive white Gaussian noise (AWGN) and fading environment. The channel model is a Laurent polynomial channel of order N^h between all transmit and receive antennas which can be described by N^h+1 coefficient matrices $H_{TD}(l)$, $0 \leq l \leq N^h$, and contains the channel fading gains. We assumed that the channel completely known by the receiver. The corresponding transfer function of the MIMO-OFDM channel is given by [106]

$$H(e^{jw}) = \sum_{l=0}^{N^h} H_{TD}(l)e^{-jwl} \qquad 0 \leq l \leq N^h, \tag{9.1}$$

and is a polynomial matrix of degree N^h in e^{jw} with the normalized frequency $0 \leq w \leq 2\pi$. Expanding (9.1) results in

$$H(e^{jw}) = H_{TD}(0) + H_{TD}(1)e^{-jw_1} + H_{TD}(2)e^{-jw_2} + \cdots + H_{TD}(N^h)e^{-jw_{N^h}}, \tag{9.2}$$

By sampling this transfer function $H(e^{jw})$ at N_c equidistant sampling frequencies, where the sampling frequency is given by

$$w_n = 2\pi n/Nc, \qquad 0 \leq n \leq N_c - 1, \tag{9.3}$$

the channel matrices at discrete carrier frequencies are given as follows.

$$H(n) = H(e^{jw_n}) = \sum_{l=0}^{N^h} H_{TD}(l)e^{-jw_n l} \qquad 0 \leq n \leq N_c - 1, \tag{9.4}$$

$$H(n) = H_{TD}(0)+H_{TD}(1)e^{-jw_n}+H_{TD}(2)e^{-j2w_n}+\cdots+H_{TD}(N^h)e^{-jN^h w_n} \qquad 0 \leq n \leq N_c-1. \tag{9.5}$$

According to (9.5) only $N^h + 1$ $H(n)$ are needed to transmit so we can find the remaining channel matrices by interpolation because the channel matrix is a Laurent polynomial matrix of degree N^h (i.e., only $N^h + 1$ carriers are required to

calculate all other $H(n)$ by interpolation). Interpolation methods can reduce the computational complexity of the system under study and reduce the cost of the system implementation since no need for complicated processors [99].

9.7.1 MIMO-OFDM Transmitter

The main operations at the MIMO-OFDM transmitter are given as follows. The information data is spliced into n_t (number of transmitter antennas) parallel data streams, commonly called layers, and then can be coded by Forward Error Correction (FEC) and then interleaved (i.e., send data vertically). Then it is modulated by any modulation scheme, typically M-QAM or M-PSK, to obtain the modulated symbols $d_i(n)$, where $1 \leq i \leq n_t$, and $0 \leq n \leq N_c - 1$. After transforming the symbols to time domain by using the inverse fast Fourier transform (IFFT), a guard interval (GI) of length N_G is added in the form of a cyclic prefix to obtain the signal $X_i(t)$ of length $N_c + N_G$. Then this signal is transmitted from the i^{th} transmit antenna. So the transmitted MIMO-OFDM signal in vector form is given by

$$\mathbf{X}(t) = [X_1(t)X_2(t)X_3(t)\dots X_{n_t}(t)]^T, \tag{9.6}$$

where

$[.]^T$: represents the transpose operation of the vector.

9.7.2 MIMO-OFDM Receiver

At the receiver stage, the main operations of a MIMO-OFDM receiver are as follows. The GI, which is in the form of a cyclic prefix, is deleted, and the FFT process (which is the reverse operation of the IFFT process at the transmitter) is used to perform the transformation back into frequency domain from the time domain. The application of the cyclic prefix and discrete Fourier transform (or Fast Fourier transform for simplicity) results in N_c orthogonal carriers in the MIMO-OFDM system. So, the corresponding received vector in the frequency domain can be given as follows [106]

$$\mathbf{Y}(n) = \mathbf{H}(n)\mathbf{X}(n) + \mathbf{W}(n), \qquad 0 \leq n \leq N_c - 1, \tag{9.7}$$

where

$\mathbf{Y}(n)$: the $n_r \times 1$ received vector in the frequency domain,

$\mathbf{H}(n)$: the $n_r \times n_t$ MIMO channel matrix in frequency domain,

$\mathbf{X}(n)$: the $n_t \times 1$ transmitted vector in frequency domain,

$\mathbf{W}(n)$: the $n_r \times 1$ Additive White Gaussian Noise vector at each receive antenna in the frequency domain.

The process of precoding/decoding in combined MIMO-OFDM systems requires decomposition of the channel matrix $\mathbf{H}$(n) for all the N_c subcarriers. This decomposition can be done by one of the several approaches of factorization like, Singular Value (SVD), QR, LU, and Cholesky decompositions. In this dissertation, we are interested in the first decomposition technique, which depends on SVD decomposition.

9.8 Singular Value Decomposition (SVD) Of MIMO-OFDM Channel Gain Matrix

In order to perform interference cancellation (IC) on subcarrier n, the channel matrix $\mathbf{H}(n)$ is decomposed using the SVD process. The SVD of the channel matrix $\mathbf{H}$ with size $n_r \times n_t$ is typically computed by finding the Eigenvalues and Eigenvectors of $\mathbf{H}\mathbf{H}^T$ and $\mathbf{H}^T\mathbf{H}$. Eigenvectors of $\mathbf{H}^T\mathbf{H}$ make up the columns of $\mathbf{V}$; the Eigenvectors of $\mathbf{H}\mathbf{H}^T$ make up the columns of $\mathbf{U}$. Also, the singular values in $\mathbf{S}$ are square roots of Eigenvalues from $\mathbf{H}\mathbf{H}^T$ or $\mathbf{H}^T\mathbf{H}$. The singular values are the diagonal entries of the $\mathbf{S}$ matrix and are arranged in descending order. The singular values are always real numbers. If the matrix $\mathbf{H}$ is a real matrix, then $\mathbf{U}$ and $\mathbf{V}$ are also real. The singular value matrix $\mathbf{S}$, which contains the singular values of the channel matrix, is known at the transmitter by feedback signal from the receiver. For example, the n^{th} subcarrier MIMO channel matrix can be decomposed using SVD as

$$\mathbf{H} = \mathbf{U}\mathbf{S}\mathbf{V}^H,$$

where $\mathbf{S}$ is the diagonal matrix with non-negative entries, with the same dimension as $\mathbf{H}$, and with nonnegative diagonal elements in decreasing order having the singular values of $\mathbf{H}$ and unitary matrices $\mathbf{V}$ and $\mathbf{U}$ with dimensions $n_t \times n_t$ and $n_r \times n_r$, respectively. Notice that $\mathbf{U}$ and $\mathbf{V}$ are unitary matrices so that $\mathbf{U^T U} = \mathbf{I}$, $\mathbf{U^T} = \mathbf{U}^{-1}$, and $\mathbf{V}\mathbf{V}^T = \mathbf{I}$, where $\mathbf{U}$ and $\mathbf{V}$ are orthogonal, and $\mathbf{I}$ is the identity matrix.

Assuming that the MIMO-OFDM receiver has perfect knowledge of the channel matrix $\mathbf{H}(n)$ using a channel estimation process; thus, at the receiver end, the received vector in frequency domain $\mathbf{Y}$ is multiplied by $\mathbf{U^H}$. It is important here to pay

attention to matrix $\mathbf{V}$, which is obtained at the transmitter side by the feedback signal from the receiver and is multiplied by the transmitted signal at the transmitter. Then, the received vector at the receiver side is given by

$$\mathbf{Y} = \mathbf{HVX} + \mathbf{W}$$

by multiplying the received vector by the filter matrix $\mathbf{U}^H$ to obtain

$$\begin{aligned}\overline{\mathbf{Y}} &= \mathbf{U}^H\mathbf{Y} \\ &= \mathbf{U}^H\mathbf{HVX} + \mathbf{U}^H\mathbf{W}\end{aligned}$$

after decomposing $\mathbf{H}$ using the SVD process to obtain

$$\begin{aligned}&= \mathbf{U}^H\mathbf{U}\ \mathbf{SV}^H\mathbf{V}\ \mathbf{X} + \mathbf{U}^H\mathbf{W} \\ &= \mathbf{S}\ \mathbf{X} + \overline{\mathbf{W}}.\end{aligned} \tag{9.8}$$

So according to the $\mathbf{S}$ matrix structure, $\overline{\mathbf{Y}}$ is free of interference (i.e., the multiplication of $\mathbf{S}$ matrix by the received signal vector $\mathbf{X}$ will achieve the interference cancellation in the MIMO-OFDM system).

9.9 SVD Through Interpolation

9.9.1 Fourier Transform Interpolation

Different interpolation techniques are used to interpolate the channel matrices in MIMO-OFDM wireless communication systems, such as Canonical basis, Lagrange, Newton, and Trigonometric interpolation [107]. An efficient approach for performing the interpolation is using IFFT and FFT since these operations exist already in

the MIMO-OFDM transmitter and receiver, respectively. Let us say we want to interpolate the vector $\mathbf{X}$ by the FFT and IFFT method. The original vector $\mathbf{X}$ is transformed to the Fourier domain using FFT and then transformed back using the IFFT with more points (oversampling). If we have vector $\mathbf{X}$ of length $= a$, and $\mathbf{X}$ has a sample interval given by dx, then, the new sample interval for vector $\mathbf{Z}$ is given by $dz = dx(a/b)$, where $\mathbf{Z}$ is the new vector and results from applying the interpolation-based Fourier transform method on the vector $\mathbf{X}$. The length of the vector $\mathbf{Z} = b$. Note that b cannot be smaller than a. If $\mathbf{H}$ is a matrix, then the interpolation based on the Fourier transform technique operates on the columns of $\mathbf{H}$, returning a matrix $\mathbf{J}$ with the same number of columns as $\mathbf{H}$, but with a higher number of rows. As we mentioned before, we consider the channel matrix $\mathbf{H(n)}$ as a Laurent Polynomial (LP) matrix of degree N^h, and if $\mathbf{H(n)}$ is known for N_k distinct subcarriers with $N_k < N_c$ and $N_k \geq N^h + 1$, then all remaining N_d channel matrices $\mathbf{H(n)}$, where $N_d = N_c - N_k$, can be calculated by interpolation. Using this philosophy, authors in [113] interpolated the channel matrices $\mathbf{H(n)}$ for the data subcarriers from the corresponding pilot carriers. Furthermore, they proposed to calculate the filter matrices (i.e., R matrices) for IC in a MIMO-OFDM system only for a limited number of carriers and to determine the remaining filter matrices by interpolation. In the following, we apply this idea for the SVD process.

9.9.2 Interpolation of SVD Decomposition

We use the philosophy of calculating the matrices resulting from applying SVD for channel matrices of a MIMO-OFDM system only for a limited number of carriers

and determine the remaining SVD filter matrices by interpolation based on the FFT and IFFT. We used FT-based interpolation since FFT and IFFT processes are exist inherently in the MIMO-OFDM system. So if the SVD filter matrices are known for distinct subcarriers N_k with $N_k \leq N_c$ and $N_k \geq N^h + 1$, then all remaining coefficients of polynomial matrices $\mathbf{H(n)}$ with $N_d = N_c - N_k$ can be calculated by interpolation-based Fourier transform technique instead of calculating the SVD for all N_c carriers, which burns heavy computational complexity.

Algorithm

- Determine the channel matrix $\mathbf{H(n)}$ for each of the N_k subcarriers, $n \in N_k$. This step could be done by sending pilot subcarrier signals, where they are already exist in the system for signaling issues.

- Perform SVD process with respect to these $\mathbf{H(n)}$ matrices, $n \in N_k$, as follows.

$$\mathbf{H} = \mathbf{USV}^H.$$

- Interpolate the N_k $\mathbf{U}, \mathbf{S}$, and $\mathbf{V}^H$ matrices to obtain the remaining N_d matrices of $\mathbf{U}, \mathbf{S}$, and $\mathbf{V}^H$, where $N_d = N_c - N_k$.

9.10 Summary and Conclusions

This chapter proposed a simple and computationally efficient interpolation-based SVD decomposition of a channel matrix to detect the received signal in MIMO-OFDM systems. The complexity is reduced significantly compared to the other

methods that perform the QR decomposition for all Nc carriers. The proposed algorithm for interpolation-based SVD decomposition for MIMO-OFDM systems can yield a computational complexity savings over the carrier-by-carrier PSQR decomposition. Due to the reduction in the computational complexity, the processing delay and time cost will also be reduced. Moreover, the interpolation through the FT for the MIMO-OFDM system needs no additional system hardware since the FT is inherently included in the system, so no additional cost is needed. Having such a study with the evaluation of BER performance and computational complexity reduction of MIMO-OFDM communication systems, enables system engineers and designers to optimize their designs before actual deployment in real situations and save the cost that may occur according to mistakes in system hardware implementation.

Chapter 10

FT-BASED INTERPOLATION TECHNIQUE FOR SVD COMPLEXITY REDUCTION: PERFORMANCE ANALYSIS

10.1 Overview

In this chapter, we analyze the computational complexity and BER performance of SVD Pre-coding and Decoding of MIMO-OFDM Systems with and without the proposed algorithm. In the sequel, we investigate the complexity of the proposed interpolation based SVD detection with respect to complex floating point operations F, and compare it to the P-SQRD detection. SVD outperforms PSQRD since SVD has no interference left, whereas the interference should be canceled successively in PSQRD. But the PSQRD does not require any process at the transmitter side, so there is no need for the CSI at the transmitter side, where as the SVD requires process at the transmitter side, so the CSI at the transmitter side is needed.

The remainder of this chapter organized as follows. In section 10.2, we present the computational complexity analysis. In section 10.3, we present the BER performance

analysis using Monte Carlo simulation. In section 10.4, we present the numerical and simulation results. Finally, Summary and conclusions are provided in section 10.5.

10.2 Computational Complexity

In this chapter we investigate the computational complexity of the proposed method with respect to complex floating point operations (flops) F, and compare it to the method proposed by [106], in which the authors propose interpolation-based full Parallel Sorted QR Decomposition (P-SQRD). For comparison purposes, we assume that the number of transmit antennas and the number of receive antennas are equal to each other (i.e., $n_t = n_r$). To compute the computational complexity using floating point operations, the mathematical operations such as addition and multiplication, division, and subtraction, count as one flop [106]. The SIC following the signal-to-interference-and-noise-ratio (SINR) approach in [106] cost

$$F_{SINR-SIC} = O((16n_t^4 + (2n_r + 1/6)n_t^3 + 3n_r n_t^2)N_C) \tag{10.1}$$

floating point operations. In [106], the authors give the overall computational complexity of interpolated PSQRD as follows:

$$F_{Int-P-SQRD} = F_{P-SQRD,Nk} + F_M + F_{Int} + F_{\triangle^2}, \tag{10.2}$$

where

$$F_{psqrd,N_k} = ((4n_r + 1/4)n_t^2 - 3/2n_r n_t)N_k, \tag{10.3}$$

$$F_M = (n_t^2 + (1 + 2n_r)n_t - 3 - 2n_r)N_k, \tag{10.4}$$

$$F_{Int} = (3/2n_t^2 + (3/2 + 3n_r)n_t)(N_c - N_k), \tag{10.5}$$

and

$$F_{\triangle^2} = (n_t - 1)(N_c - N_k)/2. \tag{10.6}$$

The SVD process of a matrix $\mathbf{H}$ with $n_t \times n_r$ size is typically computed by a two-step procedure, in the first step, the matrix is reduced to a bidiagonal matrix, which can be done using a householder reflections process. The second step is to compute the SVD of the bidiagonal matrix. The overall cost is $O(n_t n_r^2)$ flops [105]. So, for N_k channel matrices the SVD process will cost $\mathrm{O}(n_t n_r^2 N_k)$ flops. For the interpolation part, we consider the Fourier transform interpolation method which implements FFT and IFFT operations. It is well known that the quick computing of FFT of N points can be computed in only $\mathrm{O}(N \times logN)$ operations and since we apply the interpolation for just $N_c - N_k$ carriers, the computational complexity for the FFT interpolation method will cost $O(2(N_c - N_k)log(N_c - N_k))$. As a result the total computational complexity of the overall proposed process is given by

$$\begin{aligned} F_{Int-SVD} &= F_{SVD,N_k} + F_{Int} \\ &= O(n_t n_r^2 N_k) + O(2(N_c - N_k)log(2(N_c - N_k))). \end{aligned} \tag{10.7}$$

Using the Matlab platform aid, we compute the interpolation and the SVD of the channel matrices for different carriers. Also, we evaluate the computational complexity of the method proposed in [106], the results show that the computational complexity of the MIMO-OFDM receiver based on the SVD costs less than the one based on QRD, this reduction in cost increases with the increase in the number of carriers N_c, as well as the number of transmit and receive antennas.

10.3 BER performance Analysis

The simulation of BER performance analysis is described in this section. Through this BER performance analysis we assumed that he channel experienced between each transmit to the receive antenna is independent and randomly varying in time. The channel experience by each transmit antenna is independent from the channel experienced by other transmit antennas. The simulation performs the following: At the transmitter side,

- Generation of random binary sequence (10^6 bits)
- BPSK modulation (i.e., bit 0 represented as -1 and bit 1 represented as +1)
- Group the modulated symbols into pair of two symbols and send two symbols in one time slot (2×2 MIMO system)
- Assigning modulated symbols to OFDM subcarriers (IFFT process)
- Adding cyclic prefix
- Concatenation of multiple symbols to form a long transmit sequence
- Create the rayleigh fading channel
- Convolution of each symbol with the random channel
- Adding White Gaussian Noise,

and at the receiver side,

- Removing cyclic prefix and taking the desired subcarriers

- Converting to frequency domain (FFT process)
- Apply the proposed FT-based interpolation algorithm for the SVD process as explained in the previous chapter.
- Perform Maximal Ratio Combining for equalizing the new received symbol
- Demodulation and conversion to bits
- Counting the number of bit errors and compute the BER
- Repeat this process 10^8 times and take the average of the outputs (Monte Carlo runs)
- Repeat for multiple values of SIR (we consider the range from -5 to 30 dB) and plot the simulation results.

The following section presents the numerical and simulation results of this chapter.

10.4 Numerical and Simulation Results

In this section, we provide the following results of this study. Fig. 10.1 compares the computational complexity in terms of the number of floating point operations (F) for different decomposition methods of a MIMO-OFDM system with $n_r = n_t$, $N_c = 32$, and $N^h = 8$, we notice the reduction in the computational complexity due to using the proposed method and this reduction increases with the increase in the number of carriers N_c as well as the number of transmit and receive antennas. The figure

shows that the SVD based-FT interpolation requires less computational complexity than the QRD FT-based interpolation method, and this difference in the required computations becomes more significant by increasing the number of the transmit and receive antennas as well as the number of carriers.

Fig. 10.2 compares the computational complexity in terms of the number of floating point operations (F) for different decomposition methods of a MIMO-OFDM system with $n_r = n_t$, $N_c = 512$, and $N^h = 8$, we notice the reduction in the computational complexity due to using the proposed method and this reduction increases with the increase in the number of carriers N_c as well as the number of transmit and receive antennas. The figure shows that the FT-based interpolation of SVD requires less computational complexity than the FT-based interpolation of QRD method, and this difference in the required computations becomes more significant by increasing the number of the transmit and receive antennas as well as the number of carriers.

Fig. 10.3 shows the BER of BPSK MIMO-OFDM system over a Rayleigh channel with SVD pre-coding and decoding process with and without FT-based interpolation. We can see that the computational complexity due to the proposed method does not degrade the system performance level.

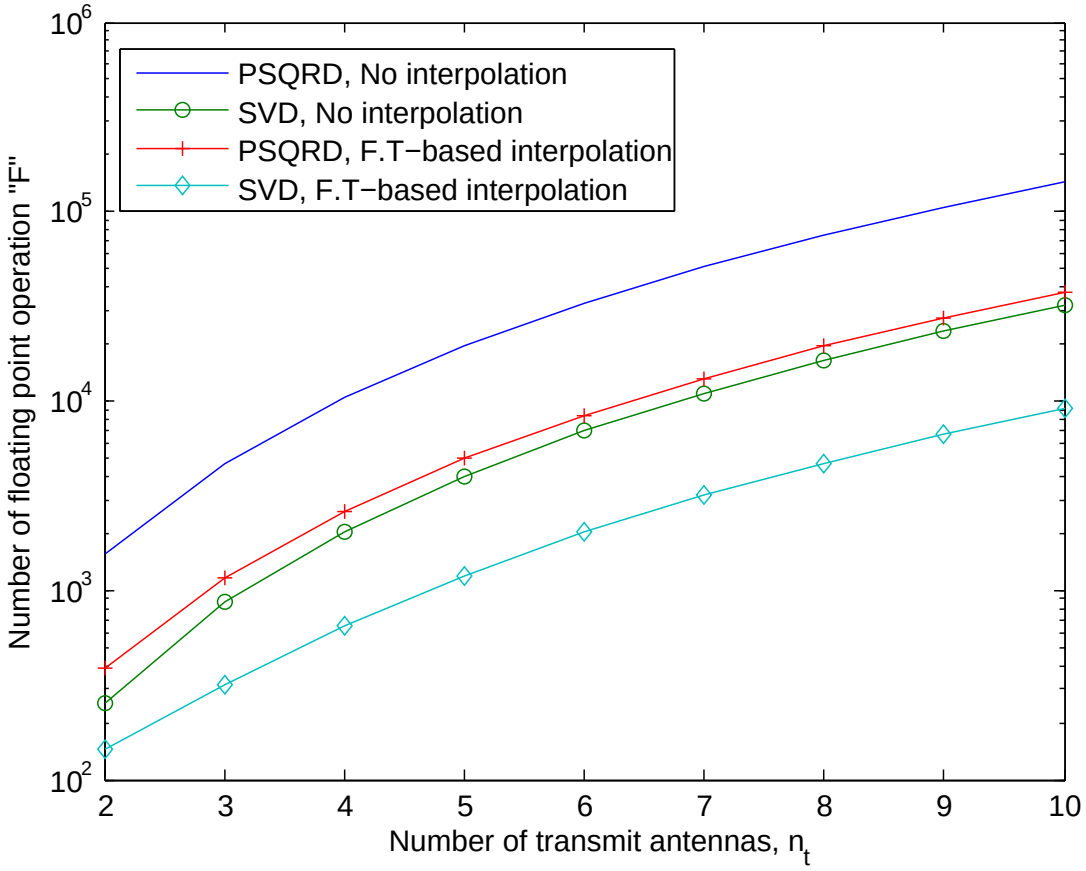

Figure 10.1. Number of floating point operations (F) for decomposition methods of a MIMO-OFDM system with $n_r = n_t$, $N_c = 32$, and $N^h = 8$.

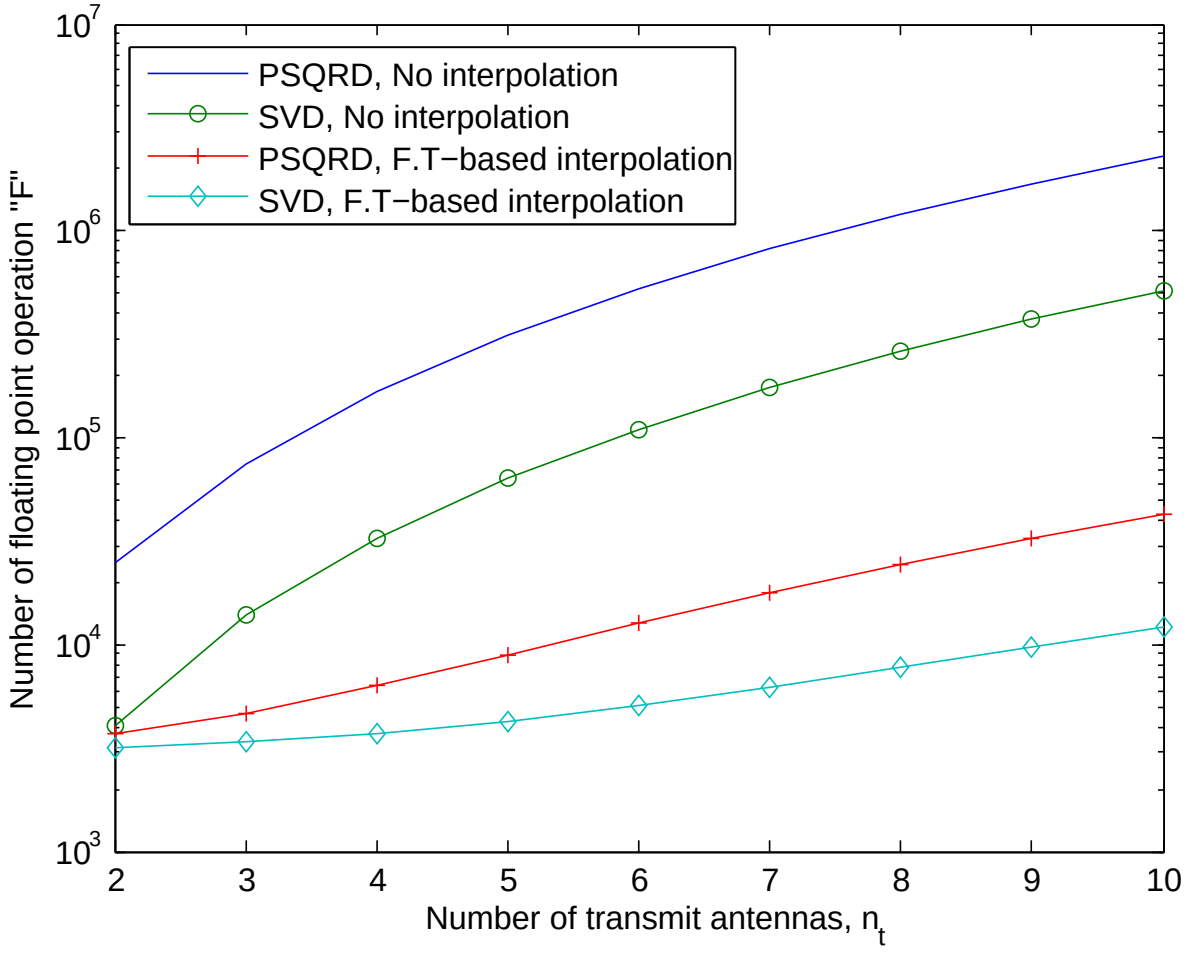

Figure 10.2. Number of floating point operations (F) for decomposition methods of a MIMO-OFDM system with $n_r = n_t$, $N_c = 512$, and $N^h = 8$

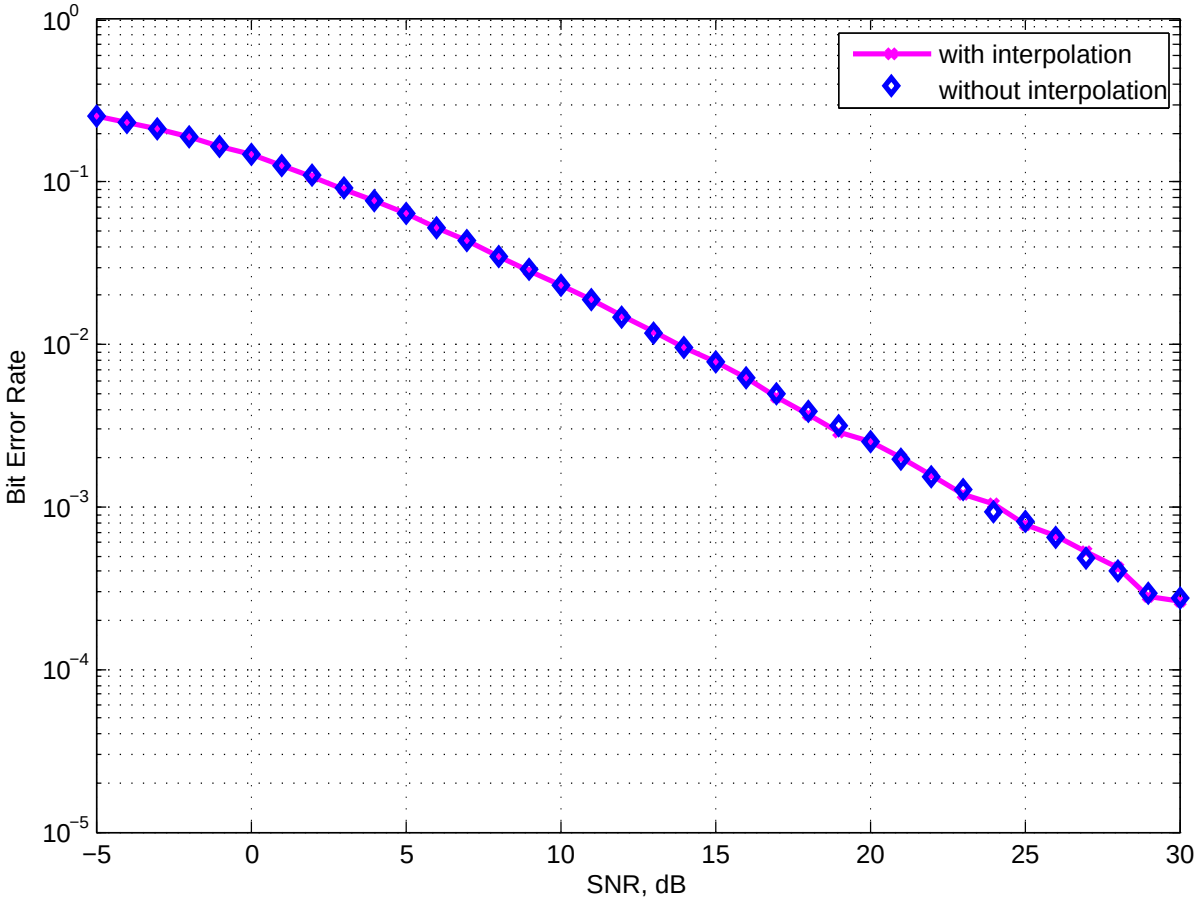

Figure 10.3. BER of BPSK MIMO-OFDM stem over a Rayleigh channel with SVD pre-coding and decoding process with and without FT interpolation

10.5 Summary and Conclusions

This chapter analyze the computation complexity and the BER performance analysis for FT-based interpolation of SVD decomposition of a channel matrix to detect the received signal in MIMO-OFDM systems. The results show that the complexity is reduced significantly compared to the other methods that perform the QR decomposition for all Nc carriers. The proposed algorithm for F.T-based interpolation of SVD decomposition for MIMO-OFDM systems can yield a computational complexity savings over the carrier-by-carrier PSQR decomposition. Due to the reduction in the computational complexity, the processing delay and time cost will also be reduced. Moreover, the interpolation through the FT for the MIMO-OFDM system needs no additional system hardware since the FT is inherently included in the system, so no additional cost is needed. Having such a study with the evaluation of BER performance and computational complexity reduction of MIMO-OFDM communication systems, enables system engineers and designers to optimize their designs before actual deployment in real situations and save the cost that may occur according to mistakes in system hardware implementation.

Chapter 11

DISSERTATION CONCLUSIONS AND FUTURE WORK

11.1 Dissertation Conclusions

In this dissertation, we have covered several interesting topics in wireless communication systems that are crucial and essential in the next generation of wireless communications. It also has provided extensive approaches in deriving different performance metrics of the newly emerging models for wireless communication systems. Moreover, the analysis of wireless communication systems with power and rate adaptation are provided in order to maximize the achievable channel capacity and throughput under the different transmission protocols. This dissertation has provided general expressions for the performance metrics by considering the small-scale fading model, the Nakagami-m distribution, which conveys the flexibility of the obtained expressions by considering other fading models as special case; namely, the Rayleigh. This dissertation contains two parts and the following points summarize the contributions and the conclusions of each part:

- In the first part, the average bit error rate (BER) performance of interference-limited dual-hop decode-and-forward (DF) relaying cooperative systems with

co-channel interference (CCI) at both the relay and destination nodes is analyzed in small-scale multipath Nakagami-m fading channels with arbitrary (integer as well as non-integer) values of m. This channel condition is assumed for both the desired signal as well as co-channel interfering signals. In addition, the practical case of unequal average fading powers between the two hops is assumed in the analysis. Accurate closed-form approximate expressions for the BER performance of different modulation schemes (i.e., binary phase shift keying (BPSK), binary frequency shift keying (BFSK), differential binary phase shift keying (DBPSK), and coherent M-ary modulation schemes) are derived. Beside that, the characteristic function approach is used to derive a limited integral form of the average BER of the M-ary modulation schemes. The analysis assumes an arbitrary number of independent and non-identically distributed (i.n.i.d.) interfering signals at both relay (R) and destination (D) nodes. The derived closed-form expressions are simple and easy to evaluate as compared to the exact one using simulation. In this part, the results show that the DPSK modulation scheme outperforms the BFSK modulation scheme, where as the BPSK modulation scheme outperforms both of them. Considering this channel distribution in cooperative and non-cooperative communication system we derived closed integral expressions for the average channel capacity (ACC) under different adaptive transmission protocols; namely, the simultaneous power and rate adaptation protocol (OPRA), the optimal rate with fixed power protocol (ORA), the channel inversion with fixed rate protocol (CIFR), and the truncated channel inversion with fixed transmit power protocol (CTIFR). Numer-

ical and simulation results are obtained to show the accuracy of the obtained expressions. The derived expressions as well as the generated performance curves are useful for several applications in the wireless communication theory, especially in the design phase of cellular network planning.

- Also, in this part, the work extended to the case when the receiver employs the maximum ratio combining (MRC) and the equal gain combining (EGC) combining schemes to exploit the diversity gain in multipath fading channels. The effect of MRC and EGC diversity on the system BER and ACC performance analysis was considered with k elements at the receiver antenna, and the results show that for a given BER or ACC, increasing K decreases the required SIR. So, the system performance can be improved by saving the energy of the transmitted signal. The numerical and the simulation results have been provided to verify the accuracy of our derived expressions. The derived expressions in this dissertation are new and have not been previously reported in the literature.

- In the second part, the large computational complexity in the encoding/decoding process in the multiple-input multiple-output and orthogonal frequency division multiplexing (MIMO-OFDM) systems is reduced by the proposed technique. The process of precoding/decoding in combined MIMO-OFDM systems requires the computation of the conventional singular value decomposition (SVD) for each of the data-carrying OFDM tones. Since MIMO-OFDM systems involve large number of data-carriers, the corresponding computational

complexity becomes significantly large. In this study, we present a computationally efficient technique for precoding/decoding MIMO-OFDM symbols at the transmitter/receiver, respectively, which depends on applying the conventional SVD process for only a limited number of subcarriers. Making the advantage of the fact that the inverse FFT (IFFT) and FFT processes are inherently implemented in the MIMO-OFDM transmitter and receiver, respectively, we propose to use the FFT-based interpolation method at the receiver to estimate the SVD decompositions for the remaining MIMO-OFDM subcarriers. The computation results show that the new proposed technique results in reduced computational complexity in encoding/decoding MIMO-OFDM symbols as compared to other schemes known in literature. The derived expressions as well as the generated performance curves are useful for several applications in the wireless communication theory, especially in the design phase of cellular network planning. Also, the work extended to investigate the effect of this complexity reduction on the system performance. The results show that the proposed algorithm does not affect the system error performance.

- Finally, dissertation conclusions and Proposed future plan are presented at the end of this manuscript. Numerical results are obtained for all of the obtained closed-form expressions. The derived expressions as well as the generated performance curves are useful for several applications in the wireless communication theory, especially in the design phase of cellular network planning. The dissertation has analyzed different aspects of the wireless communication sys-

tems and obtained expressions for different performance measures. Further investigations can be conducted to extend our research work to include more practical systems and channel conditions.

11.2 Proposed Future Plans

The dissertation has analyzed different aspects of the wireless communication systems and derived closed-form expressions for different performance metrics (i.e., BER and ACC). Further investigations can be conducted to extend our research work to include more practical systems and channel conditions. Possible extensions for the dissertation can be summarized in the following points:

- More realistic channel conditions can be considered to tackle further signal degradation phenomena, such as large-scale fading (log normal shadowing), co-channel interference in interference and noise channels, antenna shape factor, and non-flat (selective) fast fading (including both time-selective and frequency-selective fading). In addition, we can also consider other generalized multipath small-scale fading such as the $\kappa-\eta$ and the $\mu-\eta$ fading models that most recently addressed in the literature. Furthermore, possible extensions can be accomplished by considering more practical received signal replicas when using diversity combining, such as having some kind of correlation between these replicas or having each signal replica follow a certain fading model, i.e., one path follows the Rayleigh, the other one follows the Nakagami-m, Rician, Weibull, $\alpha-\mu$ model,etc. Other future work can be obtained by

considering hybrid diversity combining schemes containing both the coherent and non-coherent diversity combiners.

- Many extensions can be attained by studying other types of the channels in relay-based communications. Moreover, the analysis of a dual-hop amplify and forward cooperative communication systems acquires the determination of the harmonic mean distributions of the two hop distribution models. However, the harmonic mean distribution of all fading models, other than the Rayleigh, is a challenging task mathematically. Therefore, studying the BER performance of an amplify and forward cooperative systems with Nakagami-m, Weibull, or the $\alpha-\mu$ channel models, adds a good impact to the literature and describes a more realistic channel environment. also, we can consider other type of channel models and other diversity combiners, such as the selective combining, with the different transmission protocol.

- The MIMO-OFDM system model in this dissertation can be extended to include space time coding, time hopping, and frequency hopping. Moreover, other channel conditions can also be considered, including other signal impairments as pointed out earlier above. In addition, code division multiple access can also be considered by assigning each user with a code as well as a private encryption algorithm with distributed relay-nodes cooperative communication systems.

- The investigated problems in this dissertation could be extended to include multiuser detection and multiplexing techniques, space division multiple access,

and code division multiple access can also be considered.

LIST OF REFERENCES

References

[1] P. A. Anghel and M. Kaveh,"Exact symbol error probability of a cooperative network in a Rayleigh-fading environment" IEEE Trans. Wireless Commun., vol. 3, no. 5, pp. 14161421, Sept. 2004.

[2] A. K. Sadek, W. Su, and K. J. R. Liu, "Multinode cooperative communications in wireless networks," IEEE Trans. Signal Process., vol. 55, pp. 341-355, Jan. 2007.

[3] Valentine A. Aalo, and Jingjun Zhang, "On the effect of cochannel interference on average error rates in Nakagami-fading channels," IEEE COMMUNICATIONS LETTERS, VOL. 3, NO. 5, MAY 1999

[4] S. Savazzi and U. Spagnolini, "Cooperative space-time coded transmissions in Nakagami-m fading channels," in Proc. IEEE GLOBECOM07, pp. 4334-4338, Nov. 2007.

[5] L.-L. Yang and H.-H. Chen, "Error probability of digital communications using relay diversity over Nakagami-m fading channels," IEEE Trans. Wireless Commun., vol. 6, pp. 1806-1811, May 2008.

[6] Z. Yi and I.-M. Kim, "Diversity order analysis of the decode-and forward cooperative networks with relay selection," IEEE Trans. WirelessCommun., vol. 6, pp. 1792-1799, May 2008.

[7] Yinman Lee, Ming-Hung Tsai, and Sok-Ian Sou, "Performance of Decode-and-Forward Cooperative Communications with Multiple Dual-Hop Relays over Nakagami-m Fading Channels", IEEE Transactions on Wireless Communications, vol. 8, no. 6, June 2009.

[8] J. N. Laneman, D. N. C. Tse, and G.W.Wornell,"Cooperative diversity in wireless networks: Efficient protocols and outage behavior" IEEE Trans. Inf. Theory, vol. 50, no. 12, pp. 30623080, Dec. 2004.

[9] M. O. Hasna and M.-S. Alouini,"A performance study of dual-hop transmissions with fixed gain relays," IEEE Trans. Wireless Commun., vol. 3, pp. 1963-1968, Nov. 2004.

[10] M. O. Hasna and M. S. Alouini, "Harmonic mean and end-to-end performance of transmission systems with relays," IEEE Trans. Commun., vol. 52, pp. 130-135, Jan. 2004.

[11] A. Adinoyi and H. Yanikomeroglu,"Cooperative relaying in multiantenna fixed relay networks," IEEE Trans. Wireless Commun., vol. 6, pp. 533-544, Feb. 2007.

[12] G. K. Karagiannidis, T. A. Tsiftsis, and R. K. Mallik,"Bounds of multihop relayed communications in Nakagami-m fading," IEEE Trans. Commun., vol. 54, pp. 18-22, Jan. 2006.

[13] G. K. Karagiannidis,"Performance bounds of multihop wireless communications with blind relays over generalized fading channels," IEEE Trans. Wireless Commun., vol. 5, pp. 498-503, Mar. 2006.

[14] S. Ikki and M. H. Ahmed,"Performance analysis of cooperative diversity wireless networks over Nakagami-m channels," IEEE Commun. Lett., vol. 11, pp. 334-336, Apr. 2007.

[15] Himal A. Suraweera, George K. Karagiannidis, "closed-form error analysis of the non-identical Nakagami-m relay fading channel," IEEE Communications Letters, vol. 12, no. 4, April 2008.

[16] Fawaz S Al-Qahtani, Caijun Zhong, Khalid A. Qaraqe, Hussein Alnuweiri, Tharm Ratnarajah, "performance analysis of dual-hop AF systems in Nakagami-m fading channels in the presence of interference," IEEE ICC 2011 proceedings International conference on digital object identifire. PP. 1-5, 2011.

[17] Fawaz S Al-Qahtani, Duong, Caijun Zhong, Khalid A. Qaraqe, Hussein Alnuweiri, Tharm Ratnarajah, "performance analysis of dual-hop AF systems in Nakagami-m

fading channels in the presence of interference," IEEE signal procesing Letter, Vol. 18, Issue 8, PP. 454-457, 2011.

[18] In-Ho Lee, Dongwoo Kim, "Decouple-and-forward relaying for dual-hop alamouti transmissions," IEEE Communications Letters, Vol. 12, no. 2, February 2008.

[19] W. Su, A. K. Sadek, and K. J. R. Liu,"SER performance analysis and optimum power allocation for decode-and-forward cooperation protocol in wireless networks," in Proc. IEEE Wireless Commun. Networking Conf., vol. 2, pp. 984-989 Mar. 2005.

[20] A. K. Sadek, W. Su, and K. J. R. Liu, "Performance analysis for multinode decode-and-forward relaying in cooperative wireless networks," in Proc. IEEE Int. Conf. Acoustics, Speech, Signal Process., vol. 3, pp. 521524, Mar. 2005.

[21] Y. Lee and M.-H. Tsai, "Performance of decode-and-forward cooperative communications over Nakagami-m fading channels," IEEE Trans. Veh. Technol., vol. 58, no. 3, pp. 12181228, Mar. 2009.

[22] W. Su, "Performance analysis for a suboptimum ML receiver in decodeand- forward communications," in Proc. IEEE Global Telecommun. Conf., pp. 2962-2966 Nov. 2007.

[23] A. Mller and J. Spiedel, "Exact symbol error probability of -PSK for multihop transmission with regenerative relays," IEEE Commun. Lett., vol. 11, no. 12, pp. 952-954, Dec. 2007.

[24] D.B. da Costa and M.D. Yacoub, "Dual-hop DF relaying systems with multiple interferers and subject to arbitrary Nakagami-m fading," Electronics Letters, Volume: 47 , Issue: 17, Page(s): 999 1001, 18th August 2011.

[25] Xianfu Lei, Pingzhi Fan, Mathiopoulos, P.T., "BER and ergodic capacity of dual-hop relay channel in Nakagami-m fading," Signal Design and its Applications in Communications, IWSDA '09. Fourth International Workshop on, page(s): 173 - 176, 04 December 2009.

[26] Milosevic, N., Nikolic, Z., Dimitrijevic, B., "Performance analysis of dual hop relay link in Nakagami-m fading channel with interference at relay," Radioelektronika (RADIOELEKTRONIKA), 2011 21st International Conference, Page(s): 1 - 4, 2011.

[27] Costa, H. Ding, and J. Ge, "Interference-limited relaying transmissions in dual-hop cooperative networks over nakagami-m fading," IEEE Communications letters, Vol. 15, no. 5, May 2011.

[28] Salama S. Ikki and Sonia Assa, "Performance analysis of dual-hop relaying systems in the presence of co-channel interference," IEEE Globecom 2010.

[29] Cvetkovic, A.M., orevic, G.T. , Stefanovic, M.C. , "Performance of interference-limited dual-hop non-regenerative relays over rayleigh fading channels," Communications, IET, 17 January 2011.

[30] Caijun Zhong, Tharm Ratnarajah, and Kai-Kit Wong, "Outage analysis of decode-and-forward cognitive dual-hop systems with the interference constraint in nakagami-m fading channels," IEEE Transactions on vehicular technology, Vol. 60, NO. 6, July 2011.

[31] V. A. Aalo, , and J. Zhang, Performance Analysis of Maximal Ratio Combining in the Presence of Multiple Equal-Power Cochannel Interferers in a Nakagami Fading Channel, IEEE Trans. Veh. Tech., vol.50, no. 2, pp. 497503, March 2001.

[32] Phillips, P. C. "The true characteristic function of the F distribution," Biometrika, 69: 261-264 JSTOR 2335882,(1982)

[33] J. W. Craig, "A new, simple, and exact result for calculating the probability of error for two-dimension signal constellations," in Proc. IEEE MILCOM,pp. 571575. Oct. 1991.

[34] J.C.S. Santos Filho and M. D. Yacoub, "Nakagami-m approximation to the sum of M non-identical independent Nakagami-m variates," IET Electron. Lett., vol. 40 no. 15, app. 951-952. Jul. 2004.

[35] M. Nakagami, "The m-distribution, a general formula of intensity of rapid fading," In statistical methods in radio wave propagation, proceedings of a symposium held june 18-20, 1958, pp 3-36. permagon press, 1960.

[36] I.S. Gradshteyn, I.M. Ryzhik, Alan Jeffrey, Daniel Zwillinger, " Table of Integrals, Series, and Products," seventh edition, CA., Academic Press, 2007.

[37] M. Abramowitz, I. Stegun, "Handbook of mathematical functions ," New York: Dover, 1970.

[38] L. J. Slater, "Confluent hypergeometric functions," Cambridge, U.K.: Cambridge university Press, 1960.

[39] Andrea Goldsmith, "Wireless Communications," Stanford University, Cambridge University Press 2005.

[40] J.C.S. Santos Filho and M. D. Yacoub, "Nakagami-m approximation to the sum of M non-identical independent Nakagami-m variates," IET Electron. Lett., vol. 40 no. 15, app. 951-952. Jul. 2004.

[41] M. Nakagami. "The m-distribution, a general formula of intensity of rapid fading," In statistical methods in radio wave propagation, proceedings of a symposium held june 18-20, 1958, pp 3-36. permagon press, 1960.

[42] Danny Dyer, " The convolution of generalized F distributions," Journal of the American Statistical Association, Vol. 77, No. 377, pp. 184-189, Mar., 1982.

[43] I.S. Gradshteyn, I.M. Ryzhik, Alan Jeffrey, Daniel Zwillinger, " Table of Integrals, Series, and Products," seventh edition, CA., Academic Press, 2007.

[44] Milton Abramowitz, Irene A. Stegun, "Handbook of mathematical functions with formulas, graphs, and mathematical tables," Volume 55, New York, Issue 1972.

[45] M. Abramowitz, I. Stegun, "Handbook of mathematical functions ," New York: Dover, 1970.

[46] L. J. Slater, "Confluent hypergeometric functions," Cambridge, U.K.: Cambridge university Press, 1960.

[47] Abramowitz, M. and Stegun, I. A. (Eds.). "Hypergeometric functions," Handbook of mathematical functions with formulas, graphs, and mathematical tables, 9th printing. New York: Dover, pp. 555-566, 1972.

[48] Exton, "H. Handbook of hypergeometric integrals: theory, applications, tables, computer programs," Chichester, England: Ellis Horwood, 1978.

[49] Gasper, G. and Rahman, "M. Basic Hypergeometric series. cambridge," England: Cambridge University Press, 1990.

[50] R. M. Gagliardi, "Introduction to Communication Engineering," New York, Wily, 1988.

[51] R. V. and A. T. Craig. , "Introduction to Mathematical Statistics," 4th edition. New York, Macmillan, 1978.

[52] Mohamed-Slim Alouini, "Sum of Gamma Variates and Performance of Wireless Communication Systems Over Nakagami-Fading Channels," IEEE Trans. Veh. Technol., VOL. 50, NO. 6, NOVEMBER 2001

[53] P. G. Moschopoulos, "The distribution of the sum of independent gamma random variables," Ann. Inst. Statist. Math. (Part A), vol. 37, pp. 541544, 1985.

[54] M. K. Simon, S. M. Hinedi, and W. C. Lindsey, *Digital Communication Techniques: Signal Design and Detection.* Englewood Cliffs, New Jersey: PTR Prentice-Hall, 1995.

[55] R. V. L. Hartley, "Transmission of Information," *Bell System Technical Journal*, vol. 7, pp. 535-563, July 1928.

[56] C. E. Shannon, "A Mathematical Theory of Communication I," *Bell System Technical Journal*, vol. 27, pp. 329-423, 1948.

[57] C. E. Shannon, "A Mathematical Theory of Communication II," *Bell System Technical Journal*, vol. 27, pp. 623-656, 1948.

[58] C. E. Shannon and W. Weaver, "The Mathematical Theory of Communication," University of Illinois Press, Urbana, Illinoi, 1959.

[59] A. J. Goldsmith and P. P. Varaiya, "Capacity of Fading Channels with Channel Side Information," *IEEE Transactions on Information Theory,* vol. 43, no. 6. pp. 1986-1992, November 1997.

[60] M.-S Alouini and A. J. Goldsmith, "Capacity of Rayleigh Fading Channels Under Different Adaptive Transmission and diversity-Combining Techniques," *IEEE Transactions on Vehcular Technology,* vol. 48, no. 4, pp. 1165-1181, July, 1999.

[61] M.-S Alouini and A. J. Goldsmith, "Adaptive Modulation over Nakagami Fading Channels ," *Wireless Personal Communications,* vol . 13, no. 1-2, pp. 119-143, May, 2000.

[62] M.-S. Alouini and A. Goldsmith, "Capacity of Nakagami multipath fading channels,"*IEEE Vehicular Technology Conference*, vol. 1, pp. 358-362, 4-7 May 1997.

[63] N. C. Sagias, D. A. Zogas, G. K. Karagiannidis, and G. S. Tombras, "Channel Capacity and Second-Order Statistics in Weibull Fading," *IEEE Communication Letters*, vol. 8, no. 6, pp. 377-379, June, 2004.

[64] H. C. Yang and M. S. Alouini, "Performance analysis of multibranch switched diversity systems," *IEEE Transactions on Communications*, vol. 51, no. 5, pp. 782-794, May 2003.

[65] F. Zheng, and T. Kaiser,"On the Channel Capacity of Multiantenna Systems with Nakagami Fading," *EURASIP Journal on Applied Signal Processing,* vol. 1, pp. 1-11, March 2006.

[66] M. Kang, and M.-S. Alouini, "Capacity of correlated MIMO rayleigh fading channels," *IEEE Transaction on Wireless Communication,* vol. 5, pp. 143-155, January 2006.

[67] E. Telatar, "Capacity of Multi-Antenna Gaussian channels," *European Transaction on Telecommunication,* vol. 10, no. 6, pp. 311-335, 1998

[68] M. Chiani, M. Z. Win, and A. Zanella, "On the Capacity of Spatially Correlated MIMO Rayleigh-Fading Channels," *IEEE Transaction on Information Theory,* vol. 49, no. 10, pp. 2363-2371, October. 2003.

[69] M. Kang, and M.-S. Alouini,"Capacity of MIMO Rician Channels," *IEEE Transaction on Wireless Communication,* vol. 5, pp. 112-122, January 2006.

[70] M.-S Alouini, and A. Goldsmith, "Capacity of Nakagami Multipath Fading," *Vehicular Technology Conference,* IEEE 47th, vol. 1, pp. 358 - 362, May 1997.

[71] C. Tellambura, A. Annamalai, and V. K. Bharagava, "Unified anaylsis of switched diversity systems in independent and correlated fading channels," *IEEE Transactions on Communications*, vol. 49, no. 11, pp. 1955-1965, November 2001.

[72] A. P. Prudnikov, Yu. A. Brychkov, and O. I. Marichev, *Integrals and Series, Volume 3: More Special Functions*. Gordon and Breach Science Publishers, 1990.

[73] E. Biglieri, J. G. Proakis, and S. Shamai, "Fading Channels: Information-Theoretic and Communications Aspects," *IEEE Transaction on Information Theory,* vol. 44, no. 6, pp. 2619-2692 October 1998.

[74] Y. Zhao, M. Zhao, S. Zhou, and J. Wang, "Closed-Form Capacity Expressions for SIMO Channels with Correlated Fading," *IEEE Vehicular Technology Conference,* vol. 2, pp. 982-985 Sept. 2005.

[75] A. M. Magableh and M. M. Matalgah, "Capacity of SIMO systems over non-identically independent Nakagami-m channels," *IEEE Sarnoff Symposium 2007,* Digital Object Identifier 10.1109/SARNOF.2007.4567395, vol. 1, pp. 1-5, April 30-May 2 2007.

[76] FOSCHINI, G.J., and GANS, M.J. "On limits of wireless communications in a fading environment when using multi-element antennas," Wirel. Pers. Commun. , pp. 311-335, 1998.

[77] M. Borgmann and H. Bolcskei,"On the capacity of noncoherent wideband MIMO-OFDM systems," in IEEE Int. Symp.Inf. Theory (ISIT), Adelaide, Australia, Sept. 2005, pp. 651-655.

[78] Telatar, E.: "Capacity of multi-antenna Gaussian channels," Eur.Trans. Telecommun., 1999, 10, pp. 585-595

[79] Tarokh, V., Sheshadri, N., and Calderbank, A.R.: "Space-time codes for high data rate wireless communication: Performance criterion and code construction," IEEE Trans. Inf. Theory, 1998, 44, pp. 744-765

[80] Wolniansky, P.W., Foschini, G.J., Golden, G.D., and Valenzuela, R.A.: "V-BLAST: an architecture for realizing very high data rates over the rich-scattering wireless channel," Proc. URSI Int. Symp. On Signals, Systems, and Electronics, Sept. 1998, pp. 295-300

[81] Li, Y., Winters, J.H., and Sollenberger, N.R.: "MIMO-OFDM for wireless communications: Signal detection with enhanced channel estimation," IEEE Trans. Commun., 2002, 50, pp. 1471-1477

[82] Piechocki, R.J., Fletcher, P.N., Nix, A.R., Canagarajah, C.N., and McGeehan, J.P.: "Performance evaluation of BLAST-OFDM enhanced Hiperlan/2 using simulated and measured channel data," Electron. Lett., 2001, 37, pp. 1137-1139

[83] A. B. Gershman and N. D. Sidiropoulos, "Space-Time Processing for MIMO Communications", John Wiley, 2005.

[84] Marvin K. Simon and Mohamed-Slim Alouini, "Digital communication over fading channels: a unified approach to performance analysis", John Wiley and Sons, Inc., 2000.

[85] Wbben ,J.Rinas ,V.Khn ,and K.-D Kammeyer ,"Efficient Algorithm for detecting layered space-time codes ",in proc.international ITG conference on source and channel coding , Berlin Germany,Jan.2002,pp. 399-405.

[86] M.Borgmann and H.Bolcskei , "Interpolation Based Efficient Matrix Inversion for MIMO-OFDM Receiver," in proc .Asilomar Conference on signals, systems and computers, Pacific Grove. CA. USA, Nov.2004

[87] Cescato, M.Borgmann, H Bolcskei, J.Hansen, and A. Burg, "Interpolation Based QR Decomposition in MIMO-OFDM systems ," in IEEE Proc.workshop on signal processing Advances in wireless communication s (SPAWC), New York,USA ,June 2005.

[88] Richard van Nee and Ramjee Prasad "OFDM for Wireless Multimedia Communications," 2000.

[89] John G.Proakis, "Digital Communications," (4th Ed), McGraw-HILL (2001)

[90] H.Schuster and P.Hippe, "Inversion of polynomial Matrices by interpolation," IEEsE Trans.on Automatic Control, Vol.37, no.3, pp.363-365, Mar.1992.

[91] T.K Moon, "More Mathematical Methods and Algorithms for signal processing," 2000, online: http://www.engineering.usu.edu/ece/faculty/tmoon/books.html.

[92] Mostafa Naghizadeh, Kristopher A. Innanen, "Seismic data interpolation using a fast generalized Fourier transform," GEOPHYSICS,VOL. 76, NO. 1 FEBRUARY 2011.

[93] Chien-Cheng, Su-Ling Lee, "Design offractional delay filterusing discrete Fourier transform interpolation method," a publication of the European Association for Signal Processing (EURASIP), Signal Processing, 2010.

[94] Jihoon Choi and Robert W.Heath, Jr. "Interpolation Based Transmit Beamforming for MIMO-OFDM with Partial Feeddback," Sept.16, 2003.

[95] D. Wubben and K.-D. Kammeyer, "Parallel-SQRD for Low Complexity Successive Interference Cancellation in Per-Antenna-Coded MIMO-OFDM Schemes," in Proc.

International ITG Conference on Source and Channel Coding, Munich, Germany, Apr. 2006.

[96] D. Wubben, R. Bohnke, V. Kuhn, and K.-D. Kammeyer,"MMSE Extension of V-BLAST based on Sorted QR Decomposition,"in Proc. VTC, Orlando, FL, USA, Oct. 2003.

[97] T.K. Moon, "More Mathematical Methods and Algorithms for Signal Processing," 2000, Online: http://www.engineering.usu.edu/ece/faculty/tmoon/books.html.

[98] D. Wubben and K.-D. Kammeyer, "interpolation based successive interference cancellation for per antenna codec MIMO-OFDM systems USING P-SQRD," International ITG/IEEE Workshop on smart antennas WSA, Germany, 2006.

[99] D. Cescato, M. Borgmann, H. Bolcskei, J. Hansen, and A. Burg, "Interpolation-Based QR Decomposition in MIMO-OFDM Systems," in IEEE Proc. Workshop on Signal Processing Advances in Wireless Communications (SPAWC), New York, NY, USA, June 2005.

[100] B. Hassibi, "A Fast Square-Root Implementation for BLAST," inProc. Asilomar Conference on Signals, Systems and Computers, vol. 2,Asilomar, USA, Nov. 2000, pp. 1255 - 1259.

[101] P.W. Wolniansky, G.J. Foschini, G.D. Golden, and R.A.Valenzuela, "V-BLAST: An Architecture for Realizing Very High Data Rates Over the Rich-Scattering Wireless Channel," in Proc. International Symposium on Signals,Systems, and Electronics (ISSSE), Pisa, Italy, Sept.1998, pp. 295-300.

[102] D. Wubben, J. Rinas, R. Bohnke, V. Kuhn, and K.-D.Kammeyer, "Efficient Algorithm for Detecting Layered Space-Time Codes," in Proc. International ITG Conference on Source and Channel Coding, Berlin, Germany,Jan. 2002, pp. 399-405. vol. 37, no. 3, pp. 363-365,Mar. 1992.

[103] Xiaodong Wang,H. Vincent Poor,"Wireless Communication Systems: Advanced Techniques for Signal Reception", prentice hall communication engineering and emerging technologies series, theodore S.Rappapot, series editor.

[104] Helmut Bolcskei," MIMO-OFDM Wireless Systems: Basics, Perspectives, and Challenges Communication Technology Laboratory, ETH Zurich,8092 Zurich, Switzerland

[105] Luc Knockaert, Bernard De Backer, and Daniel De Zutter, "SVD Compression, Unitary Transforms, and Computational Complexity", IEEE TRANSACTIONS ON SIGNAL PROCESSING, VOL. 47, NO. 10, OCTOBER 1999

[106] D. Wubben and K.-D. Kammeyer, "Low Complexity Successive Interference Cancellation for Per-Antenna-Coded MIMO-OFDM Schemes by Applying Parallel- SQRD," in IEEE Proc. Vehicular Technology Conference(VTC), Spring, Melbourne, Australia, May 2006.

[107] J-K. Zhang, A. Kavcic, and K. M. Wong, "Equal diagonal QR decomposition and its application to precoder design for successive-cancellation detection," IEEE Trans. on Information Theory,vol. 51,pp. 154-172. , Jan 2005.

[108] D.Wubben, R.Bohnke, V.Kuhn,andK.-D.Kammeyer, MMSE Extension of V-BLAST based on Sorted QR Decomposition, in IEEE Proc. Vehicular Technology Conference (VTC), Orlando, FL, USA, Oct. 2003.

[109] Chien-Hung Pan "Complexity reduction by using triangular matrix multiplication in computing capacity for an optimal transmission," WSEAS TRANSACTIONS on COMMUNICATIONS, Volume 8 , Issue 8 ,August 2009.

[110] D. Cescato, M. Borgmann, H. Bolcskei, J. Hansen, and A. Burg, "Interpolation-Based QR Decomposition in MIMO-OFDM Systems," in IEEE Proc. Workshop on Signal Processing Advances in Wireless Communications (SPAWC), New York, NY, USA, June 2005.

[111] Cheng-Zhou Zhan, Kai-Yuan Jheng, Yen-Lian Chen, Ting-Jhun Jheng, An-Yeu Wu, "High-convergence-speed low-computation-complexity SVD algorithm for MIMO-OFDM systems", VLSI Design, Automation and Test, Grad. Inst. of Electron. Eng., Nat. Taiwan Univ., Taipei, Taiwan, 2009.

[112] Zamiri-Jafarian, H. ; Rajabzadeh, M. ;"A Polynomial Matrix SVD Approach for Time Domain Broadband Beamforming in MIMO-OFDM Systems", IEEE On page 802, Vehicular Technology Conference, Singapore, VTC Spring 2008.

[113] Davide Cescato, Helmut Blcskei, "Algorithms for Interpolation-Based QR Decomposition in MIMO-OFDM Systems ", IEEE TRANSACTIONS ON SIGNAL PROCESSING, VOL. 59, NO. December 28, 2010

[114] M. K. Simon, S. M. Hinedi, and W. C. Lindsey,"Digital Communication Techniques: Signal Design and Detection." Englewood Cliffs, New Jersey: PTR Prentice-Hall, 1995.

[115] C. E. Shannon, A Mathematical Theory of Communication, Bell System Technical Journal, vol. 27, pp.329-423, 623-656, 1948.

[116] N. C. Beaulieu, J. Cheng, Precise Error-Rate Analysis of Bandwidth-Efficient BPSK in Nakagami Fading and Cochannel Interference IEEE Trans.on Comm.,vol. 52, no. 1, pp. 149-158, Jan. 2004

[117] Fawaz S Al-Qahtani, Duong, Caijun Zhong, Khalid A. Qaraqe, Hussein Alnuweiri, Tharm Ratnarajah, "Performance analysis of dual-hop AF systems in Nakagami-m fading channels in the presence of interference," IEEE signal procesing Letter, Vol. 18, Issue 8, PP. 454-457, 2011.

[118] D.B. da Costa and M.D. Yacoub, "Dual-hop DF relaying systems with multiple interferers and subject to arbitrary Nakagami-m fading," Electronics Letters, Vol. 47 No. 17, 18th August 2011.

[119] A. J. Goldsmith and P. P. Varaiya, "Capacity of Fading Channels with Channel Side Information," *IEEE Transactions on Information Theory,*" vol. 43, no. 6. pp. 1986-1992, November 1997.

[120] M.-S Alouini and A. J. Goldsmith, "Capacity of Rayleigh Fading Channels Under Different Adaptive Transmission and diversity-Combining Techniques," *IEEE Transactions on Vehcular Technology,* vol. 48, no. 4, pp. 1165-1181, July, 1999.

[121] M.-S Alouini and A. J. Goldsmith, "Adaptive Modulation over Nakagami Fading Channels ," *Wireless Personal Communications,* vol . 13, no. 1-2, pp. 119-143, May, 2000.

[122] M.-S. Alouini and A. Goldsmith, "Capacity of Nakagami multipath fading channels,"*IEEE Vehicular Technology Conference*," vol. 1, pp. 358-362, 4-7 May 1997.

[123] Bhuvan Modi, A. Annamalai, O. Olabiyi, and R. Chembil Palat, " Ergodic capacity analysis of cooperative amplify-and-forward relay networks over Rice and Nakagami fading channels," International Journal of Wireless and Mobile Networks (IJWMN) Vol. 4, No. 1, February 2012.

[124] Golnaz Farhadi and Norman C. Beaulieu, " On the ergodic capacity of multi-hop wireless relaying systems," IEEE TRANSACTIONS ON WIRELESS COMMUNICATIONS, VOL. 8, NO. 5, MAY 2009.

[125] J. N. Laneman, D. N. C. Tse, and G. W. Wornell, "Cooperative diversity in wireless networks: effecient protocols and outage behavior," IEEE Trans. Inform. Theory, vol. 50, no. 12, pp. 3062-3080, Dec. 2004.

[126] Shi Jin, Matthew R. McKay, Caijun Zhong, and Kai-Kit Wong, " Ergodic capacity analysis of amplify-and-forward mimo dual-hop systems," IEEE TRANSACTIONS ON INFORMATION THEORY, VOL. 56, NO. 5, MAY 2010.

[127] A. P. Prudnikov, Yu. A. Brychkov, and O. I. Marichev, "*Integrals and Series, Volume 3: More Special Functions*. Gordon and Breach Science Publishers," 1990.

[128] W. Su, "Performance analysis for a suboptimum ML receiver in decode-and-forward communications," in Proc. IEEE Global Telecommun. Conf., pp. 2962-2966 Nov. 2007.

[129] A. Maller and J. Spiedel, "Exact symbol error probability of BPSK for multihop transmission with regenerative relays," IEEE Commun. Lett., vol. 11, no. 12, pp. 952-954, Dec. 2007.

[130] R. M. Gagliardi, "Introduction to Communication Engineering," New York, Wily, 1988.

[131] J.C.S. Santos Filho and M. D. Yacoub, "Nakagami-m approximation to the sum of M non-identical independent Nakagami-m variates," IET Electron. Lett., vol. 40 no. 15, app. 951-952. Jul. 2004.

[132] I.S. Gradshteyn, I.M. Ryzhik, Alan Jeffrey, Daniel Zwillinger, " Table of Integrals, Series, and Products," seventh edition, CA., Academic Press, 2007.

[133] M. Abramowitz, I. Stegun, "Handbook of mathematical functions ," New York: Dover, 1970.

[134] L. J. Slater, "Confluent hypergeometric functions," Cambridge, U.K.: Cambridge university Press, 1960.

[135] Andrea Goldsmith, "Wireless Communications," Stanford University, Cambridge University Press 2005.

VITA

Mohammed Shaker Akhoirshida was born in Jordan, in 1980. He received a Bachelor's degree in Electrical Engineering with emphasis in Electronics and Communications from Jordan University of Science and Technology (JUST), Irbid, Jordan, in 2003, and a Master's degree in Engineering Science with an emphasis in Communications from The University of Jordan (UJ), Amman, Jordan, in 2007. From August 2003 to January 2004, he was a Teaching Assistant in the Department of Electrical Engineering at JUST. From February 2004 to April 2005, he worked as a full time Electronics and Communication Engineer with Communication Directorate, Amman, Jordan. From April 2005 to January 2009, he worked as a full time Electrical and Communication Engineer with the Special Communication Commission, Amman, Jordan. From January 2009 to September 2009, he worked as a full time instructor at the Electrical Engineering Department at the Tafila Technical University, Tafila, Jordan. During the period of September 2009 to present 2012, he has been with the Center for Wireless Communications (CWC) at the University of Mississippi, Oxford, MS, USA, as a Research Assistant and Graduate Instructor where he pursued his Ph.D. degree in Electrical Engineering. His research interests include several areas in wireless communications with emphasis on the performance evaluation of cooperative network of the wireless communication systems over fading

channels and MIMO-OFDM wireless systems. Mr. Akhoirshida is the recipient of a dissertation fellowship award, graduate school, university of Mississippi, USA, fall 2012, a Research Grant, graduate school, university of Mississippi, USA, fall 2010, in recognition of his research work at the University of Mississippi. Mr. Akhoirshida served as a reviewer for several refereed international journals and conferences, a member of the Institute of Electrical and Electronics Engineers (IEEE), USA , a member of the Graduate Students Council (GSC) since 2010, a member of the Mississippi Academy of Sciences, Physics and Engineering Division, and a member of the Jordanian Engineering Association since 2003.